Technical Report Documentation Page

1. Report No.	2. Government Accession No.	3. Recipient's Catalog No.
FHWA/TX-1995/1243-4		

4. Title and Subtitle	5. Report Date
PRELIMINARY STUDIES TO DEVELOP A TRAILER-MOUNTED SYSTEM TO DELINEATE IRREGULARITIES IN RIGID PAVEMENTS	December 1994
	6. Performing Organization Code

7. Author(s)	8. Performing Organization Report No.
Blake E. Cotton, Kenneth H. Stokoe, II, and Jose M. Roesset	Research Report 1243-4

9. Performing Organization Name and Address	10. Work Unit No. (TRAIS)
Center for Transportation Research The University of Texas at Austin 3208 Red River, Suite 200 Austin, Texas 78705-2650	11. Contract or Grant No. Research Study 0-1243
	13. Type of Report and Period Covered Interim
12. Sponsoring Agency Name and Address Texas Department of Transportation Research and Technology Transfer Office P. O. Box 5080 Austin, Texas 78763-5080	14. Sponsoring Agency Code

15. Supplementary Notes

Study conducted in cooperation with the U.S. Department of Transportation, Federal Highway Administration. Research study title: "Automated Equipment for Characterizing the Properties and Thicknesses of Pavements"

16. Abstract

This study involved preliminary investigation of the components needed to develop a low-cost, prototype, trailer-mounted system to nondestructively delineate irregularities and flaws in rigid pavements while rolling. The proposed system should be capable of delineating cracks, voids, debondings, and delaminations within a rigid pavement system. The design concept consists of introducing stress waves at one point on top of the pavement, and sensing the waves at another point. With this design concept, source and receiver wheels were experimentally studied, small trailer systems were prototyped, and systems to isolate the source and receiver were investigated. Preliminary full-scale tests were performed at the rigid concrete pavement test facility at The University of Texas at Austin. Testing consisted of evaluating individual components at various levels of development in a stationary mode. No successful rolling tests were performed These tests showed that a source wheel should input stress waves with frequencies up to 25 kHz and force levels above several hundred pounds (> 1000 N). The receiver wheel is, however, the critical design element in a moving system and no successful receiver wheels were developed. A critical aspect is the negative impact that the rough texture of a rigid pavement has on the inability to couple high frequencies into the receiver wheel. Suggestions for future efforts and directions are given.

17. Key Words	18. Distribution Statement
Non-destructive pavement testing, rigid pavements, voids, delaminations, rolling tests	No restrictions. This document is available to the public through the National Technical Information Service, Springfield, Virginia 22161.

19. Security Classif. (of this report)	20. Security Classif. (of this page)	21. No. of Pages	22. Price
Unclassified	Unclassified	253	

PRELIMINARY STUDIES TO DEVELOP A TRAILER-MOUNTED SYSTEM TO DELINEATE IRREGULARITIES IN RIGID PAVEMENTS

by

Blake E. Cotton
Kenneth H. Stokoe, II
J. M. Roesset

Research Report 1243-4

Research Project 0-1243
Automated Equipment for Characterizing the
Properties and Thicknesses of Pavements

conducted for the

Texas Department of Transportation

in cooperation with the

U.S. Department of Transportation
Federal Highway Administration

by the

CENTER FOR TRANSPORTATION RESEARCH
Bureau of Engineering Research
THE UNIVERSITY OF TEXAS AT AUSTIN

December 1994

IMPLEMENTATION STATEMENT

The results of studies to develop a trailer-mounted system to nondestructively evaluate rigid pavements are presented. The proposed system would be used to delineate cracks, voids, debondings, and delaminations within the rigid pavement. The results show that a high-energy piezoelectric shaker can be used as the "source wheel." However, further studies are necessary to develop the appropriate "receiver wheel" so that testing can be performed while moving. Therefore, a trailer-mounted system is not ready for implementation at this time.

Prepared in cooperation with the Texas Department of Transportation and the U.S. Department of Transportation, Federal Highway Administration.

DISCLAIMERS

The content of this report reflect the views of the authors, who are responsible for the facts and the accuracy of the data presented herein. The contents do not necessarily reflect the official views of policies of the Federal Highway Administration or the Texas Department of Transportation. This report does not constitute a standard, specification, or regulation.

NOT INTENDED FOR CONSTRUCTION, BIDDING, OR PERMIT PURPOSES

Kenneth H. Stokoe, II (Texas No. 49095)
Research Supervisor

ACKNOWLEDGMENTS

The writers are grateful to the many graduate students who assisted in various aspects of this work. James Bay and Mark Fuhriman offered much assistance. Ron Andrus, Marwan Aouad, Sung-Ho Joh, Seon-Keun Hwang, Thomas Wesling, and Chris Noack were also very helpful. The assistance of the staff at the University of Texas is also appreciated. Mr. James Stewart, Mr. Johnie Williams Jr., Mr. Gonzalo Zapata, Mrs. Teresa Tice-Boggs, Ms. Heather L. Rankine, and Ms. Linda M. Iverson all helped in this work.

Thanks and appreciation are extended to Mr. Larry Olson for providing pertinent data and valuable comments during this project, to Dr. Nazarian for his useful data and cooperation, to Mr. Robert Briggs, project director, for his helpful guidance, and the Texas DOT for the financial support to accomplish this research.

TABLE OF CONTENTS

SUMMARY

Preliminary studies were undertaken to develop a low-cost, prototype, trailer-mounted system to nondestructively and continuously monitor rigid pavements. The proposed system should be capable of delineating cracks, voids, debondings, and delaminations within a rigid pavement system while moving. The design concept consists of inducing seismic body and surface waves at one point on top of the pavement system. These waves propagate through the system and are altered by the interior structure. The waves are sensed at another, nearby point on the pavement surface. The received signal is analyzed and interpreted to reveal any superficial and/or subsurface irregularities in the pavement system.

Using the design concept and detailed analyses of both equipment and road noises, pertinent design parameters were established which in turn dictated the optimum design of the prototype trailer-mounted system. The design evolution covered five major redesigns and several minor modifications. Initially, a system consisting of separate trailers for both the source and the receiver was attempted. In addition, an electromagnetic shaker was initially utilized to generate the necessary signal. Owing to various problems encountered during the design and development process, the design was modified and refined several times. The resulting prototype system consists of a piezoelectric shaker on a "source wheel," which is used to beam the desired signal into the pavement. The altered signal is received using a high-sensitivity piezoelectric accelerometer on a "receiver wheel."

It should be noted that problems were encountered with the final prototype system. The problems were isolated to the receiver mechanism and the inability to develop a strong coupling to the pavement. Therefore, the receiver mechanism needs to be replaced to improve the performance in future systems. The entire system consists of a single trailer in which the source and receiver are isolated from one another. In addition the trailer itself is isolated from any outside noise interference using acoustical sound chambers around both the source and receiver.

The prototype trailer was tested at the rigid concrete pavement test facility at The University of Texas at Austin. This facility contains such known defects as cracks, voids, and delaminations. First, the design concept was validated by characterizing each of the pavement anomalies using the source and receiver directly on the pavement surface and, again, using the "source wheel" component of the trailer. This was successful in establishing a "signature" for each defect. Finally, the prototype trailer-mounted system was tested using several different testing configurations, including a series of individual trailer component tests.

Chapter One
Introduction

1.1 Pavement Irregularities

Pavement irregularities, both superficial and subsurface, decrease the usable life of a rigid pavement system. Therefore, locating and correcting these anomalies is a major concern in an effective pavement management plan. Most pavement irregularities are caused by internal stresses associated with environmental conditions, material anomalies, or irregular loading. The most critical irregularities occurring in rigid pavements include cracks, delaminations, and voids. These anomalies are illustrated in Figure 1.1.

Pavement cracking, the most widespread defect (Ayyub and White, 1987), refers to any variety of vertically oriented discontinuities in the pavement. Cracking is caused by thermal expansion and contraction within the pavement or by excessive loading conditions and may be limited to only the surface layer or it may extend to the sublayers. Cracking is not considered a serious structural defect by itself. However, cracking allows easy access to the inner pavement layers and the reinforcing steel for moisture and chemicals such as salt. Such access results in deterioration of the pavement layers and corrosion of the reinforcing steel.

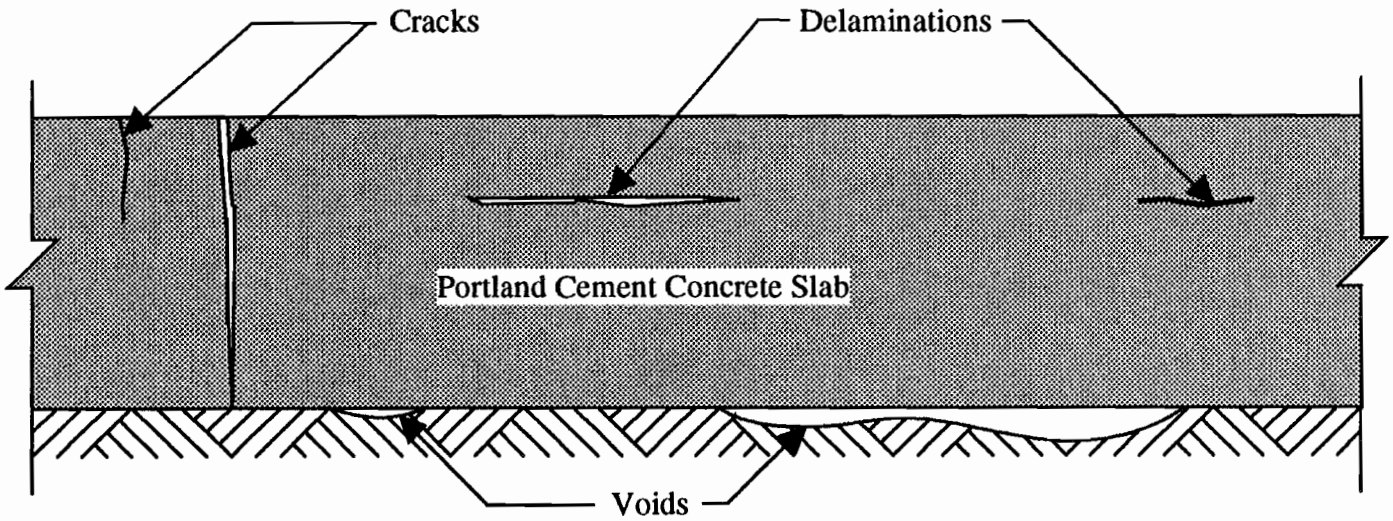

Figure 1.1: Illustration of Typical Cracks, Voids, and Delaminations and Their Relative Locations in a Rigid Concrete Pavement

Corrosion of the reinforcing steel is the major cause of the development of delaminations (Ayyub and White, 1987). The corrosive material occupies more space than the steel alone. Thus, internal stresses develop. These stresses can become quite large and result in a horizontal crack or subsurface fracture plane. The fracture plane, or delamination, is usually located at or just above the top reinforcement and may be limited to a small area or it may extend over a considerable portion of the pavement. In addition, more than one delamination may occur on various horizontal planes above the reinforcing steel (Ayyub and White, 1987). The combination of cracks and delaminations results in spalling of the pavement (more commonly called "potholes"). Both delaminations and cracks are easiest to repair in their early stages of development. When pavement spalling occurs, the repairs can be quite extensive and costly.

Unlike cracks and delaminations, voids are not located within the pavement but rather below the pavement. Voids are cavities that form beneath the pavement usually at the edge or near a joint. They can occur in a variety of ways such as the shrinkage of subsurface material or the decomposition of organic material beneath the pavement. Voids can vary in depth from thousandths of an inch to over several inches. Voids result in a loss of support, the severity of which is determined by the depth and lateral extent of the void. Any loss of support will cause increased stresses and increased

deflections, both of which will result in a significant reduction in the fatigue life of the pavement. In addition, voids can cause superficial and subsurface cracking which can lead to delaminations and pavement spalling (Uddin et al., 1987). In the early stages, voids are fairly easy to repair. However, at the extreme conditions, voids can require extensive and costly repairs.

1.2 Purpose and Experimental Study

Obviously, the early detection of pavement irregularities is a vital concern of State Department of Transportation (DOT) offices and a necessity in any effective pavement management plan. Thus, a nondestructive method capable of detecting these anomalies is desirable. Ideally, the method would allow both stationary and mobile measurements, be easy to operate, be simplistic in data interpretation, and consist of "off-the-shelf" equipment which is fairly inexpensive. Therefore, the overall objective of this work is to investigate the possibility of using nondestructive methods to delineate irregularities in rigid pavement layers. This objective is being investigated both analytically and experimentally. The focus of this study, which is the experimental portion of the project, is to design and develop a vehicle capable of delineating irregularities in rigid pavement layers.

A previously constructed concrete pavement research facility at the Balcones Research Center at the University of Texas at

Austin was used to perform the experimental study. The research facility contains known pavement irregularities making it well suited for such a project.

Experimental results are reported and discussed for all three anomalies. In addition, data from outside sources involving "state-of-the-art" methods are discussed in an effort to establish a considerable data base for a variety of pavement systems.

1.3 Organization of the Thesis

Since the early detection of pavement irregularities has received some attention, the various methods that have been developed to detect pavement irregularities are presented in Chapter Two. Methods applicable to each of the three critical anomalies are discussed separately.

The process involved in the design and development of a prototype vehicle which satisfies the design criteria is initially discussed in Chapter Three. Included in this chapter is a discussion on all applicable equipment and other relevant design considerations.

The design and development process, begun in Chapter Three, is continued in Chapter Four. Chapter Four concludes with a presentation of the proposed prototype trailer-mounted system.

Preliminary field studies, including a detailed description of the concrete pavement facility, are presented in Chapter Five. Testing and characterization of each anomaly and the preliminary

results of the prototype trailer-mounted system are also presented. In addition, data from outside sources concerning "state-of-the-art" methods, applicable to this research, are discussed in Chapter Five.

Finally, the major findings and recommendations for further research are presented in Chapter Five.

Chapter Two
Existing Pavement Monitoring Techniques

2.1 Introduction

As discussed in Chapter One, the presence of defects in pavement systems, both visually and subsurface, is of great interest. Early detection of such defects significantly impacts the effectiveness of an overall pavement management plan. Therefore, effective pavement testing methods are a critical aspect of any successful management plan. As might be expected, a variety of testing methods are presently available to monitor pavement conditions. These include both destructive and nondestructive techniques which range in complexity from visual surveys to such advanced schemes as radar and thermography. However, no method has yet evolved into an optimum and accepted standard.

In this chapter, various nondestructive methods for pavement monitoring are examined. First, those methods currently used to detect voids are reviewed. A discussion of delamination detection techniques then follows. Finally, crack detection methods are presented. It should be noted that voids are generally associated only with rigid concrete pavements. On the other hand, delaminations and cracks are generally associated with both asphalt and concrete pavements. The examination of pavement testing

methods highlights their diversity, relative costs, advantages, and disadvantages while establishing justification for this research.

2.2 Void Detection Methods

Void detection methods are numerous and diverse. The methods range from visual surveys to ground penetrating radar and include deflection based and acoustic methods. The void detection methods presented herein are summarized in Table 2.1.

2.2.1 Visual Surveys

In research performed for the Federal Highway Administration (FHWA), Torres and McCullough (1983) and Uddin et al. (1987) report the major visual criterion, indicative of a void, is edge pumping. The location of deposits of pumped material or the presence of water stains along the pavement edge is assumed to indicate the presence of a void beneath the pavement at that location. However, the actual location of suspected voids may vary considerably from the location of the pumped material deposits due to the drainage characteristics of the pavement (Torres and McCullough, 1983). In addition to edge pumping, as heavy vehicles travel over a pavement system, the ejection of water and fine materials may occur which is indicative of a void. Other visual signs, which might suggest the presence of a void, include the faulting of transverse joints and corner cracking (Uddin et al. 1987).

Table 2.1: Comparison of Void Detection Methods

Method	Vehicle Requirements	Training	Inspection Speed	Traffic Control	Independent of Bonded Overlays	Independent of Debonded Overlays
Visual Survey	Transport Vehicle	Moderate	Very Slow	Lane closure	Yes	Yes
Static Deflection	Transport Vehicle and Load Truck	Moderate	Slow	Lane Closure	Unknown	Unknown
Dynamic Deflection	Instrumented Towing Vehicle	Moderate	Slow	LaneClosure	Unknown	Unknown
Acoustic Methods	Transport Vehicle	Moderate/ Extensive	Very Slow	Lane Closure	Unknown	Unknown
Ground Penetrating Radar	Instrumented Vehicle	Extensive	Fast	Moving Lane Closure	Yes	Yes
Infrared Thermography	Instrumented Vehicle	Extensive	Fast	Moving Lane Closure	Unknown	Unknown
Radioactive Tracer	Unknown	Extensive	Very Slow	Lane Closure	Unknown	Unknown

Table 2.1(con't): Comparison of Void Detection Methods

Method	Field Data Processing	Office Data Processing	Data Interpretation	Non-contacting	Independent of Weather	Relative Cost
Visual Survey	Routine	Not Required	Simple	Yes	No	Inexpensive
Static Deflection	Moderate	Not Required	Simple	No	Unknown	Moderate
Dynamic Deflection	Moderate to Extensive	Moderate	Moderate	No	Unknown	Moderate
Acoustic Methods	Moderate to Extensive	Moderate	Moderate	No	Yes	Moderate
Ground Penetrating Radar	Extensive	Moderate	Difficult	Yes	Yes	Moderate to High
Infrared Thermography	Moderate to Extensive	Routine to Moderate	Moderate	Yes	No	Moderate to High
Radioactive Tracer	Extensive	Unknown	Unknown	No	Unknown	Unknown

The advantage of visual surveys is the simplicity and negligible equipment cost. In addition, visual surveys are unaffected by pavement overlays. However, Birkoff and McCullough (1979) reported the method to be only 50 percent reliable in void detection. Therefore, researchers have recommended the use of visual surveys only to support other methods (Uddin et al., 1987). For example, Torres and McCullough (1983) found a combination of visual surveys and the Dynaflect deflection method to be a reliable means for void detection.

2.2.2 Deflection Based Methods

Deflection based methods originate from the intrinsic deflectional characteristics of pavements. Either the deflection profile along the edge is compared to the deflection profile along the inside lane (Uddin et al., 1983) or deflections are measured under a given load and compared to an allowable deflection specification (Uddin et al., 1987). For both cases, an area showing large deviations in the compared values is presumed to contain voids underneath the pavement at that location. The methods used to determine a pavements deflectional response to loading can be separated into two categories: static and dynamic. This classification simply refers to the method of loading (Uddin et al., 1983).

Static deflection methods use a static load such as a standard 18-kip single axle. Deflections are measured with a Benkelman Beam or similar device and are compared to the allowable specifications (Uddin et al., 1987). Dynamic deflection methods use counter rotating masses, hydraulic actuated masses, or similar means to produce a dynamic load. Deflections are usually measured using a series of receivers, such as geophones. Unlike static methods, dynamic deflection methods house the loading device and receivers in one unit. The available dynamic deflection equipment includes the Dynaflect, Road Rater, and Falling Weight Deflectometer (Uddin et al., 1983, Uddin et al., 1987, and Barenberg et al., 1988). In addition to these methods the French have developed a Collograph which has possible applications in void detection. However, the Collograph's response to voids has received little investigation (Le Laboratoire Central des Ponts et Chaussees, 1983). The Collograph method is discussed in Sections 2.3.2 and 2.4.4.

It should be noted that climatic factors, such as temperature, affect the deflectional behavior of rigid pavements. Therefore, the American Association of State Highway Officials, AASHO, recommends testing pavements between midnight and 10:00am to minimize the effects of thermal expansion (Uddin et al., 1987).

2.2.3 Acoustic Methods

Acoustic methods for void detection are based on either the vibrational characteristics of the pavement system or the characteristics of seismic wave propagation through the system. (Acoustic method classification is explained in more detail in Section 2.3.1.) Currently, there are only a few acoustic methods which have shown positive results in void detection. These include the use of vibratory equipment (Torres and McCullough, 1983) and the Transient Dynamic Response (TDR) method (Uddin et al., 1987). Methods involving tapping steel rods/hammers on the pavement surface or dragging heavy chains across the pavement surface are not reported in the literature for void detection. This is most likely because the accuracy of these acoustical methods diminishes with depth making voids, which are located at the bottom of rigid concrete pavements, more difficult to detect.

Vibratory equipment has been widely used and consists of applying a sinusoidal force of varying frequencies to the pavement and then examining the characteristics of the resulting signal. A force generator typically creates the input, and the output is received by a geophone. This method is primarily used to determine the dynamic moduli of the various pavement layers, however, a sharp change or discontinuity in the output is assumed to indicate the presence of a void (Torres and McCullough, 1983).

Similar to this is Testconsult CEBTP Ltd.'s Transient Dynamic Response method (Uddin et al., 1987). This method, also known as the Impulse-Response method, was originally utilized for integrity testing of drilled shafts (Olson et al., 1990). The method consists of using a small hammer to strike a load cell on the pavement surface. The generated signals are then received by a geophone. The analysis of the frequency response provides a large amount of information about the pavement including the degree of support provided by the base layer. From this analysis, those areas with a loss of support obviously contain a void in the base layer (Uddin et al., 1987).

2.2.4 Ground Penetrating Radar

One of the most promising methods for void detection seems to be ground penetrating radar (GPR). Typical GPR units are shown in Figure 2.1. GPR has been used extensively to identify a variety of subsurface structures such as voids, tunnels, and buried pipes (Uddin et al., 1987 and Geophysical Survey Systems, Inc., 1989). There is a variety of ground penetrating radar systems, including hand-pulled and van-mounted units. In addition, these units have either contact or non-contact transducers (i.e. the combined transmitter and receiver) which affect the testing speed (Uddin et al., 1987).

Ground penetrating radar is based on the behavior of electromagnetic energy as it pertains to changes in dielectric

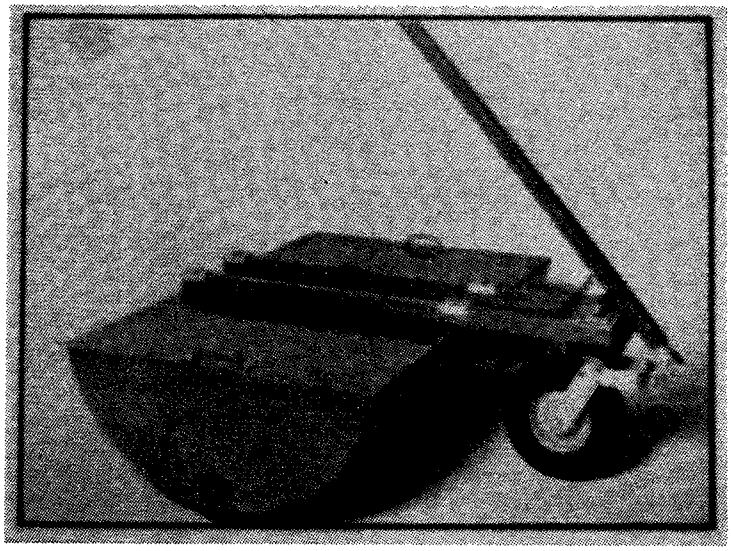

A. Geophysical Survey Systems, Inc. Model 3112 (Center Frequency = 80 MHz)

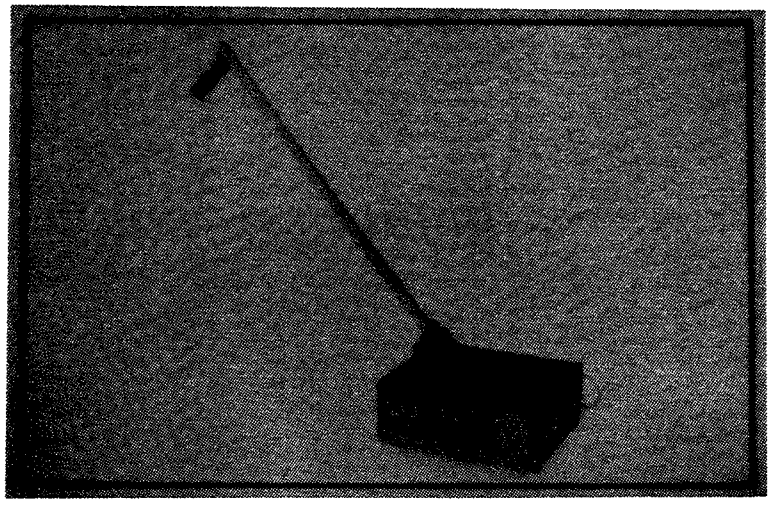

B. Geophysical Survey Systems, Inc. Model 3102 (Center Frequency = 500 MHz)

Figure 2.1: Typical Ground Penetrating Radar (GPR) Units (Geophysical Survey Systems, Inc., 1989)

properties within a pavement system (Clemena et al., 1986, Ransom and Kunz, 1986, and Uddin et al., 1987). A short pulse of high frequency energy is directed into the pavement by the transmitter. As the electromagnetic energy encounters a change in the dielectric properties at each material boundary, a portion of the energy is reflected back to the receiver where it is amplified. The amplified signal is then recorded on both magnetic tape and a chart recorder (Holt and Eales, 1987). This reflection-penetration process continues until all of the energy has dissipated. If a void is encountered, an extra reflection is created as shown in Figures 2.2 and 2.3 (Clemena et al., 1986, and Ransom and Kunz, 1986).

The resolution of GPR systems is a function of the signal frequency and bandwidth. It should be noted that this does not consider the effect of soil properties in the base and subgrade. Low frequencies and narrow bandwidths have deep penetration with lower resolution whereas high frequencies and wide bandwidths have shallow penetration with higher resolution. Therefore, to detect small defects, such as voids, high-frequency radar units are used (Cantor, 1984). It should be noted that the presence of asphaltic overlays has little impact on the ability of ground penetrating radar to detect voids. Overlays merely create an extra interface which shows up on the output profile (Clemena et al., 1986).

The accuracy of GPR can still be less than desirable. Clemena et al. (1986) reported ground penetrating radar was able to

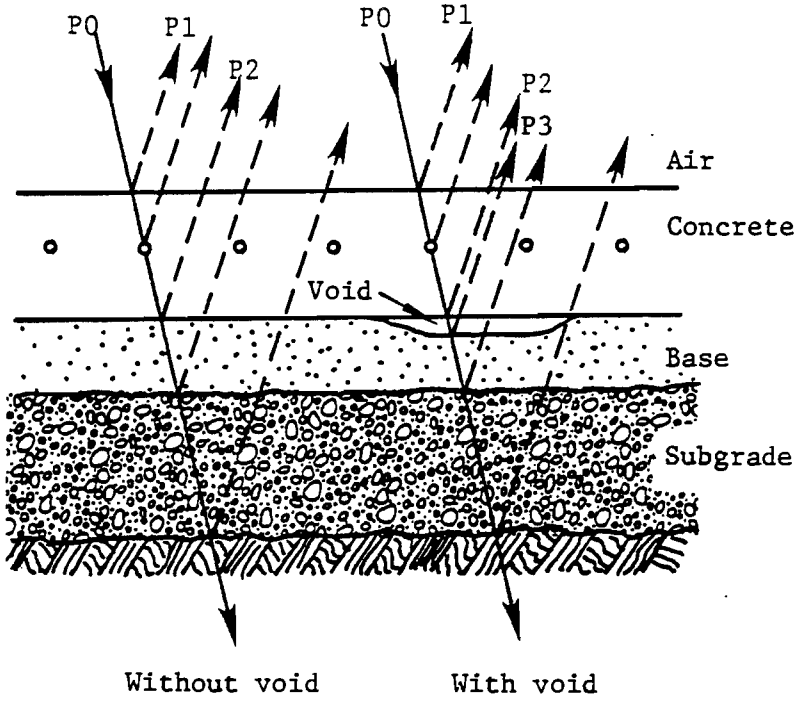

Figure 2.2: Propogation of Electromagnetic Energy Through a Concrete Pavement, Without and With a Void Underneath the Concrete Slab (after Clemena et. al., 1986)

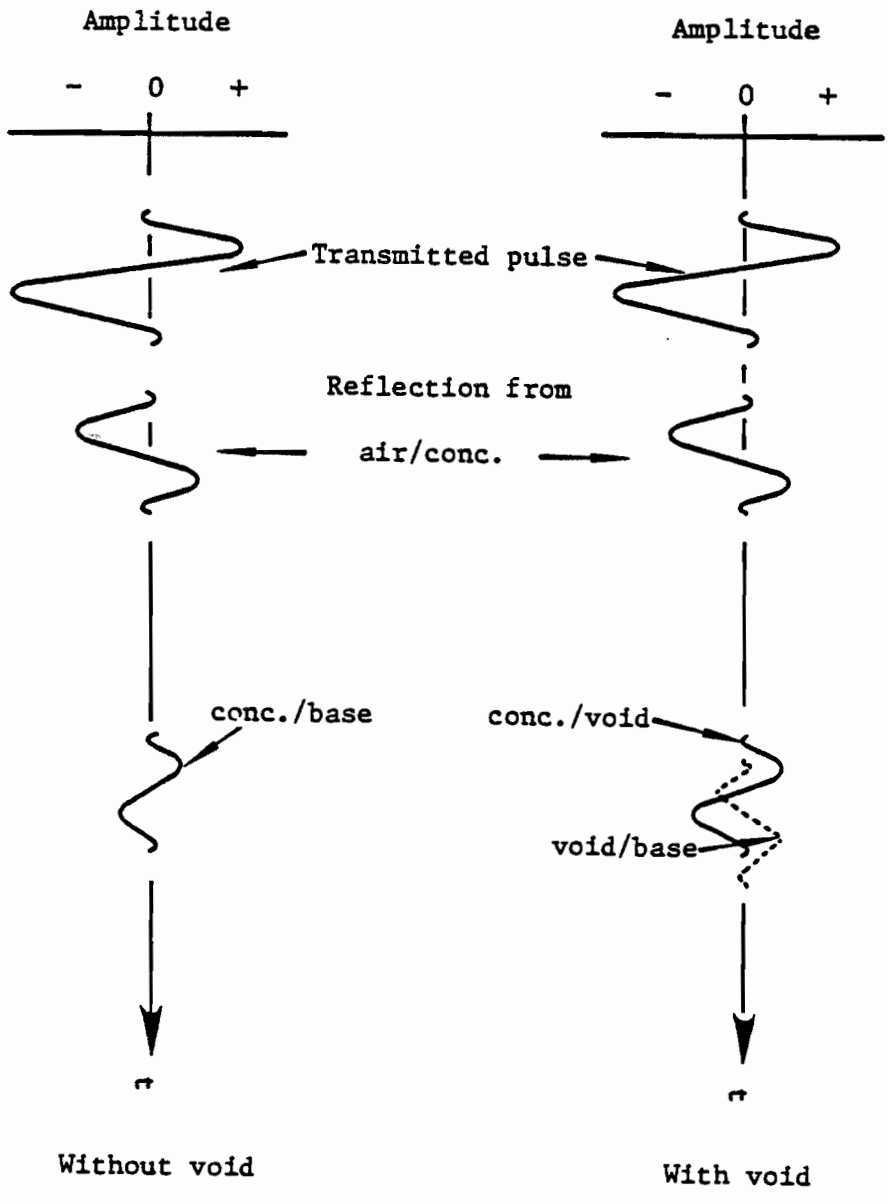

Figure 2.3: Electromagnetic Energy Reflection Profile for Concrete Pavement, Without and With a Void (after Clemena et. al., 1986).

detect voids, greater than 0.125 in. (3.175 mm) and generally less than 12 in. (304.8 mm) thick, 90 percent of the time. For voids less than 0.125 in. (3.175 mm) thick, GPR was only 54 percent accurate. This translates into an overall effectiveness of 68 percent. Clemena et al. (1986) also reported that this deficiency could possibly be eliminated with further development of radar technology.

2.2.5 Other Methods

In addition to the previously mentioned methods, both infrared thermography and the radioactive tracer method are of interest in void detection. Infrared thermography is based on the theory that pavement sections above voids will exhibit a considerably different temperature than sound pavement (Torres and McCullough, 1983). An entire lane is scanned at one time with a van-mounted infrared camera. The data are recorded to produce an infrared map of the pavement. Simultaneously, a real-time video of the pavement is recorded for reference (Holt and Eales, 1987). Tests conducted at the Balcones Research Center at the University of Texas at Austin (UT) have shown infrared thermography to be effective in void detection (Torres and McCullough, 1983). It should be noted that environmental conditions can adversely affect the ability to detect a discernible temperature differential. These conditions are explained in greater detail in Section 2.3.4.

The radioactive tracer method is not a widely used method due to its complexity and potential danger. This method has been used in France for void detection with reasonable success. Water contaminated with a radioactive tracer is injected into the soil-pavement plane. The location and extent of voids are determined from the concentration of radioactively contaminated water (tracer configuration) along the soil-pavement plane (Torres and McCullough, 1983).

2.3 Delamination Detection Methods

Delaminations are basically horizontal cracks which usually occur within what is generally considered the top pavement layer of both rigid concrete pavements and flexible asphalt pavements. It should be noted that the separation of asphalt overlays from the surface is called debonding and is similar to a delamination. As stated in Chapter One, delaminations are located reasonably close to the surface (Figure 1.1). Therefore, since acoustic methods are most effective in detecting defects near the surface, the majority of delamination detection methods are acoustic methods. Other delamination detection methods include the Collograph, ground penetrating radar, and infrared thermography. These delamination detection methods are summarized in Table 2.2.

Table 2.2: Comparison of Delamination Detection Methods

Method	Vehicle Requirements	Training	Inspection Speed	Traffic Control	Independent of Bonded Overlays	Independent of Debonded Overlays
Acoustic: Sonic 0 to 20KHz	Transport Vehicle	Moderate to Extensive	Slow to Moderate	Lane Closure	Uncertain	No
Ultrasonic >20KHz	Transport Vehicle	Moderate to Extensive	Slow	Lane Closure	Yes	No
The Collograph	Transport vehicle	Moderate to Extensive	Slow to Moderate	Lane Closure	Uncertain	Uncertain
Ground Penetrating Radar	Instrumented Vehicle	Extensive	Fast	Moving lane Closure	Yes	Yes
Infrared Thermography	Instrumented Vehicle	Extensive	Fast	Moving lane Closure	Unknown	Unknown
Nuclear Techniques	Unknown	Extensive	Very Slow	Unknown	Yes	Yes

Table 2.2 (con't): Comparison of Delamination Detection Methods

Method	Field Data Processing	Office Data Processing	Data Interpretation	Non-contacting	Independent of Weather	Relative Cost
Acoustic: Sonic 0 to 20KHz	Routine	Not Required	Moderate	No	Yes	Low to Moderate
Ultrasonic >20KHz	Moderate	Routine	Difficult	No	Yes	Moderate
Collograph	Moderate	Moderate	Difficult	No	Unknown	Moderate to High
Ground Penetrating Radar	Extensive	Moderate	Very Difficult	Yes	Yes	High
Infrared Thermography	Moderate to Extensive	Routine to Moderate	Moderate	Yes	No	Moderate to High
Nuclear Techniques	Moderate to Extensive	Unknown	Moderate	Yes	Yes	High

2.3.1 Acoustic Methods

Acoustic methods can be subdivided into sonic and ultrasonic techniques. Sonic techniques involve compressive stress waves within a frequency range generally considered to be in the audible range of 0 to 20KHz. They exploit the mechanical vibrational characteristics of the pavement system. An impulse is used to excite free vibrations within the pavement system. In contrast, ultrasonic techniques involve compressive stress waves within a frequency range greater than 20KHz which is generally considered above the audible range. They use seismic wave propagation through the pavement system. Utilizing this, ultrasonic methods can either measure seismic wave velocities within the pavement or seismic energy attenuation by the pavement (Joyce, 1985).

2.3.1.1 Sonic Methods

Sonic methods are further subdivided into either manual or automatic methods depending on the operator involvement. Manual methods are simplistic but rely heavily on the operators judgement to interpret the audible characteristics of the pavement (Joyce, 1985). A variety of manual sounding devices, including hammers, iron rods, and heavy chains, are used. The operator uses one of these tools to "strike" the pavement surface at various locations. The number of locations tested depends on the desired resolution. Sound pavement

emits a "ringing" sound when struck whereas delaminated pavement has a distinctive "hollow" sound (Sansalone and Carino, 1989).

The resonance characteristics of the striking device are influential in the ability to detect delaminated areas with sonic methods. The difference between sound and delaminated concrete is hard to distinguish with highly resonant striking devices such as steel rods and claw hammers. For this reason, dragging a heavy chain across the pavement surface has been the most effective manual sounding method. However, this is still time consuming and dependent on the operators judgement, which can be adversely affected by conditions such as traffic, weather, and the presence of overlays (Ayyub and White, 1986).

Automatic sonic methods alleviate a majority of the problems associated with manual methods. The most reported automatic sonic delamination detection technique is Delamtect. Developed at Texas A&M University and shown in Figure 2.4, Delamtect is a three wheel push cart which contains a detection unit, a signal processing unit, and recording instrumentation (Joyce, 1985, and Hagen, 1984). Delamtect introduces a signal into the pavement and then evaluates the acoustic response to detect delaminations. The tapping device (source) operates at 60 Hz. To enhance the ability to detect delaminations, a bandpass filter restricts the received frequencies to between 300 and 1200 Hz. In addition, the signal is gated, thereby receiving only the first 3 milliseconds of the

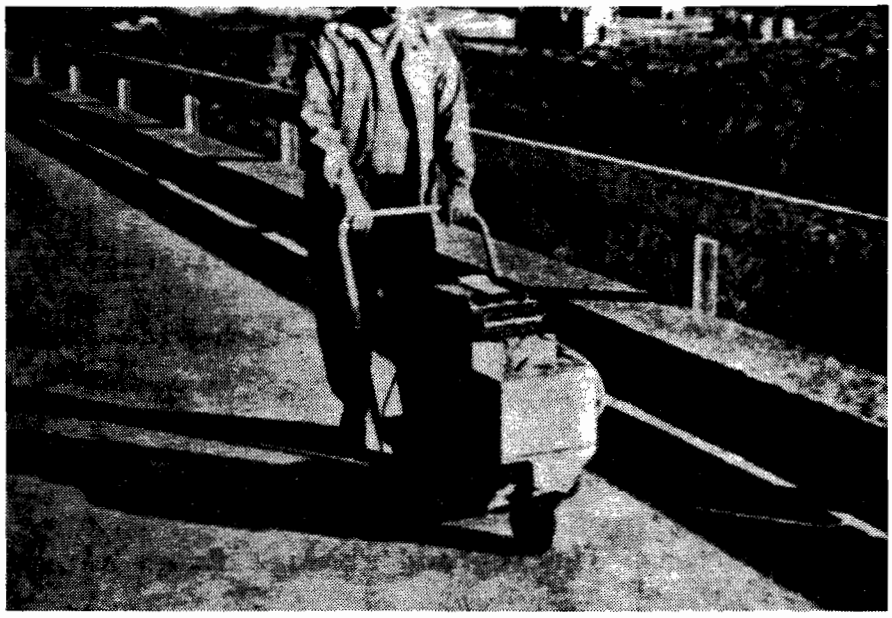

A: Delamtect in Operation

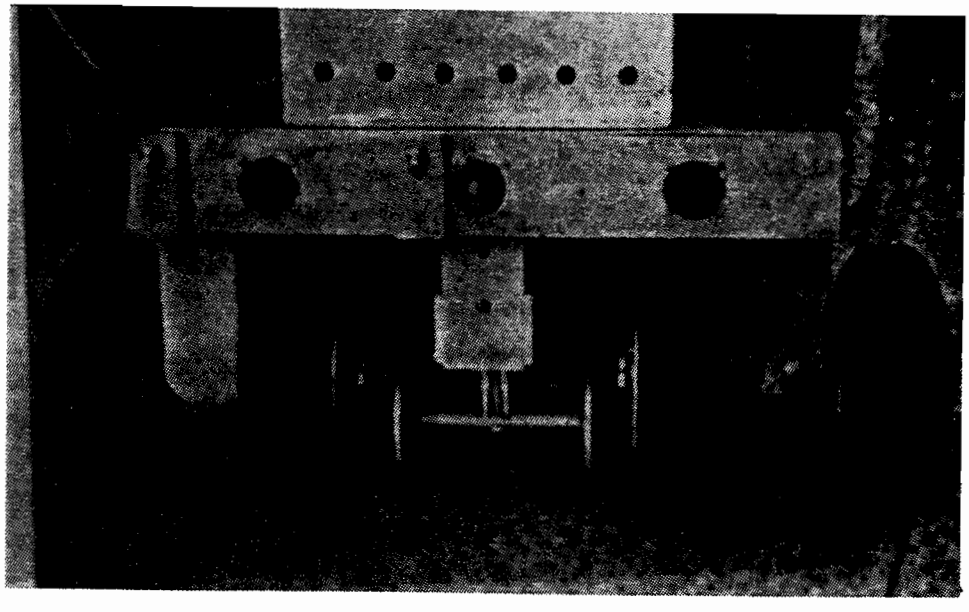

B: Rear View of Delamtect

Figure 2.4: Delamtect Delamination Detection Unit (Moore et. al., 1970)

signal after each tap (Moore et al., 1970). The signal is then conditioned using a DC rectifier, and a voltage output is achieved with which delaminations can be identified (Ayyub and White, 1986). A quick examination of the specifications leads to some uncertainties. It appears the maximum number of cycles that are received, due to the gating, is 3.6 at 1200 Hz. If the intention is to achieve a resonance within the pavement for the delaminated areas, it seems doubtful that this is achieved in so few cycles. Nevertheless, Delamtect appears to be effective in delamination detection (Moore et al., 1970). By automating the procedure and removing the subjectivity, Delamtect is obviously more effective than the manual sonic methods in detecting delaminations. However, Joyce (1985) reported Delamtect has a tendency to miss small delaminations less than 4 in. (101.6 mm) in length, is time consuming, and requires lane closures. All of these characteristics make Delamtect less appealing as a delamination detection method.

2.3.1.2 Ultrasonic Methods

Ultrasonic methods are based on the customization of geophysical techniques to pavement analysis applications. More specifically, ultrasonics use either reflection or refraction surveying concepts to detect delaminations. Two methods currently reported are the impact-echo and microseismic refraction methods (Ayyub and White, 1986, and Sansalone and Carino, 1989).

The principles of reflection surveying form the foundation of impact-echo testing. An impact on the free surface introduces a transient stress pulse into the pavement. This energy propagates as compressional (P), shear (S), and Rayleigh (R) waves. Among these, the P-wave has the greatest velocity followed by the S-wave. Both P- and S-waves are body waves and, thus, propagate into the pavement whereas Rayleigh waves propagate along the pavement surface. Body waves travel into the pavement until they encounter a contrasting impedance (such as an interface between materials) where they are reflected back to the receiver located at the surface next to the impact location. At locations close to the impact, P-waves produce larger vertical displacements than S-waves. Therefore, the P-wave reflection is the largest amplitude measured. Using the P-wave velocity (V_p) and the frequency of P-wave reflections (f_p), the depth (H) to a reflective interface is calculated as:

$$H = \frac{Vp}{2fp} \tag{2.1}$$

Equation 2.1 is only valid for reflections received close to the impact location where the travel path is assumed to be twice the depth to the reflective interface (Sansalone and Carino, 1989).

A typical impact-echo result and sample calculation are illustrated in Figure 2.5. This method involves performing a Fast

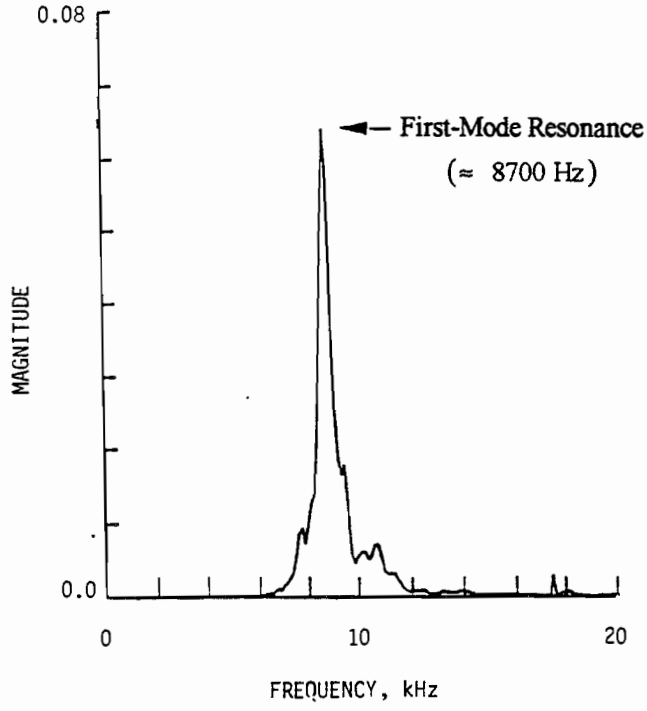

A. Typical Impact-Echo Measurement on a Concrete Slab (Nazarian and Baker, 1992)

Measured Compression Wave Velocity = 12,500 ft/sec

Resonant (Return) Frequency = 8700 Hz (from Figure 2.5A)

Nominal Slab Thickness = 8.0 inches

$$H = \frac{V_p}{2f} \qquad H = \frac{12500 \text{ ft/sec}}{2(8700 \text{ Hz})} \qquad H = .718 \text{ ft (8.62 in.)}$$

B. Sample Calculation Based on Record in Figure 2.5A (Nazarian, 1992)

Figure 2.5: Typical Impact-Echo Measurement and the Corresponding Sample Calculation

Fourier Transform on the time-domain displacement waveform to determine the first-mode resonant frequency. This frequency corresponds to f_p in Equation 2.1 which is based on resonating a "free-free" system. As can be seen in Figure 2.5b, one needs to estimate the P-wave velocity before the thickness can be calculated. In the example, Professor Nazarian was contacted and he indicated the measurement shown in Figure 2.5a was performed on a very young concrete which had an estimated V_p of about 12,500 ft/sec (3812.5 m/sec). Therefore, a thickness of 8.6in. (21.8 cm) was calculated. This thickness compares with the cast thickness of 8.0 in. (20.3 cm).

Generally, if the calculated thickness is within 10 percent of the cast thickness, the slab is considered good. Values of H which are much less than the cast pavement thickness indicate a delamination. Since the results are only valid at the exact location tested, the resolution of this method is dependent on the number of locations tested. Joyce (1985) and Sansalone and Carino (1989) report the impact-echo method is an effective delamination detection technique but is time consuming and requires lane closures.

Like the impact-echo method, microseismic refraction deals with the propagation of seismic waves through the pavement. However, microseismic refraction is based on the principles of refraction surveying. A transient stress pulse is introduced into the pavement. The resulting signal is received at a receiver located a

fixed distance away from the impact. By varying this distance, a travel-time graph (Figure 2.6) is compiled which contains the arrivals of both the direct waves and the refracted waves. The point at which the refracted wave and the direct wave arrive at the same time is known as the critical point. Knowing this location and the P-wave velocities from the travel-time graph, the depth to an underlying layer can be determined. However, the microseismic refraction technique is primarily used to examine the quality of concrete by comparing the calculated P-wave velocities with the expected values for sound concrete (Ayyub and White, 1986).

Ayyub and White (1986) reported the use of microseismic refraction for delamination detection is impractical because it is time consuming, the data interpretation is difficult, and the extent of the deterioration cannot be determined. However, microseismic refraction seems to have a serious problem in delamination detection that is not reported in the literature. Microseismic refraction cannot exploit areas where a lower velocity material is beneath a higher velocity material which is generally indicative of a zone of weakness. The travel time graph for the higher velocity material will "over shadow" any lower velocity material and hence, no critical point will be visible.

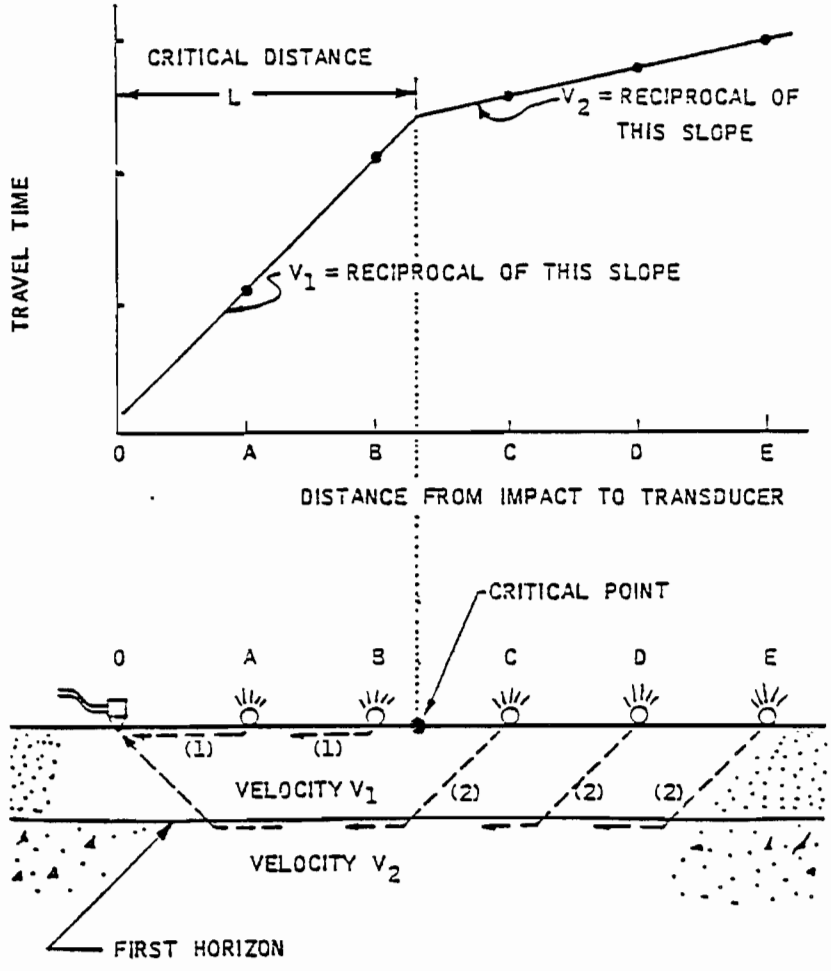

Figure 2.6: Travel Time Graph and Refracted Wave Path from Microseismic Refraction Method for Delamination Detection (after Ayyub and White, 1986).

2.3.2 Collograph

Developed in France, the Collograph is simply a small self-powered vehicle containing a rotating mass, hydrophonic receiver, and data acquisition unit. The Collograph, shown in Figure 2.7, is based on the continuous integral measurement of the dynamic deflection of a pavement system subjected to a moving vibratory load. The source is a small roller which houses a rotating mass. The rotating mass produces a force, f, expressed by:

$$f = F \cdot \sin(\omega \cdot t) + m \cdot g \qquad (2.2).$$

The weight of the mass (m·g) is 3000N (~675lb) and F is 2000N (~450lb) for the source operating at 60 Hz. This produces a force which cycles from a minimum of 1000N (~225lb) to a maximum of 5000N (~1125lb) creating large deflections in the pavement.

The deflections created by the Collograph are detected at the receiver. The receiver is a liquid filled soft rubber wheel which contains four vertically oriented hydrophones. The hydrophones produce a voltage output corresponding to the vertical displacement. The voltage output is displayed on a graphic recorder which allows immediate on-site evaluation of the results. Normal pavements produce a virtually constant amplitude output whereas delaminations produce a highly modulated amplitude output as shown in Figure 2.8 (Le Laboratoire Central des Ponts et Chaussees, 1983).

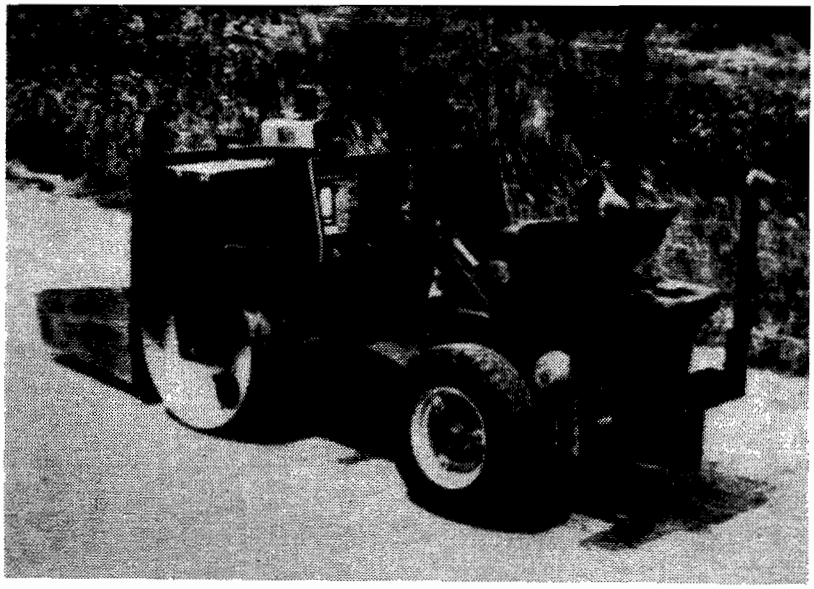

Figure 2.7: The Collograph (Le Laboratoire Central des Ponts et Chaussees, 1983).

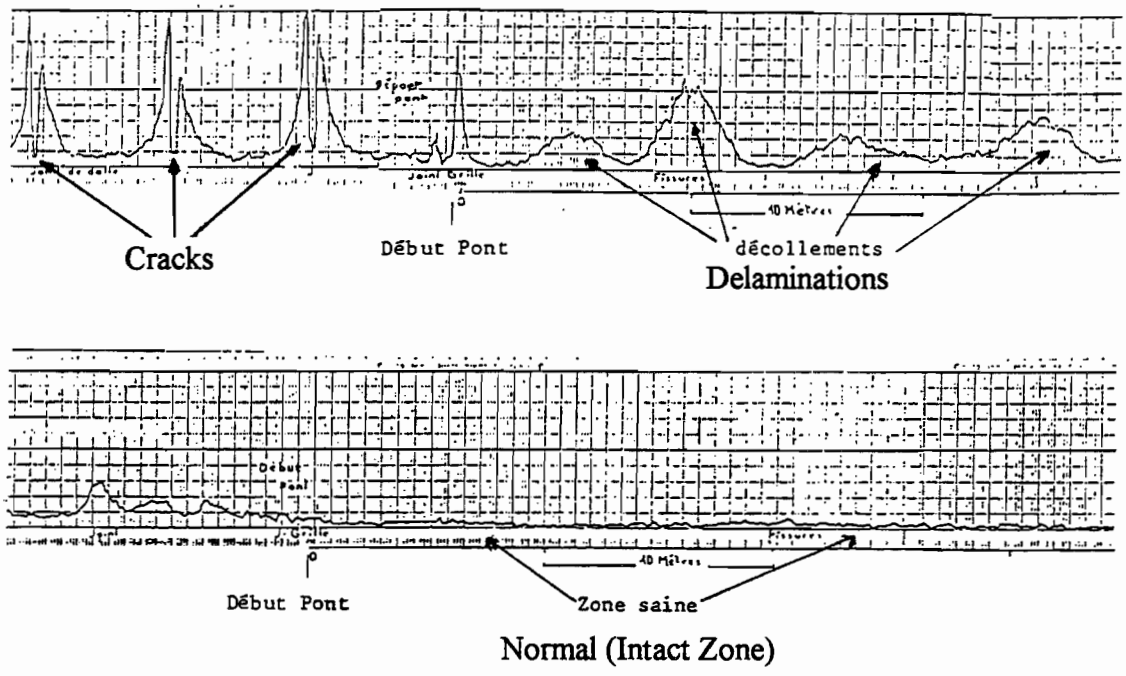

Figure 2.8: Typical Output from the Collograph Showing Delaminations and Cracks (Le Laboratoire Central des Ponts et Chaussees, 1983)

Delamination detection appears very promising with the Collograph. However, the performance is not well documented in the literature and, therefore, the overall reliability is unknown.

2.3.3 Ground Penetrating Radar

As mentioned in Section 2.2.4 on void detection, the principle of ground penetrating radar is based on reflections of high-frequency electromagnetic energy caused by differences in the dielectric properties of the pavement system being investigated. These reflections occur at all dielectric discontinuities such as material changes and defects. Therefore, ground penetrating radar can be applied to delamination detection. However, due to the usually smaller size of delaminations, the radar system must have a much higher degree of resolution than is acceptable for void detection (Joyce, 1987).

Currently, there are two types of radar systems used to evaluate pavements for delaminations: 1) swept frequency and 2) short-pulse radar. Swept frequency radar systems are sometimes referred to as continuous wave, frequency modulated systems. These systems have a slow speed of frequency variation and, hence, are not suitable for rapid inspection applications. Because of this, the most widely used ground penetrating radar system is the short-pulse system.

In contrast to the swept frequency radar, the short-pulse radar directs high frequency (center frequencies ranging from 80MHz to greater than 1GHz), short pulse signals into the pavement (Clemena, 1982, Joyce, 1985, and Ayyub and White, 1987). A detailed description of the principle of short pulse ground penetrating radar is presented in Section 2.2.4. GPR has a few notable qualities including the ability to measure the thickness of asphalt on an asphalt overlaid surface. In addition, GPR is virtually independent of environmental conditions. However, short-pulsed radar is adversely affected if the pavement surface is wet. Also, because of its limited testing area, ground penetrating radar requires several passes per pavement section to obtain a clear picture of the pavement and, in some cases, may still miss small delaminations (Ayyub and White, 1986).

2.3.4 Other Methods

Both infrared thermography and various nuclear techniques have been applied in the detection of delaminations. Infrared thermography is essentially the same for delamination detection and void detection. Accordingly, the thermographic images, which map temperature levels in the pavement, highlight the areas of heat concentration. These concentrations correspond to subsurface deterioration (Masliwec, 1990, Clemena and McKeel, 1977, and Hafermann, 1983). Delaminated concrete is warmer than sound

concrete under direct solar heating and is most visible generally between 10:00am and 2:00pm as shown in Figure 2.9. However, certain environmental conditions must be present to obtain a discernible temperature differential including a clear, sunny day with less than 50-60 percent broken clouds. In addition, the pavement must be dry, and the wind speed must be less than 15-20 mph (24.2-32.2 km/hr) (Ayyub and White, 1986).

As described in Section 2.2.5, an entire lane is scanned with an infrared camera. The data is recorded and an overall thermographic map is produced. Along with the infrared scan, a visible scan is performed to discriminate between temperature differences due to defects and those due to a change in the surface emissivity such as sand cover and skid marks (Joyce, 1985). In addition to delaminations, infrared thermography has the capability to detect debonded asphalt overlays (Ayyub and White, 1986).

Finally, nuclear techniques offer promise as a potential delamination detection method. Currently, only single-compton-scatter density gauges and compton-scatter tomography are specific enough to detect local hidden defects (Ayyub and White, 1986). Single-compton-scatter density gauges consist of a collimated source and detector. Only a narrow channel is irradiated and viewed. It has the potential to detect defects; however, the inspection speed is extremely slow. Compton-scatter tomography uses radiation transmission to generate a cross-sectional view. This offers the

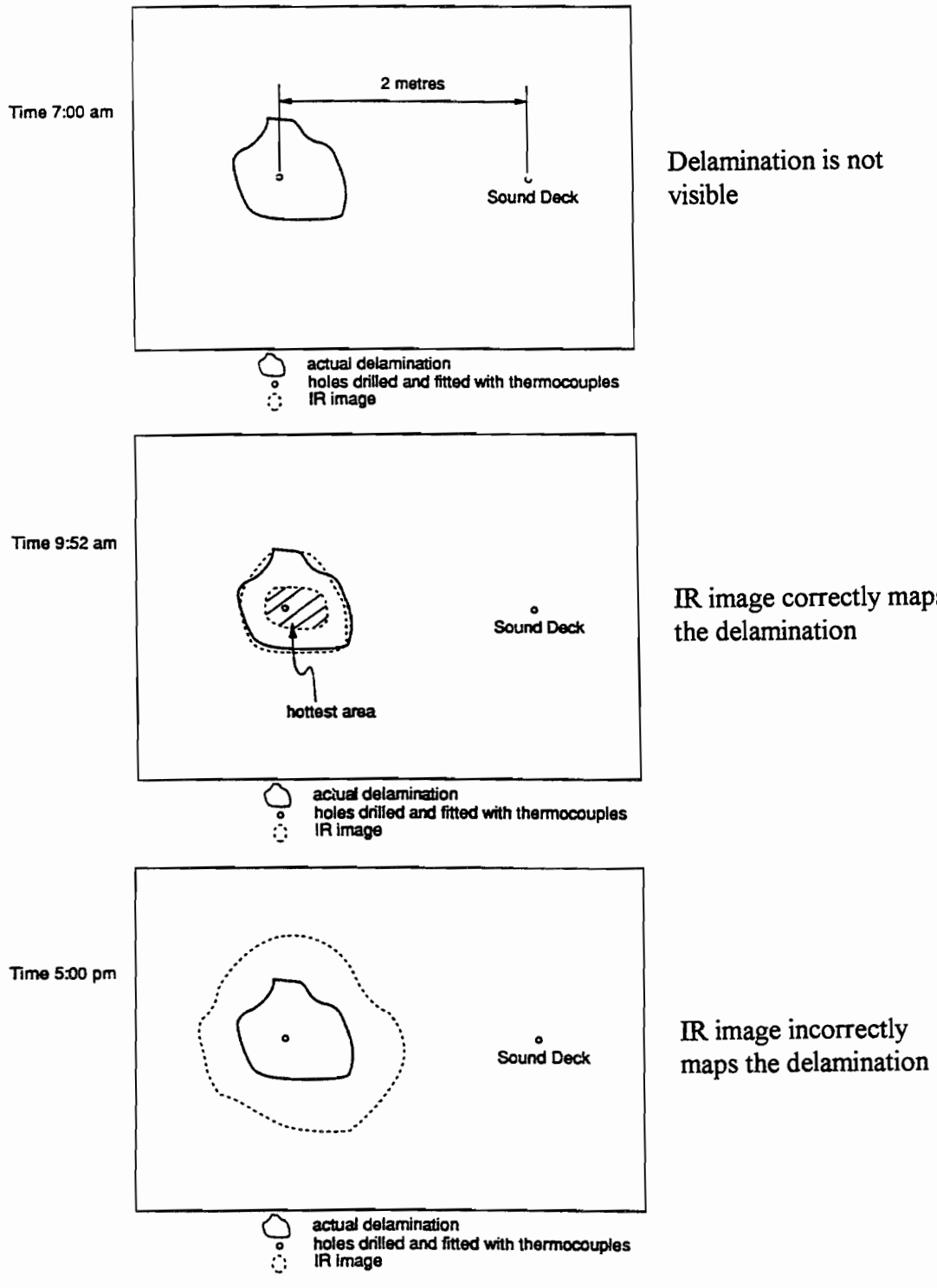

Figure 2.9: Typical Data Obtained from Infrared Thermography at Various Times in Ontario, Canada (Masliwec, 1988)

advantage of exposing all relevant details such as voids, delaminations, reinforcing bars, and aggregate distribution. Thus, nuclear technology has the potential to support the detection of delaminations in pavement systems. However, the previously mentioned nuclear techniques have not been developed sufficiently and, hence, field equipment is unavailable (Joyce, 1985).

2.4 Crack Detection Methods

Due to the nature of pavement cracking, unique possibilities are available for crack detection methods. Unlike voids and delaminations, cracks are often visible on the pavement surface. Therefore, crack detection lends itself to a variety of visual and photographic techniques. In fact, a majority of crack detection methods in use today are either visual or photographic. Other crack detection methods currently in use include slit integration and the Collograph. These methods are summarized in Table 2.3.

2.4.1 Visual Methods

Visual methods for crack detection are simple and relatively inexpensive. Many Department of Transportation (DOT) offices use the visual survey method which involves an on-site visual analysis to determine the extent of pavement cracking. During this process, the pavement cracks are individually categorized according to their width and pattern (Hintz et al., 1988). Examples of the Florida

Table 2.3: Comparison of Crack Detection Methods

Method	Vehicle Requirements	Training	Inspection Speed	Traffic Control	Independent of Bonded Overlays	Independent of Debonded Overlays
Visual Methods	Transport Vehicle	Routine to Moderate	Slow	Lane Closure	Yes	Yes
Photologging	Instrumented Vehicle	Moderate	Fast	Moving Lane Closure	Yes	Yes
Slit Integration	Instrumented Vehicle	Moderate to Extensive	Fast	Moving Lane Closure	Yes	Yes
Collograph	Transport Vehicle	Moderate to Extensive	Slow to Moderate	Lane Closure	Uncertain	Uncertain

Table 2.3 (con't): Comparison of Crack Detection Methods

Method	Field Data Processing	Office Data Processing	Data Interpretation	Non-contacting	Independent of Weather	Relative Cost
Visual Methods	Routine	Routine to Moderate	Basic	Yes	No	Low
Photologging	Routine to Moderate	Moderate to Extensive	Basic	Yes	No	Moderate to High
Slit Integration	Moderate	Moderate	Moderate	Yes	No	High
Collograph	Moderate	Routine to Moderate	Moderate	No	Unknown	Moderate to High

DOT's categorizing system are shown in Figures 2.10 and 2.11. With the information from the visual survey, the type and extent of cracking is produced. These results are then used to analyze the pavement condition. To achieve consistent results, visual survey personnel must undergo extensive training (Hintz et al., 1988).

In addition to the visual survey method, many DOTs use the Present Serviceability Index (PSI)[1] to analyze the pavement condition. Several factors contribute to this index including the square footage of cracking per 1000 ft^2 (92.9m^2) of pavement. This factor is obtained by visual analysis (Cable and Dankbar, 1990). Therefore, the PSI gives an indirect measurement of pavement cracking through visual analysis.

Visual methods for crack detection are advantageous for their simplicity and low equipment cost. However, there are several disadvantages associated with these methods. The output from a visual method does not contain a permanent record of the pavement surface. This would be useful for a more detailed or future evaluation as well as to document long-term pavement performance. In addition, visual methods cannot detect cracks that do not reach the surface. Finally, regardless of the high level of personnel

[1]For a detailed explanation of the Present Serviceability Index, the reader is referred to Cable and Dankbar, 1990 or Yoder and Witczak, 1975.

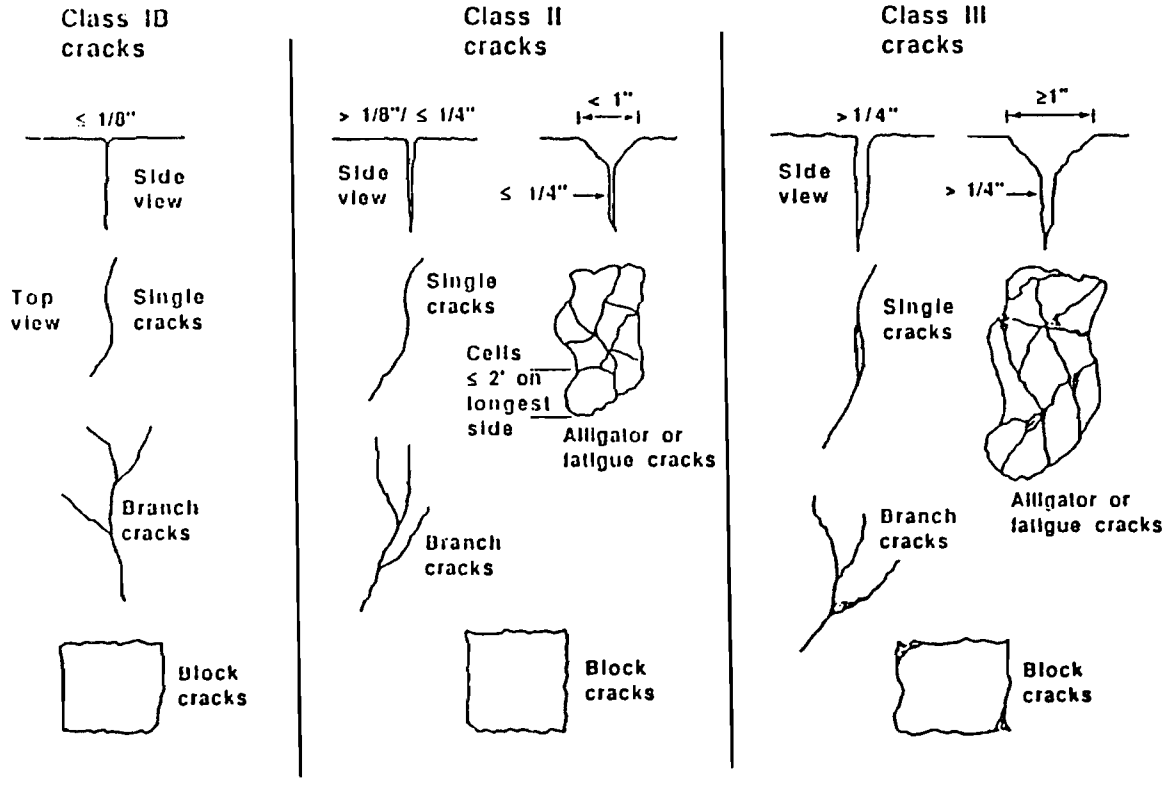

Figure 2.10: Crack Classifications for the Florida Department of Transportation (Hintz et. al., 1988)

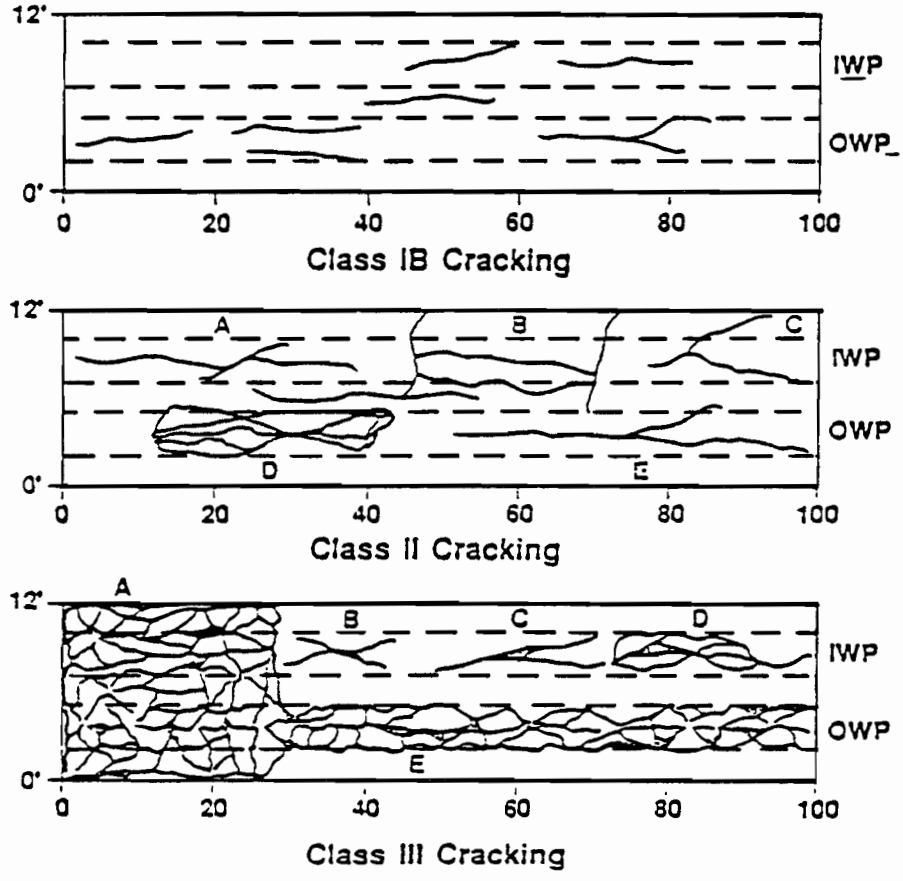

Figure 2.11: Crack Classification Patterns for the Florida Department of Transportation (Hintz et. al., 1988)

training, visual methods still involve a high level of human subjectiveness.

2.4.2 Photologging Techniques

Several crack detection methods utilize a process known as photologging. Photologging simply refers to the use of photographs, filmed from a moving vehicle, for pavement analysis (Hintz et al., 1988). All photologging techniques involve a similar type of data acquisition. A large vehicle, usually a van, houses the system. One or more cameras are mounted on the vehicle so that the pavement surface may be viewed with little, if any, distortion. The actual placement of the cameras varies with each method. The cameras are connected to an operator-controlled recording system inside the vehicle (Hintz et al., 1988 and Cable and Dankbar, 1990) Therefore, the camera can film the pavement surface while the vehicle is in motion. Although data acquisition is similar among all photologging techniques, the level of data processing is quite varied. The French developed GERPHO (Group for the Examination of Roads by Photography) and the Japanese developed PASCO. Both systems involve very simple processing techniques. Once the pavement is filmed, the tape is visually analyzed in the office where the percentage of cracking and,hence, the pavement condition is determined (Hintz et al., 1988, Cable and Dankbar, 1990, and Christory, 1981).

In an effort to improve processing and increase accuracy in photologging, Hintz et al. (1988) developed a computerized processing procedure for the Florida DOT. From the pavement film, each crack is digitized, using an analytical stereoplotter, for computer analysis. Taking this process a step further, Pavdex Inc. developed the PAS I road survey system. In addition to computer processing in the office, the Pavdex system partially evaluates the pavement during the photologging process. The testing vehicle contains a viewing monitor which displays the pavement as it is being filmed. From here, a trained observer identifies the visible distress types, severity, and amount and enters this information into an on board computer. The computer then collates the information and stores it for future evaluation (Cable and Dankbar, 1990).

There are several advantages to the fore-mentioned photologging techniques. Photologging produces a permanent record of the pavement which may be used for future reference and analysis. Because of this, the human subjectivity is reduced. In addition, a few of the methods involve computer analysis which increases the reliability. However, photologging involves high equipment costs and is only applicable to surface cracks. Lastly, the results from the various photologging techniques are not readily available since the data processing is done away from the testing site.

2.4.3 Slit Integration

In an effort to eliminate human subjectivity and develop a real-time system, Mendelsohn (1988) proposed the use of slit integration for crack detection. This method detects transverse and longitudinal surface cracks using two separate sensors mounted to a testing vehicle. Other crack orientations are detected by their longitudinal and transverse components. Each sensor is a lightmeter, with a narrow field of view, oriented in either the longitudinal or transverse directions. Figures 2.12 and 2.13 illustrate this principle. As the vehicle drives down a road, the sensors are constantly averaging the reflectivity of the pavement. When a sensor passes over a crack, the signal output dips. To eliminate false signals, the slit integration system uses cross correlation to verify each signal drop encountered. The final output consists of crack density indices for the tested pavement sections. The vehicle is capable of testing at speeds between 20 and 60 mph (32.2 and 96.6 km/hr). Since this system performs all data reduction in real-time, the crack density indices are immediately available as the vehicle passes over each pavement section (Mendelsohn, 1988)

In addition to the many advantages of the slit integration system, there are a few disadvantages which should be noted. This system is only capable of detecting surface cracks. Also, cracks less than 0.125 in. (3.175mm) in width, cracks that are light in color, and cracks which are angled +/- 20° from either the longitudinal or

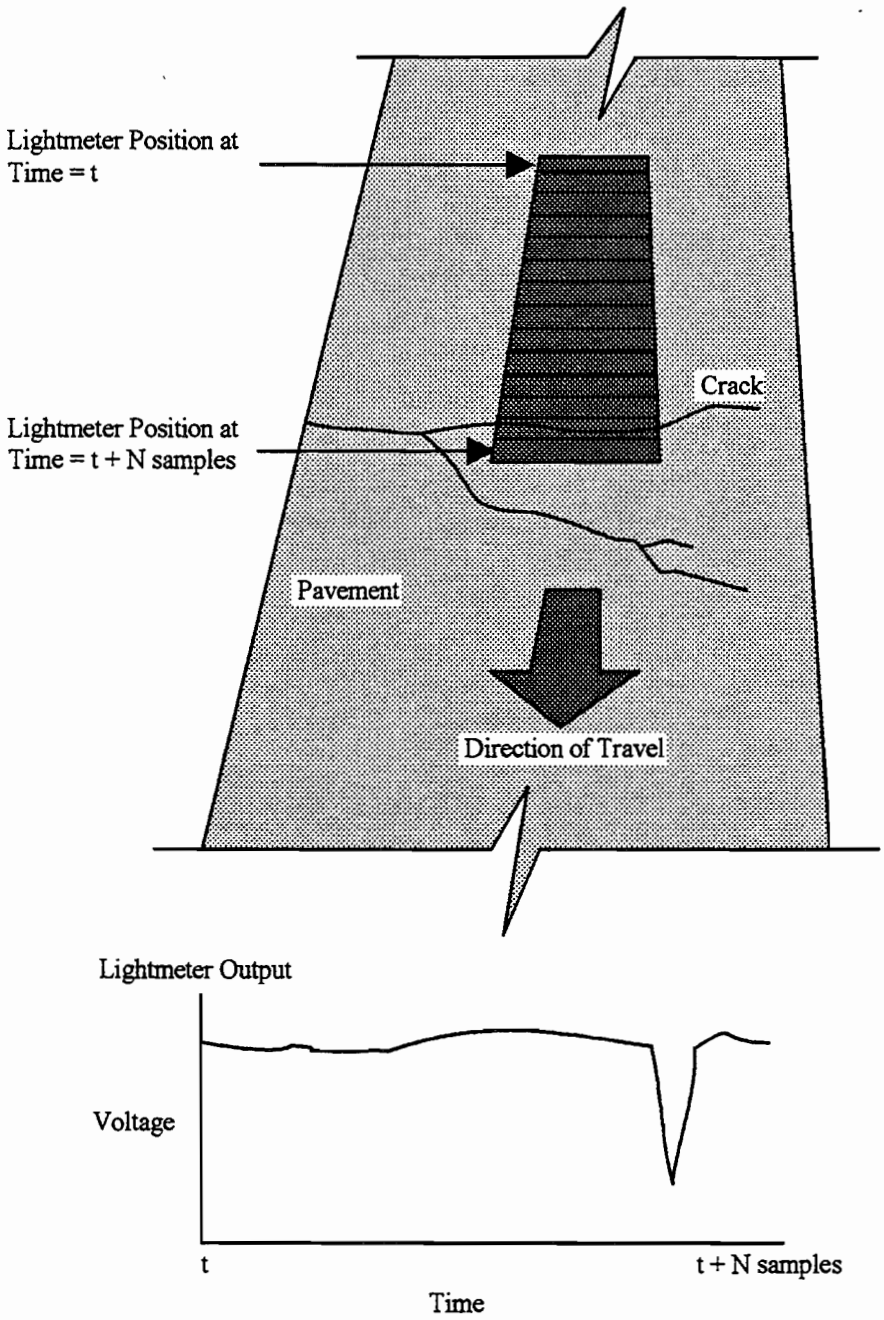

Figure 2.12: Principle of Slit Integration for Transverse Crack Detection (after Mendelson, 1988)

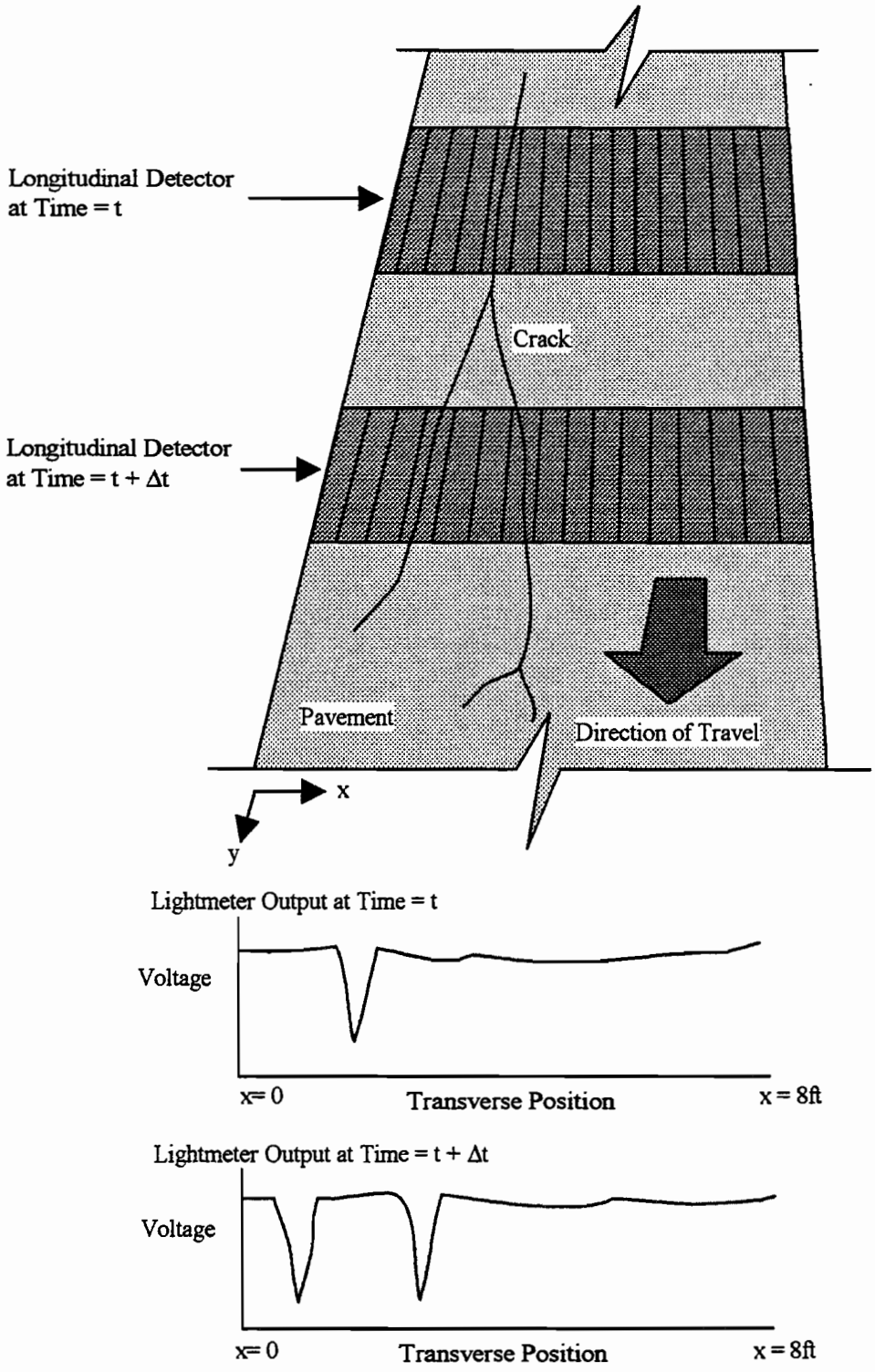

Figure 2.13: Principle of Slit Integration for Longitudinal Crack Detection (after Mendelson, 1988)

transverse axes are generally not detectable. Lastly, this system was designed to measure crack density and, therefore, does not indicate the severity or location of each crack (Mendelson, 1988).

2.4.4 Collograph

As described in Section 2.3.2, the Collograph is a dynamic deflection measurement system. Through the use of a rotating mass source and hydrophonic receiver array, the Collograph is able to detect pavement layer anomalies. The principle of operation for crack detection is identical to that for delamination detection as described in Section 2.3.2. The major advantage of the Collograph is its ability to detect subsurface as well as surface cracks. The graphic recorder output, called a collogram, has a distinct "signature" for each anomaly. For surface cracks, the output has two peaks separated by a minimum. The minimum corresponds to the point at which the source and receiver are on opposite sides of the crack. For partial cracks, that is subsurface cracks that do not penetrate the surface, the output has one sharp peak (Le Laboratoire Central des Ponts et Chaussees, 1983). These signature are illustrated in Figure 2.14 and actual data are shown in Figure 2.8. The Collograph is a very promising method for crack detection, however, as previously mentioned, this system is not well documented in the literature and, therefore, the actual performance and reliability are unknown.

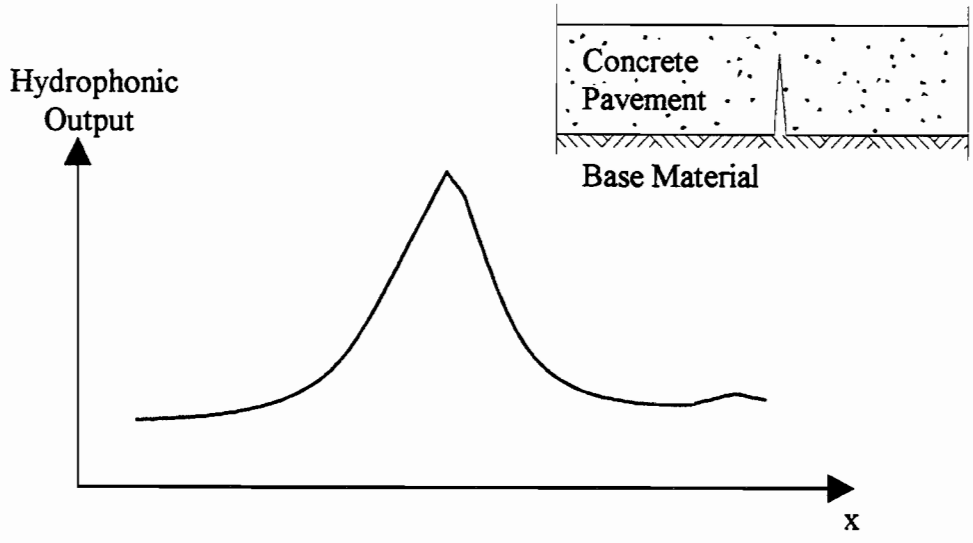

A. Signature for Partial Crack

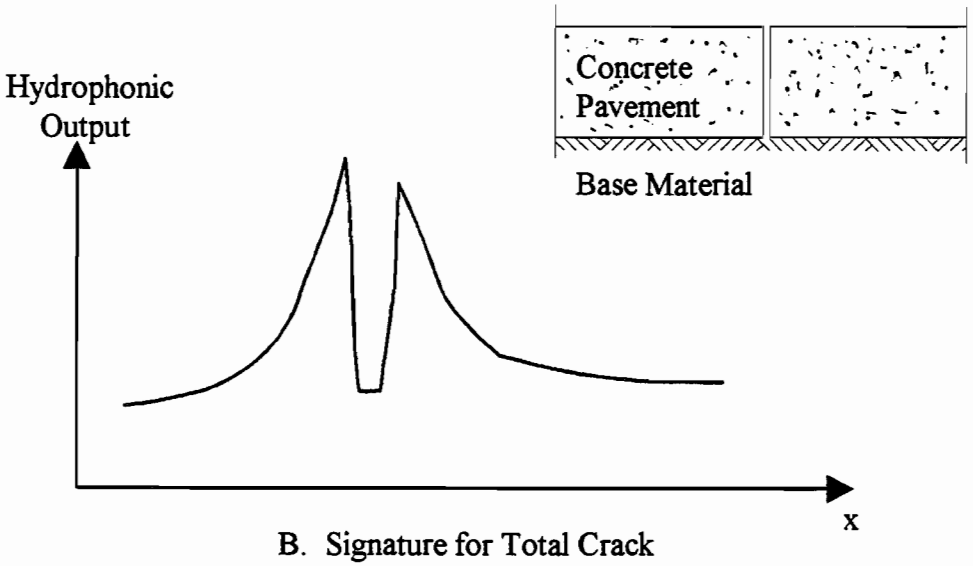

B. Signature for Total Crack

Figure 2.14: Collograph "Signatures" for Various Crack Configurations (after Le Laboratoire Central des Ponts et Chaussees, 1983)

2.4.5 Other Methods

Several other techniques have been explored as possibilities for use in pavement crack detection. However, these methods have had little, if any, success with respect to pavement testing applications. They include holographic (Luxmoore, 1973), laser (Payne and Walker, 1988), and x-ray (Whittmann, 1983) techniques.

2.5 Summary

The presence of irregularities, such as cracks, voids, and delaminations, within rigid concrete pavement layers adversely affects the overall pavement performance. Therefore, there is a significant need to develop fast, economical, and conclusive methods to detect irregularities. Past research has yielded a wide variety of detection methods which have been applied with varying degrees of sucess for each of the three anomalies.

Deflection-based methods are traditionally popular and effective for void detection and most state DOT's have one or more Falling Weight Deflectometers. In addition, ground penetrating radar (GPR) is very effective for void detection and also provides adequate delamination detection. However, GPR involves high equipment costs and extensive operator training. Visual and photographic methods are extensively used for crack detection but are limited to superficial pavement cracking and can be influenced by

human subjectivity. The Collograph is the only researched method which seems to have the ability to detect cracks, voids, and delaminations. However, the system performance has not been adequately documented and, thus, the reliability and accuracy are unknown.

Chapter Three
Design and Development of Prototypes 1 and 2

3.1 Introduction

A fundamental concept of the measurement scheme is necessary to design and develop a prototype vehicle capable of detecting cracks, voids, and delaminations in a rigid pavement system. Design stipulations suggested that the solution should be capable of taking both stationary and mobile measurements, easy to operate, simplistic in data interpretation, fairly inexpensive, and consist of "off-the-shelf" equipment as much as possible.

The original design concept, shown in Figure 3.1, consisted of a "source wheel" and a "receiving wheel" moving along the pavement surface. The "source wheel" transfers a constant controlled signal from a source to the pavement. The signal propagates through the pavement layers and is altered according to their structural characteristics. The receiving wheel transfers the altered signal to a receiver where the data can be processed and interpreted.

The transition from concept to prototype is started in this chapter. Design considerations, such as equipment characteristics, are discussed to establish the foundation and framework for the design process. In an effort to establish optimum testing parameters,

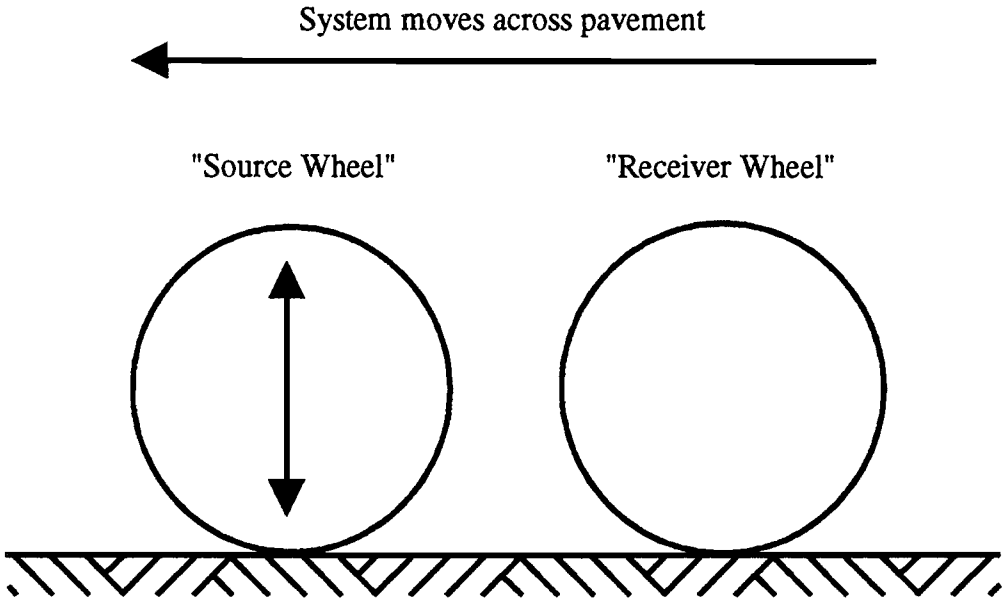

NOTE: Drawing not to scale

Figure 3.1: Original Design Concept

both equipment noise and applicable road noise are included in this discussion. Finally, the first and second attempts at prototype development are examined, with an emphasis on laboratory testing to justify the evolution.

3.2 Design Considerations

Initial stages of the design process required that certain fundamental design parameters be established. For instance, a minimum response level and a testing frequency or frequency range had to be established. Several factors, such as available sources, available receivers, and road and equipment noise levels, influence these parameters. To start this work, potential sources were investigated. Likewise, various receivers were then examined. Lastly, the effect of equipment noise and road noise were considered.

3.2.1 Sources

The signal used to analyze pavement layers is created by applying a dynamic vertical load to the pavement surface via the "source wheel". The dynamic vertical load may be generated by a variety of sources. Sinusoidal and impulsive sources are both common for pavement applications.

Sinusoidal sources generate energy at a constant amplitude either for a specific frequency or over a "sweep" of one frequency after another. This energy is usually created by either an electromagnetic shaker (for operation from low to moderately high frequencies, approximately 5 to 5000 Hz) or a piezoelectric shaker (for operation from medium to ultrasonic frequencies, approximately 1000 to 50,000 Hz). Electromagnetic shakers operate by using a permanent magnetic field to drive a coil. The resulting dynamic electromagnetic coil field actuates the "moving element". The force produced is proportional to the input current. The electromagnetic shaker used at the University of Texas at Austin for this research was a M.B. Dynamics PM100 Vibration Exciter. The PM100 is driven by an M.B. Dynamics SS530 amplifier and produces a peak force output of 100 pounds (444.8 N) with forced air cooling and 50 pounds (222.4 N) with natural convection cooling. In addition, the shaker system is controlled with a function generator or a waveform analyzer. The electromagnetic shaker and amplifier are shown in Figure 3.2.

In contrast, piezoelectric shakers utilize piezoelectric crystals which expand or contract proportionally to an applied voltage. Because the displacements are very small, large forces are obtained at high frequencies by using multiple crystals and high drive voltages. The piezoelectric shaker used at the University of Texas at

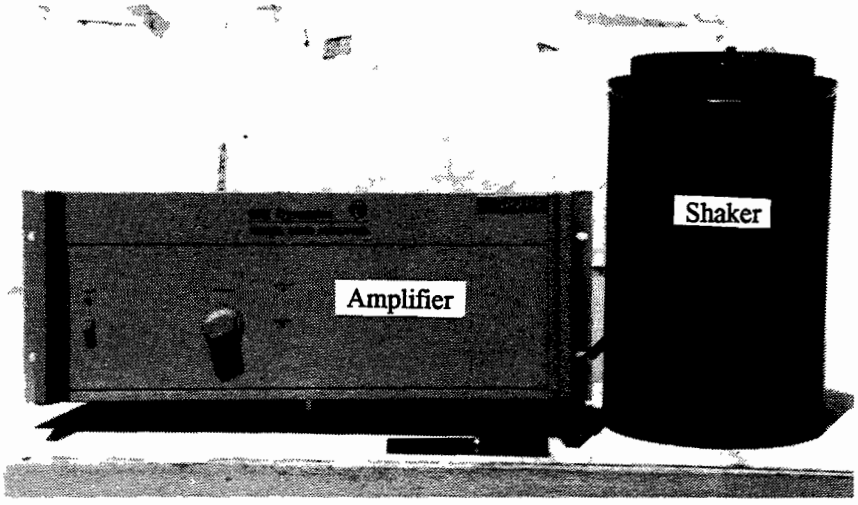

Note: Function generator used to control system not shown

Figure 3.2: M.B. Dynamics Electromagnetic Shaker System

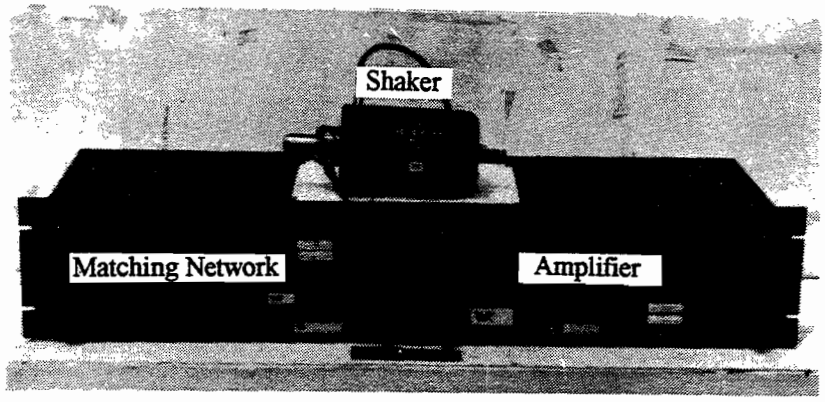

Note: Function generator used to control system not shown

Figure 3.3: Wilcoxon Piezoelectric Shaker System

Austin for this research was a Wilcoxon model F8 Piezoelectric Vibration Generator. The model F8 is powered by a Wilcoxon model PA8 Power Amplifier and a Wilcoxon model N8H Matching Network. As with the electromagnetic shaker system, the piezoelectric shaker system is controlled by a function generator or a waveform analyzer. The piezoelectric shaker, amplifier, and matching network are shown in Figure 3.3. The peak blocked force output for this system is approximately 2000 pounds (8896.4 N).

Impulsive sources generate a burst of energy over a wide range of frequencies. Generally, neither the exact frequency range nor the amplitude are controllable. A typical impulsive source is an instrumented hammer. Since not consistent with the design concept, an impulsive source was only used to simulate other methods of pavement analysis, such as the impact-echo method (Sansalone and Carino, 1989), as discussed in Chapter 2. The impulsive sources used at the University of Texas at Austin for this research were PCB Piezotronics Series 086B01 and 086B20 Modally Tuned Impact Hammers. These hammers, shown in Figure 3.4, are powered by PCB Piezotronics Model 480D06 Power Unit/Signal Amplifiers.

Each of the possible testing sources were evaluated to establish their response over a wide range of frequencies. The source/receiver configuration for these tests, shown in Figure 3.5b, is modeled directly after the original design concept. The frequency

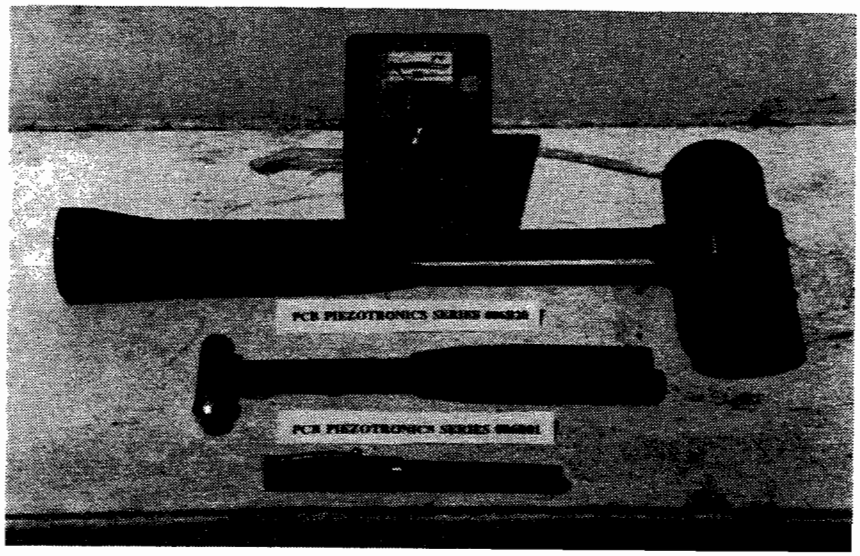

Figure 3.4: PCB Piezotronics Modally Tuned Impact Hammers

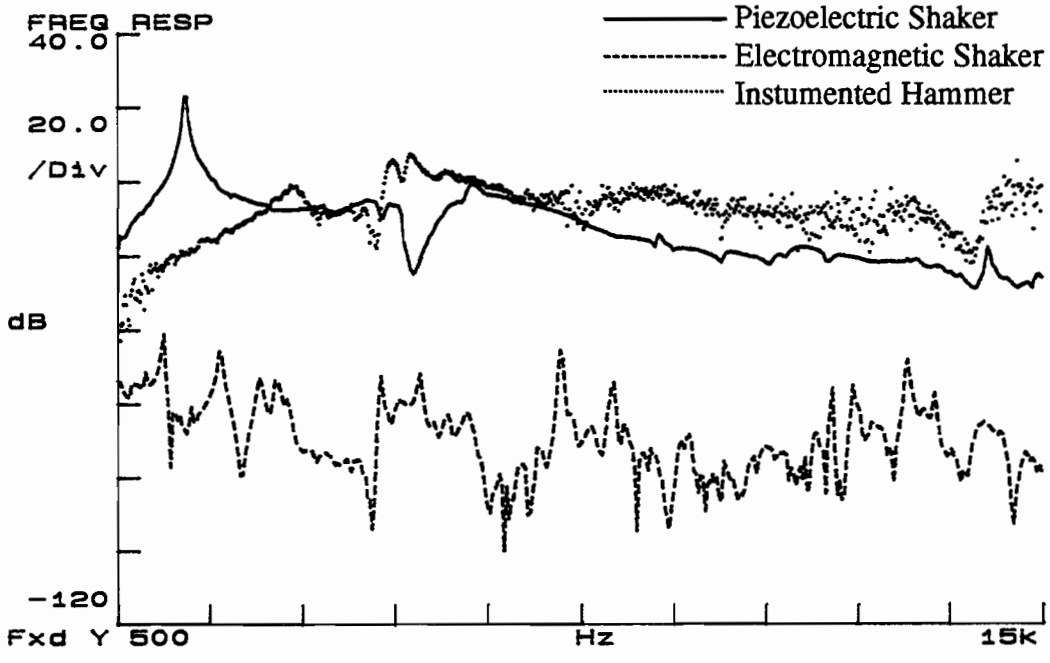

A. Frequency Response Comparisons of Possible Sources

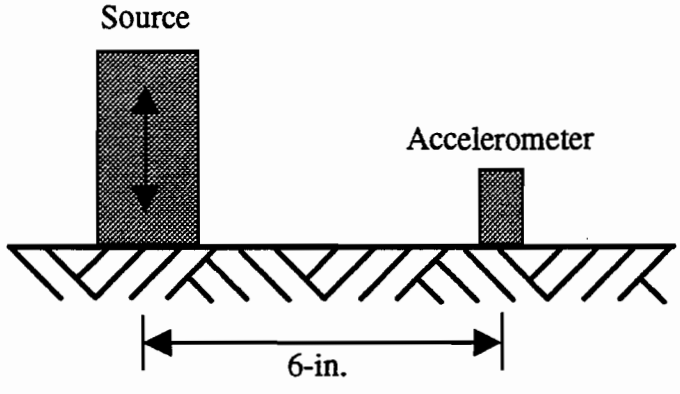

NOTE: Drawing not to scale

B. Source/Receiver Configuration for Testing in Figure 3.5A

Figure 3.5: Comparison of Possible Testing Sources

response for each of the possible testing sources is shown in Figure 3.5a. The frequency response[1], sometimes called the "transfer function", is the ratio of a system's output to its input. For the piezoelectric shaker and the instrumented hammer, the frequency response was the ratio of the receiver output to the force output of the corresponding source. However, since the electromagnetic shaker does not have a load cell to determine the force output, the frequency response was the ratio of the receiver output to the source input (approximately one volt). The response of the piezoelectric shaker and the instrumented hammer are similar throughout the frequency span of 500 to 15,000 Hz. However, the response of the electromagnetic shaker was approximately 60dB (dB = decibels[2]) below the other sources. This corresponds to a linear magnitude of approximately 1000 times. The low response was partially expected since the electromagnetic shaker produces much lower forces than either the piezoelectric shaker or the instrumented hammer. however, it is believed that the low response was also partially due to the coupling between the shaker and the ground surface and, therefore, the coupling was a major design consideration when using the electromagnetic shaker.

[1]The frequency response is defined in Figure 3.13.

[2]The decibel concept is defined in Figure 3.9.

3.2.2 Receivers

Once the generated signal has been directed into the pavement, it must be transferred, via the "receiver wheel", to a vibration monitor (receiver) for analysis. The vibration monitor detects particle displacement, velocity, or acceleration depending on the frequency content of the signal. For pavement analysis, high-frequency measurements are most common and, thus, particle acceleration is of interest.

Piezoelectric accelerometers are good detectors of particle acceleration at high frequencies. Accelerometers vary in frequency response and sensitivity. The amplitude of the received signal establishes the maximum allowable sensitivity. High amplitude signals should be analyzed with low-sensitivity ($\approx 10\,mV/g$) accelerometers, and low amplitude signals are best analyzed by high-sensitivity ($> 100\,mV/g$) accelerometers.

The accelerometers used at the University of Texas at Austin for this research are Wilcoxon Model 728T High Sensitivity, Low Noise Accelerometers and Wilcoxon Model 736 High Sensitivity, High Frequency Accelerometers. The Model 728T has a frequency response of 1-10,000 Hz with a ±3dB deviation and a sensitivity of $500\,mV/g$. The Model 736 has a frequency response of 2-25,000 Hz with a ±3dB deviation and a sensitivity of $100\,mV/g$. The

signal from either accelerometer is amplified using a Wilcoxon Model P702 Power Unit/Amplifier. The accelerometers and power unit/amplifier are shown in Figure 3.6.

3.2.3 Noise Considerations

Before proceeding with the design process, it was necessary to analyze the equipment noise and the applicable road noise to establish a threshold level of the receiver signal. First, the equipment noise was analyzed. In addition to the previously mentioned source and receiver equipment, the recording equipment currently used at the University of Texas at Austin consists of a Hewlett Packard 3562A Dynamic Signal Analyzer. The 3562A is a two-channel, fast fourier transformation (FFT) based analyzer which features network, spectrum, waveform, and transient analyses. Also used in data collection is a Wavetek System 716 Brickwall Filter and a Hewlett Packard 3478A Digital Multimeter.

The configuration used for the equipment noise analysis is shown in Figure 3.7. The accelerometer was contained in an anechoic chamber. This soundproof room, shown in Figure 3.8, insured that all signals were due entirely to equipment noise. The towing vehicle used for field testing was also considered in the noise evaluation. The engine and generator noise of the towing van were analyzed by simply recording the response of an accelerometer

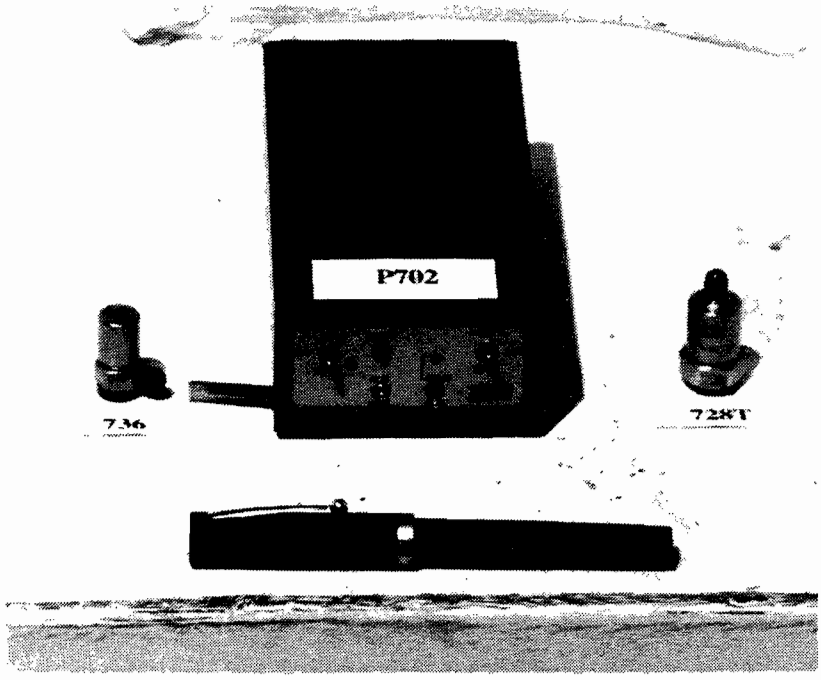

Figure 3.6: Wilcoxon Accelerometers and Power Unit/Amplifier

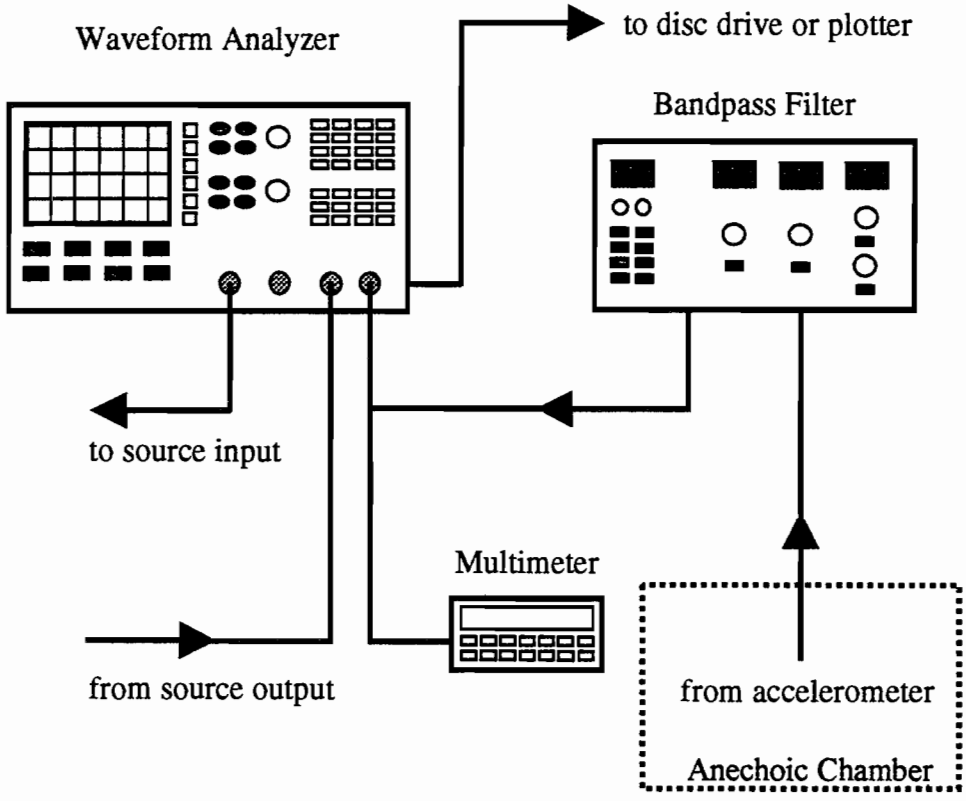

Figure 3.7: Typical Equipment Configuration for Testing and Noise Analyses

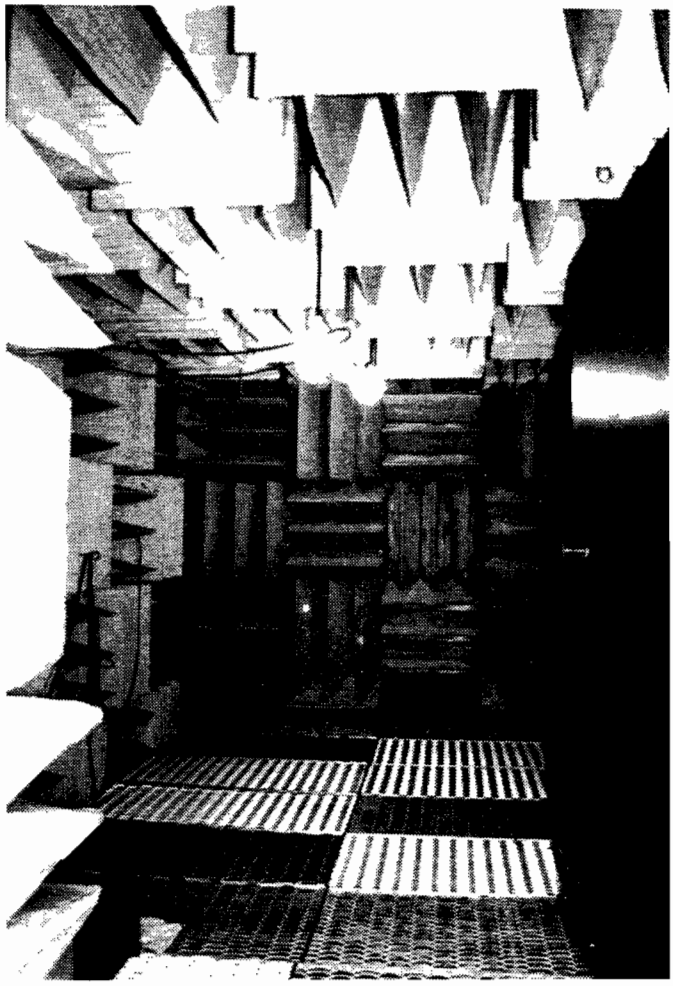

Figure 3.8: Anechoic Chamber at the University of Texas at Austin

placed on the pavement at the approximate location of the prototype trailer receiver. The power spectrum functions for the equipment noise evaluation are shown in Figure 3.9. The power spectrum is defined as the power level of the incoming signal at the measurement frequency for each point measured during the sweep. It is calculated as the FFT of the signal multiplied by its complex conjugate as shown in Figure 3.10. The resulting magnitude is then converted to decibels using the formula in Figure 3.9. The average equipment noise level was approximately -120 dB and was relatively constant over the frequency span of 1 to 10 kHz. This was about 15dB lower than the average towing vehicle noise level of -104 dB. Therefore, a minimum receiver signal strength of $\geq$ -104 dB was established. Actually, since the noise is slightly variable a safer threshold was set at $\geq$ -100 dB.

After evaluating the equipment noise, typical road locations were tested. To adequately address noise concerns on various roads, three locations were tested under typical traffic levels. These locations included 26th street in Austin, Texas during medium to heavy traffic conditions, IH-35 in Austin, Texas during medium traffic conditions, and IH-77 outside Kingsville, Texas during heavy traffic conditions. The peak roadway noise as a function of frequency is shown in Figure 3.11. The largest roadway noise levels occurred on IH-77 at an average intensity of -93dB and a peak

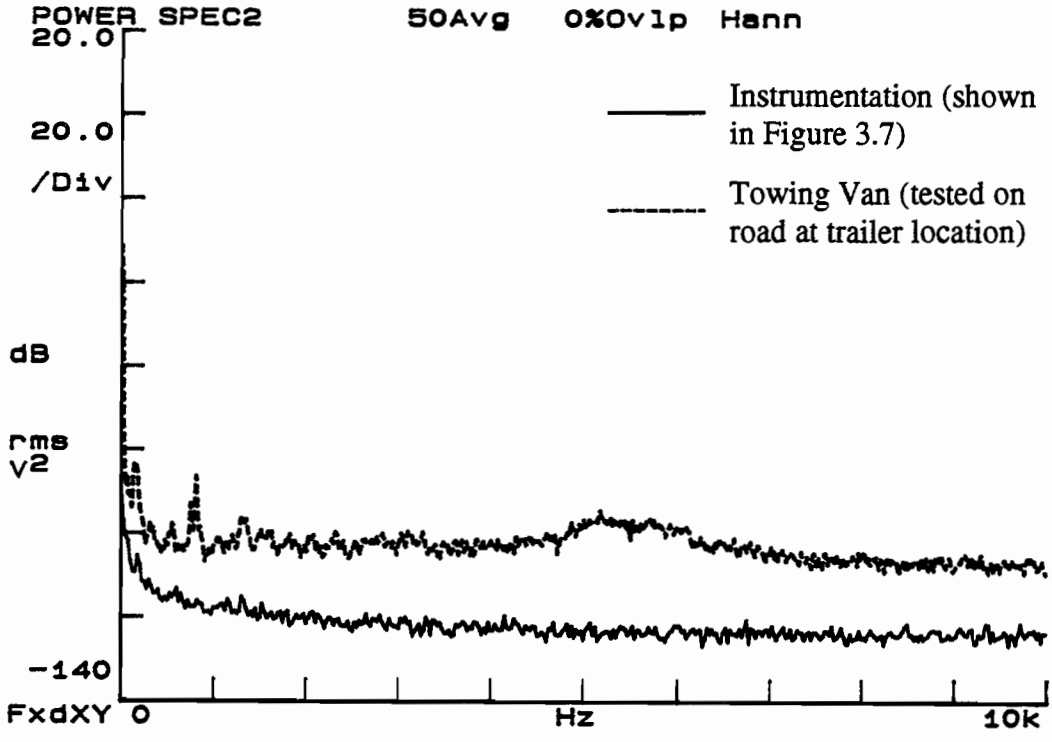

A. Noise Levels for 0 - 10KHz

Mag. (dB) = 20 log (x volts/1 volt)

NOTE: Decibel magnitude referenced to 1 volt

B. Decibel (dB) Concept

Figure 3.9: Evaluation of Noise Levels in Testing Instrumentation

$$\mathbf{H(f) = \frac{G_{xy}}{G_{xx}}}$$

where: G_{xy} is the cross spectrum
G_{xx} is the Channel 1 power spectrum

A. Frequency Response Concept

$$\gamma^2 = \frac{G_{xy}G_{xy}^*}{G_{xx}G_{yy}}$$

where: G_{xy} is the cross spectrum
G_{xy}^* is its complex conjugate
G_{xx} is the Channel 1 power spectrum
G_{yy} is the Channel 2 power spectrum

B. Coherence Function Concept

$$\mathbf{G_{xx} = F_x F_x^*}$$

where: F_x is the linear spectrum (FFT)
F_x^* is its complex conjugate

C. Power Spectrum Concept

Figure 3.10: Definition of the Frequency Response, Coherence, and Power Spectrum Concepts (Hewlett Packard, 1985)

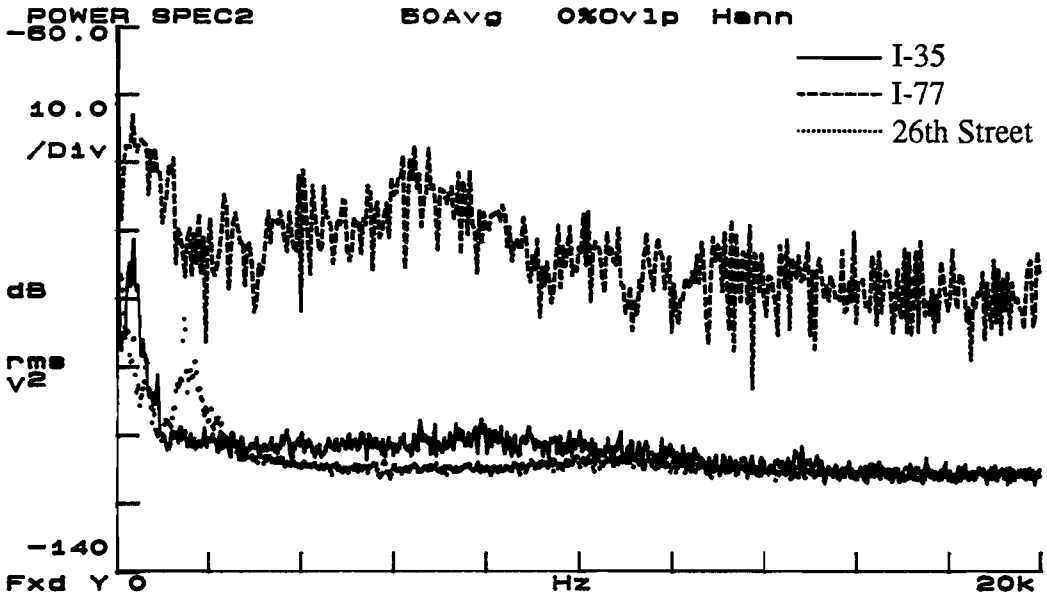

A. Noise Levels for 0 - 20 kHz

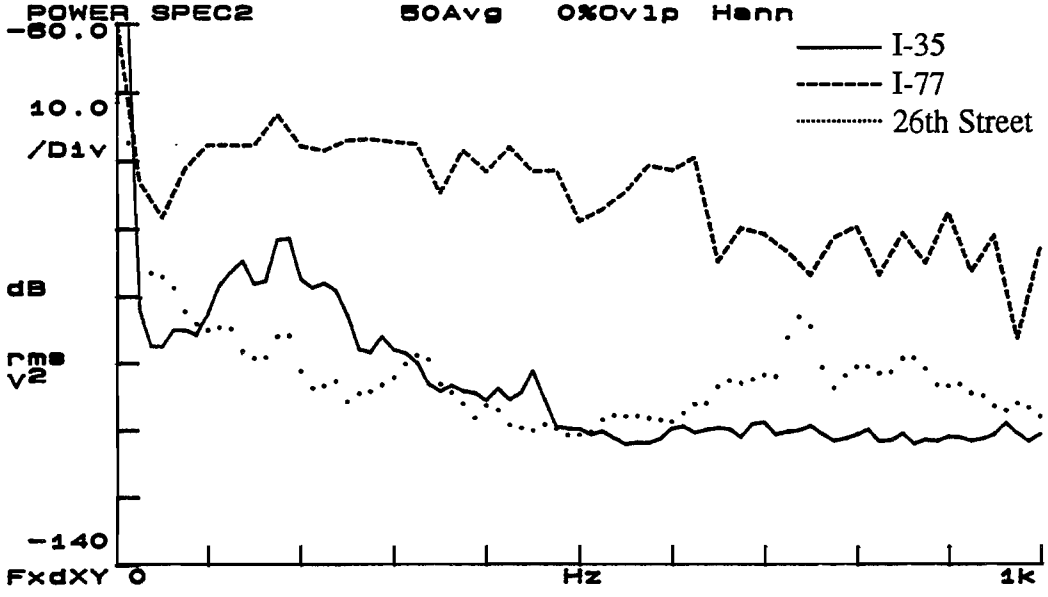

B. Noise Levels for 0 - 1 kHz

Figure 3.11: Evaluation of Noise Levels at Selected Roadways

intensity of -75dB at 175 Hz. This was about 30dB above the average noise levels of 26th street and IH-35. It was also noted that a majority of the road noise was concentrated in the 0 to 1 kHz frequency range as can be seen in Figure 3.11a. Thus, possible testing frequencies were limited to $\geq$ 1 kHz. According to the possible peak roadway noise, the threshold receiver signal strength was changed to $\geq$ -80 dB.

3.3 Prototype 1

In the initial design stages, the electromagnetic shaker system was used because it posed a fairly simplistic design solution and was easier to operate than the piezoelectric shaker system. Along with the M.B. Dynamics shaker, a Wilcoxon Model 728T accelerometer was used to receive the pavement signal due to its high sensitivity over a frequency span consistent with the electromagnetic shaker.

The first attempt at a prototype is shown in Figure 3.12. Solid rigid casters were chosen for both the "source wheel" and the "receiver wheel" to minimize signal loss. Separate trailers were designed for the source and receiver to insure the transmitted signal traveled through the pavement. Both trailers were constructed of aluminum to minimize the weight. The source trailer supported the M.B. Dynamics PM100 Vibration Exciter. The shaker was anchored

A. Overall View

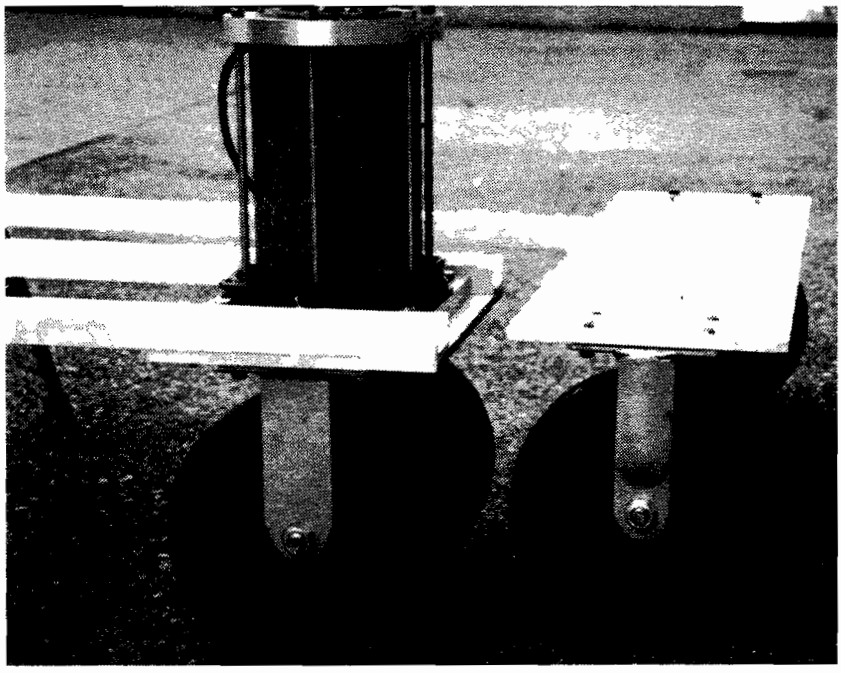

B. Detail of "Source Wheel" and "Receiver Wheel"

Figure 3.12: Prototype 1

to the trailer with a specially designed "cage" in an effort to increase the frequency response of the system. The shaker signal was transferred to the pavement via two, 12-in. (30.48-cm) diameter solid rigid casters. These casters have a 0.375-in. (9.53-mm) thick, stiff polyurethane tread. The receiver trailer was designed so that the receiver wheel, also a 12-in. (30.48-cm) diameter solid rigid caster with a 0.375-in. (9.53-mm) thick, stiff polyurethane tread, tracks directly behind and between the two "source wheels". A second wheel, a 12-in. (30.48-cm) diameter pneumatic rigid caster, was used to stabilize the receiver trailer.

Testing was conducted in the basement of the Civil Engineering building, at the University of Texas, on Prototype 1 to assess its signal transmission capabilities. An accelerometer was placed at three locations on the source trailer to evaluate signal loss in the system. The three locations are shown in Figure 3.13 and are labeled A, B, and C. It should be noted that the testing was conducted on a polished concrete floor which, since that time, has been found to be an inaccurate representation of a typical pavement surface. (Signals are transferred to a polished concrete floor much better than to a brushed concrete pavement.) However, for the preliminary laboratory tests, this was considered acceptable.

For these tests involving the electromagnetic shaker, channel one of the analyzer was connected to the source input from

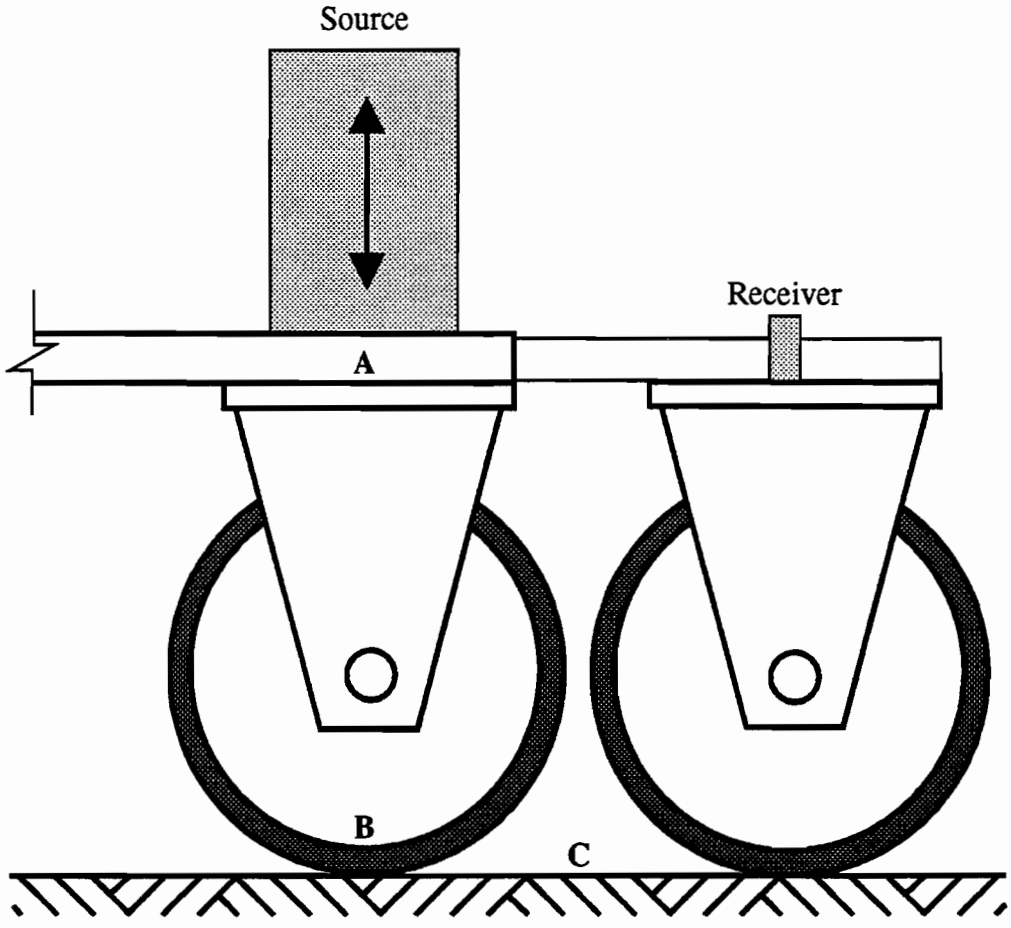

NOTE: Drawing not to scale

Figure 3.13: Schematic of Prototype 1 with Testing Locations A-C for Table 3.1 and Figures A.1 through A.12

the analyzer and channel two was connected to the accelerometer. The tests were performed using a swept sinusoid mode with a constant voltage output of one volt from the analyzer to the source. In addition, the amplifier output was set at approximately 70% to prevent any signal clipping (caused by excessive input signal or improper load impedance) that might occur over the frequency span. This input gives an estimated peak force output from the shaker of 35 pounds (155.7 N). A frequency span of 1 to 10 kHz was chosen for testing due to the frequency response of the Model 728T accelerometer and the noise considerations discussed in Section 3.2.3 The frequency responses and coherence functions[1] from these tests are shown in Appendix A (Figures A.1 through A.6). In addition, a summary plot is shown in Figure 3.14. The coherence function is an indication of the statistical validity of the frequency response. It therefore defines what portion of the channel 2 signal (receiver output) at a given frequency is directly related to the channel 1 signal (source output) at that same frequency. A coherence of 1.0 means 100% of the accelerometers output came from the source. Coherence values less than 1.0 are caused by system nonlinearities and extraneous noise. In addition to the frequency response and coherence, the power spectra[1] for each

[1]Frequency response, coherence, and power spectrum are defined in Figure 3.10.

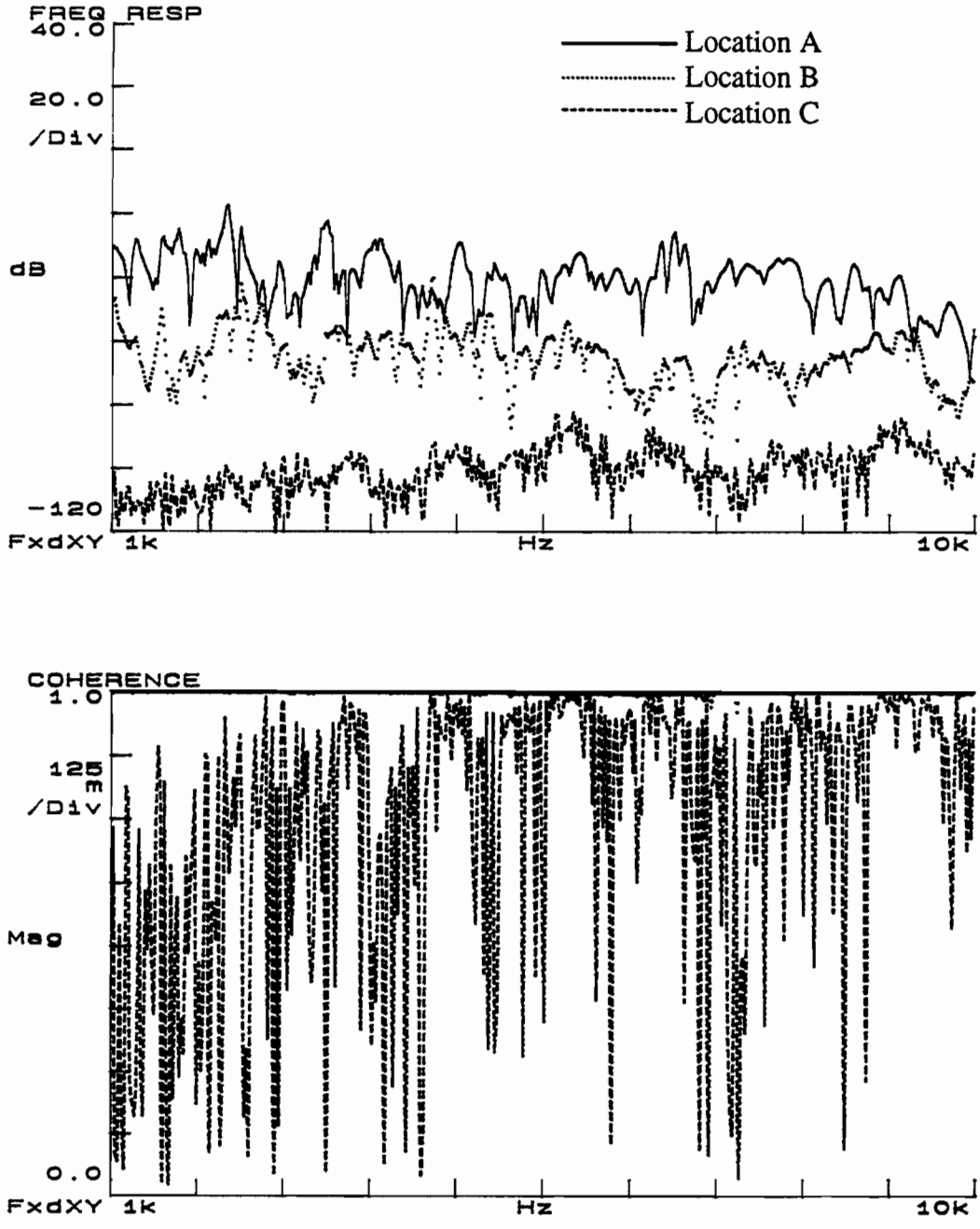

Figure 3.14: Summary Plot of the Frequency Response and Coherence for Testing Signal Transmission Capabilities on Prototype 1 at Locations A-C from Figure 3.13

channel were also examined.

The results of the transmission tests are summarized in Table 3.1. As shown in the table, the average frequency response at location A is approximately -41dB with excellent coherence. However, on the ground at location C, the frequency response is notably weak ($\approx$ -101 dB) with a very questionable coherence. The reduction of the signal strength by 60dB in the source wheel alone corresponds to a magnitude reduction of 1000 times. The accelerometer output (power spectrum for channel two) at location C has an average value of approximately -104dB which is coincidental with the towing vehicle noise level (Section 3.2.3) because the towing vehicle was not used in these laboratory tests. Due to this poor response, Prototype 1 was judged unacceptable and a design reevaluation was conducted.

3.4 Prototype 2.

Prototype 2 evolved as a mere modification of Prototype 1. Since the focus of Prototype 2 was to overcome the weak signal transmitted to the pavement in Prototype 1, modifications to the shaker were considered. According to Newton's Law, $F=m \cdot a$, the logical way to achieve a higher force output from the electromagnetic shaker would be to increase the mass of the moving element. From tests on Prototype 1, the estimated peak force output

Table 3.1: Summary of Laboratory Tests on Prototype 1 Evaluating the Vibration Level Transmitted into the Pavement

Accelerometer Location (from Fig. 3.13)	Frequency Response (1 to 10 kHz) (in dB)			Coherence (quality)	Power Spectrum Ch.2 (Accelerometer Output in dB)		
	Maximum	Average	Minimum		Maximum	Average	Minimum
A	-17.39	-40.74	-71.19	Excellent	-22.30	-45.65	-76.10
B	-39.81	-65.08	-91.00	Excellent	-44.71	-69.98	-95.74
C	-81.75	-100.82	-127.24	Poor	-86.59	-103.92	-121.72

Notes:

1 One volt source input
2 Swept frequency mode of operation
3 Estimated peak shaker force output = 35 lbs. (155.7 N)

was 35 pounds (155.7 N). A mass attachment had already been designed for the Model PM100 shaker. This mass attachment was simply incorporated into the design, and the resulting Prototype 2 is shown in Figure 3.15. The mass attachment added approximately 65 pounds (289.1 N) to the moving element. It should be noted that the specified peak force output for the Model PM100 shaker is derived from a peak acceleration based on the mass of the moving element and any attachments. As a result, the peak acceleration of the moving element decreases as the mass increases. Therefore, the addition of the mass attachment may not significantly affect the peak force output. Regardless, the mass attachment was utilized in Prototype 2 to attempt to improve the signal transmission into the pavement. Other than the mass attachment, the design remained identical to Prototype 1.

Prototype 2 was then tested in the laboratory to evaluate the effect of the added mass on the response of the system using the same configuration as that for Prototype 1 shown in Figure 3.13. The input voltage and amplifier output remained the same at one volt and 70% respectively. It is believed that the peak force output from the shaker with the mass attachment was approximately 49 pounds (218.0 N). The frequency responses, coherence functions, and power spectra for these tests are located in Appendix A, Figures A.7 through A.12. A summary plot is shown in Figure 3.16. In addition,

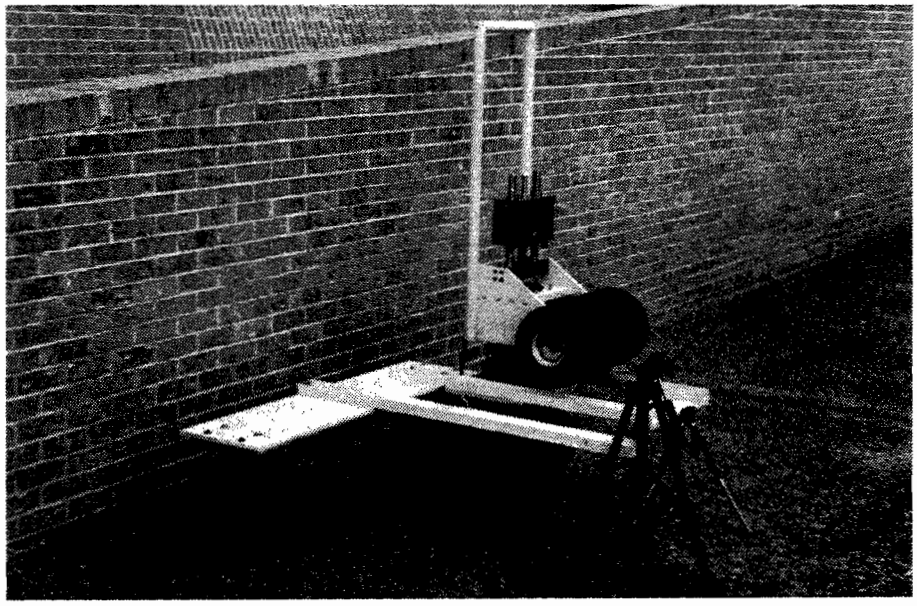

Figure 3.15: Prototype 2

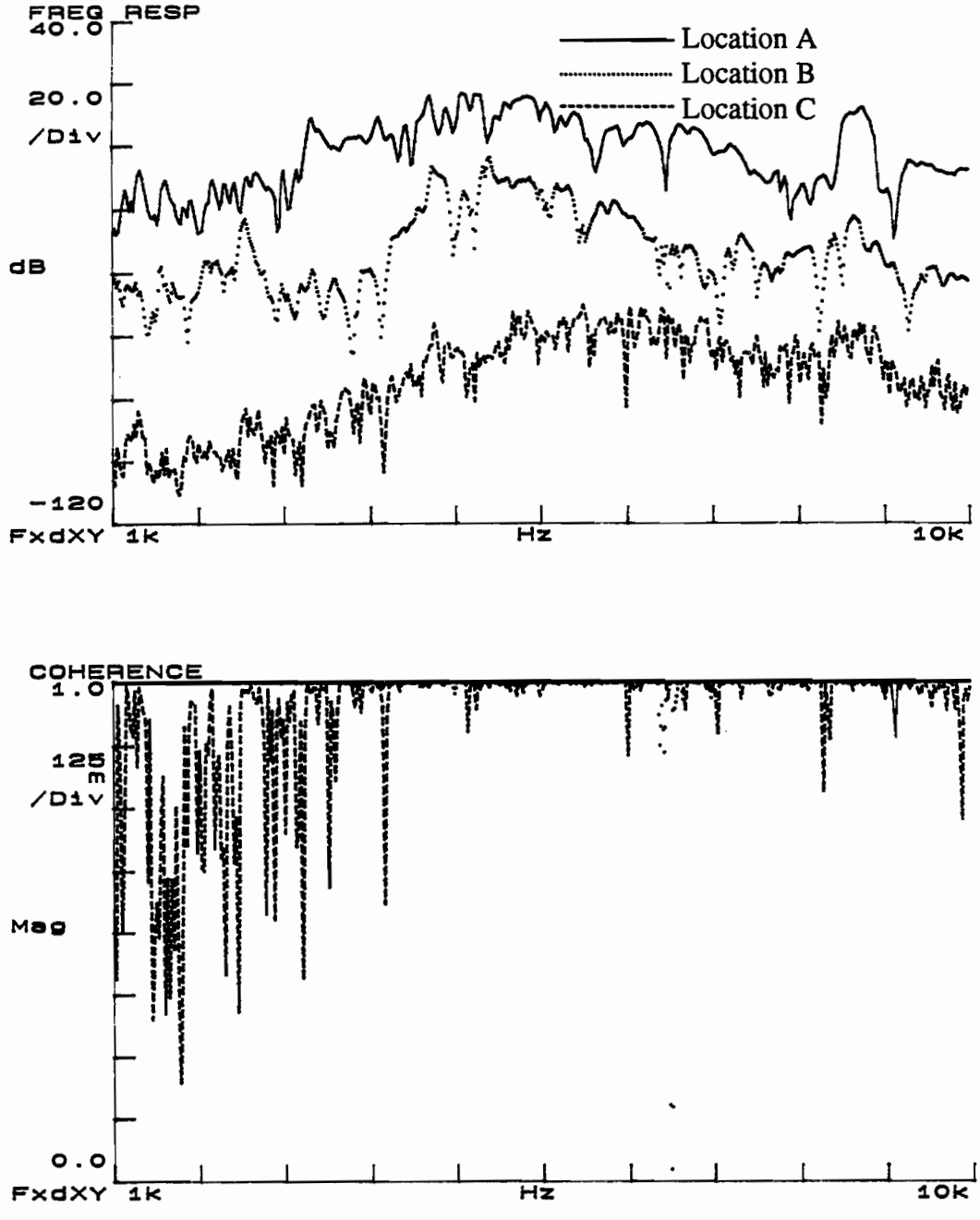

Figure 3.16: Summary Plot of the Frequency Response and Coherence for Testing Signal Transmission Capabilities on Prototype 2 at Locations A-C from Figure 3.13

the results are summarized in Table 3.2. The response of Prototype 2 was slightly better than the response of Prototype 1. There is a stronger signal at location A (–3dB) which diminishes to approximately -74dB at location C. This drop of 71 dB corresponds to a magnitude change of about 3000 times which is much greater than that found in Prototype 1. The coherence between 1kHz and 4kHz at location C is poor. In addition, a majority of the accelerometer output at location C was at or below the recording equipment noise level and only slightly above the road noise level as discussed in Section 3.2.3. Therefore, the addition of the mass to the moving element only slightly improved the signal strength transmitted into the pavement. However, the improvement was not enough to be acceptable. Because of this unacceptable signal level, it was determined that the electromagnetic shaker was not capable of generating the required signal. Therefore, a complete redesign was conducted.

3.5 Summary

A fundamental scheme consisting of a "source wheel" and a "receiver wheel" translating along the pavement surface formed the basis for the design of a prototype vehicle capable of detecting cracks, voids, and delaminations in pavement layers. A variety of dynamic, vertically loading sources were investigated in the

Table 3.2: Summary of Laboratory Tests on Prototype 2 Evaluating the Vibration Level Transmitted into the Pavement

Accelerometer Location (from Fig. 3.13)	Frequency Response (1 to 10 kHz) (in dB)			Coherence (quality)	Power Spectrum Ch.2 (Accelerometer Output in dB)		
	Maximum	Average	Minimum		Maximum	Average	Minimum
A	16.70	-3.03	-29.11	Excellent	11.79	-7.94	-34.21
B	-3.71	-34.04	-65.57	Good	-8.62	-38.91	-70.18
C	-50.24	-74.37	-110.58	Fair to Poor	-55.14	-78.81	-110.26

Notes:

1 One volt source input
2 Swept frequency mode of operation
3 Estimated peak shaker force output = 49 lbs. (218.0 N)

preliminary design phases. In addition, several accelerometers were considered for signal reception. The basic design parameters for this system were established by analyzing noise levels for both the equipment and typical roadways. The threshold receiver signal strength was determined to be -80dB from the noise analysis. Furthermore, the noise analysis defined a minimum testing frequency of 1 kHz if typical noise in the roadways was to be avoided.

After establishing pertinent design parameters, the prototype vehicle design process was initiated. Prototypes 1 and 2 were designed with an electromagnetic shaker as the source. The performance of these prototypes were investigated by constructing actual trailers on which the sources were placed. Based on the results of tests involving Prototypes 1 and 2, it was concluded that the electromagnetic shaker was unacceptable for application in pavement analysis under the established design parameters because the signal imparted to the pavement was too small.

Chapter Four
Design and Development of Prototypes 3 and 4

4.1 Introduction

Before continuing with the design and development process, Prototypes 1 and 2 were reexamined. In evaluating Prototypes 1 and 2, several performance flaws became apparent. First, the electromagnetic shaker could not generate the force needed to excite the pavement an appreciable amount. Therefore, in the redesign, the source would need to be capable of generating a force output much larger than 35 to 49 lbs. (155.7 to 218.0 N), which was the estimated peak force output of the MB Dynamics Model PM100 electromagnetic shaker. Thus, a piezoelectric shaker was selected for use in Prototypes 3 and 4. This shaker existed in the Soil Dynamics Laboratory at UT and was capable of generating more than ten times as much force over the frequency range of concern.

In addition to the force level, there was a great deal of signal loss within the solid rigid casters ("wheels") in the trailer. Due to this, smaller diameter rigid casters were considered in Prototypes 3 and 4. Finally, the source trailer and the receiver trailer were combined into one trailer to minimize signal loss in the pavement by placing the "source wheel" as close as possible to the "receiver wheel". To prohibit transmission of the signal through the trailer, natural rubber isolators were placed at all connections.

In addition to the above mentioned design modifications, an acrylic shield was installed between the "source wheel" and the "receiver wheel" to minimize any signal transmission through the air. It should be noted that signal transmission through the air was investigated using the previously mentioned anechoic chamber. The piezoelectric shaker and an accelerometer were independently suspended in the anechoic chamber at the same distance above the chamber floor and 6 in. (15.24 cm) apart. This arrangement was established to best model the relative locations of the shaker and accelerometer in Prototypes 3 and 4. The results from that testing, shown in Figure 4.1, yielded a signal strength just below the recording equipment noise (Figure 3.9) and well below the roadway noise level (Figure 3.11). Thus, it was concluded that air transmission was not a major concern and the acrylic shield was added to merely reinforce this conclusion.

4.2 Prototype 3

Incorporating the design modifications described above, the resulting Prototype 3 is shown in Figure 4.2. Both the "source wheel" and the "receiver wheel" were 4-inch (10.16 cm) diameter solid rigid casters. These casters have a 0.25-inch (0.635 cm) thick stiff polyurethane tread. A comparison between the 12-inch (30.48 cm) diameter rigid casters and the 4-inch (10.16 cm) diameter rigid casters is shown in Figure 4.3. Once again a 12-inch (30.48 cm)

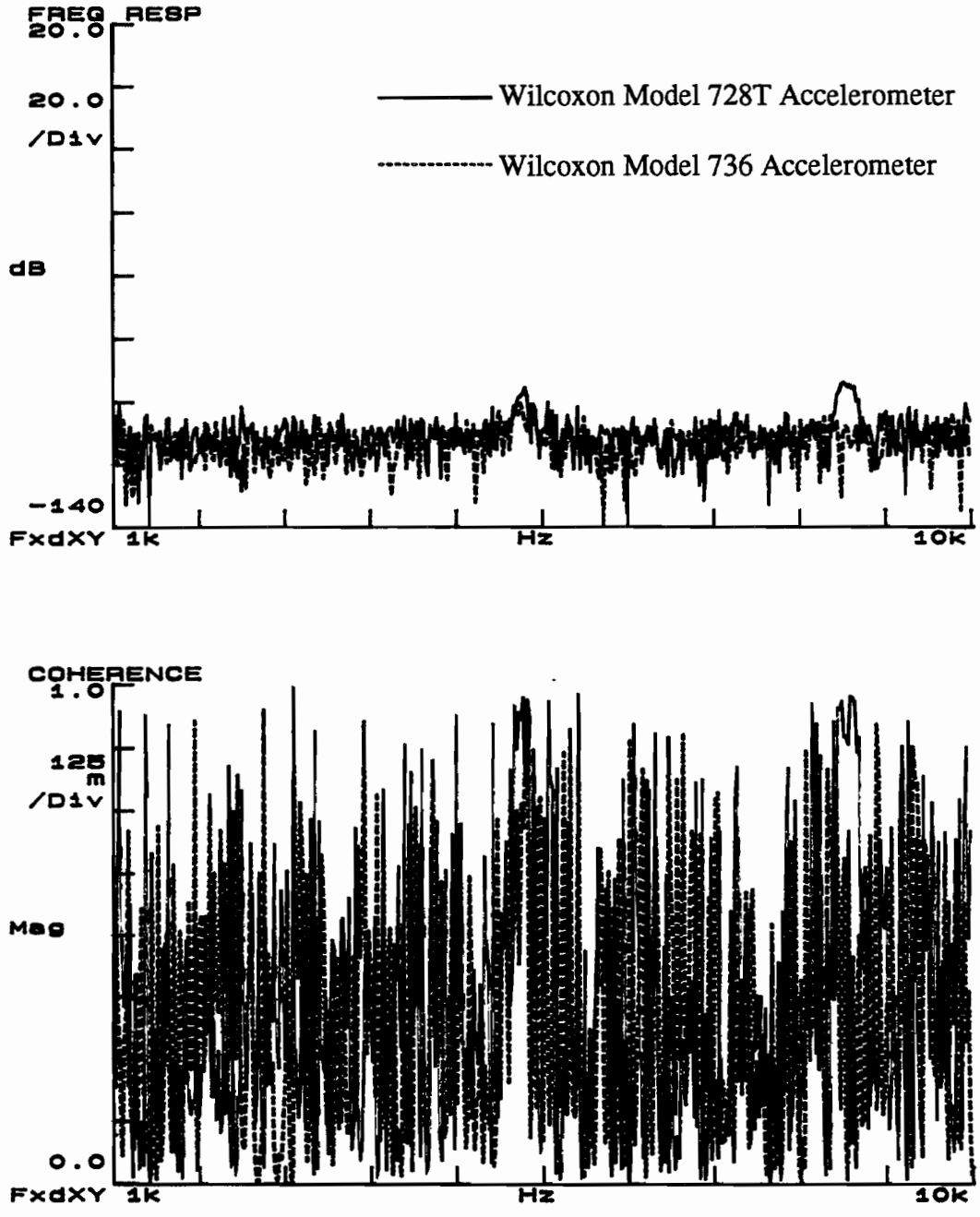

Figure 4.1: Frequency Response and Coherence for Air Signal Transmission Testing in the Anechoic Chamber Utilizing the Piezoelectric Shaker and both the Wilcoxon Models 728T and 736 Accelerometers

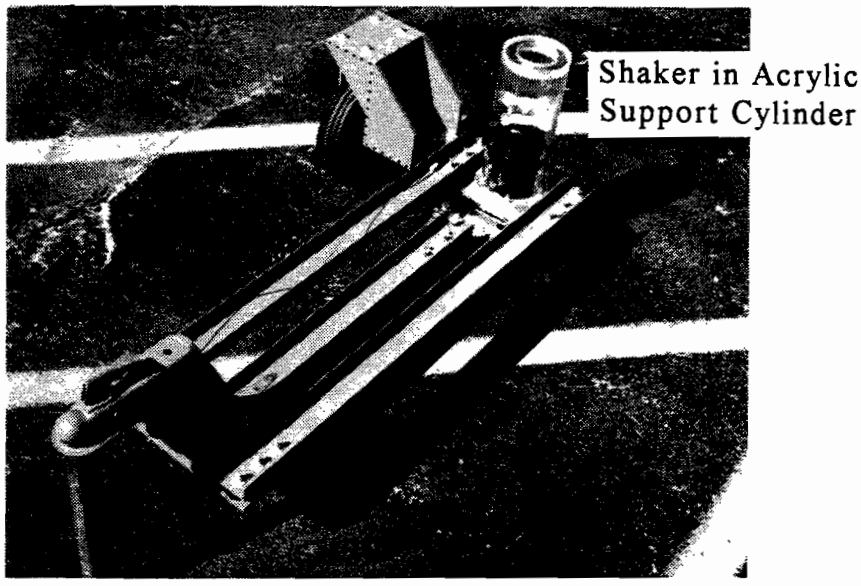

A. Overall View

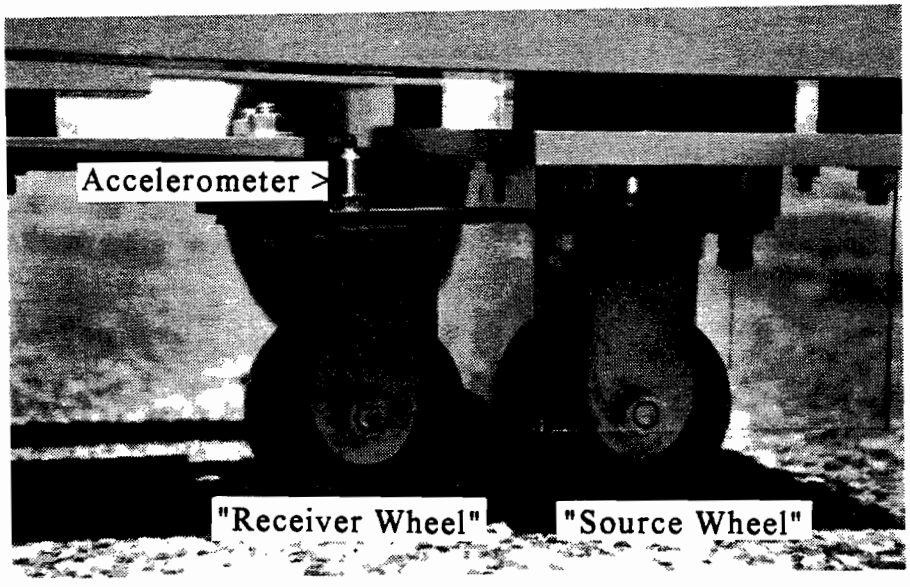

B. Detail of Source and Receiver Wheels

Figure 4.2: Prototype 3

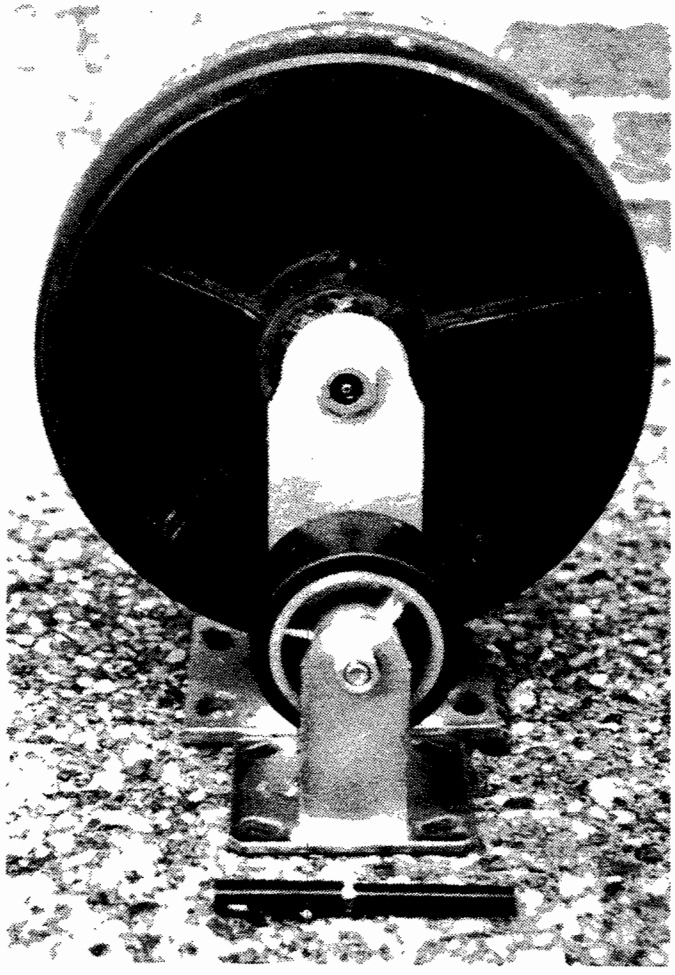

Figure 4.3: Comparison Between 12-inch Diameter Rigid Caster and 4-inch Diameter Rigid Caster

diameter pneumatic rigid caster was used for stability. The Wilcoxon Model F8 piezoelectric shaker rests directly on the "source wheel". The shaker was supported by a specially designed acrylic cylinder that prohibits horizontal movement but allows vertical movement. This type of housing was necessary due to the delicate nature of the piezoelectric shaker. Because of the continued need for a highly sensitive receiver, the Wilcoxon Model 728T accelerometer was also utilized in Prototype 3 as can be seen in Figure 4.2b.

As before with Prototypes 1 and 2, tests were conducted in the basement laboratory of the Civil Engineering building at UT to evaluate the performance of the proposed Prototype 3 design. As mentioned in Section 3.3, it should be again noted that the laboratory testing floor had a polished concrete surface which does not accurately represent a typical brushed pavement surface. However, for preliminary laboratory testing, this was considered acceptable from a relative standpoint. Accelerometers were again placed at various locations on the trailer to determine the signal loss through the trailer. The accelerometer placement for tests performed on Prototype 3 is shown in Figure 4.4. Channel one of the Hewlett Packard 3562A Dynamic Signal Analyzer was connected to the force transducer on the Model F8 shaker and channel two was again connected to the accelerometer. The signal from the force transducer went through a charge converter before it was amplified.

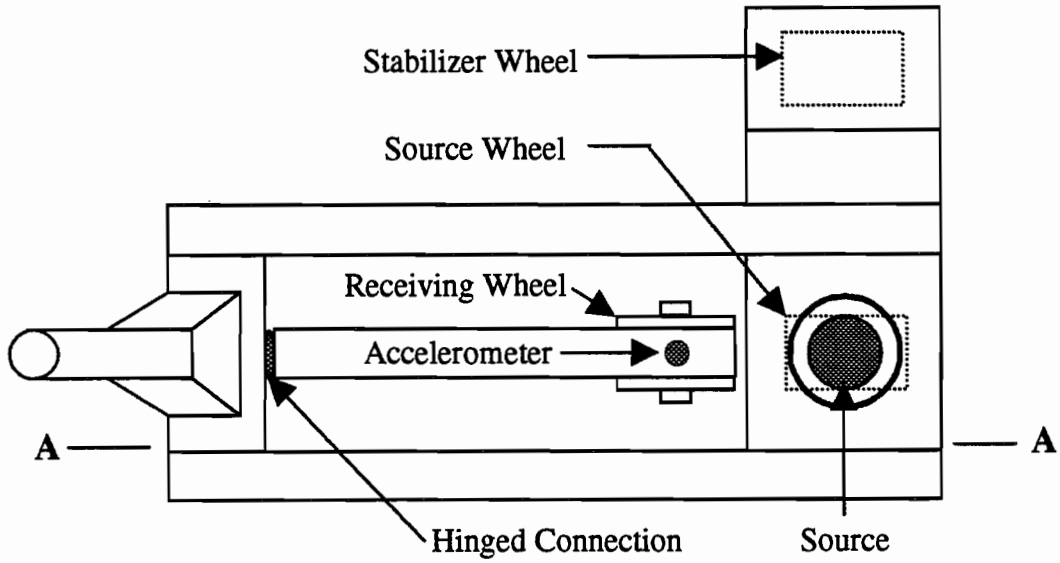

NOTE: Drawing not to scale

A. Plan View

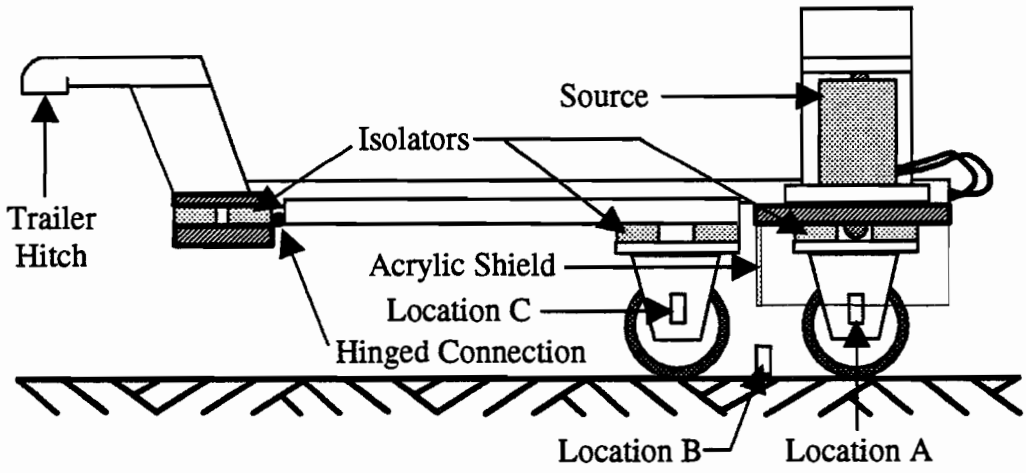

NOTE: Drawing not to scale

B. Section A-A

Figure 4.4: Plan and Cross-Sectional Views of Prototype 3 Showing Testing Locations A-C for Table 3.3 and Figures A.13 through A.24

The resulting force gage sensitivity was $10\,^{mV}/_{lb}$. A swept sinusoid mode was used for controlling the shaker. The Model PA8 amplifier was driven with a one volt constant input and the Model N8H matching network was set at 800 Vrms. It should be noted that although the amplifier has a maximum input of three volts, the input was limited to one volt because certain frequencies encountered when sweeping through a wide frequency span can cause various resonances within the system. These resonances overdrive the accelerometers, and thus the data are unreliable.

Figure 4.5 summarizes the signal transmission from location A to location C in terms of the frequency responses. In addition, the frequency responses, coherence functions, and power spectra from tests on Prototype 3 (Figures A.13 through A.18) are summarized in Table 4.1. The frequency response at locations A and B were stronger than in any of the previous tests (an average increase of $\approx$14dB and $\approx$11dB, respectively). Equally as important as the response improvement was the substantial improvement in the coherence at all testing locations over the entire frequency span. However, the accelerometer output (power spectrum for channel 2) at location B was fairly weak at an average value of $\approx$–64dB. The signal at location C was also low.

A comparison of the previously measured roadway noise levels (Section 3.2.3) to the accelerometer outputs (power spectrum from channel 2) at locations A through C is illustrated in Figure 4.6.

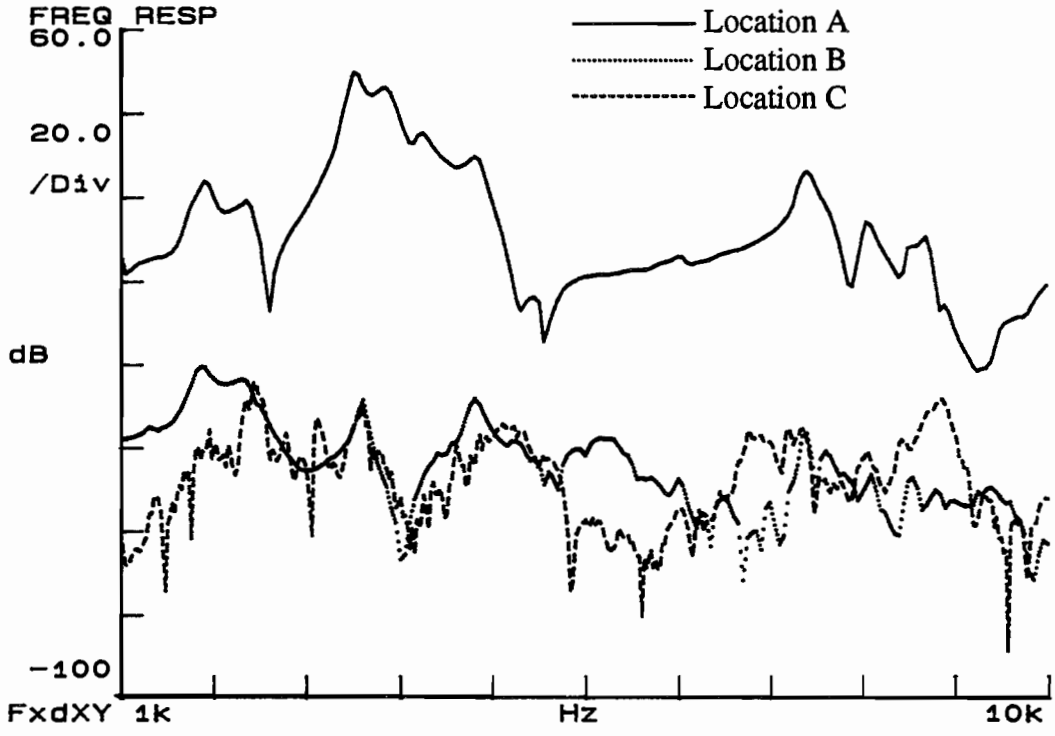

Figure 4.5: Summary Plot of the Frequency Response for Testing Signal Transmission Capabilities on Prototype 3 at Locations A-C from Figure 4.4

Table 4.1: Summary of Laboratory Tests on Prototype 3 Evaluating the Vibration Level Transmitted Through the Pavement

Accelerometer Location (from fig. 3.17)	Frequency Response 1 to 10KHz (in dB)		Coherence (quality)	Power Spectrum Ch.1 (Force Output from Shaker) (in pounds)		Power Spectrum Ch. 2 (Accelerometer Output) (in dB)	
A	Maximum	49.91	Excellent	Maximum	738.93	Maximum	20.04
	Average	10.56		Average	11.49	Average	-8.23
	Minimum	-21.90		Minimum	0.22	Minimum	-47.09
B	Maximum	-20.54	Excellent	Maximum	731.64	Maximum	-31.61
	Average	-44.86		Average	11.44	Average	-63.69
	Minimum	-71.81		Minimum	0.20	Minimum	-90.85
C	Maximum	-24.02	Excellent	Maximum	404.88	Maximum	-29.90
	Average	-47.99		Average	15.47	Average	-64.19
	Minimum	-88.76		Minimum	0.47	Minimum	-112.78

Notes:

1 One volt source input
2 Swept frequency mode of operation

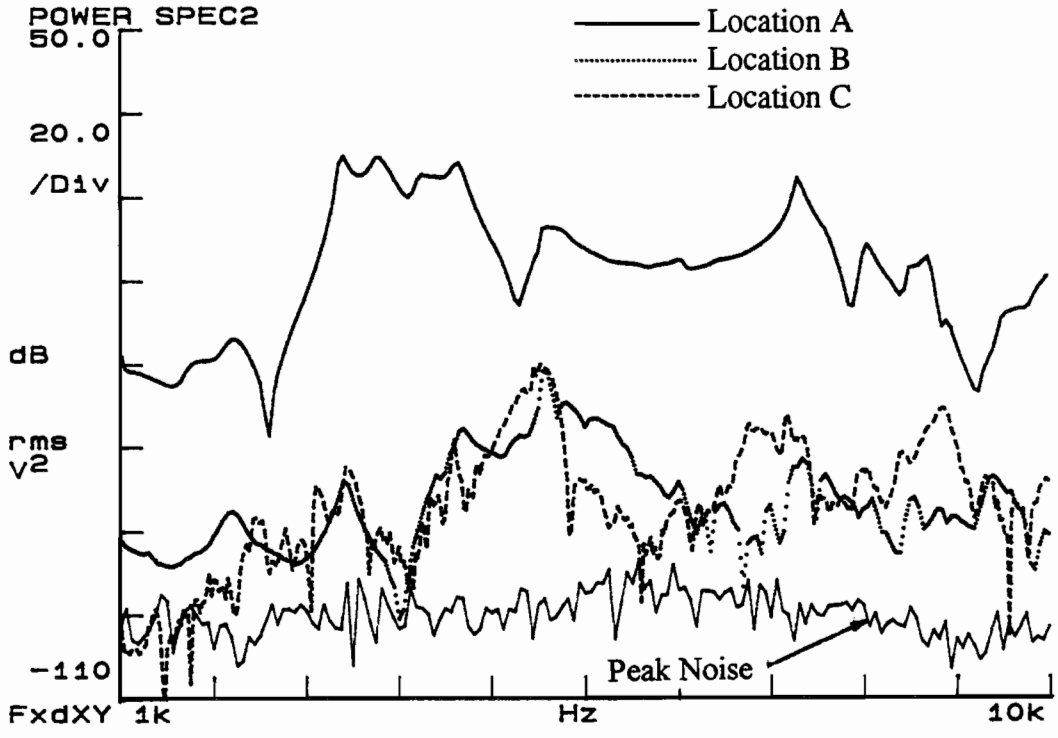

Figure 4.6: Summary Plot of the Power Spectrum for Testing Signal Transmission Capabilities on Prototype 3 at Locations A-C from Figure 4.4 Relative to the Established Roadway Noise Level from Section 3.2.3

Although the response at location A was well above the peak roadway noise level, the response at locations B and C was within 10 dB, on the average, of the recorded magnitude of the peak noise. Based on the above results, the design was reevaluated because it was felt that the performance on an actual road would be less than that measured in the laboratory.

4.3 Prototype 4

In examining the frequency responses and the power spectra from tests performed on Prototype 3, it was determined that a majority of the signal loss was occurring within the wheels. The problem was either in signal transfer from the yoke to the wheel or in the actual wheel assembly. Both possible problems were addressed. First, the axles were redesigned using one-inch (2.54-cm) diameter brass stock. The "receiver wheel" axle was also specially modified so that the accelerometer could be mounted directly on it, thus reducing the travel path of the signal and reducing the number of interfaces encountered by the signal. Furthermore, the individual wheels were redesigned. Instead of the prefabricated aluminum wheels a 4-inch (10.16 cm) diameter segment of stainless steel was used. To reduce losses, the wheels were milled so that they just fit on the axle with very little clearance. To obtain the best possible signal transmission, no bearings or bushings were allowed and no coating (tread) was used on the stainless steel. A comparison of the

wheels is shown in Figure 4.7. The intensive wheel redesign was the only modification made for Prototype 4 (Figure 4.8). A plan and cross-sectional view of Prototype 4 is shown in Figure 4.9.

The laboratory testing procedure and accelerometer configuration for Prototype 4 were identical to that of Prototype 3 (Figure 4.4). A summary of the signal transmission from location A to location C in terms of the frequency responses is shown in Figure 4.10. The overall results are summarized in Table 4.2 and the individual frequency responses, coherence functions, and power spectra are shown in Figures A.19 through A.24. The response of the trailer and the output of the accelerometer at location A were very similar to that of Prototype 3 as was expected since no modifications from the previous design were made on the signal travel path between the source and location A. The advantage gained by the wheel modification became evident in the signal magnitude at locations B and C. On the average the frequency response at locations B and C increased $\approx$22dB and $\approx$14dB, respectively, from that in Prototype 3. The real increase in performance was seen in the accelerometer output (power spectrum from channel 2) at locations B and C which improved $\approx$26dB and $\approx$14dB, respectively. The response of Prototype 4 was well within the established performance parameters.

As a result of this acceptable preliminary laboratory performance, more extensive testing was conducted to understand

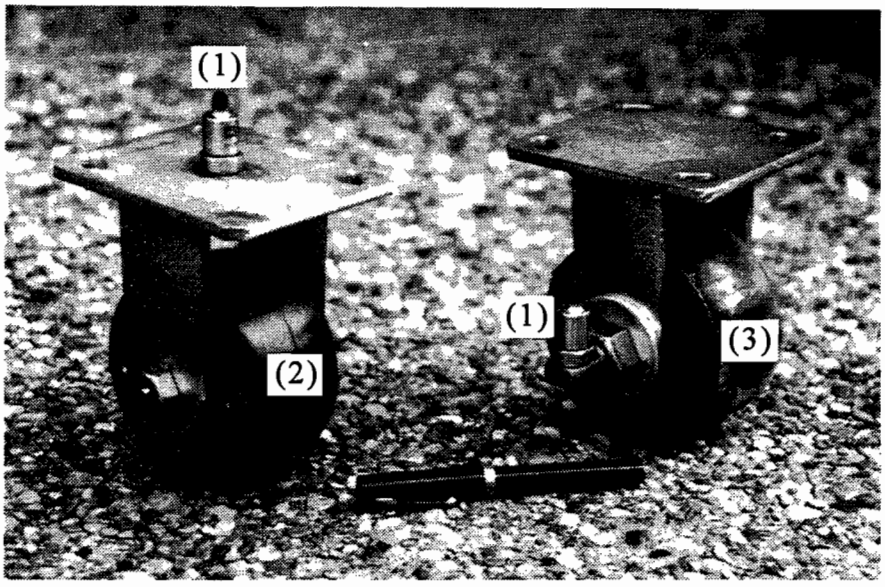

(1) Wilcoxon Model 728T Accelerometer
(2) Prefabricated Aluminum Wheel
(3) Specially Designed Stainless Steel Wheel

Figure 4.7: Comparison Between Prefabricated Aluminum Wheel and Specially Designed Solid Stainless Steel Wheel

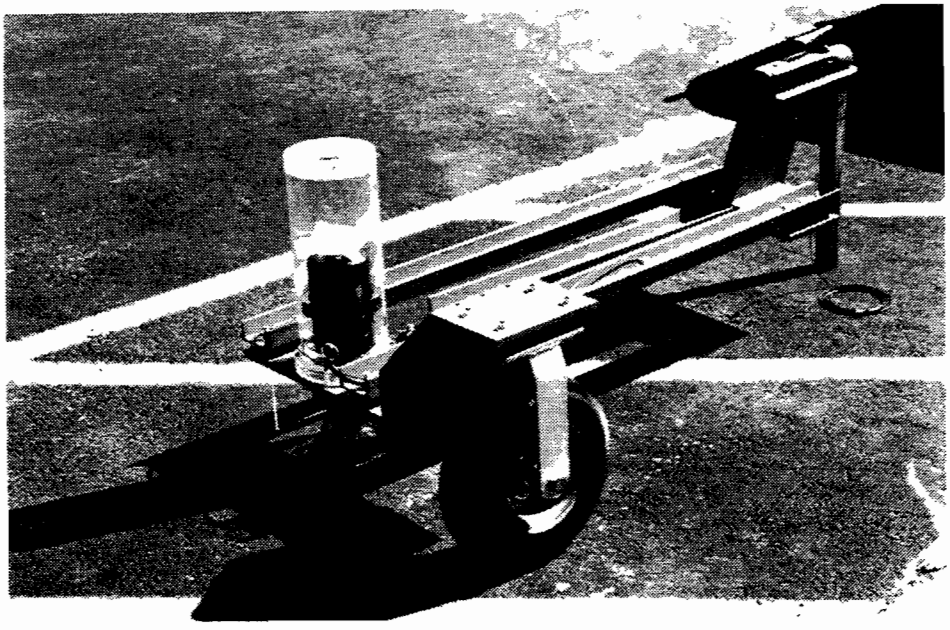

A. Overall View

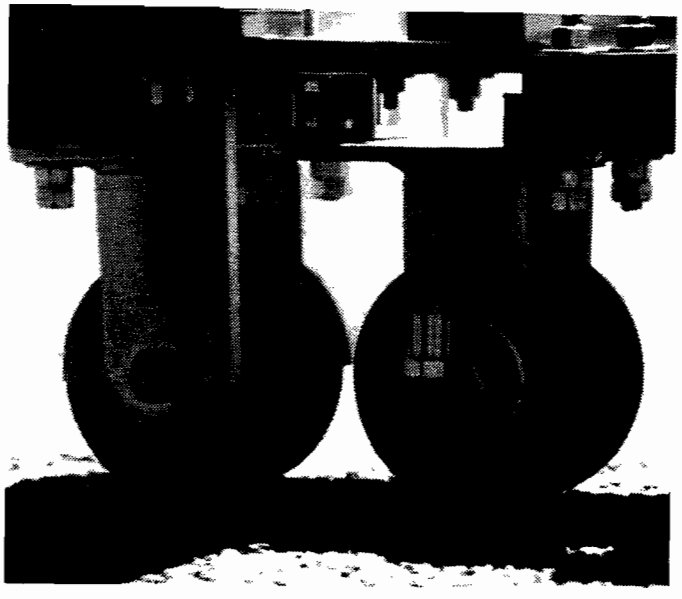

B. Detail of Source and Receiver Wheels

Figure 4.8: Prototype 4

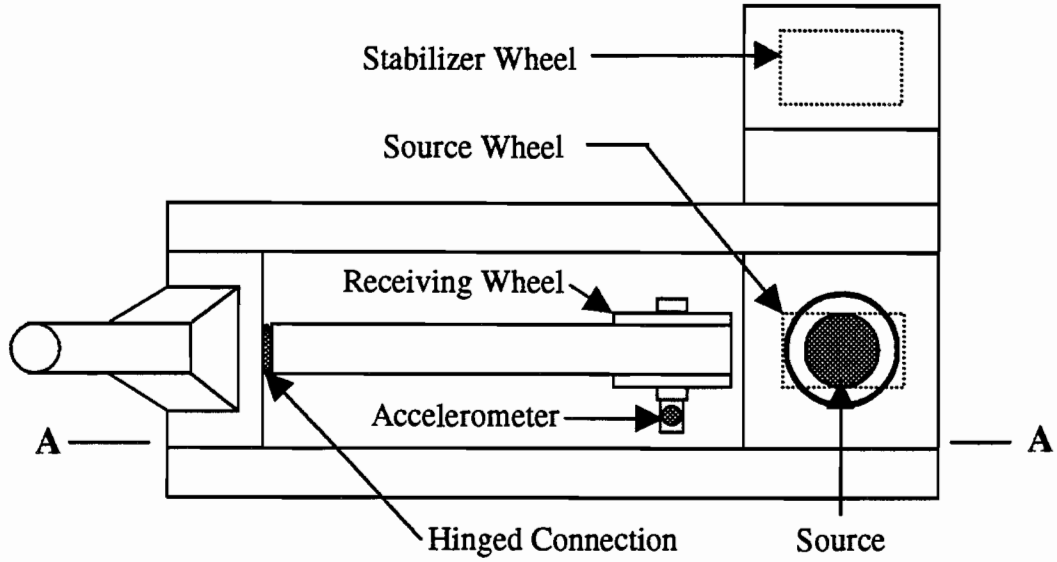

NOTE: Drawing not to scale

A. Plan View

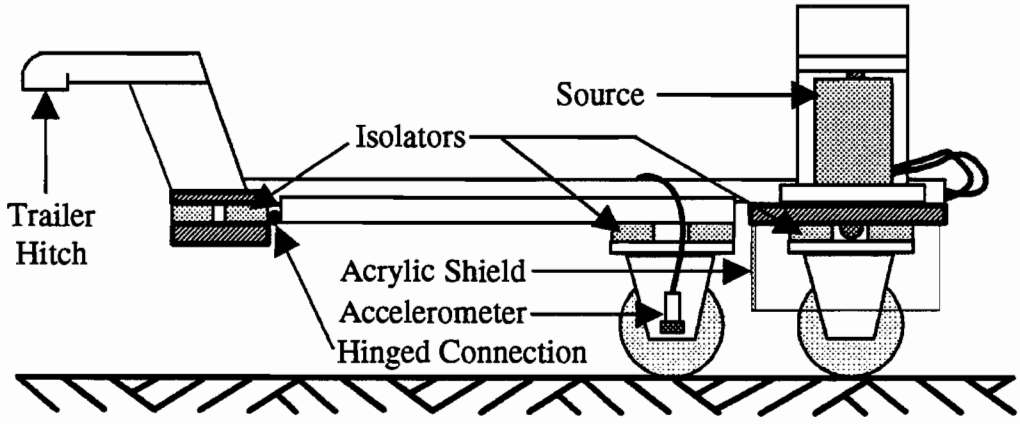

NOTE: Drawing not to scale

B. Section A-A

Figure 4.9: Plan and Cross-Sectional Views of Prototype 4

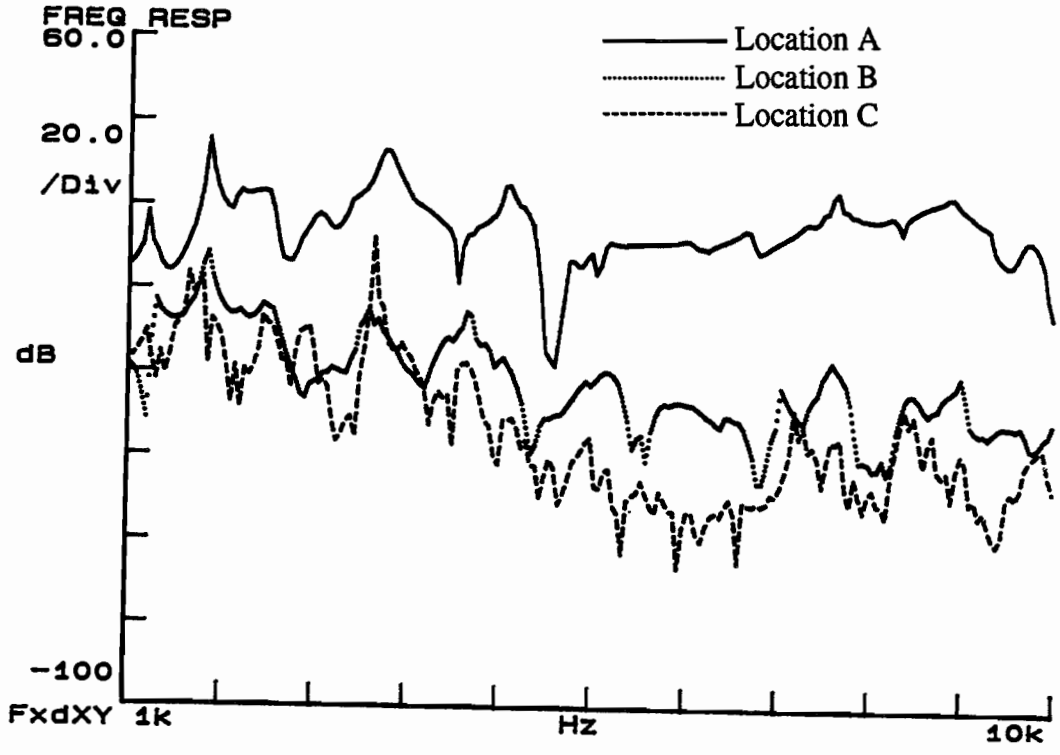

Figure 4.10: Summary Plot of the Frequency Response for Testing Signal Transmission Capabilities on Prototype 4 at Locations A-C from Figure 4.4

Table 4.2: Summary of Laboratory Tests on Prototype 4 Evaluating the Vibration Level Transmitted Through the Pavement

Accelerometer Location (from fig. 3.17)	Frequency Response 1 to 10KHz (in dB)		Coherence (quality)	Power Spectrum Ch.1 (Force Output from Shaker) (in pounds)		Power Spectrum Ch. 2 (Accelerometer Output) (in dB)	
A	Maximum	35.74	Excellent	Maximum	562.25	Maximum	20.21
	Average	14.63		Average	14.52	Average	-2.13
	Minimum	-18.54		Minimum	0.10	Minimum	-33.88
B	Maximum	8.67	Excellent	Maximum	179.99	Maximum	-23.44
	Average	-22.79		Average	18.45	Average	-37.46
	Minimum	-45.87		Minimum	0.19	Minimum	-66.10
C	Maximum	12.95	Excellent	Maximum	134.62	Maximum	-31.83
	Average	-34.45		Average	16.71	Average	-49.98
	Minimum	-66.14		Minimum	0.19	Minimum	-74.66

Notes

1 One volt source input

2 Swept frequency mode of operation

and document more aspects of signal transmission and loss through Prototype 4. The set of tests are conceptually illustrated in Figure 4.11. These tests were performed to understand how each component performed. The "source wheel" was analyzed separately by conducting a test with the source on the "source wheel" and the accelerometer directly on the ground next to the "source wheel" (Figure 4.11a). In addition, the "receiver wheel" was analyzed separately by performing a test with the accelerometer on the "receiver wheel" and the source directly on the ground next to the "receiver wheel" (Figure 4.11b). Finally, the entire system was analyzed by conducting a test with the source on the "source wheel" and the accelerometer on the "receiver wheel" (Figure 4.11c). For comparison purposes, a test was conducted with both the source and the accelerometer directly on the ground (Figure 4.11d), approximately 6 inches (15.2 cm) apart.

These component tests were performed on the polished concrete floor in the UT Civil Engineering basement laboratory just like the prototype tests. The results of the component tests are tabulated in Table 4.3. A comparison of the frequency responses for the ground, "source wheel", and "receiver wheel" are shown in Figure 4.12. In addition, a comparison of the frequency responses for the entire system and the ground are shown in Figure 4.13. The individual frequency responses, coherence functions, and power spectra for these tests are located in Figures B.1 through B.8.

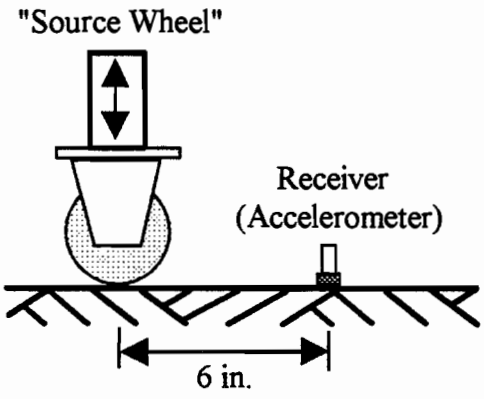

A. Configuration for the "Source Wheel" Test

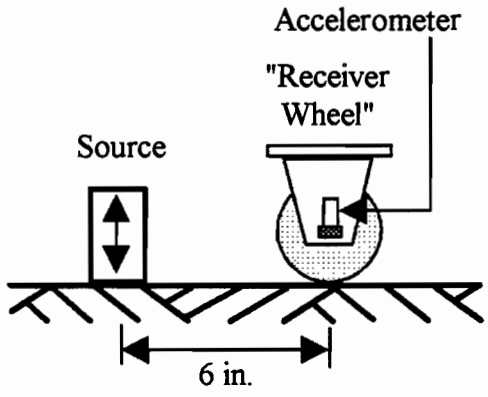

B. Configuration for the "Receiver Wheel" Test

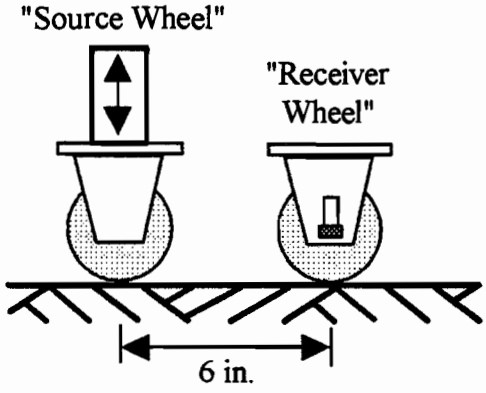

C. Configuration for the "Entire System" Test

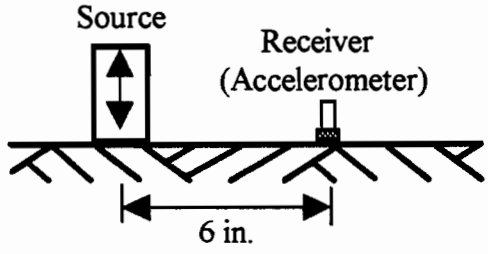

D. Configuration for the Ground Comparison Test

Figure 4.11: Conceptual Illustration of the Configuration for Individual Component Laboratory Testing on Prototype 4

Table 4.3: Summary of Laboratory Testing on Prototype 4 Evaluating Signal Transmission Through Each Trailer Component

Source/ Accelerometer Location	Frequency Response 1 to 10KHz (in dB)		Coherence (quality)	Power Spectrum Ch.1 (Force Output from Shaker) (in pounds)		Power Spectrum Ch. 2 (Accelerometer Output) (in dB)	
Ground/Ground	Maximum	22.89	Excellent	Maximum	341.54	Maximum	4.86
	Average	-3.12		Average	22.03	Average	-16.24
	Minimum	-29.51		Minimum	0.07	Minimum	-46.43
Source Wheel/ Ground	Maximum	8.67	Excellent	Maximum	179.99	Maximum	-23.44
	Average	-22.79		Average	18.45	Average	-37.46
	Minimum	-45.87		Minimum	0.19	Minimum	-66.10
Ground/ Receiver Wheel	Maximum	-3.32	Excellent	Maximum	342.74	Maximum	-22.11
	Average	-35.26		Average	21.08	Average	-48.78
	Minimum	-62.47		Minimum	0.11	Minimum	-73.50
Source Wheel/ Receiver Wheel	Maximum	12.95	Excellent	Maximum	134.62	Maximum	-31.83
	Average	-34.45		Average	16.71	Average	-49.98
	Minimum	-66.14		Minimum	0.02	Minimum	-74.66

Notes

1 One volt source input
2 Swept frequency mode of operation

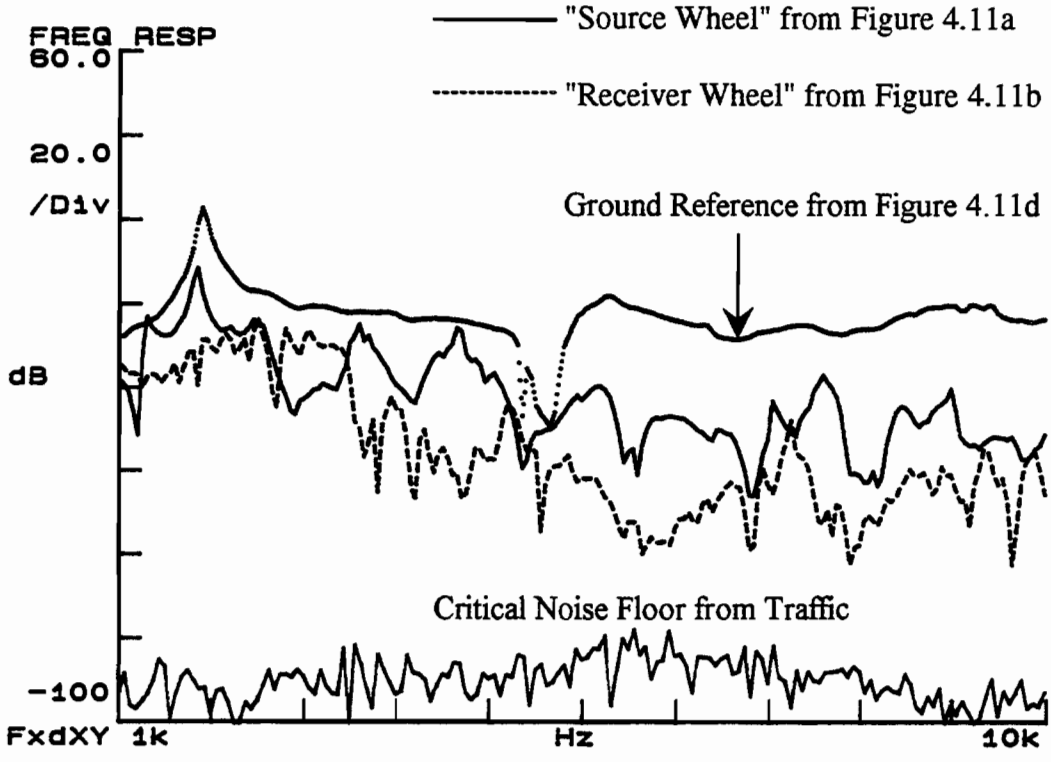

Figure 4.12: Comparison Plot of the Frequency Response for Testing Signal Transmission Capabilities Through the "Source Wheel", the "Receiver Wheel", and the Ground on Prototype 4

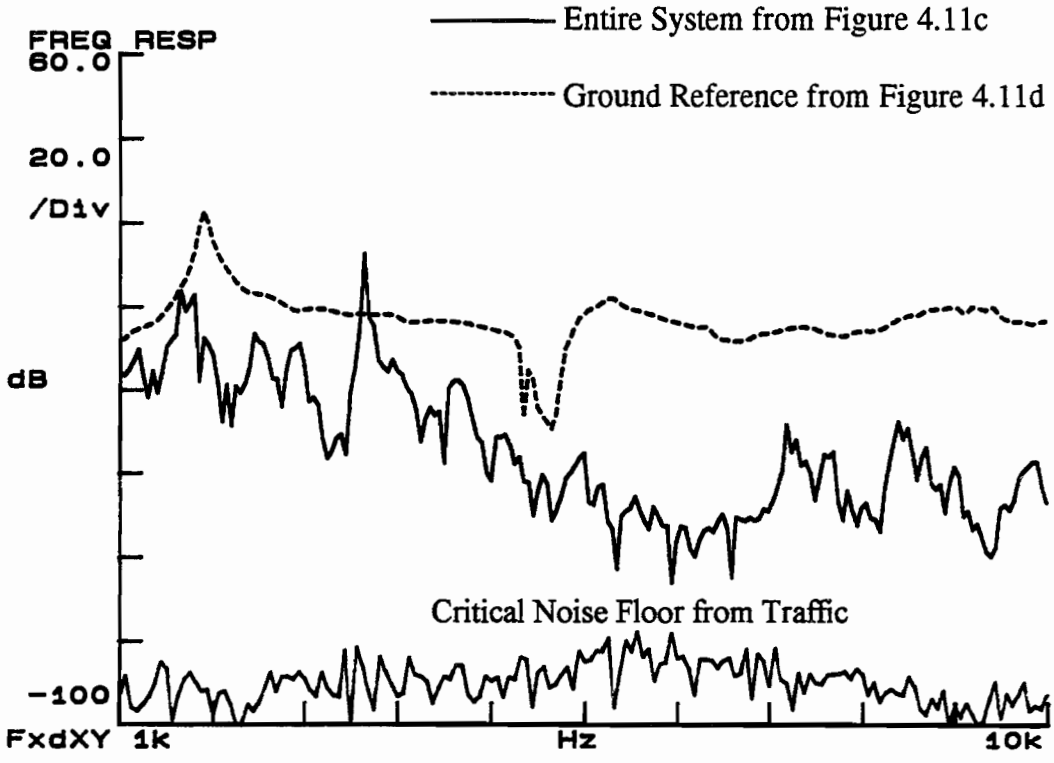

Figure 4.13: Comparison Plot of the Frequency Response for Testing Signal Transmission Capabilities Through the Entire System Relative to the Ground on Prototype 4

As shown in Table 4.3 and Figure 4.12, approximately 4.5 times (on a linear scale) more of the signal was lost in the "receiver wheel" than in the "source wheel". In addition, a larger peak force output was obtained with the shaker on the ground than with the shaker on the "source wheel", approximately 342 lbs. (1521.3 N) versus 180 lbs. (800.7 N) respectively. This was expected since the ground more closely represents an infinite impedance than does the "source wheel". Again, it should be noted that the piezoelectric shaker is capable of much higher forces than those reported in Table 4.3. However, resonances within the system while sweeping from 1 to 10 kHz caused excessively large accelerations and, thus the accelerometer faulted at a higher force output at certain frequencies resulting in unreliable data. Therefore, once a testing frequency is established in the actual system, a higher force output may be obtained depending on the system response at that frequency. Finally, Table 4.3 suggests a slight increase in the signal strength with the shaker on the "source wheel" and the accelerometer on the "receiver wheel" relative to the combined losses through both the "receiver wheel" and the "source wheel". This might infer that signal transmission was occurring through the trailer, problems were occurring with the equipment, or signal transmission was occurring through the air. This problem had to be evaluated and corrected in the final prototype trailer-mounted system.

4.4 Prototype Trailer-Mounted System

To address the previously discussed problem, transmission through the trailer was first evaluated. Tests were conducted in the laboratory with the "receiver wheel" both on the ground and suspended. (The "ground is actually the polished floor in the basement of the UT Civil Engineering building.) In addition, tests were also conducted with the hinge connected and disconnected. For all four cases, shown in Figures 4.14 and 4.15, channel 1 on the analyzer was connected to the source output and channel 2 was connected to the accelerometer output. The source was located on the "source wheel" and the receiver was on the "receiver wheel". The results are shown in Figures 4.16 through 4.19. The power spectra are shown in Figures C.1 through C.4. With both the "source wheel" and "receiver wheel" on the ground and the hinge disconnected (Figure 4.17) there was almost no change in the frequency response compared to the response with the hinge connected (Figure 4.16). With the "receiver wheel" suspended (Figure 4.18), there was only a slight decrease in the signal intensity compared to the response with the "receiver wheel" on the ground (Figure 4.16). The decrease occurred between 1 kHz and approximately 2.5 kHz. Throughout the remainder of the frequency span, the responses were almost identical. Finally, with the hinge disconnected and the "receiver wheel" suspended (Figure 4.19), the response again remained similar to the previous test with the hinge

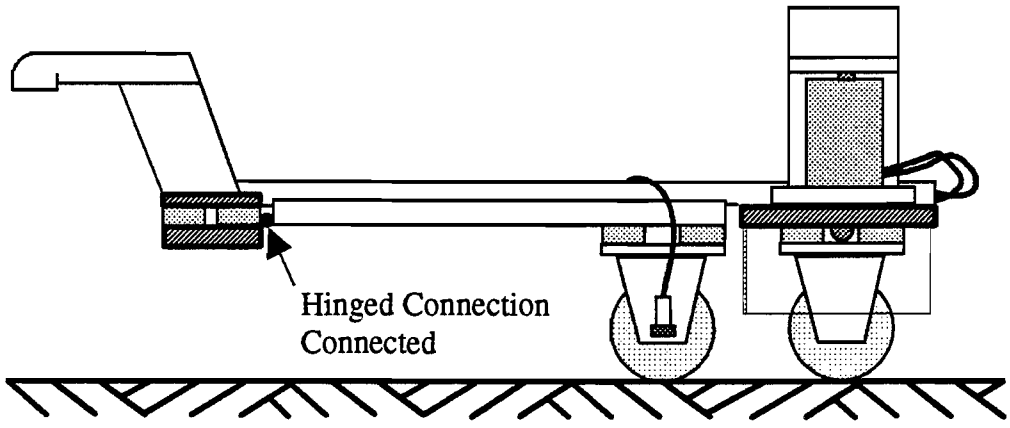

Notes: 1) Drawing not to scale
2) Section A-A from Figure 4.9

A. Fundamental Testing Configuration for Prototype 4

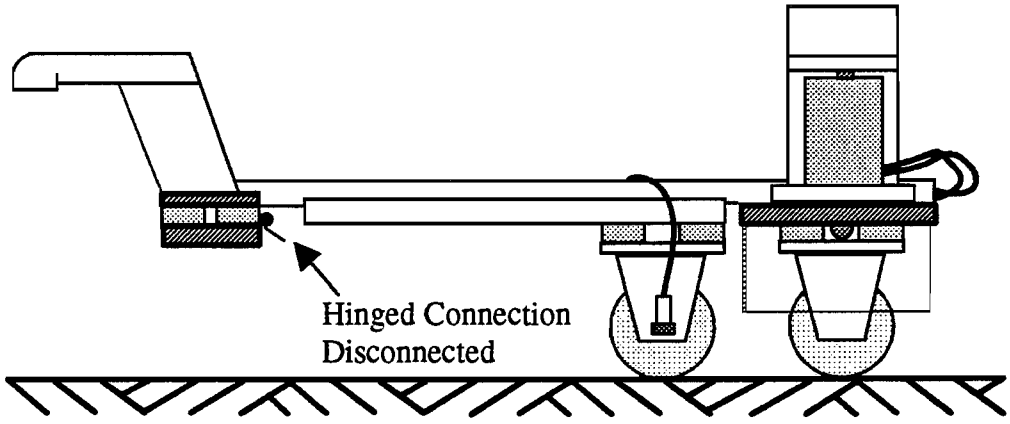

Notes: 1) Drawing not to scale
2) Section A-A from Figure 4.9

B. Fundamental Testing Configuration for Prototype 4 with the Hinge Disconnected

Figure 4.14: Fundamental Testing Configuration for Prototype 4 Laboratory Tests

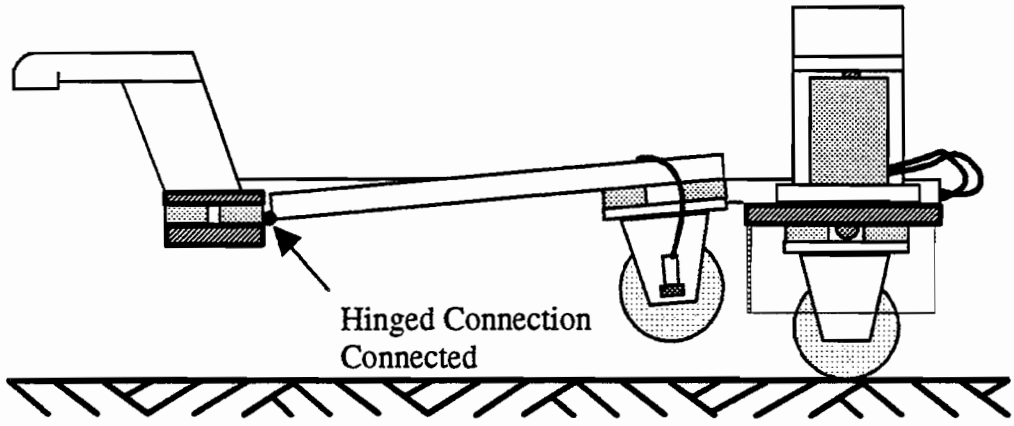

Notes: 1) Drawing not to scale
2) Section A-A from Figure 4.9

A. Testing Configuration for Prototype 4 with the "Receiver Wheel" Suspended

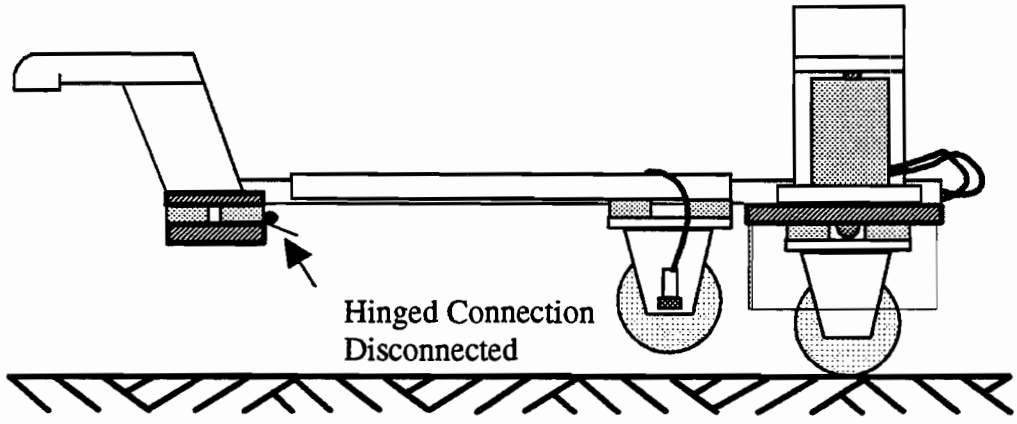

Notes: 1) Drawing not to scale
2) Section A-A from Figure 4.9

B. Testing Configuration for Prototype 4 with the "Receiver Wheel" Suspended and the Hinge Disconnected

Figure 4.15: Testing Configuration for Prototype 4 Laboratory Tests Involving the Suspension of the "Receiver Wheel"

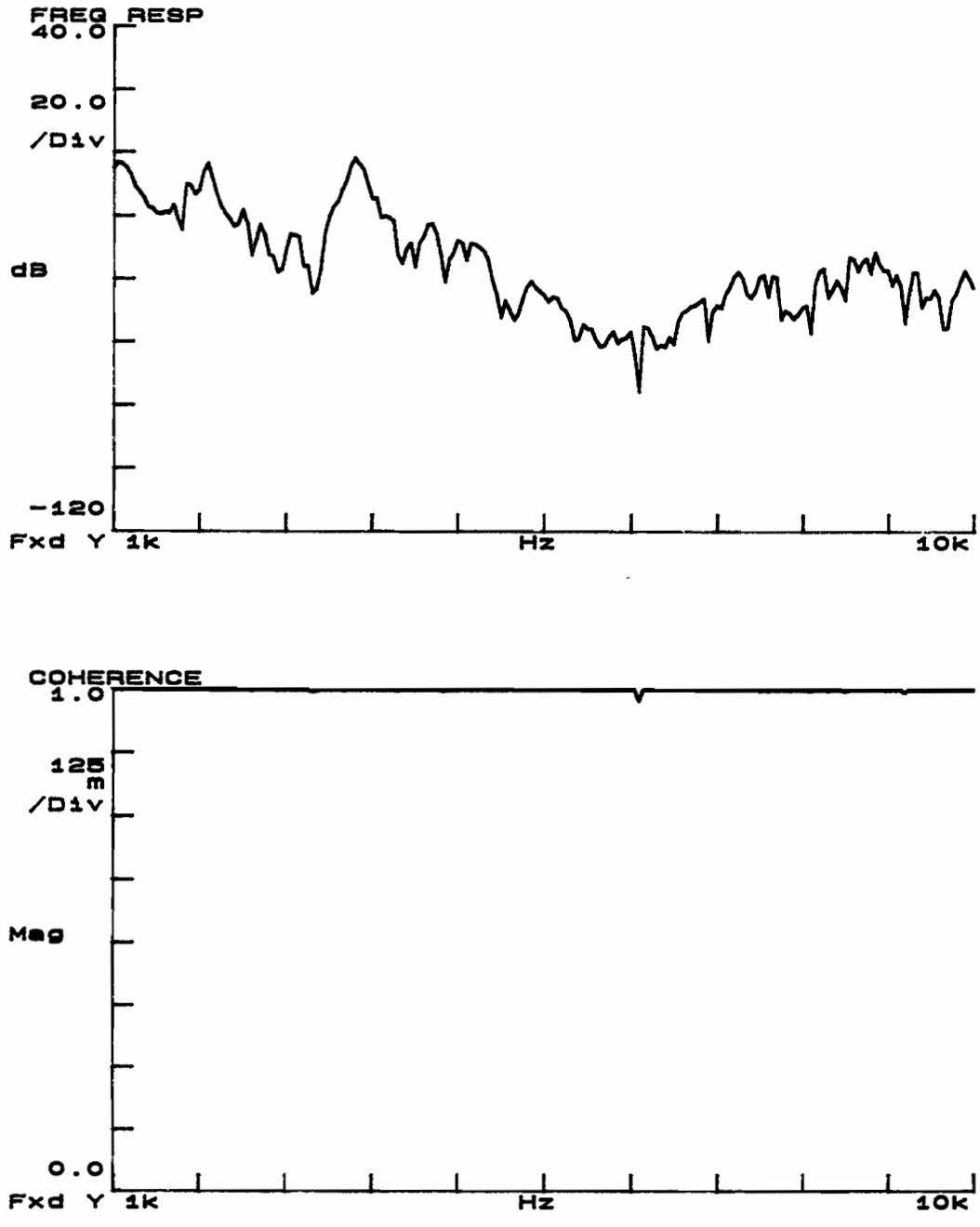

Figure 4.16: Frequency Response and Coherence for Signal Transmission Testing on Prototype 4 with Channel 1 Connected to the F8 Shaker Output and Channel 2 Connected to the Accelerometer on the "Receiver Wheel" as Shown in Figure 4.14a

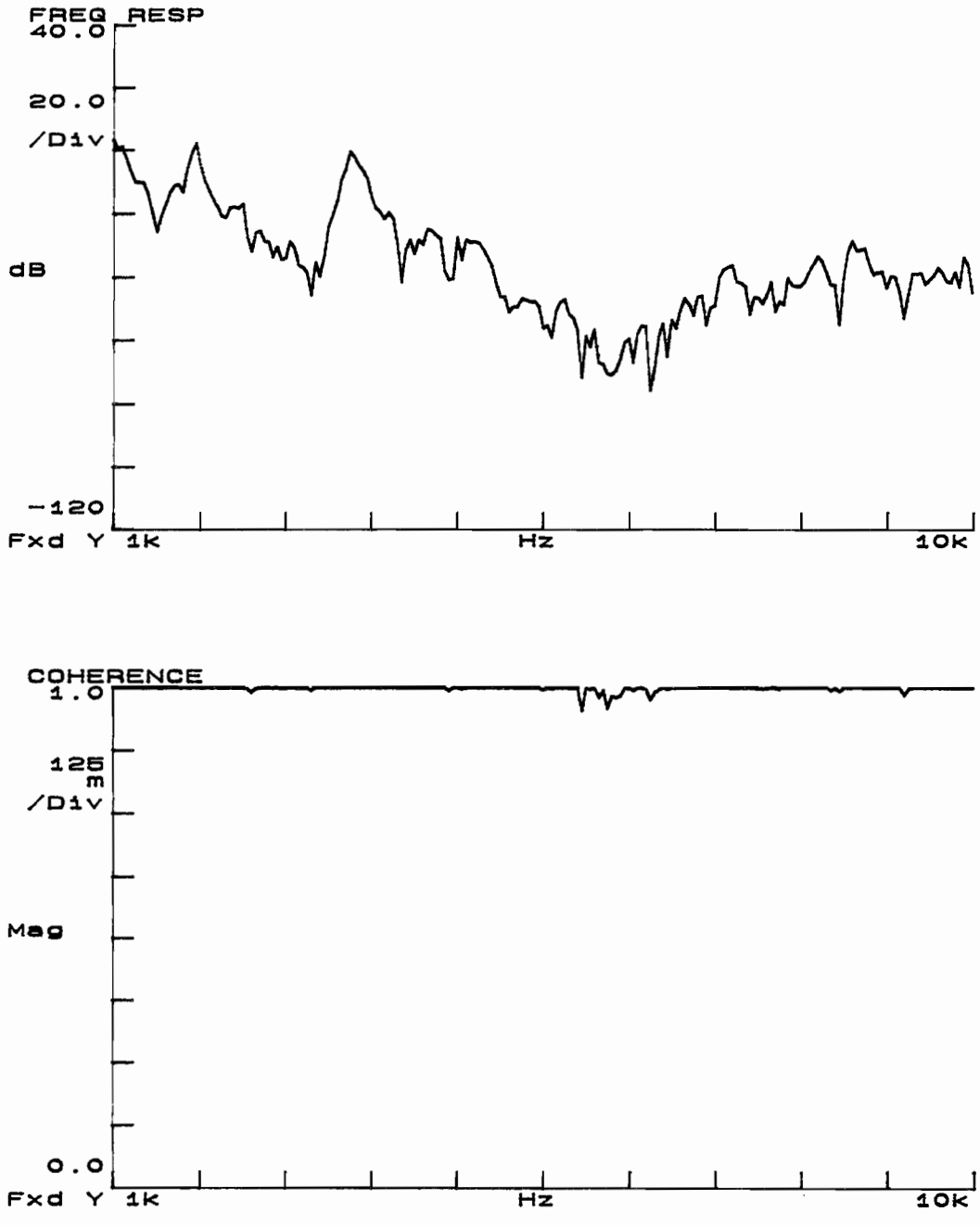

Figure 4.17: Frequency Response and Coherence for Signal Transmission Testing on Prototype 4 with the Hinge Disconnected, Channel 1 Connected to the F8 Shaker Output, and Channel 2 Connected to the Accelerometer on the "Receiver Wheel" as Shown in Figure 4.14b

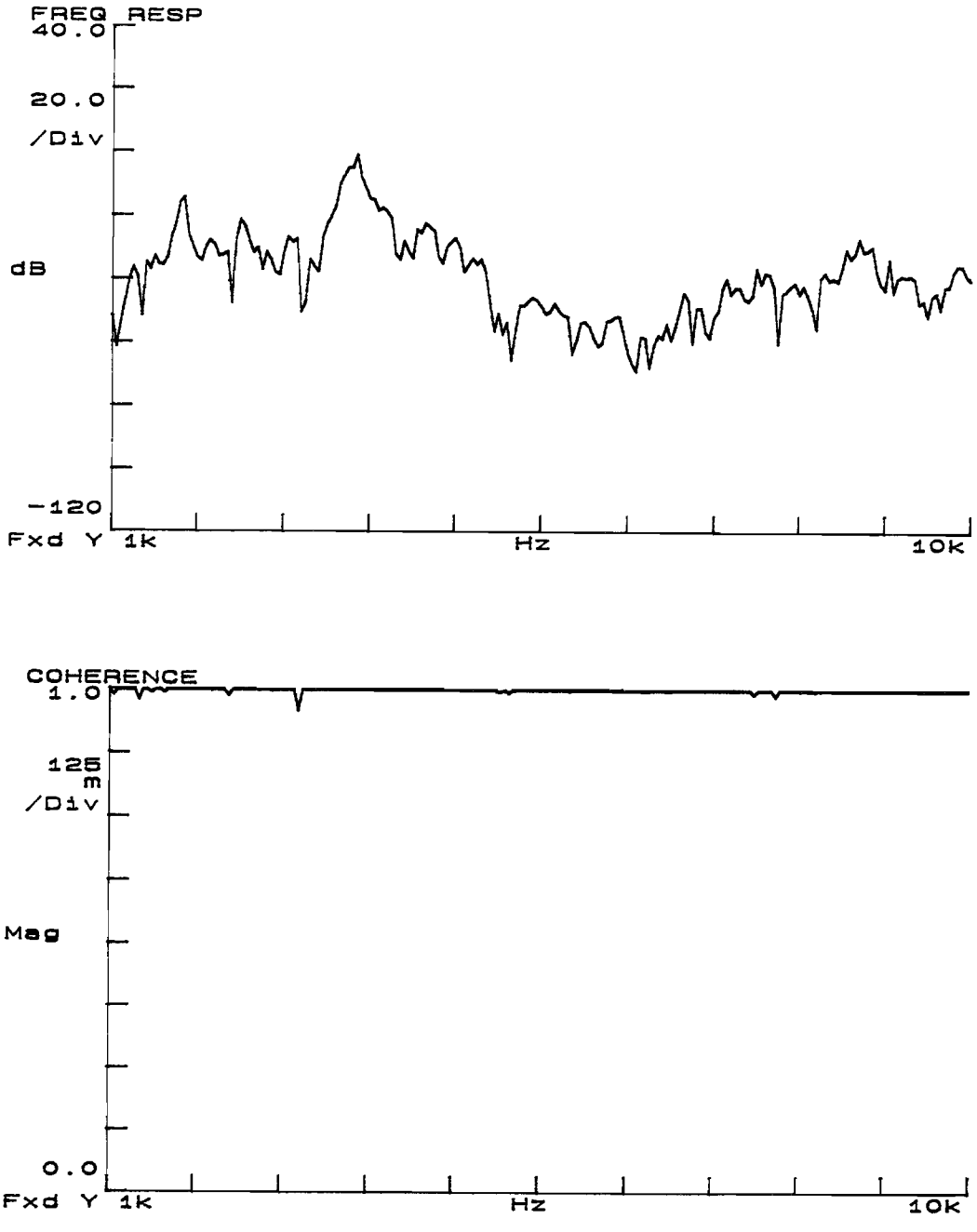

Figure 4.18: Frequency Response and Coherence for Signal Transmission Testing on Prototype 4 with the "Receiver Wheel" Suspended, Channel 1 Connected to the F8 Shaker Output, and Channel 2 Connected to the Accelerometer on the "Receiver Wheel" as Shown in Figure 4.15a

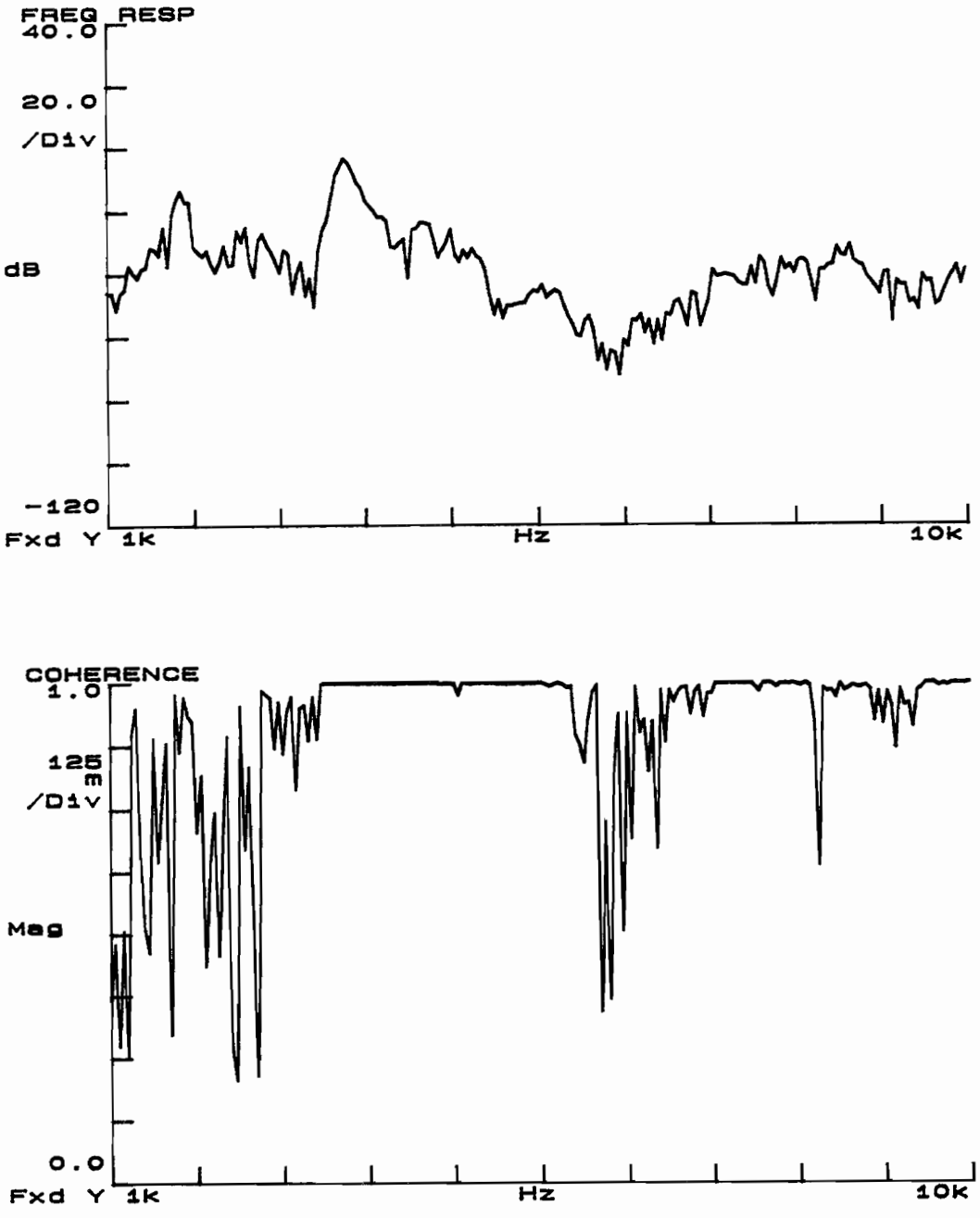

Figure 4.19: Frequency Response and Coherence for Signal Transmission Testing on Prototype 4 with the "Receiver Wheel" Suspended, the Hinged Connection Disconnected, Channel 1 Connected to the F8 Shaker Output, and Channel 2 Connected to the Accelerometer on the "Receiver Wheel" as Shown in Figure 4.15b

connected and the "receiver wheel" on the ground. However, there was a breakdown in the coherence between 1 kHz an about 3.2 kHz and again between about 5.8 kHz and 7.5Khz as shown in Figure 4.19.

These comparisons seem to indicate that the signal from the source was not transmitting through the trailer. However, due to the breakdown in coherence with the hinge disconnected and the "receiver wheel" suspended, the hinged trailer connection was modified. This was accomplished by using small rubber washer isolators and very soft Styrofoam pads between the hinge and the aluminum channel as shown in Figure 4.20.

Since the frequency responses remained almost constant during all of the previous tests, it was concluded that the signal transmission problem must be either equipment related or occurring through the air. First, testing was conducted to asses the sensitivity of the accelerometer. The concept was to determine if the receiver could accurately detect an order of magnitude change in the intensity of the source signal. Two sets of tests were conducted. One with the source operating at 750 mV and one with the source operating at 75 mV. Each set included the "source wheel" alone, the "receiver" wheel alone, and the entire system. The results (Appendix D) show an average receiver signal intensity drop of 20dB for a corresponding single order of magnitude drop in the source signal, which is consistent with the decibel concept defined in Figure 3.9.

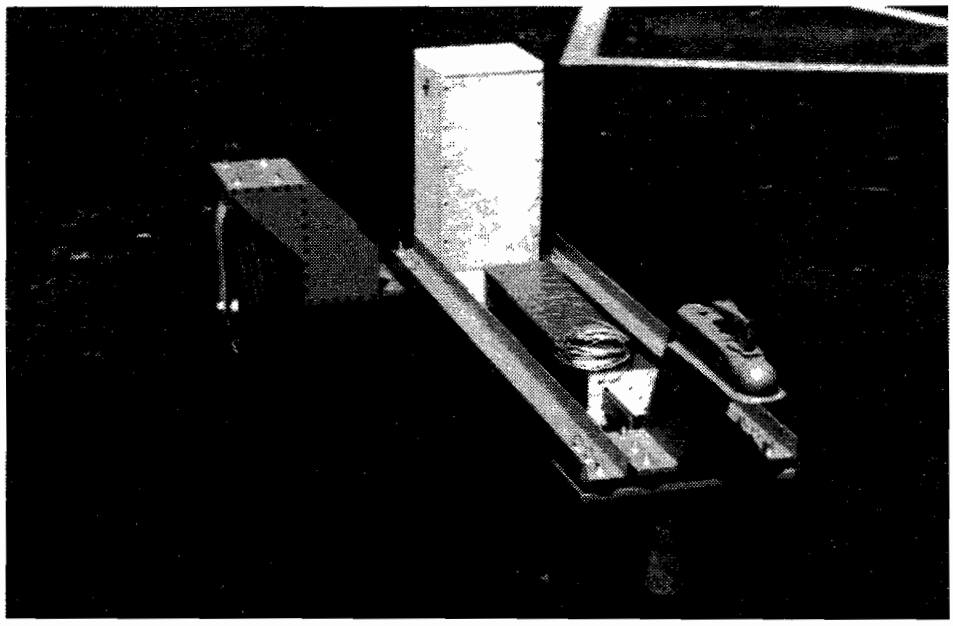

A. Overall View of Final Prototype Trailer-Mounted System

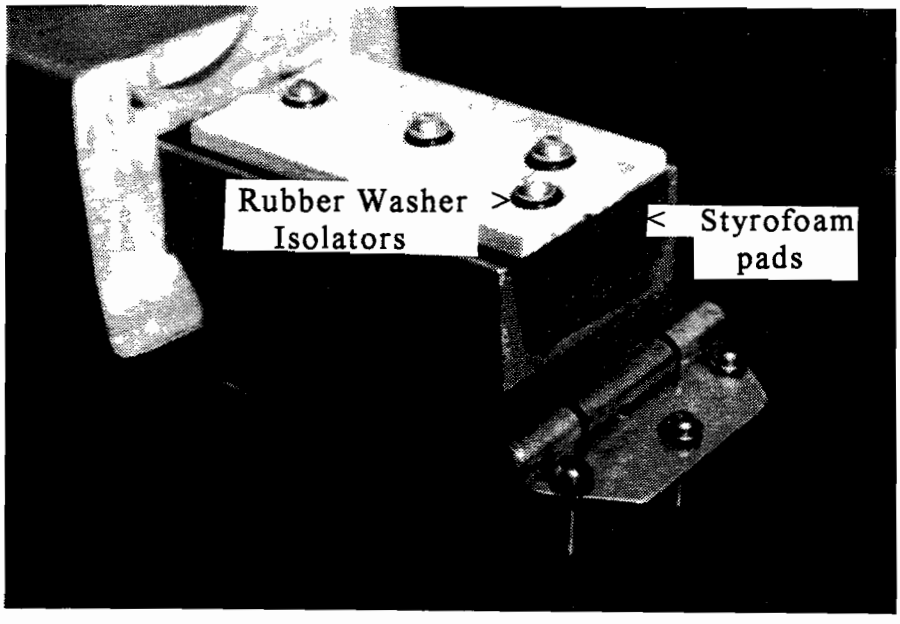

B. Detail of Hinge Modification to Correct Signal Transmission through the Trailer

Figure 4.20: Prototype Trailer-Mounted System and Corresponding Hinge Modification

Because of the receiver accelerometer's ability to detect the magnitude difference in the signal intensity, it was concluded that the accelerometer sensitivity was not the problem and thus, the signal transmission problem must have been occurring through the air. It should be noted that previous testing (Section 4.1) concluded air transmission would not be a problem. However, these tests did not take into account the effect of the trailer or the pavement on signal propagation through the air, that is, reflections from these elements contributing to the transmission through the air. Therefore, modifications were made to the trailer to isolate, as completely as possible, the source and minimize any air transmission. The modifications consisted of building acoustical boxes, similar to high-quality speaker cabinets, around the source and "source wheel" and the "receiver wheel". In addition, the aluminum channel connecting the "receiver wheel" to the main trailer frame was covered with acoustical foam tiles. Finally, the source was rigidly attached to the "source wheel" to improve the signal transmission. The resulting prototype trailer-mounted system (Figure 4.20a) was tested using the same equipment, parameters, and configuration as previously tested. As before, tests were run with the "receiver wheel" both on the "ground" (smooth concrete floor in the laboratory) and suspended. The results are shown in Figures 4.21 through 4.24. The power spectra are shown in Appendix E. Tests were also conducted to evaluate transmission through the "source wheel", the "receiver

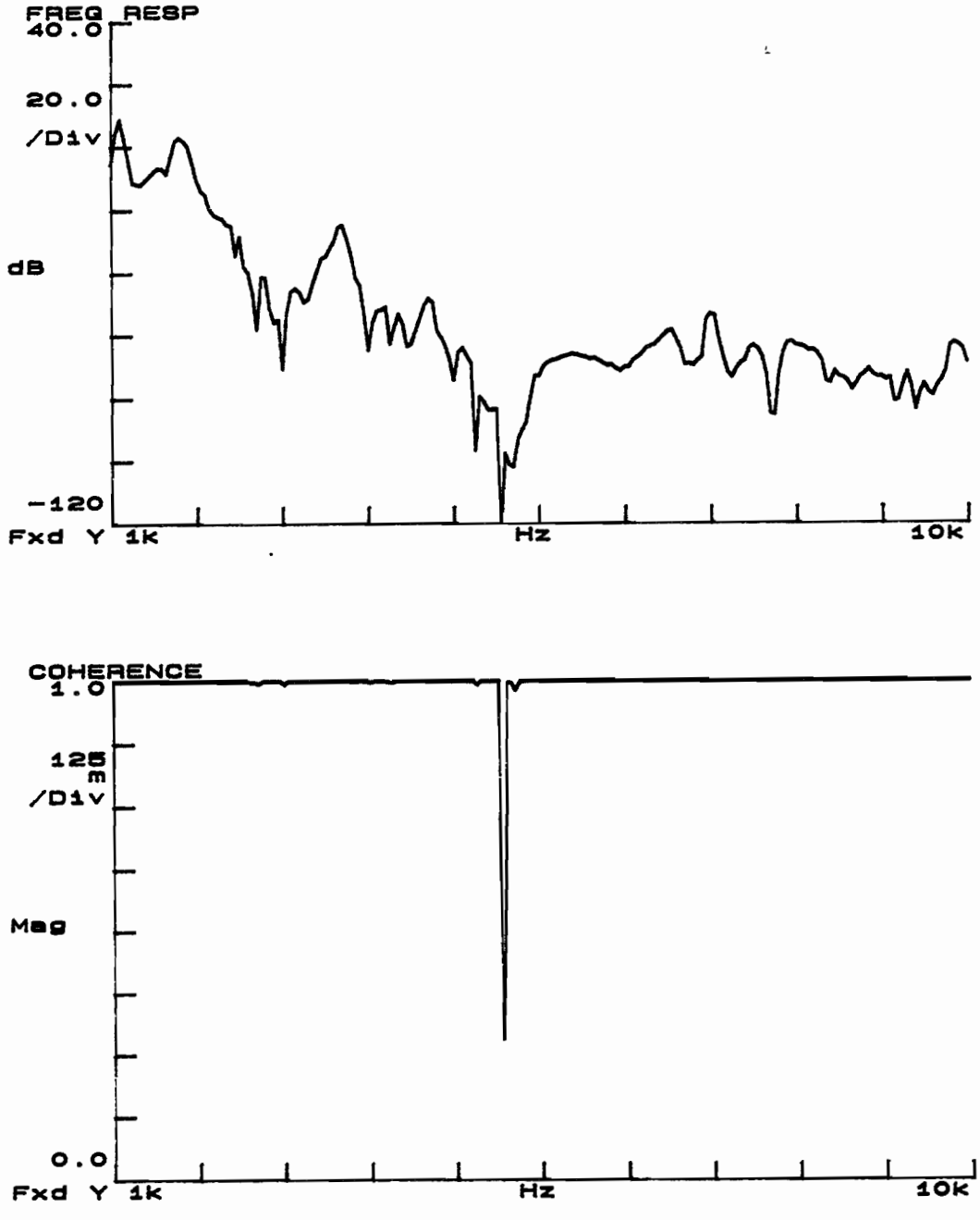

Figure 4.21: Frequency Response and Coherence for Signal Transmission Testing on Prototype Trailer-Mounted System with Channel 1 Connected to the F8 Shaker Output and Channel 2 Connected to the Accelerometer on the "Receiver Wheel" as Shown in Figure 4.14a

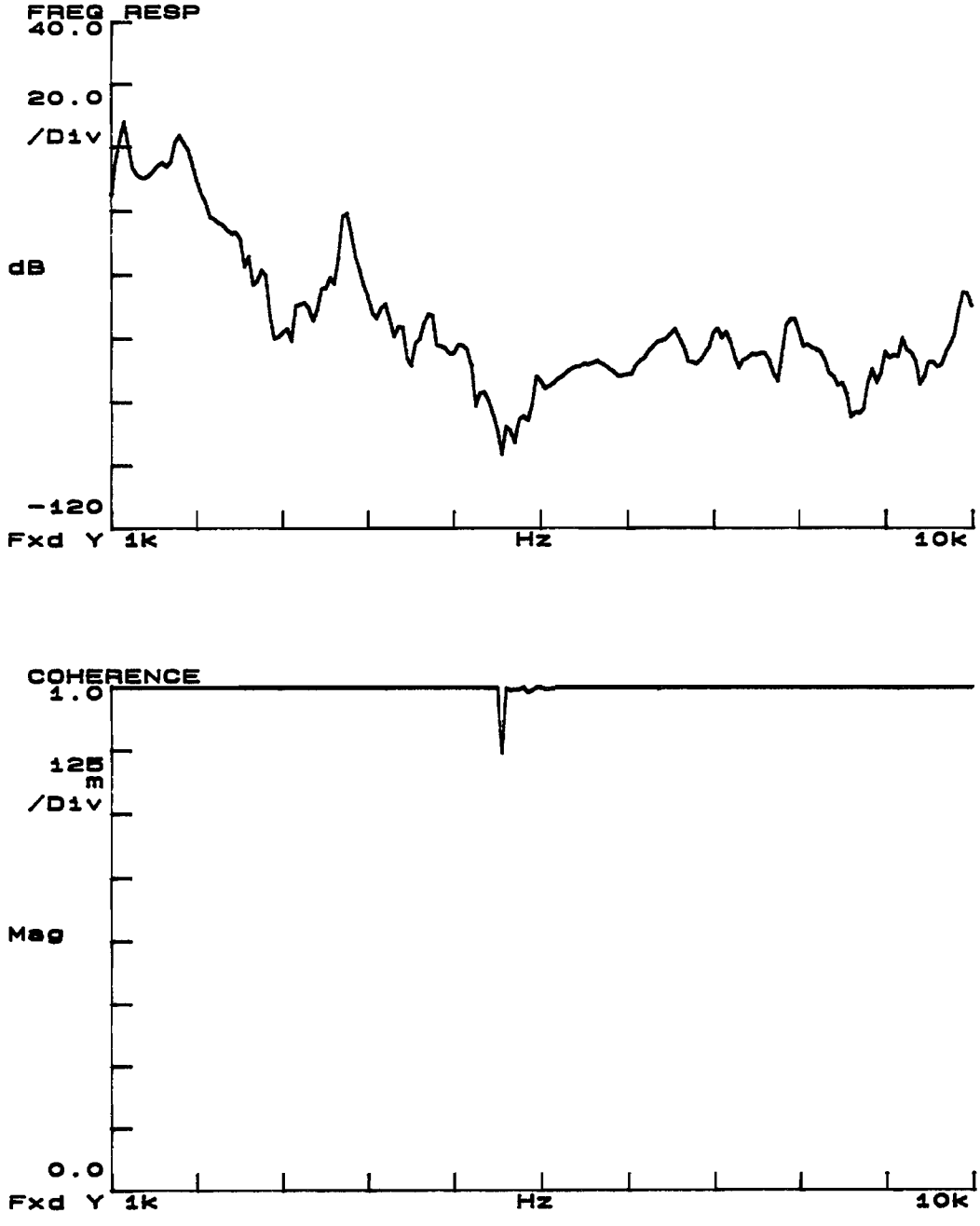

Figure 4.22: Frequency Response and Coherence for Signal Transmission Testing on Prototype Trailer-Mounted System with the Hinge Disconnected, Channel 1 Connected to the F8 Shaker Output, and Channel 2 Connected to the Accelerometer on the "Receiver Wheel" as Shown in Figure 4.14b

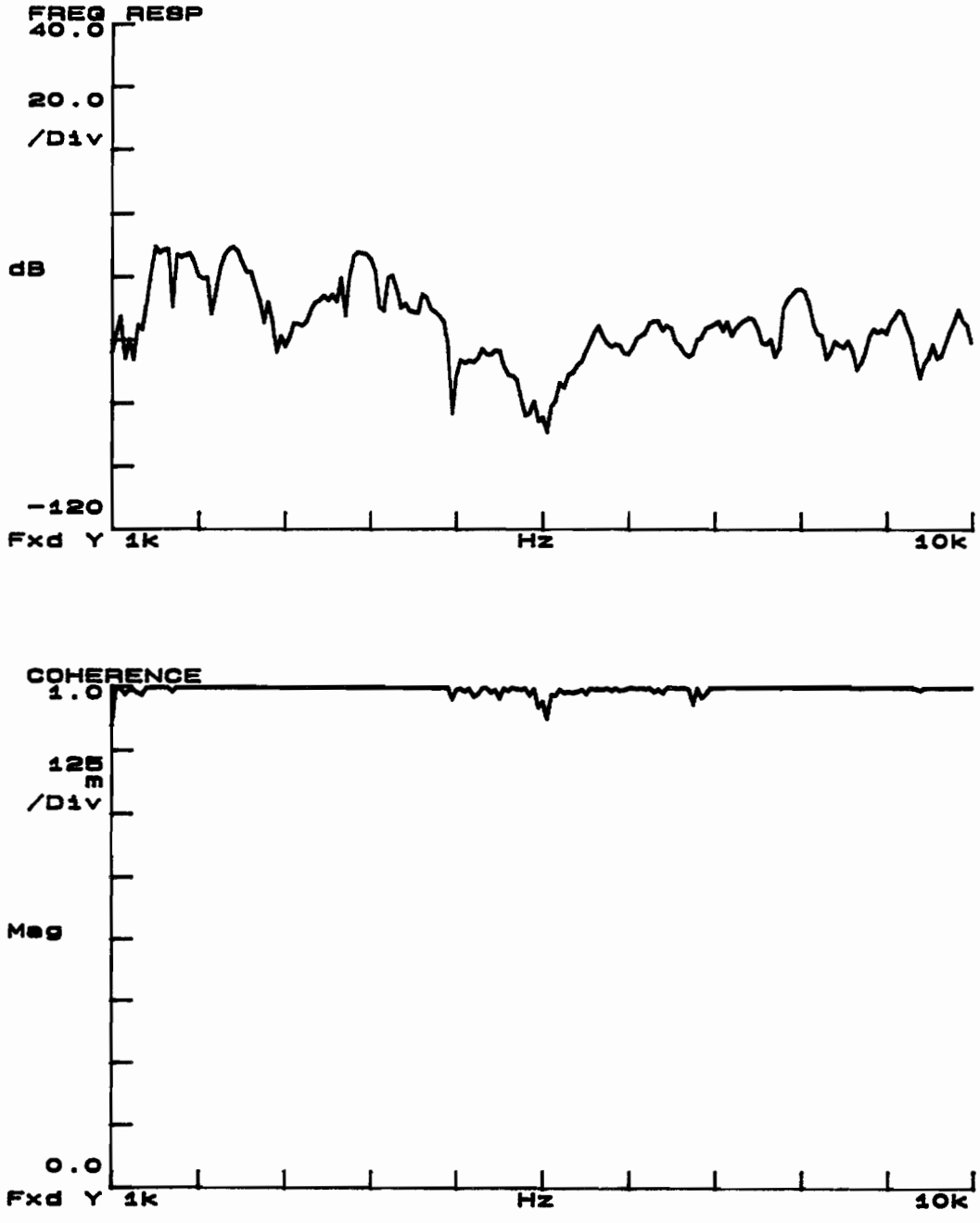

Figure 4.23: Frequency Response and Coherence for Signal Transmission Testing on Prototype Trailer-Mounted System with the "Receiver Wheel" Suspended, Channel 1 Connected to the F8 Shaker Output, and Channel 2 Connected to the Accelerometer on the "Receiver Wheel" as Shown in Figure 4.15a

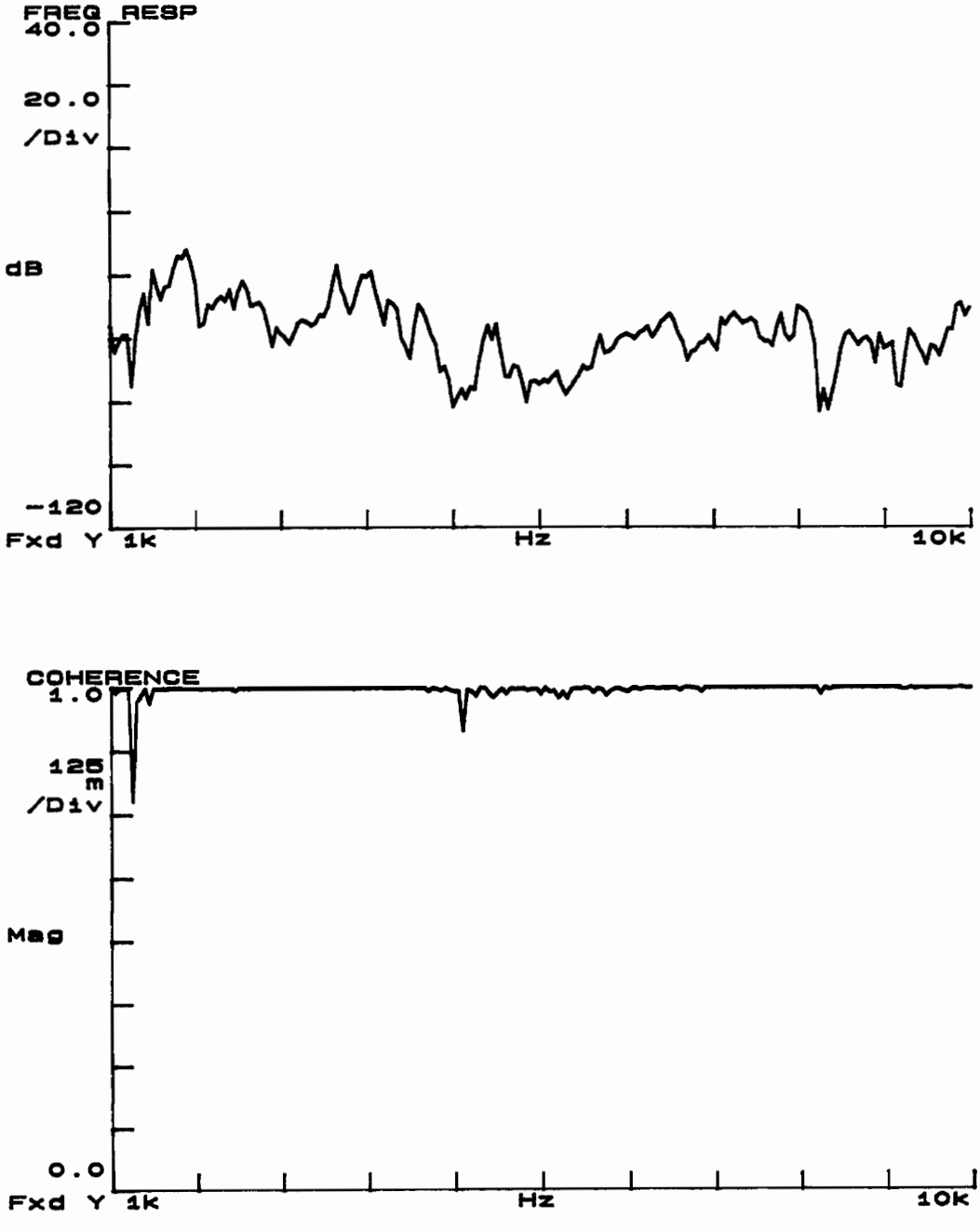

Figure 4.24: Frequency Response and Coherence for Signal Transmission Testing on Prototype Trailer-Mounted System with the "Receiver Wheel" Suspended, the Hinged Connection Disconnected, Channel 1 Connected to the F8 Shaker Output, and Channel 2 Connected to the Accelerometer on the "Receiver Wheel" as Shown in Figure 4.15b

wheel", and the entire system. The frequency responses are summarized in Figures 4.25 and 4.26 and the overall results are tabulated in Table 4.4. The individual frequency responses, coherence functions, and power spectra are located in Figures F1 through F8.

The overall results are tabulated in Table 4.4. They generally show an overall decrease in the magnitude of the signal for the tests performed. This was most likely due to the substantial reduction of any outside noise interference which may have been present in any previous tests. In addition, there still appears to be a large signal loss in the "receiver wheel" compared to the "source wheel". However, there is a slight improvement ($\leq$ 20dB) in the trailer response between 1 kHz and $\approx$ 2.5KHz. Furthermore, the performance of the prototype trailer-mounted system is above the minimum level (-80 dB roadway noise level) previously determined. Based on the design and analysis, this was determined to be the best possible solution that would meet the original design criteria.

As previously reported in Figure 3.5a, the maximum response for the piezoelectric shaker occurred at approximately 2 kHz. In addition, the blocked force output reported by Wilcoxon for the Model F8 shaker at 2 kHz is approximately 200 lbs (890.0 N), as shown in Figure 4.27, which is roughly 150 lbs. (667.2 N) above the estimated peak force for the electromagnetic shaker (Section 3.4). Therefore, it was determined that the prototype trailer-mounted

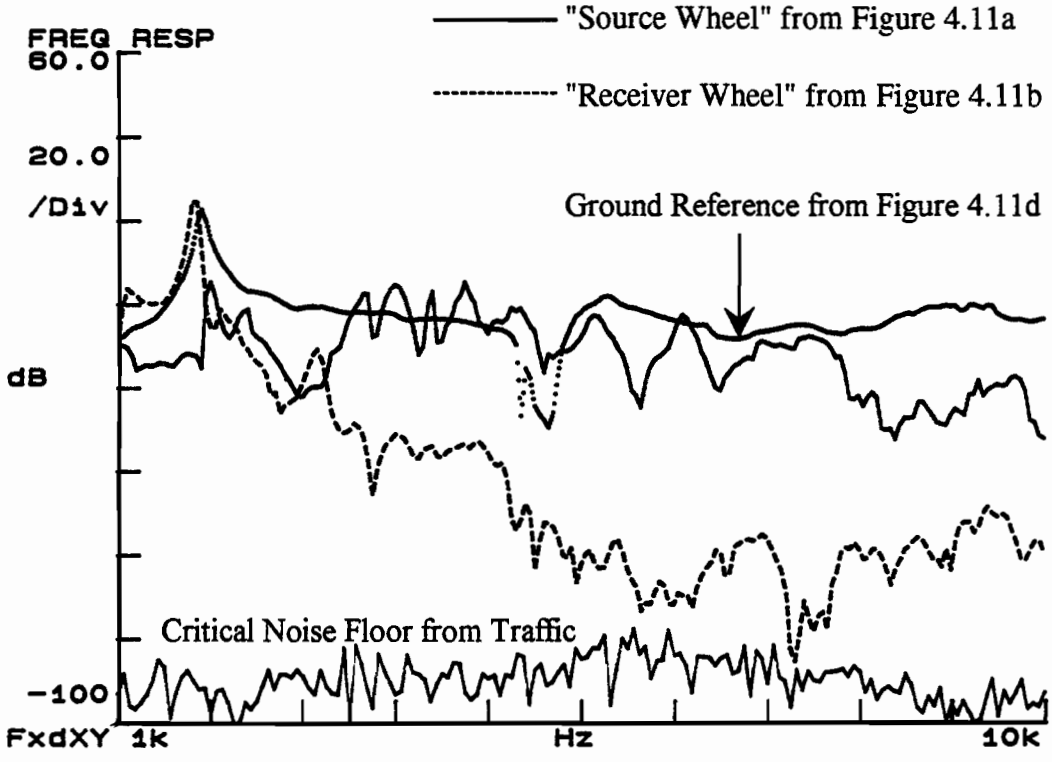

Figure 4.25: Comparison Plot of the Frequency Response for Testing Signal Transmission Capabilities Through the "Source Wheel", the "Receiver Wheel", and the Ground on Prototype 4 with Acoustical Insulation Around Both the Source and the Receiver

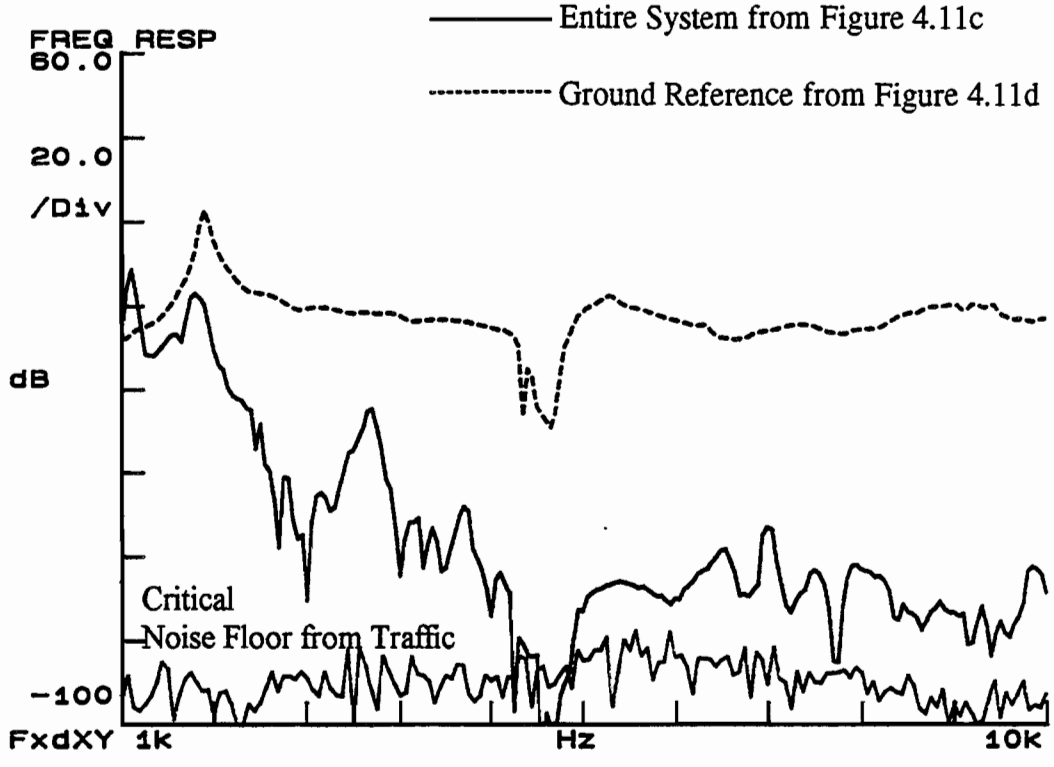

Figure 4.26: Comparison Plot of the Frequency Response for Testing Signal Transmission Capabilities Through the Entire System Relative to the Ground on Prototype 4 with Acoustical Insulation Around Both the Source and the Receiver

Table 4.4: Summary of Laboratory Testing on the Prototype Trailer-Mounted System Evaluating Signal Transmission Through Each Trailer Component

Source/ Accelerometer Location	Frequency Response 1 to 10KHz (in dB)		Coherence (quality)	Power Spectrum Ch.1 (Force Output from Shaker) (in pounds)		Power Spectrum Ch. 2 (Accelerometer Output) (in dB)	
Ground/Ground	Maximum	30.76	Excellent	Maximum	172.02	Maximum	-4.41
	Average	-3.11		Average	6.42	Average	-26.96
	Minimum	-20.73		Minimum	0.03	Minimum	-52.35
Source Wheel/ Ground	Maximum	16.35	Excellent	Maximum	295.80	Maximum	-20.73
	Average	-31.51		Average	8.92	Average	-52.52
	Minimum	-70.36		Minimum	0.14	Minimum	-80.02
Ground/ Receiver Wheel	Maximum	16.40	Excellent	Maximum	193.34	Maximum	-30.85
	Average	-34.06		Average	6.20	Average	-58.17
	Minimum	-73.21		Minimum	0.02	Minimum	-80.92
Source Wheel/ Receiver Wheel	Maximum	-3.69	Good	Maximum	297.90	Maximum	-41.72
	Average	-52.36		Average	9.16	Average	-72.97
	Minimum	-88.98		Minimum	0.00	Minimum	-90.48

Notes

1 One volt source input

2 Swept frequency mode of operation

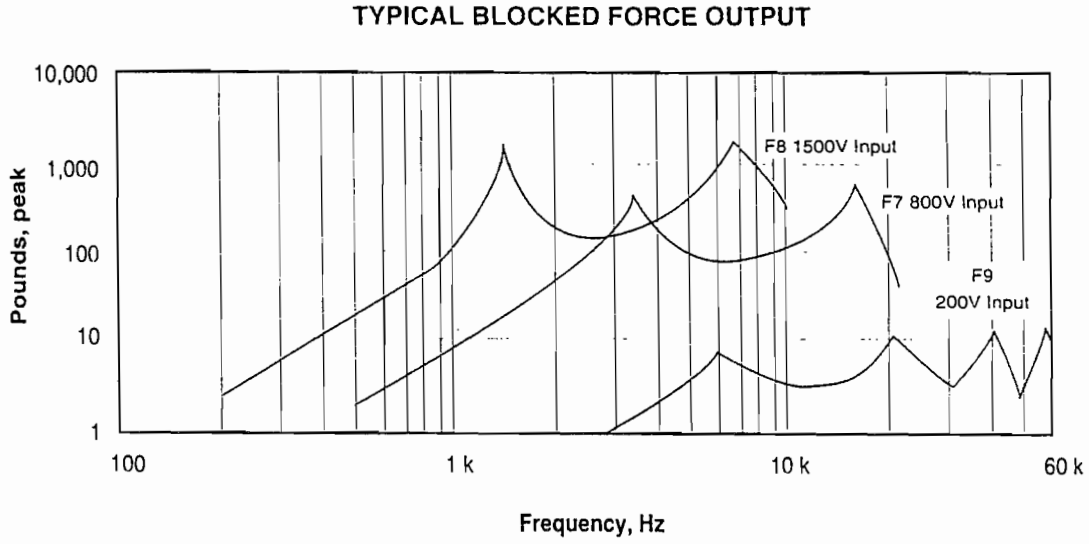

Figure 4.27: Typical Blocked Force Output for the Wilcoxon Models F7, F8, and F9 Piezoelectric Shakers (Wilcoxon Research, 1990)

system should be operated at 2 kHz to take advantage of the performance improvement from previous attempts at prototype. However, operating near 1.5 kHz, which shows a peak force in excess of 1000 lbs (4448.2 N), would be even better and should be considered in the future.

4.5 Summary

The design and development process involved a long and tedious evolution. The final result was a trailer-mounted system. A single trailer supports both the "source wheel" and the "receiver wheel". Signal transmission through the trailer was avoided by an intricate hinge design and by isolating the signal at all connection locations. Signal transmission into and out of the pavement was optimized by custom designing both the "source wheel" and the "receiver wheel", with special attention given to the axles. In addition, acoustical boxes were added to both the "source wheel" and "receiver wheel" to eliminate the influence of any outside noise components and any airborne noise generated by the source. Laboratory testing of the prototype vehicle and an analysis of the piezoelectric shaker established a source testing frequency of 2 kHz, with testing at 1.5 kHz showing even more promise. The Wilcoxon F8 Piezoelectric Shaker System was used to generate the required signal. This signal was received by a high sensitivity Wilcoxon

Model 728T accelerometer. With the prototype trailer-mounted system developed, field testing could be initiated.

Chapter Five
Preliminary Field Studies

5.1 Introduction

Field studies were conducted at a previously constructed concrete pavement research facility at the Balcones Research Center (BRC) of UT. This pavement facility was designed and built with known defects, including a crack, void and delamination, making the facility ideal for initial testing and pavement irregularity characterization. The facility and the results from the pavement irregularity testing are first discussed in this chapter. The results of testing with the prototype trailer-mounted system at BRC are then examined and compared with the initial tests.

5.2 Rigid Concrete Pavement Test Facility

Preliminary testing was conducted at the concrete pavement research facility at BRC. Fundamental tests were conducted with the source and receiver directly on the pavement to characterize the various irregularities. After establishing a "signature" for each irregularity, the prototype trailer-mounted system was tested. The results were then compared to the established "signatures".

The BRC test facility was designed and built for the application of nondestructive testing techniques, such as the Dynaflect, the Falling Weight Deflectometer, and the Spectral

Analysis of Surface Waves (SASW), on a rigid concrete pavement system (White et al., 1986). A plan view and material profile of the BRC test facility are shown in Figures 5.1 and 5.2, respectively. The test facility contains two voids that are approximately 3 feet by 3 feet by 1 inch deep (91.4 cm x 91.4 cm x 2.5 cm). The "voids" were created by placing foamed styrene into preformed void locations. After the concrete was poured and dry, a solvent was sprayed into the void to dissolve the styrene.

In addition to the voids, the test facility has a movable section of pavement used to examine load transfer across various joint sizes. For the purpose of this study, the joint was assumed to represent a crack and the movable section (which was underlain by 3 sheets of 4 mil polyethylene) was assumed to represent a delaminated pavement. It should be noted that delaminations typically occur at or above the level of reinforcing steel within what is generally considered the top pavement layer. However, since the BRC test facility was already constructed at the time of this research, use of the movable slab to represent a delaminated system was considered reasonable.

5.3 Preliminary Field Test Configuration

Before characterizing the known pavement irregularities, a preliminary testing configuration, consistent with the original design concept, was established. The configuration involved utilization of

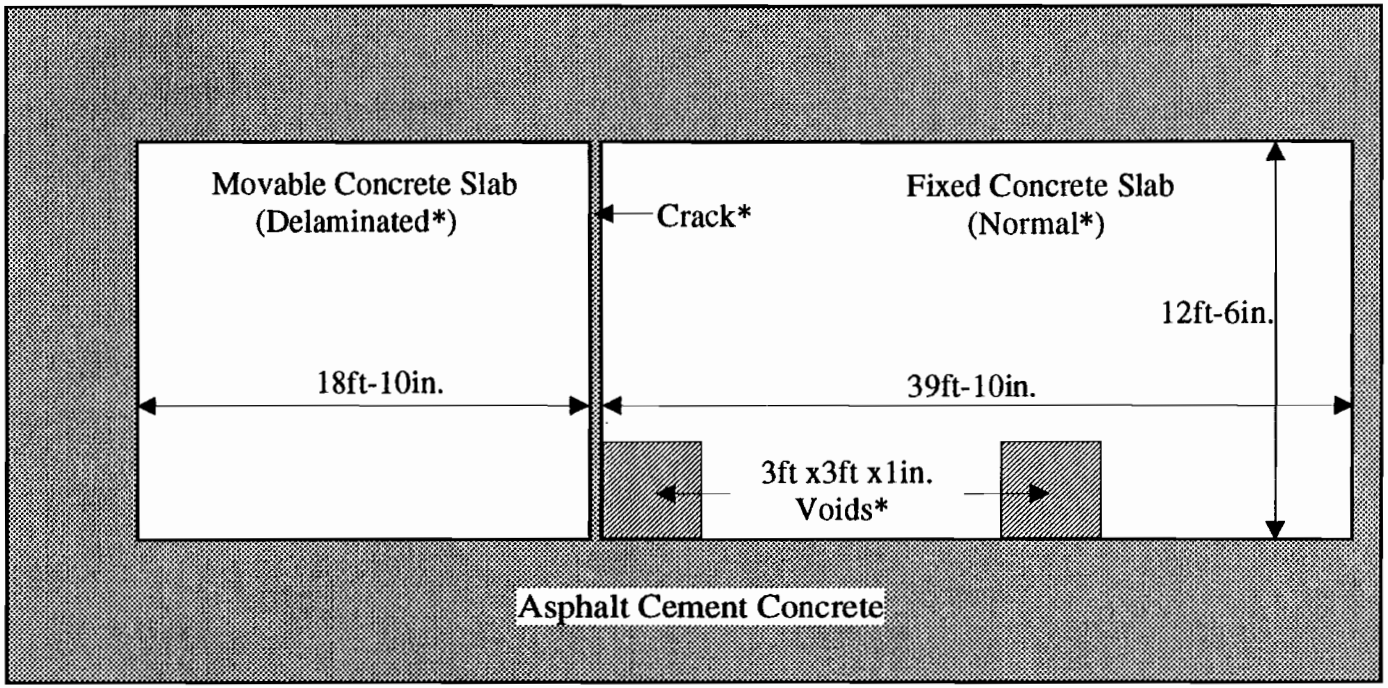

NOTE: Drawing not to scale

* Refers to descriptions used in Chapter 5

Figure 5.1: Plan View of BRC Pavement Test Facility Showing Pavement Irregularity Locations (from Sheu, 1987)

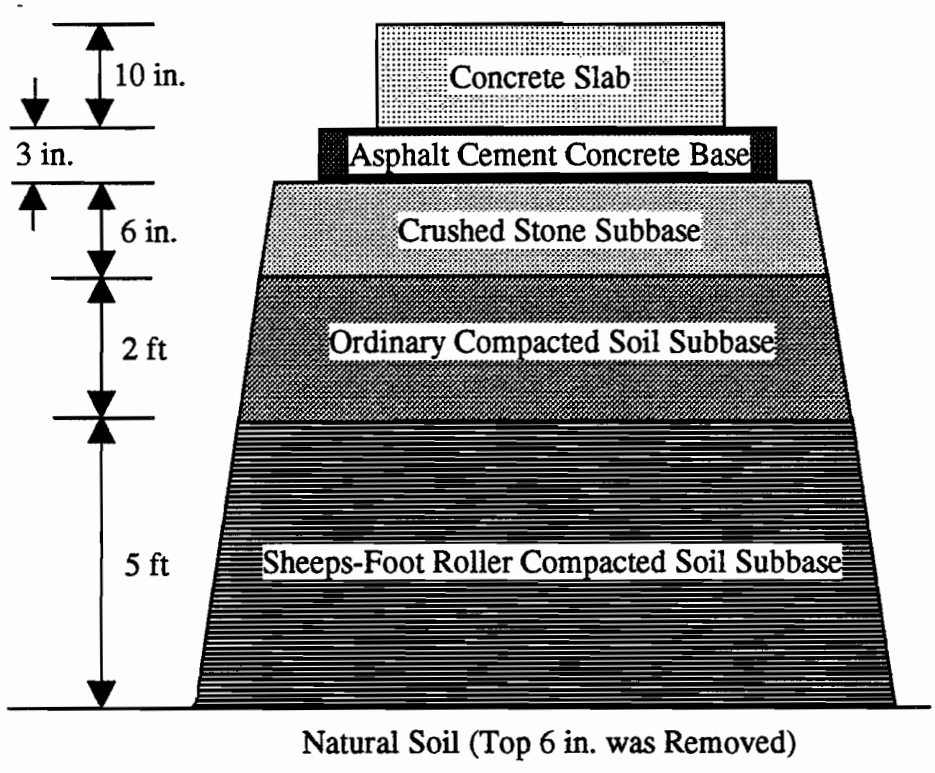

NOTE: Drawing not to scale

Figue 5.2: Material Profile at BRC Pavement Test Facility (after Sheu, 1987)

the source and receiver directly on the pavement, which represents the optimum performance. In addition, the configuration was designed to closely model the prototype trailer-mounted system. The configuration, shown in Figure 5.3, was based on a "marching" concept. This concept involved the source and receiver "marching" along the pavement in two-inch (5.1-cm) increments at a fixed source-to-receiver spacing of six inches (15.2 cm). The six-inch (15.2-cm) source-to-receiver spacing was based upon the distance between the "source wheel" and the "receiver wheel" on the prototype vehicle.

Testing with this configuration at the BRC Test Facility is shown in Figure 5.4. The Wilcoxon Model F8 piezoelectric shaker (Section 3.2.1), used to generate the signal, is contained in a wood and acrylic support system so that the moving element is in direct contact with the pavement. The Wilcoxon Model 728T accelerometer (Section 3.2.2), used to receive the signal, is magnetically placed on washers which are epoxy glued to the pavement surface. The washers are placed in two-inch (5.1-cm) increments across each of the pavement defects and a 6-inch 15.2-cm) source-to-receiver distance was used. By testing at each washer location, the effect of each anomaly can be evaluated under optimum testing conditions.

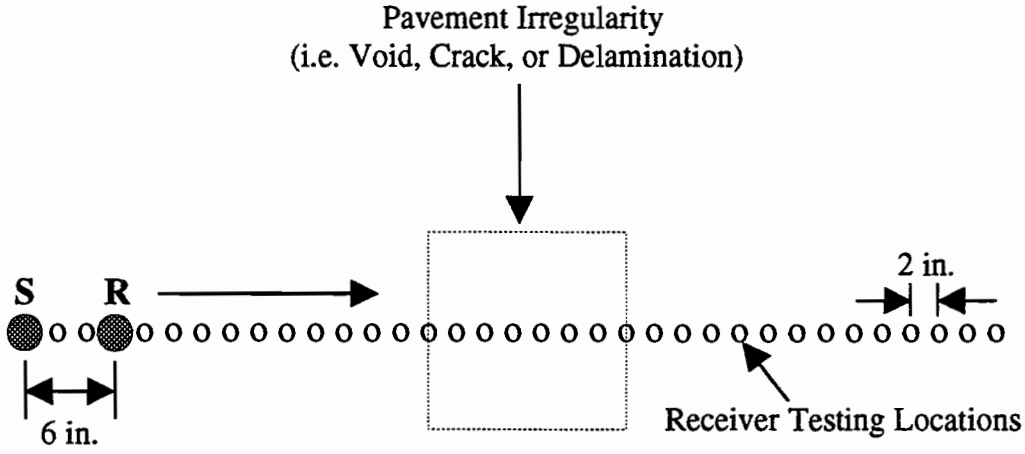

Note: S=Source; R=Receiver(Accelerometer)

Concept: Source and Receiver "march" along in two-inch increments at a fixed source-to-receiver distance of six inches

Figure 5.3: Testing Configuration Showing the "Marching" Concept used in Preliminary Testing at the BRC Test Facility

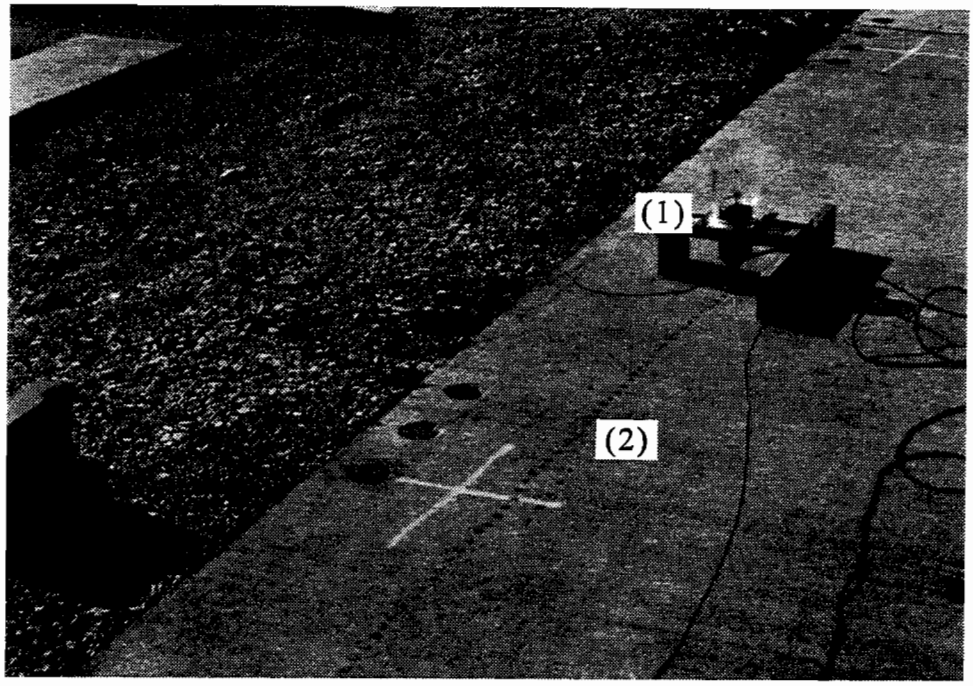

(1) Piezoelectric Shaker in the Wood/Acrylic Support System
(2) Washers Affixed to the Pavement Surface to Magnetically Attach the Accelerometer

Figure 5.4: Application of Field Testing Configuration at the BRC Test Facility

5.3.1 Characterization of Pavement Irregularities

The prototype vehicle generates a 2-kHz fixed sinusoid, as discussed in Chapter 4, and then looks at differences in the voltage output from the pavement at that frequency. Therefore, a 2-kHz fixed sinusoid was used in the characterization process. Furthermore, the source was operated with an input level of 2 volts, which corresponded to an approximately 61.5 lb (273.6 N) shaker force output. It should be noted that Wilcoxon reports the Model F8 shaker to have an approximately 200 lb (890.0 N) force output at 2 kHz as discussed in Section 4.4. However, this is with an infinite impedance, a voltage input of approximately 3 volts, and the matching network set at 1150 Vrms.

Only the voltage output from the accelerometer was used in the characterization process. This output was read directly from the multimeter and corresponds to the amplitude of the power spectrum at 2 kHz from channel 2 on the analyzer. Using the previously described configuration (Section 5.3), each pavement anomaly was tested. Each test was conducted and reported twice to confirm the proposed "signature".

5.3.2 Crack Characterization

The first irregularity tested was the crack. The testing began 24 inches (61.0 cm) before the crack. As described in Section 5.3, tests were conducted every two inches (5.1 cm). Since the

"delaminated" section was on one side of the crack, tests could not be conducted while traveling across the crack. Therefore, to accurately test the pavement while passing over the crack, the pavement was tested by approaching the crack from the side considered to be "normal". When the receiver had just crossed the crack, the source and receiver configuration were turned around, and tests were continued while leaving the crack on the "normal" pavement. Therefore, the approaching data and the leaving data were collected on the same side of the crack.

The voltage output from the accelerometer is plotted versus distance in Figures 5.5 and 5.6 for the two sets of tests conducted on the crack. The test results reported in Figure 5.5 were obtained in September, 1991 while the results in Figure 5.6 were obtained in July, 1992. For both cases, initially a constant average signal level was observed which exhibited fluctuations on the order of 40 to 50 percent of the average signal level. The average signal was about 80 mV in Figure 5.5 and 90 mV in Figure 5.6. When the receiver was approximately 4 inches (10.2 cm) from the crack, the signal began to amplify and peaked when the receiver was just before the crack. The signal dropped to slightly above the ambient noise level when the receiver just crossed over the crack and the source was on the opposite side of the crack. When the source crossed the crack to the same side as the receiver, the signal peaked again. As the source and receiver "marched" away from the crack, the signal decreased.

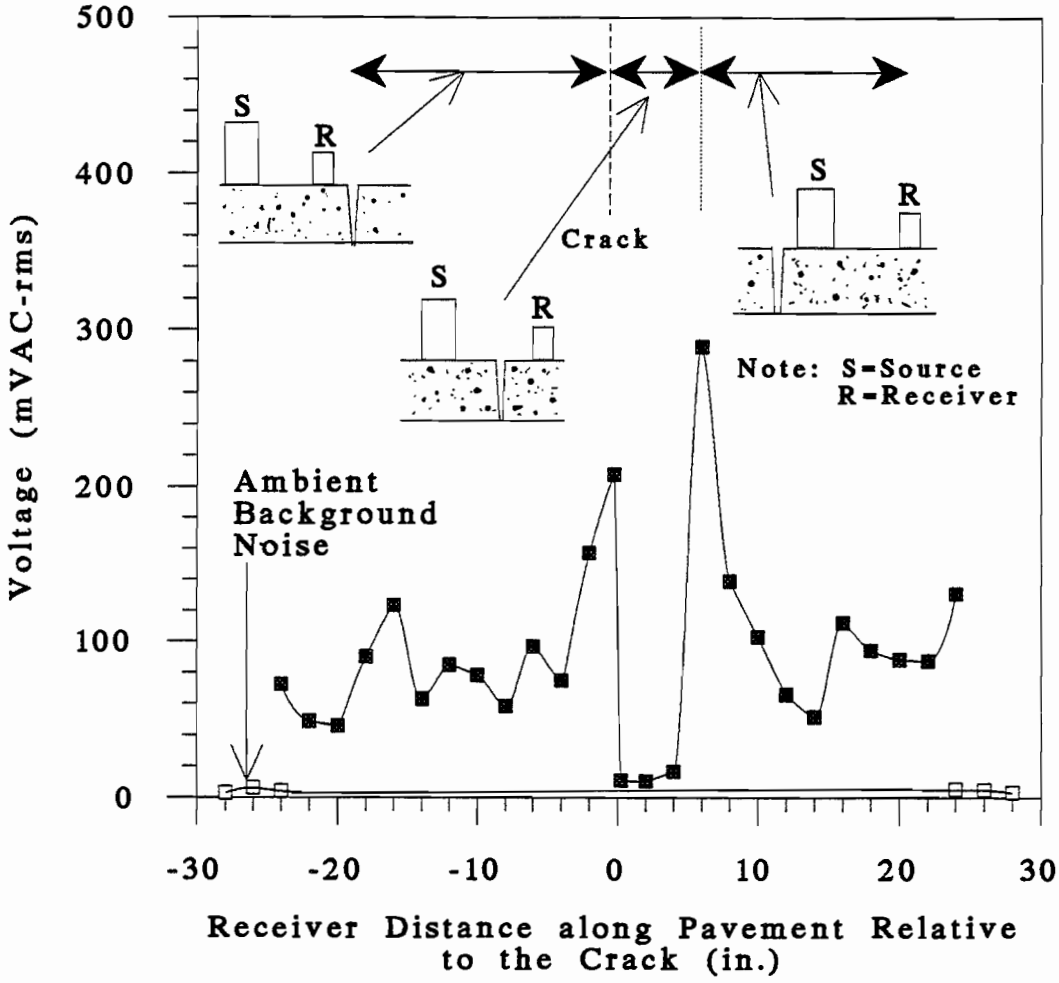

Note: Peak Force Level was Approximately 61.5 lbs (273.6 N) at a 2 kHz Fixed Sinusoid

Figure 5.5: AC Voltmeter Voltage Output Versus Distance for Testing Across Pavement Crack at the BRC Test Facility (Trial 1 Performed in September, 1991)

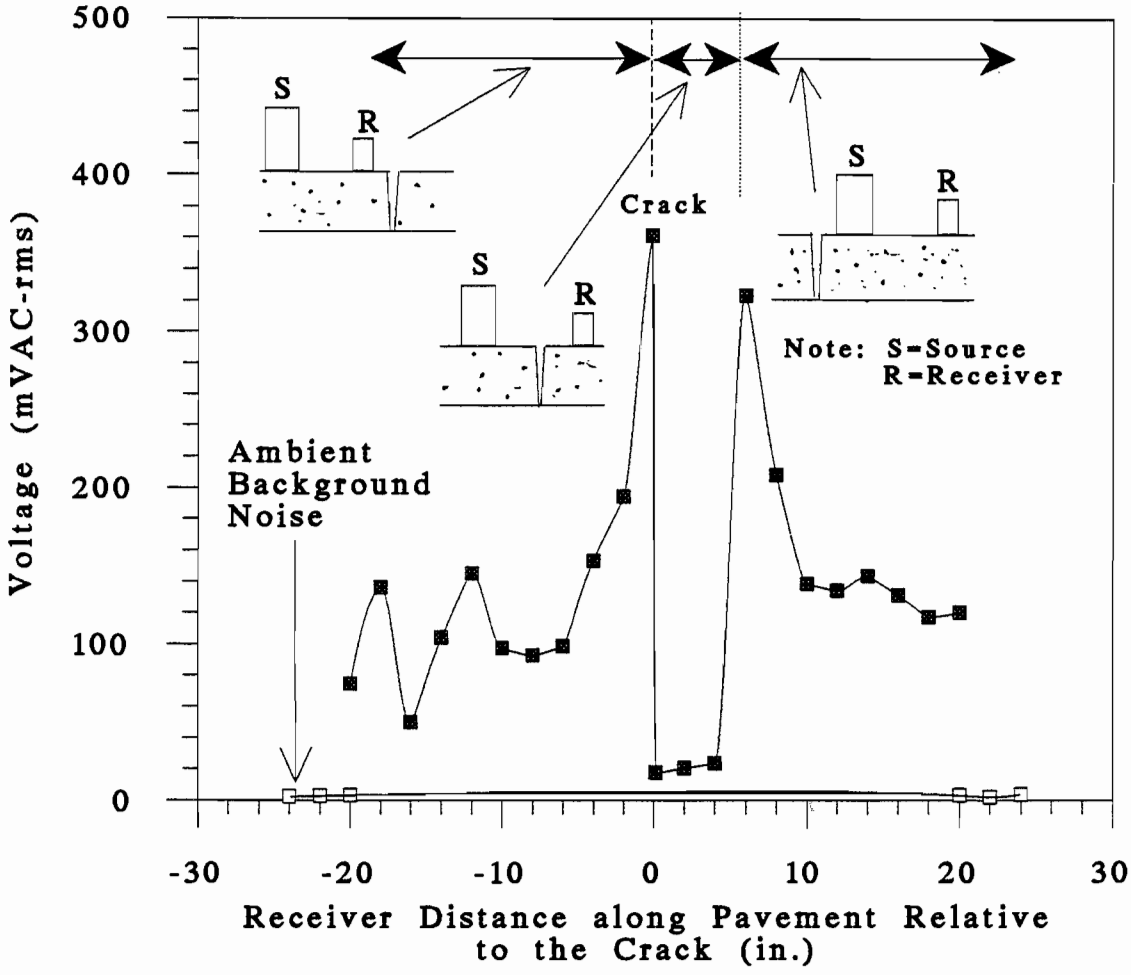

Note: Peak Force Level was Approximately 61.5 lbs (273.6 N) at a 2 kHz Fixed Sinusoid

Figure 5.6: AC Voltmeter Voltage Output Versus Distance for Testing Across Pavement Crack at the BRC Test Facility (Trial 2 Performed in July, 1992)

When the source was approximately 4 inches (10.2 cm) past the crack, the signal had reached a constant average level again, with fluctuations similar to those initially reported.

It should be emphasized that these tests show that the crack was only visible when either the source or receiver was within approximately 4 inches (10.2 cm) of the crack. It is also important to note that the peak values obtained before and after the crack are only on the order of 2 to 4 times the average signal level, and the average signal level contains significant ($\pm$ 50%) fluctuations. Regardless of this inherent scatter, the test was very successful in establishing a "signature" for cracks which was in close agreement with the Collograph (French) results.

5.3.3 Delamination Characterization

Due to the physical layout of the BRC test facility, tests could not be conducted to examine the accelerometer output while approaching a delamination. Instead tests were run on the "delaminated" section to establish an average voltage level and typical fluctuations that would be representative of a delamination. This testing was accomplished by simply "marching" along a portion of the delaminated section. For comparison, the same testing was performed on the "normal" section of the test pavement. The results are shown in Figures 5.7 and 5.8. The data reported in Figure 5.7 were obtained in September, 1991, whereas the results reported in

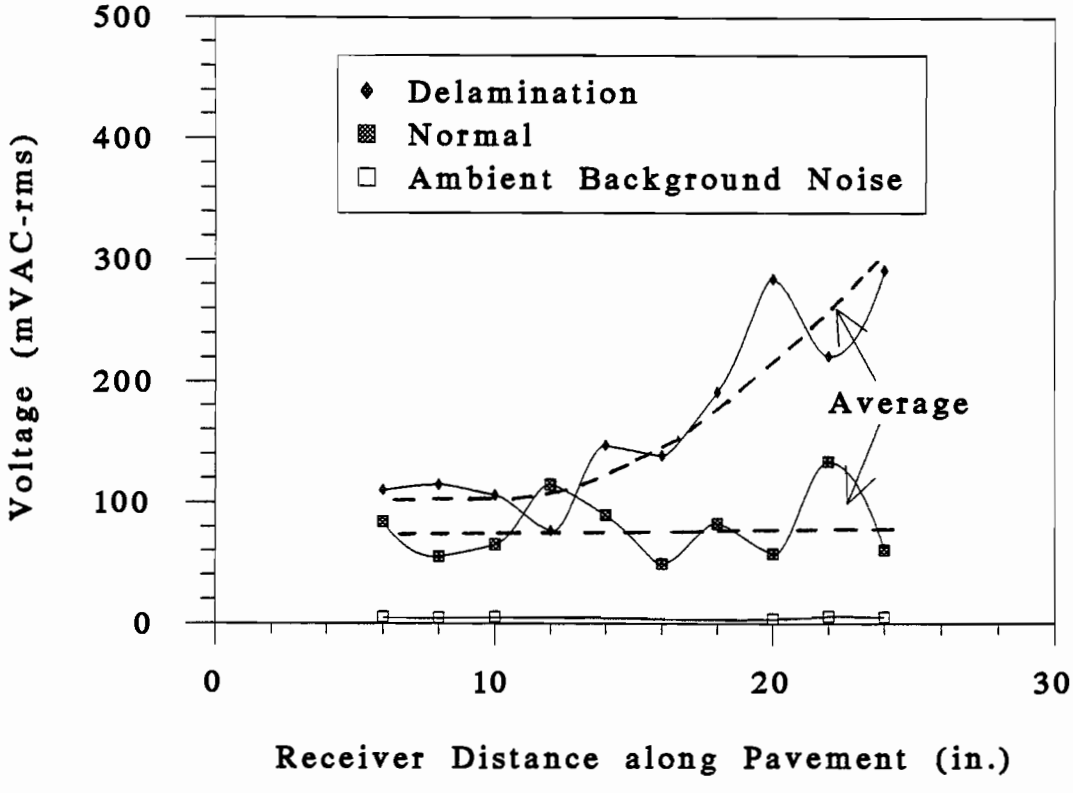

Figure 5.7: AC Voltmeter Voltage Output Versus Distance for Testing Across Normal and Delaminated Pavements at the BRC Test Facility (Trial 1 Performed in September, 1991)

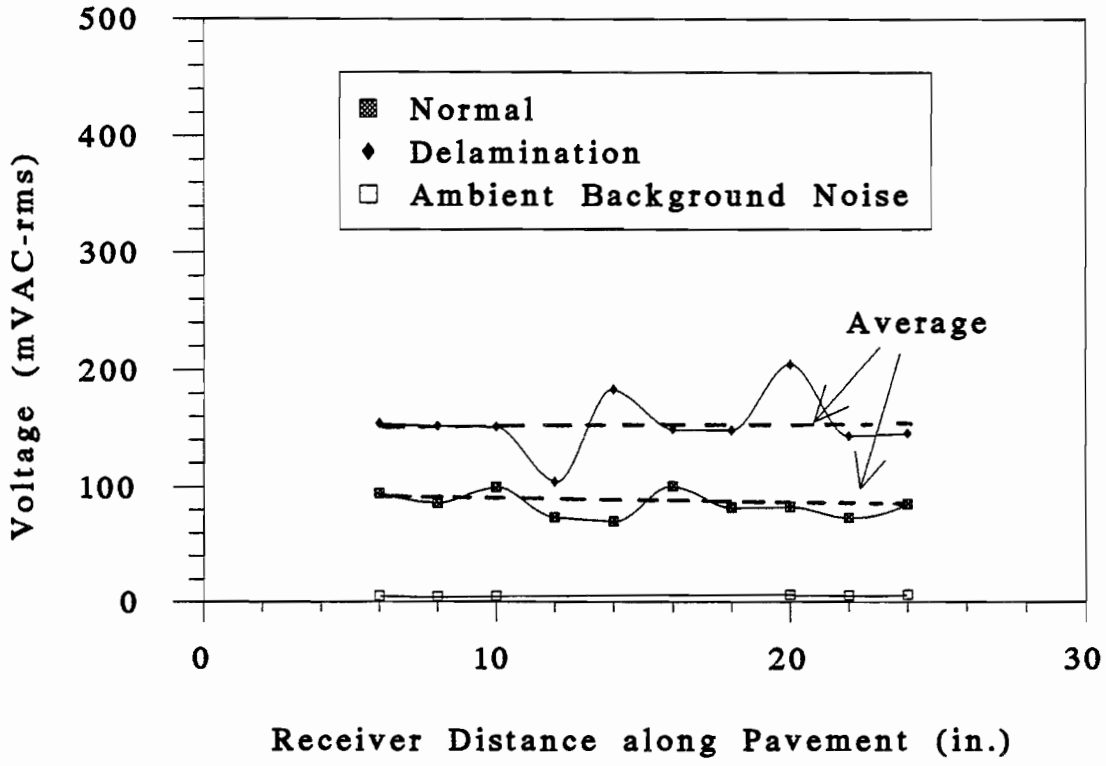

Figure 5.8: AC Voltmeter Voltage Output Versus Distance for Testing Across Normal and Delaminated Pavements at the BRC Test Facility (Trial 2 Performed in July, 1992)

Figure 5.8 were obtained in July, 1992. The normal section had a lower average voltage output than the delaminated section as was expected since delaminations provide a strong reflective interface. As seen before with the crack characterization testing, fluctuations on the order of 40 to 50 percent of the average signal level were encountered.

The delamination testing revealed several key points. First, the data are real since the average signal level is 20 to 100 times the ambient background noise level. In addition, questionable pavement sections must be tested over some distance, and not just at one point, due to the fluctuations in the signal level. Finally, it should be noted that the average signal level obtained over the delamination was on the order of 1.5 to 2 times the signal level over a normal pavement.

It is believed that the testing frequency may be an important characteristic for detecting delaminations. It is also believed that the delamination may have been more visible at the first-mode resonant frequency of the delaminated section. Therefore, the pavement was tested to determine the resonant frequency over the delamination. The testing was conducted over a 1 to 10 kHz frequency span using the PCB Piezotronics Series 086B01 instrumented hammer and a Wilcoxon Model 728T accelerometer, magnetically attached to the pavement. The resonant frequency was found by striking the delaminated pavement next to the

accelerometer. The peak response, from the frequency response, occurs at the first-mode resonant frequency. This method is described in detail in the next section dealing with void detection.

The resonant frequency for the delaminated pavement section at BRC occurred at 7.96 kHz as shown in Figure 5.9a. In addition, a similar test was conducted using the Wilcoxon Model F8 piezoelectric shaker. The resonant frequency, using the swept sine mode with the shaker, occurred at 7.92 kHz. The frequency response, for the 6 to 9 kHz sweep, is shown in Figure 5.9b. By using Equation 2.1 with a V_p = 13,500 ft/sec (4117.5 m/sec) and a f_p = 7940 Hz, the calculated thickness is 10.2 in. (25.9 cm). This compares very well with the 10-in. (25.4-cm) actual thickness.

5.3.4 Void Characterization

Fixed-Frequency Investigations- After investigating the "delamination", analysis and characterization of the void was initiated. The void that was positioned away from the "crack" was chosen for testing since it allowed testing to be performed while approaching and leaving the defect. As with the crack, testing on the void began 24 inches (61.0 cm) before the defect and continued to 24 inches (61.0 cm) beyond. The same testing configuration and parameters used for the crack and delamination testing (2-kHz fixed sinusoid and 2-volt source input) were also utilized on the void.

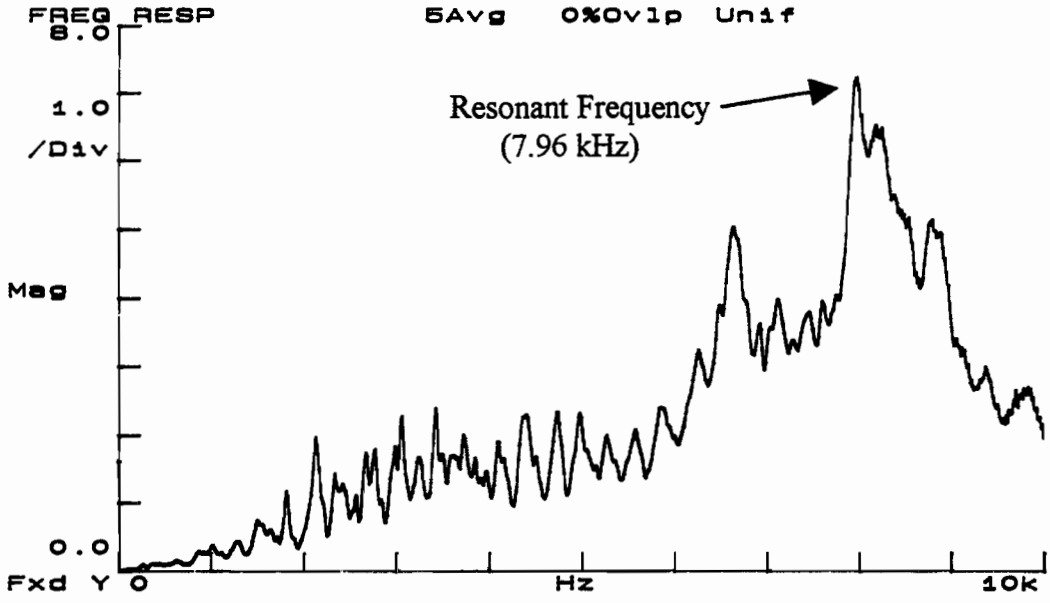

A. Frequency Response Using PCB 086B01 Instrumented Hammer

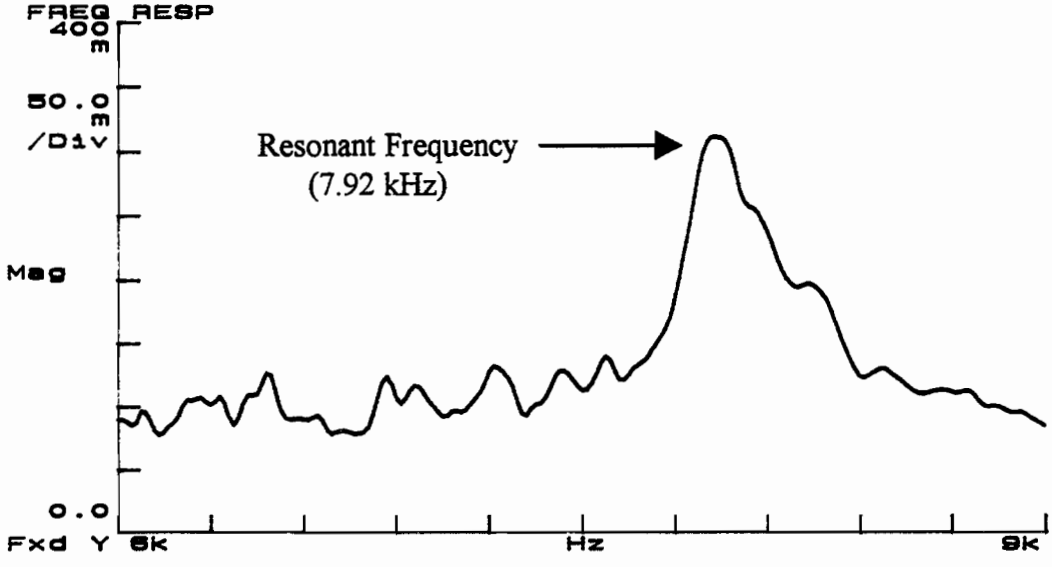

B. Frequency Response Using Wilcoxin F8 Piezoelectric Shaker

Figure 5.9: Frequency Response for Pavement Section Over the Delamination Using both the PCB Instrumented Hammer and the Wilcoxon Piezoelectric Shaker

The receiver output as testing moved across the void is shown in Figures 5.10 and 5.11. The void was not detected in either trial. The output level throughout both sweeps remained fairly constant at an average value consistent with what was determined for a normal pavement under a 2-kHz fixed sinusoid and 1-volt source input. A slight increase in the average output over the void occurred in the tests performed in September, 1991. However, this increase was not sufficient to permit positive identification. Therefore, it was concluded that, with the test parameters used, a void could not be detected.

To determine if void detection was possible with other frequencies near the 2 kHz signal, several frequencies were tested. Therefore, several other frequencies, within the established constraints, were tested. These included fixed sinusoids of 1.5 kHz, 2.175 kHz, 2.35 kHz, and 2.5 kHz. The voltage output versus distance for these tests are shown in Figures G1 through G4. The voltage outputs were more inconsistent and less uniform than the output at 2 kHz, and the void was still not visible. Like that found over the delamination, an amplification in the voltage output was expected since the air interface is such a strong signal reflector. Although some amplifications were present, the output over the entire void was only sporadically higher than that over the normal section. It should be noted that the BRC test facility pavement is an extremely stiff system and, hence, it may be very difficult to detect

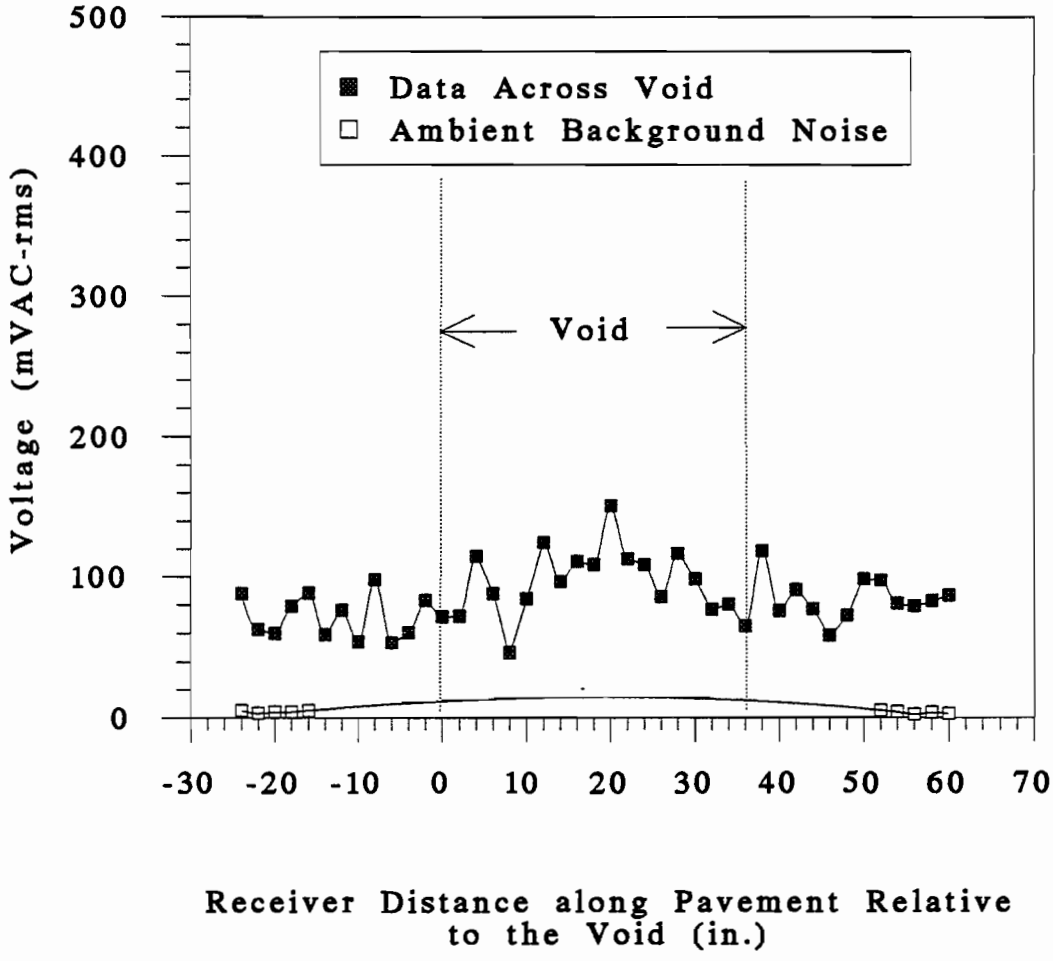

Figure 5.10: AC Voltmeter Voltage Output Versus Distance for Testing Across Pavement Void at the BRC Test Facility (Trial 1 Performed in September, 1991)

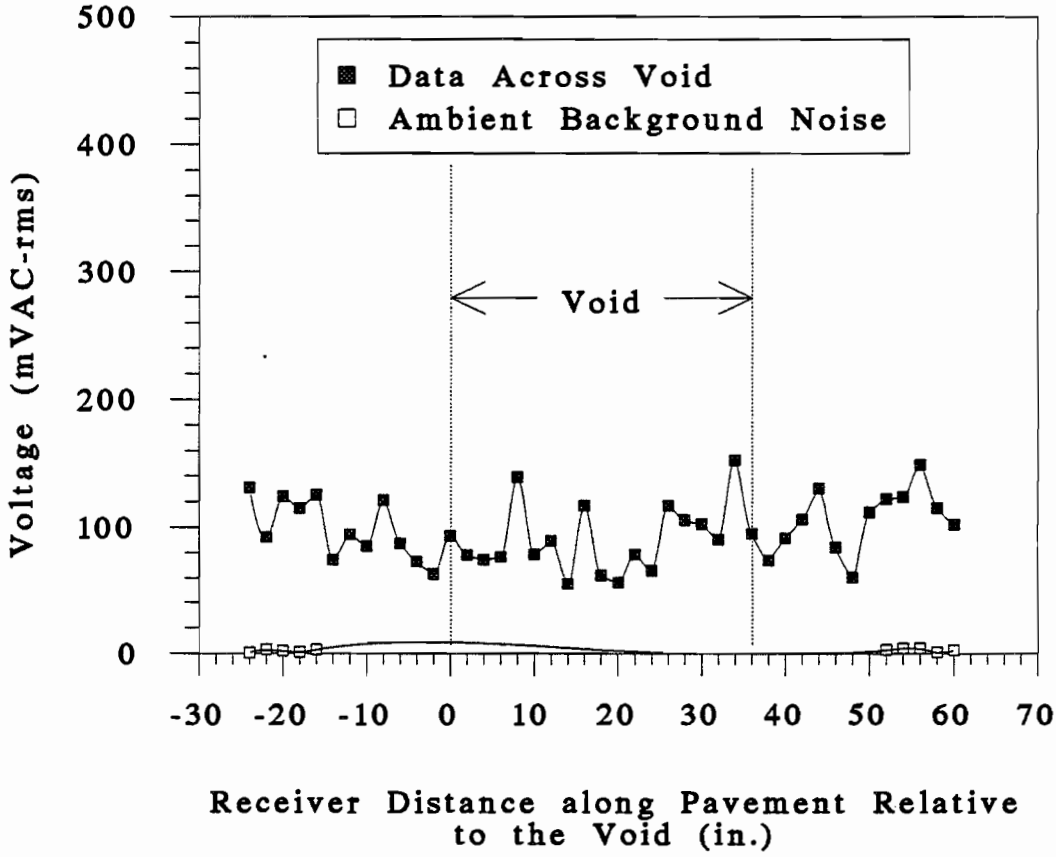

Figure 5.11: AC Voltmeter Voltage Output Versus Distance for Testing Across Pavement Void ath the BRC Test Facility (Trial 2 Performed July, 1992)

small anomalies that are located near or at the bottom of the slab. Thus, within the constraints of the presently designed system, it was determined that the void was undetectable.

Resonance Investigations- The resonance characteristics of the pavement section over the void were then examined to confirm that a void was indeed present at that location. Assuming that the pavement over the void behaves dynamically like a "free-free" system, the resonant frequency over the void was predicted. The resonant frequency for a "free-free" system can be calculated as:

$$f_n = \frac{V_p}{2l} \tag{4.1}$$

where f_n is the first mode resonant frequency, V_p is the constrained compression wave velocity, and l is the length (Richart et al., 1970). (Equation 4.1 is simply a rearrangement of Equation 2.1.) Based on data from Sheu (1987), the P-wave velocity for the slab at the BRC test facility is approximately 13,500 ft/sec (4114.8 m/sec). Using a slab thickness of 10 inches (25.4 cm), the predicted first-mode resonant frequency is 8100 Hz.

The pavement section over the void was then tested with the PCB Piezotronics Series 086B01 instrumented hammer over a 0 to 10 kHz frequency span. This method of testing is similar to the impact-echo method of void detection described in Chapter 2. In addition,

the void was also tested with the piezoelectric shaker using the swept sine mode. These tests were performed to determine the actual resonant frequency over the void. The frequency response for both the instrumented hammer test and the piezoelectric shaker test are shown in Figure 5.12. Similar tests were also performed over the normal section for comparison and are shown in Figure 5.13. It should be noted that the two tests are reported using different scales.

The frequency-response tests conducted over the void show a clear first-mode resonant frequency. The frequency response in Figure 5.12a gives a frequency of approximately 7850 Hz and the frequency response in Figure 5.12b gives a frequency of 7550 Hz. Both tests show good agreement. This is very close to the predicted value of 8100Hz. Using the average field value (7700Hz) and the known wave velocity (13,500 ft/sec) in Equation 4.1, the resulting thickness of the pavement over the void is 10.5 inches (26.7 cm). It is interesting to note that the amplitude of the response at the resonant frequency for the void (Figure 5.12) is nearly same as it was for the delamination (Figure 5.9).

The frequency response over the normal pavement section did not show a similar resonance as that found over the void. In fact, the resonant frequency of the normal pavement section is not easily seen. As shown in Figure 5.13a, the resonant frequency appears to be at about 9500 Hz. However, the peak is not clearly

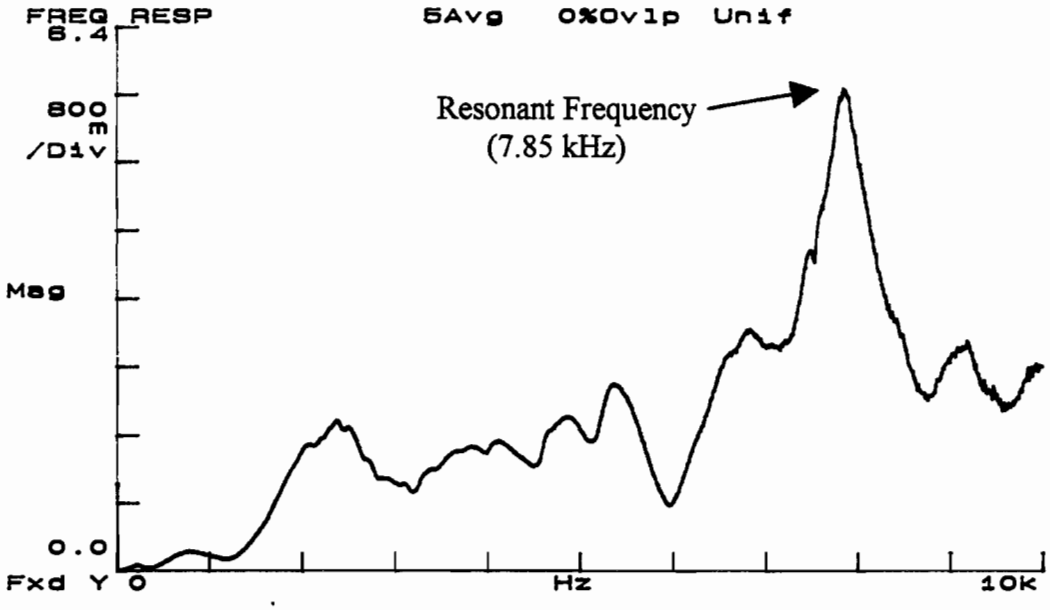

A. Frequency Response Using PCB 086B01 Instrumented Hammer

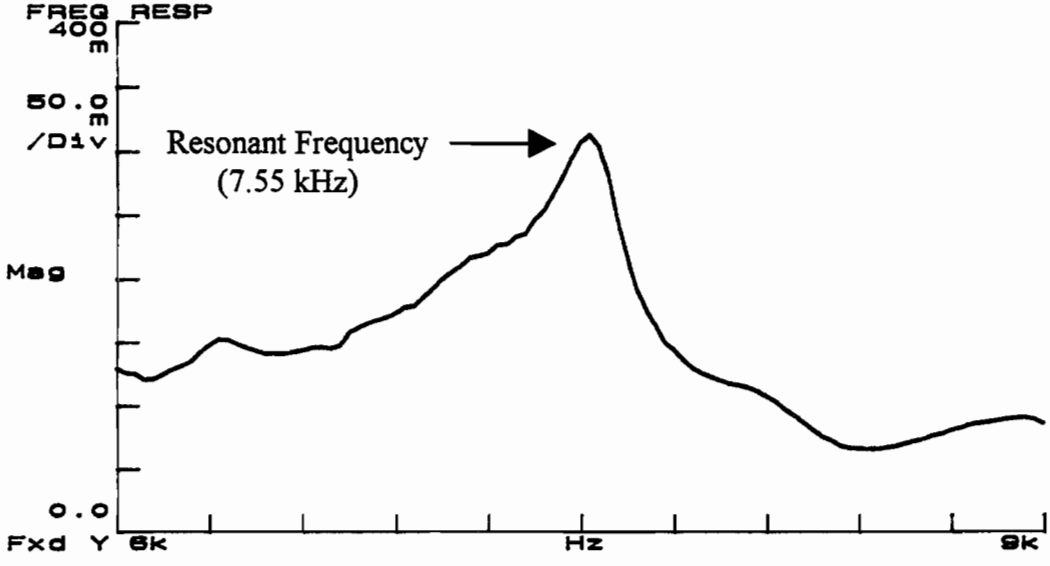

B. Frequency Response Using Wilcoxin F8 Piezoelectric Shaker

Figure 5.12: Frequency Response for Pavement Section Over the Void Using both the PCB Instrumented Hammer and the Wilcoxon Piezoelectric Shaker

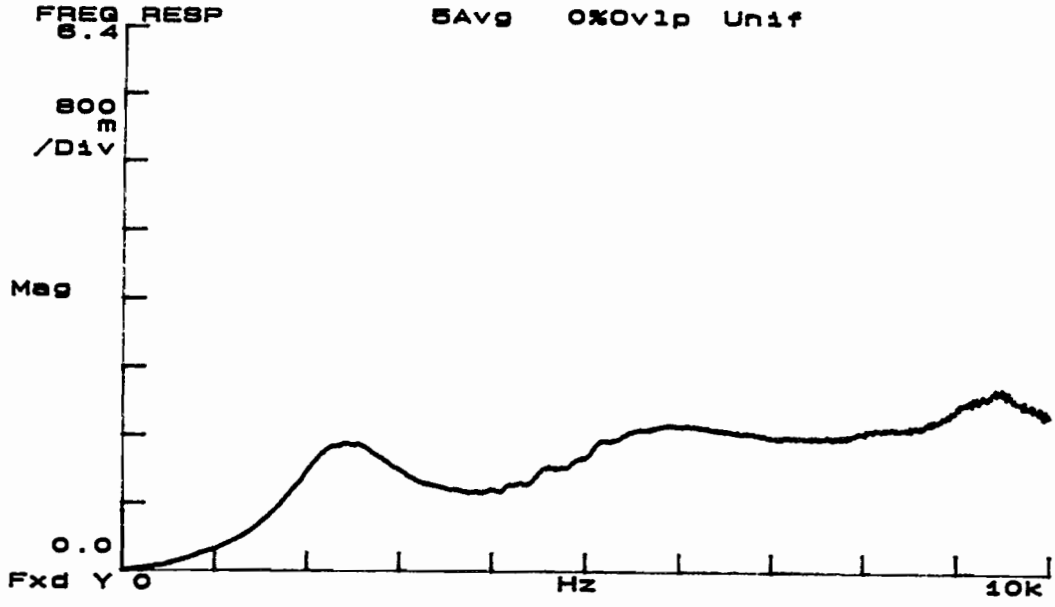

A. Frequency Response Using PCB 086B Instrumented Hammer

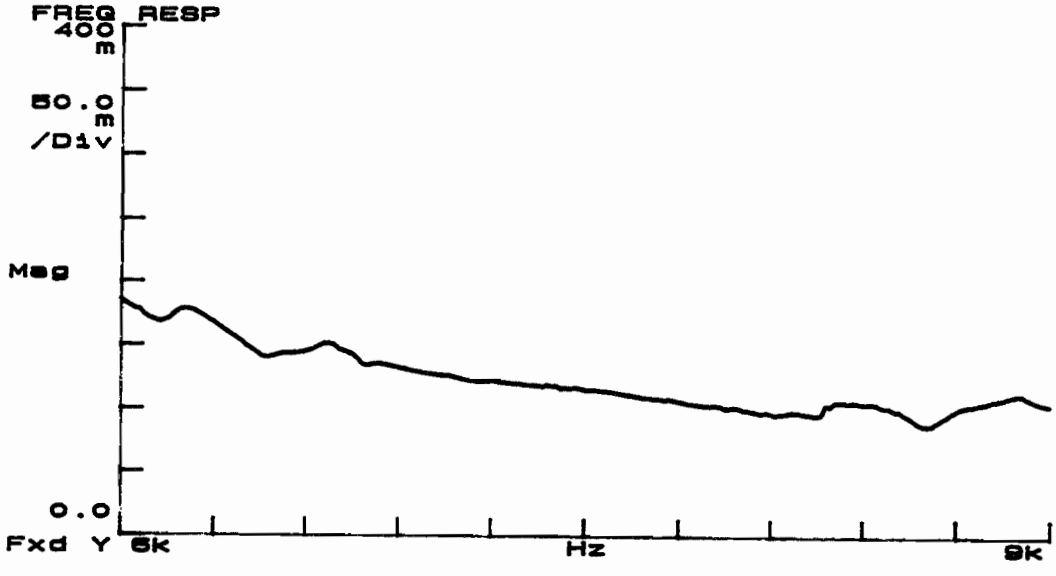

B. Frequency Response Using Wilcoxon F8 Piezoelectric Shaker

Figure 5.13: Frequency Response for the Normal Pavement Section Using both the PCB Instrumented Hammer and the Wilcoxon Peizoelectric Shaker

defined. This was expected since the normal pavement section is generally assumed to have a good bond with the Asphalt Concrete base and, hence, a majority of the signal does not reflect back to the surface at this interface. Thus, the resonant frequency, if visible, will not be clearly defined.

Based on these resonance investigations, it was concluded that a void located beneath an approximately 10.5 in (26.7 cm) thick slab was present at the location tested. From these results, it was determined that a system capable of operating at approximately the first-mode resonant frequency would be more successful in detecting voids in such a stiff system as that found at the BRC test facility.

5.4 Impulse-Response Results

The impulse-response (IR) method is somewhat similar to the impact-echo method described in Chapter 2. IR testing involves using an instrumented hammer to generate an impulsive signal. The signal is captured using a receiver such as a geophone (rather than an accelerometer used in impact-echo testing). The impulse and response signals are processed using a signal analyzer, and a plot of the velocity divided by pounds force (V/F) versus frequency is produced. This curve is the mechanical admittance (mobility) for the system. The inverse of this mechanical admittance curve is known as the impedance of the system (Olson-Church, Inc., 1986).

The impulse-response method utilizes two key aspects of the V/F plot. First, the slope of the V/F plot, from 0 to approximately 100 Hz, gives the flexibility of the slab being tested. The inverse of this slope is the dynamic stiffness (K') of the slab which is generally a function of the subgrade support. A lack of subgrade support will result in a reduction in the dynamic stiffness. Secondly, the average mechanical admittance up to approximately 800 Hz is also indicative of the subgrade support. High values of the average admittance indicate a lack of subgrade support (Olson-Church, Inc., 1986).

In May, 1986, the impulse-response method was used to investigate the void at the BRC test facility. The testing was conducted by Mr. L. Olson. The testing configuration used is shown in Figure 5.14. Figures 5.15 and 5.16 show the dynamic stiffness data and mechanical admittance data, respectively, for tests performed on the slab at the BRC test facility. In addition, a typical V/F plot from the testing at the BRC test facility is shown in Figure 5.17. The data shown in Figure 5.15 indicate an average reduction in the dynamic stiffness over the void of approximately 25 to 50 percent. The results in Figure 5.16 show an average increase in the mechanical admittance over the void of approximately 50 to 100 percent. Both of these results are indicative of a loss of subgrade support. However, the data do not clearly define the extent of the void. In fact, only the corner of the slab clearly shows a loss of

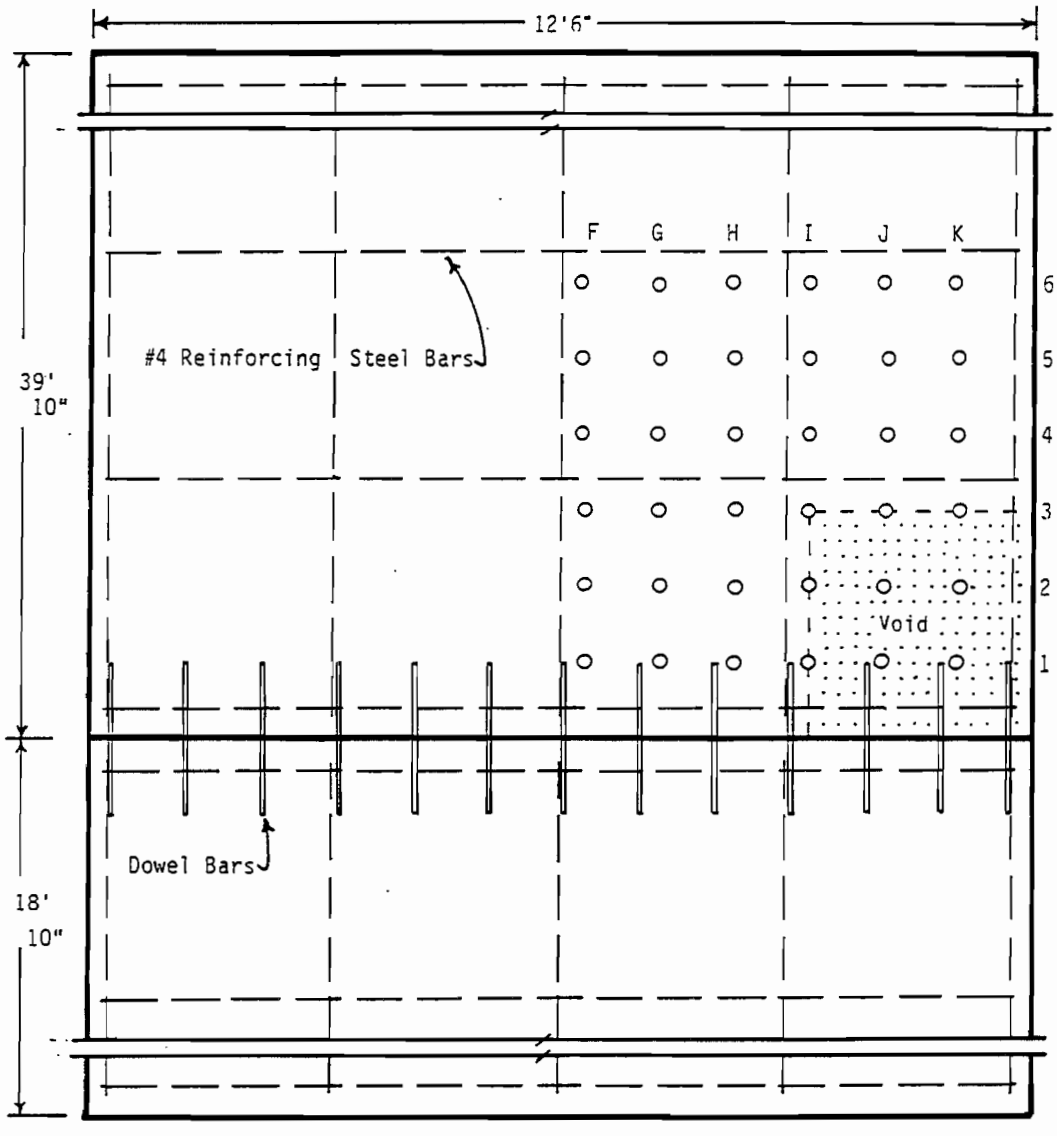

Figure 5.14: Testing Configuration for Impulse-Response Testing on the Void at the BRC Test Facility (Olson-Church, Inc., 1986)

Dynamic Stiffnesses over 20-80 Hertz Range

Row	Column / Hertz	F K'	F COH	G K'	G COH	H K'	H COH	I K'	I COH	J K'	J COH	K K'	K COH
6	20	2260	0.978	2340	0.947	2600	0.968	2280	0.997	2470	0.943	1870	0.946
	40	3680	0.983	3700	0.998	3750	0.993	3680	0.998	3360	0.997	2640	0.997
	60	4730	0.985	5220	0.964	5290	0.959	5250	0.974	4460	0.970	4080	0.992
	80	5460	0.997	5590	1.000	5900	0.998	6040	1.000	5320	0.998	4120	1.000
5	20	2670	0.955	2580	0.939	2720	0.911	2610	0.810	2030	0.986	2010	0.955
	40	3760	0.994	4070	0.795	3700	1.000	3800	0.997	3450	0.995	2780	0.993
	60	4770	0.964	5630	0.957	5260	0.975	5260	0.953	4570	0.973	3940	0.965
	80	5330	0.998	5810	0.997	5780	1.000	5920	1.000	5380	0.997	4080	0.995
4	20	4650	0.371	2580	0.994	2480	0.927	930	0.843	2450	0.975	1490	0.959
	40	3750	0.997	4020	0.997	3940	0.992	3210	0.983	3410	0.997	2640	0.995
	60	5620	0.960	5700	0.962	5460	0.960	4990	0.904	4590	0.982	3420	0.981
	80	5570	1.000	5950	0.998	6060	0.997	5570	0.993	5190	0.997	3850	0.997
3	20	2240	0.998	2260	0.997	2190	0.992	2340	0.994	2000	0.994	1850	0.955
	40	3700	0.997	3730	0.997	3660	0.997	3600	0.994	3120	0.998	2370	0.985
	60	5760	0.956	5590	0.946	5190	0.926	5360	0.982	4670	0.960	3230	0.982
	80	5810	0.998	5870	0.995	5920	0.998	6010	0.998	5040	0.998	3600	0.998
										Void			
2	20	2350	0.997	2280	0.973	2200	0.990	2120	1.000	2020	0.997	1650	0.997
	40	3410	0.998	3640	0.994	3470	0.998	3400	0.997	3040	0.988	2210	0.992
	60	5650	0.946	5990	0.946	5060	0.981	5240	0.960	4030	0.979	2780	0.988
	80	5920	0.998	6210	0.997	6020	0.997	5750	0.998	4960	0.992	3330	0.993
1	20	2140	0.994	2000	0.995	2090	0.998	2090	0.997	2030	0.985	1100	0.994
	40	3230	0.995	3050	0.997	2960	0.997	2940	0.998	2420	0.994	1980	0.988
	60	4800	0.986	4820	0.942	5050	0.933	4630	0.964	3530	0.973	2460	0.973
	80	5870	0.995	5460	0.997	5250	0.998	4990	0.998	3910	0.995	2680	0.998

Statistical Summary

		F	G	H	I	J	K
6	Avg	4033	4213	4385	4313	3903	3178
	Std	1389	1492	1495	1673	1247	1111
5	Avg	4133	4523	4365	4398	3858	3203
	Std	1172	1512	1408	1485	1453	986
4	Avg	4898	4563	4485	3675	3910	2850
	Std	885	1575	1607	2087	1222	1036
3	Avg	4378	4363	4240	4328	3708	2763
	Std	1731	1693	1660	1671	1410	797
2	Avg	4333	4530	4188	4128	3513	2493
	Std	1736	1898	1692	1676	1267	724
						Void	
1	Avg	4010	3833	3838	3663	2973	2055
	Std	1652	1591	1559	1378	891	701

Figure 5.15: Dynamic Stiffness Data from Impulse-Response Testing on the Void at the BRC Test Facility (Olson-Church, Inc., 1986)

Mobility or Mechanical Admittance (ips/lbf)

Row	Column / Hertz	F	G	H	I	J	K
6	200	9.0E-05	9.0E-05	1.0E-04	9.0E-05	8.0E-05	1.0E-04
	400	1.4E-04	1.3E-04	1.2E-04	1.2E-04	1.1E-04	1.0E-04
	600	1.5E-04	1.5E-04	1.6E-04	1.5E-04	1.5E-04	1.2E-04
	800	2.2E-04	2.0E-04	2.1E-04	2.0E-04	2.0E-04	1.9E-04
5	200	9.0E-05	8.0E-05	9.0E-05	8.0E-05	8.0E-05	1.1E-04
	400	1.3E-04	1.2E-04	1.1E-04	1.2E-04	1.1E-04	1.0E-04
	600	1.5E-04	1.6E-04	1.5E-04	1.4E-04	1.4E-04	1.1E-04
	800	2.2E-04	2.0E-04	2.0E-04	2.1E-04	2.2E-04	2.0E-04
4	200	9.0E-05	1.0E-04	1.0E-04	9.0E-05	1.0E-04	1.3E-04
	400	1.3E-04	1.1E-04	1.0E-04	1.2E-04	1.1E-04	1.0E-04
	600	1.4E-04	1.5E-04	1.4E-04	1.4E-04	1.5E-04	1.2E-04
	800	2.1E-04	2.0E-04	2.1E-04	2.1E-04	2.1E-04	2.0E-04
3	200	9.0E-05	9.0E-05	1.0E-04	1.0E-04	1.2E-04	1.9E-04
	400	1.2E-04	1.1E-04	1.1E-04	1.1E-04	1.2E-04	1.3E-04
	600	1.3E-04	1.5E-04	1.5E-04	1.4E-04	1.5E-04	1.5E-04
	800	2.1E-04	2.1E-04	2.5E-04	1.8E-04	2.1E-04	2.1E-04
2	200	9.0E-05	9.0E-05	1.0E-04	1.0E-04	1.3E-04	2.3E-04
	400	1.2E-04	1.1E-04	1.1E-04	1.4E-04	1.4E-04	2.3E-04
	600	1.3E-04	1.4E-04	1.4E-04	1.7E-04	2.0E-04	1.7E-04
	800	2.1E-04	2.0E-04	2.2E-04	2.0E-04	3.4E-04	1.9E-04
1	200	9.0E-05	9.0E-05	1.0E-04	1.1E-04	1.5E-04	2.8E-04
	400	1.2E-04	1.1E-04	1.2E-04	1.4E-04	1.4E-04	2.9E-04
	600	1.2E-04	1.4E-04	1.2E-04	1.8E-04	2.2E-04	2.3E-04
	800	1.9E-04	2.1E-04	1.8E-04	2.5E-04	4.1E-04	2.1E-04

Void

Statistical Summary

		F	G	H	I	J	K
6	Avg	1.5E-04	1.4E-04	1.5E-04	1.4E-04	1.4E-04	1.3E-04
	Std	5.4E-05	4.6E-05	4.9E-05	4.7E-05	5.2E-05	4.3E-05
5	Avg	1.5E-04	1.4E-04	1.4E-04	1.4E-04	1.4E-04	1.3E-04
	Std	5.4E-05	5.2E-05	4.9E-05	5.4E-05	6.0E-05	4.7E-05
4	Avg	1.4E-04	1.4E-04	1.4E-04	1.4E-04	1.4E-04	1.4E-04
	Std	5.0E-05	4.5E-05	5.2E-05	5.1E-05	5.0E-05	4.3E-05
3	Avg	1.4E-04	1.4E-04	1.5E-04	1.3E-04	1.5E-04	1.8E-04
	Std	5.1E-05	5.3E-05	6.8E-05	3.6E-05	4.2E-05	3.0E-05
2	Avg	1.4E-04	1.4E-04	1.4E-04	1.5E-04	2.0E-04	2.1E-04
	Std	5.1E-05	4.8E-05	5.4E-05	4.3E-05	9.7E-05	3.0E-05
1	Avg	1.3E-04	1.4E-04	1.3E-04	1.7E-04	2.3E-04	2.5E-04
	Std	4.2E-05	5.3E-05	3.5E-05	6.1E-05	1.3E-04	3.8E-05

Void

Figure 5.16: Mechanical Admittance Data from Impulse-Response Testing on the Void at the BRC Test Facility (Olson-Church, Inc., 1986)

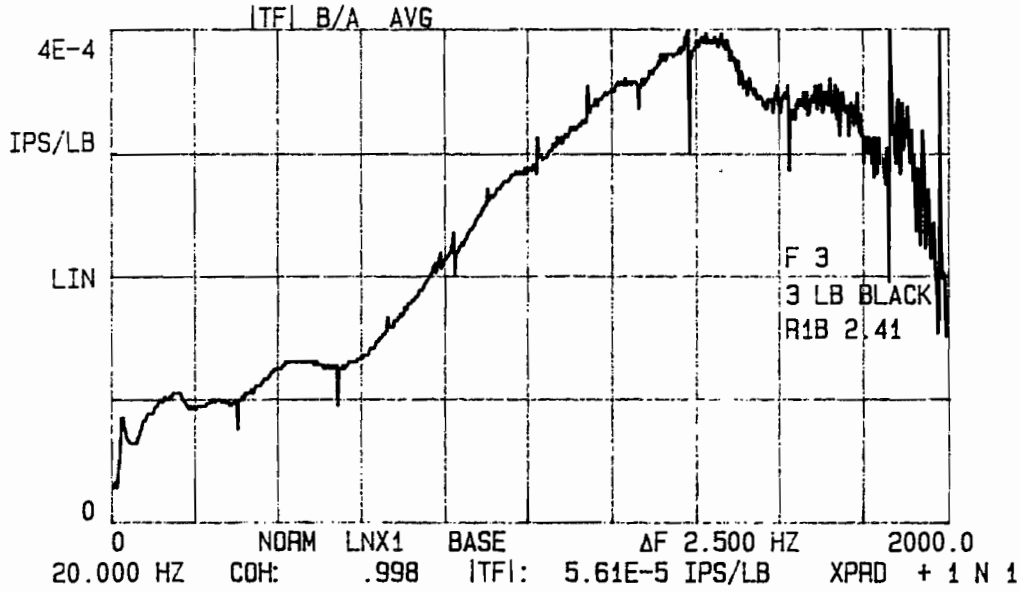

Figure 5.17: Typical V/F Plot Obtained During Impulse-Response Testing on the Void at the BRC Test Facility (Olson-Church, Inc., 1986)

support which one might expect to find without of the presence of a void. Unfortunately, data were not reported for a corner of the slab not containing a void. From the reported results, it is difficult to assess the applicability of using the impulse-response method to detect irregularities in rigid pavements, but it does appear that there is potential. One must remember that, for the thick slab tested, it is likely that only a factor of two may exist in the output between the "defective" and the "normal" pavement.

5.5 Prototype Trailer-Mounted System Response

After characterizing the anomalies within the design constraints under optimum conditions, the response of the prototype trailer-mounted system was investigated. Since the crack was the most visible defect, only data obtained while crossing the crack is reported. However, it should be noted that in conducting the prototype system tests, the entire pavement was tested over several passes.

As previously established, a 2-kHz fixed sinusoid was used for the prototype system testing. However, the source input was increased to three volts to increase the signal generated into the pavement. This generated a peak force of about 100 lbs (444.8 N). The trailer was first tested while being pulled behind a towing vehicle at a continuous and very slow speed (≈ 1 mph, ≈ 1.6 km/hr). The response when crossing the crack is shown in Figure 5.18.

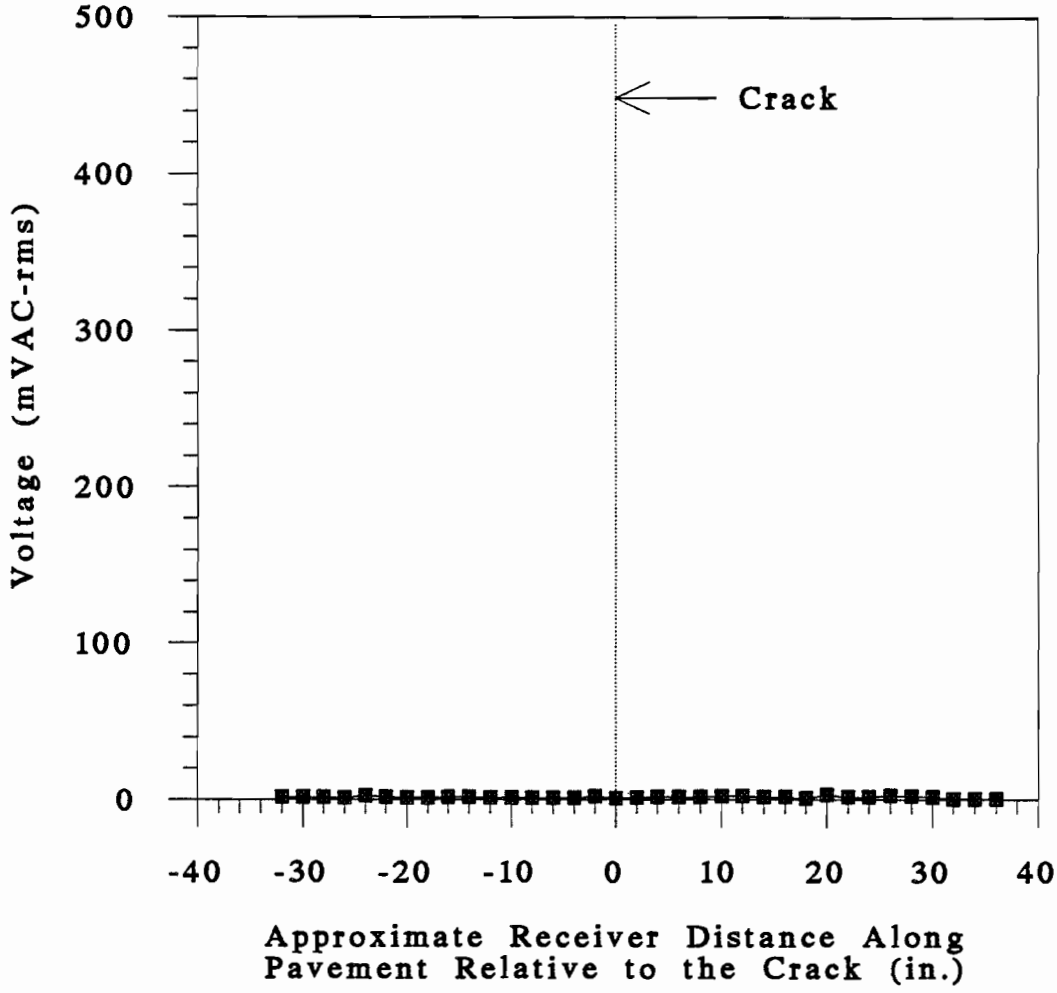

Figure 5.18: AC Voltmeter Voltage Output Versus Distance for Testing Across the Pavement Crack at the BRC Test Facility Using the Prototype Trailer-Mounted System in Continuous Motion

Unfortunately, the crack could not be detected with the trailer-mounted configuration. In fact, the voltage output was at the same level as the ambient background noise. Because of this, a second set of tests were conducted in which the trailer, pulled by the towing vehicle, was stopped every time a measurement was taken (approximately every two inches, 5.1 cm). This incremental testing resulted in an output that was above the ambient noise level. However, as shown in Figure 5.19, the crack was still not detectable.

It was determined that the poor performance problem could probably be isolated either to the "source wheel" or the "receiver wheel". More specifically, the problem appeared to be either a poor coupling between the wheel and the pavement or a drastic loss of signal within the wheel itself. Therefore, each trailer component was tested separately at the BRC test facility to isolate the problem.

First, the "source wheel" was tested. This was accomplished by testing across the pavement crack using the marching concept (Figure 5.3) with the source on the "source wheel" and the receiver magnetically coupled to the pavement. The crack was easily detected as shown in Figure 5.20. However, even with the increased source input voltage, the overall voltage output level was somewhat less than was previously found. Therefore, the test was conducted again using water on the pavement in an attempt to improve the coupling between the "source wheel" and the pavement.

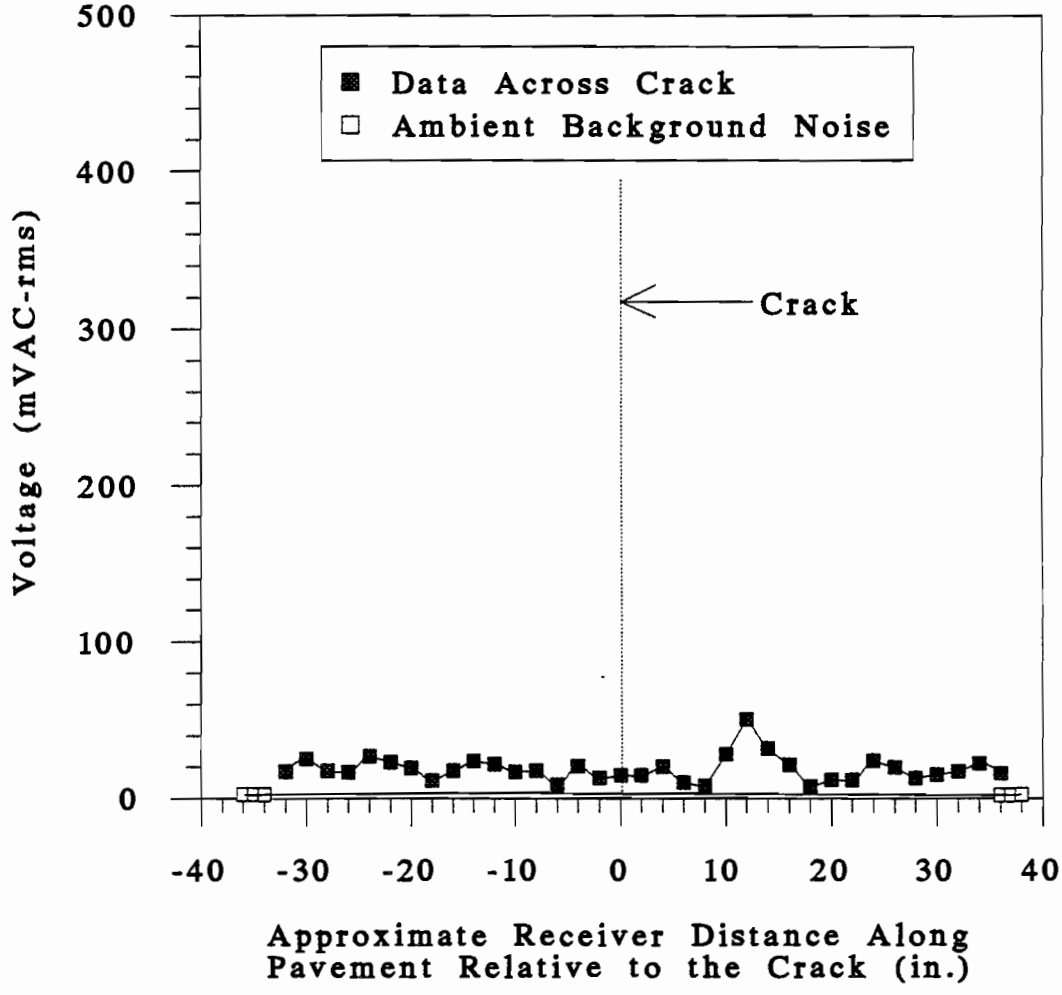

Figure 5.19: AC Voltmeter Voltage Output Versus Distance for Testing Across the Pavement Crack at the BRC Test Facility Using the Prototype Trailer-Mounted System Incrementally

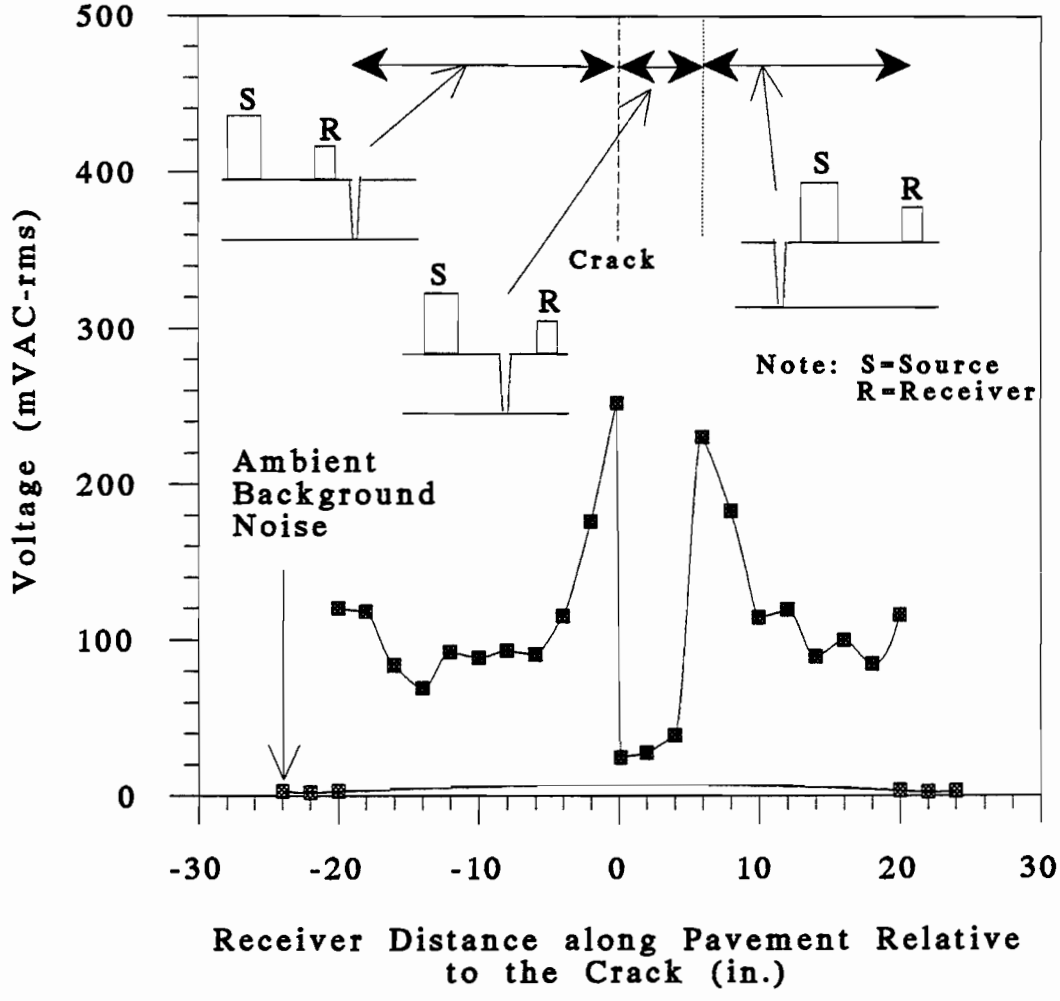

Figure 5.20: AC Voltmeter Voltage Output Versus Distance for Prototype Trailer-Mounted System Component Testing Across the Pavement Crack with the Source on the Source Wheel and the Receiver on the Pavement

The response is shown in Figure 5.21. The water had very little effect on the performance of the "source wheel".

Next, tests were conducted to analyze the "receiver wheel" performance using the same scheme as used for the "source wheel" analysis. The response with the source on the pavement and the receiver on the "receiver wheel", using water to optimize the coupling between the pavement and the "receiver wheel", is shown in Figure 5.22. This response was very similar to the response obtained by incrementally testing the entire system (Figure 5.19). It was concluded that the prototype trailer-mounted system was capable of generating the required signal into the pavement but was not able to receive the signal for analysis. To correct the problem, the "receiver wheel" would need to be extensively redesigned, paying particular attention to the materials used, the location of the receiver (or receivers), and the coupling between both the wheel and the pavement and the wheel and the receiver (or receivers). This work was not within the time frame of this researcher and hence, has been left to the next researcher.

5.6 Summary

Preliminary field testing was conducted at a concrete pavement test facility at the Balcones Research Center. This rigid pavement facility contains known pavement defects including cracks, voids, and delaminations. Before testing the prototype trailer-

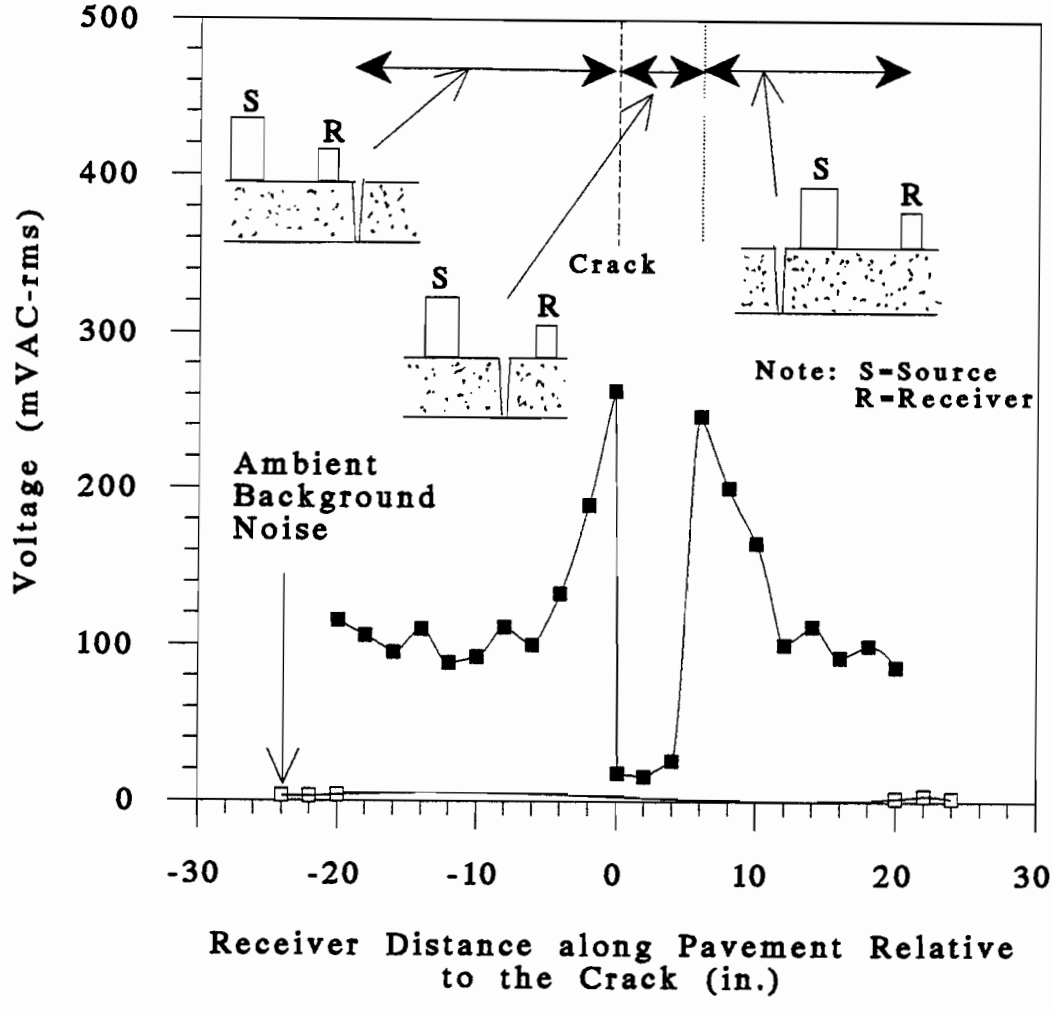

Figure 5.21: AC Voltmeter Voltage Output Versus Distance for Prototype Trailer-Mounted System Component Testing Across the Pavement Crack with the Source on the Source Wheel, Water Under the Source Wheel for Coupling, and the Receiver on the Pavement

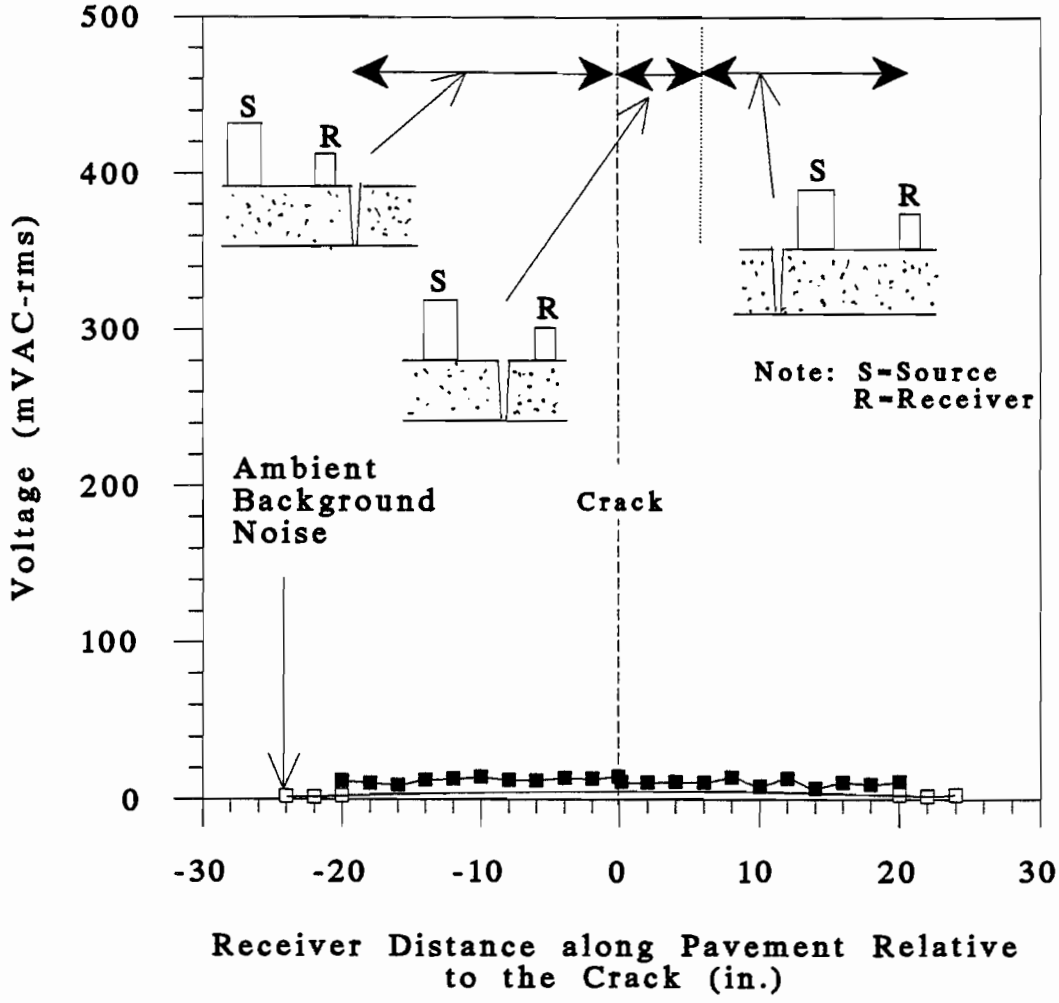

Figure 5.22: AC Voltmeter Voltage Output Versus Distance for Prototype Trailer-Mounted System Component Testing Across the Pavement Crack with the Source on the Pavement, the Receiver on the Receiver Wheel, and Water Under the Receiver Wheel for Coupling

mounted system, the various pavement anomalies were characterized using a source and receiver placed directly on the pavement. Using this test configuration that accurately modeled the prototype system, each defect was tested by incrementally "marching" across the defect. A "signature" for both the crack and the delamination was established. However, the void was not detectable because the testing was not conducted at the first-mode resonant frequency but rather at 2 kHz. Once , the void was tested at the resonant frequency (≈ 8 kHz), it was clearly seen. It is interesting to note that in all tests, generally only a factor of 2 or 3 was present between "good" and "defective" conditions for this test facility.

After the preliminary investigations were completed, the prototype trailer-mounted system response for the crack was analyzed. Several testing schemes were used in the system analysis but all failed to see the crack. As a result a series of trailer-component tests were performed to analyze the "source wheel" and the "receiver wheel". These tests isolated the problem to be within the system. It was concluded that the solution would require extensive research into the design of a new "receiver wheel" which was left to be accomplished by the next researcher.

Chapter Six
Summary, Conclusions, and Recommendations

6.1 Summary

The early detection and rehabilitation of both superficial and subsurface anomalies in rigid pavements such as cracks, voids, and delaminations is essential for the effective management of any pavement system. Numerous methods for the detection of such irregularities have been proposed, and several methods have been developed with varying degrees of success. However, a need still exists for an effective method to locate irregularities in rigid pavements. Therefore, in this work, development of the basis for a low-cost, prototype trailer-mounted system to nondestructively and continuously monitor pavements is presented. The proposed system should be capable of delineating cracks, voids, and delaminations within a rigid pavement system.

The design concept consists of inducing seismic body and surface waves at one point on top of the pavement system. These waves propagate through the system and are altered by the interior structure. The waves are sensed at another, nearby point on the pavement surface. The received signal is analyzed and interpreted to reveal any superficial and/or subsurface irregularities in the pavement system. Utilizing the design concept and a detailed analysis of both equipment and road noise, pertinent design

parameters were established which in turn dictated the optimum design of the prototype trailer-mounted system. The design evolution covered five major redesigns and several minor modifications. Initially, a system consisting of separate trailers for both the source and the receiver was attempted. In addition, an electromagnetic shaker was initially utilized to generate the necessary signal. Due to various problems encountered during the design and development process, such as signal transmission through the trailers and weak signals from the source, the design was modified and refined several times. The resulting prototype system is shown in Figure 6.1. A Wilcoxon Model F8 piezoelectric shaker is used to generate the desired signal into the pavement. The altered signal is received using a Wilcoxon 728T high-sensitivity accelerometer.

It should be noted that problems were encountered with the final prototype system. The problems were isolated to the receiver mechanism and the inability to develop a strong coupling to the pavement. Therefore, the receiver mechanism needs to be replaced to improve the performance in future versions. The entire system consists of a single trailer in which the source and receiver are isolated from one another. In addition the trailer itself is isolated from any outside noise interference using acoustical sound chambers around both the source and receiver.

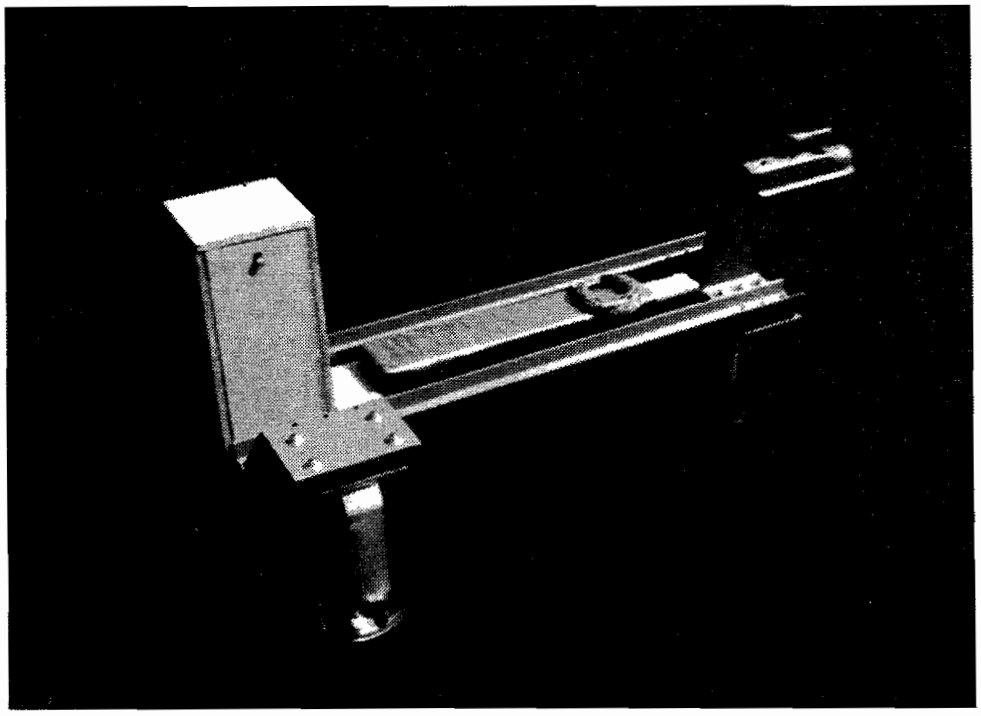

Figure 6.1: Prototype Trailer-Mounted System to Delineate Irregularities in Rigid Pavements

The prototype trailer was tested at the rigid concrete test facility at the Balcones Research Center of the University of Texas at Austin. This facility contains known defects including cracks, voids, and delaminations. First, the design concept was validated by characterizing each of the pavement anomalies using the source and receiver directly on the pavement surface and again using the "source wheel" component of the trailer. This was successful in establishing a "signature" for each defect. Finally, the prototype trailer-mounted system was tested using several different testing configurations including a series of individual trailer component tests.

6.2 Conclusions

Nondestructive seismic testing utilizing the preliminary field test configuration (Figure 5.3) was successfully applied in the detection of pavement anomalies within rigid pavements. The 2-kHz testing frequency was able to clearly detect anomalies near the surface, such as cracks. However, for deeper anomalies, such as delaminations and voids, a testing frequency close to the first-mode resonant frequency of the system, which is approximately 7800 Hz for a 10-in thick slab, was required to detect the irregularity.

The stress wave tests established "signatures" for the various anomalies tested. The "signature" for a crack consisted of a nearly constant average signal well before and after the crack. The signal peaked with the source and receiver just before and just after

the crack. The signal was at a minimum when the source and receiver were on opposite sides of the crack. The void and delamination had similar "signatures". The average signal was fairly constant well before and after both the void and the delamination. The signal was then amplified over both the void and delamination. The amplifications experienced for all three anomalies were only on the order of 2 to 3 times. In addition, it was noted that, due to fluctuations in the signal, pavements must be tested over a distance, and not a one point, to properly delineate irregularities.

Unfortunately, the prototype trailer-mounted system was unsuccessful in detecting any pavement anomalies. Two conclusions, derived from this study, are summarized below.

(1) The source must be capable of operating over a wide range of frequencies to include the first-mode resonant frequency for a variety of rigid pavement thicknesses. The source should be capable of a force output of several hundred pounds (> 1000 N). The influence of the force output of the shaker was not researched extensively and , hence, the effect of larger forces is unknown. However, based on this work, it is obvious that 500 to 1000 lbs (2224.1 to 4448.2 N) would be excellent.

(2) The "receiver wheel" is the critical design element in a moving system consisting of a vehicle utilizing nondestructive seismic methods to continuously monitoring pavement systems for irregularities. Special attention must be given to the following

areas: 1) the actual wheel design including materials; 2) the placement and number of receivers within the "receiver wheel"; 3) the coupling between the receiver(s) and the wheel itself; and 4) the coupling between the wheel and the pavement.

6.3 Recommendations

Since the prototype vehicle discussed in this research was only successfully developed for a stationary system, the following recommendations are made concerning future research in the development of a moving system which utilizes a prototype vehicle to delineate irregularities within pavement layers.

(1) The research started here, concerning rigid concrete pavements, should be continued with the following suggestions: (a) a source capable of generating significant forces (>1000lbs) over a large range of frequencies (1 to 25 kHz) to include first-mode resonances at a variety of thicknesses should be investigated; (b) the "receiving wheel" should be intricately designed so as to be highly sensitive to the generated pavement signal over a variety of surface textures. Various other receivers could be addressed at this point including velocity and displacement based units. In addition, the affect of pavement thickness, base and subbase materials, overlays, and temperature could be addressed.

(2) One could investigate the possibility of expanding the scope the above research to include delineating irregularities in asphalt pavements. Such variables as the thickness, stiffness, material profile, and temperature should be addressed.

(3) One could investigate the possibility of addressing the original problem using a different seismic method such as the Spectral-Analysis-of-Surface-Waves (SASW) method. This investigation would include both rigid and flexible pavement systems.

Appendix A

Spectral Functions Measured During Preliminary Laboratory Testing of Prototypes 1 through 4

Prototype 1 - Figures A.1 through A.6
- Approximate peak force developed by source = 35 lbs. (155.7N)
- Swept mode of operation
- Source: MB Dynamics Model PM100 electromagnetic shaker
- Receiver: Wilcoxon Model 728T accelerometer

Prototype 2 - Figures A.7 through A.12
- Approximate peak force developed by source = 35 lbs. (155.7N)
- Swept mode of operation
- Source: MB Dynamics Model PM100 electromagnetic shaker with 65lb (289.1 N) mass attachment
- Receiver: Wilcoxon Model 728T accelerometer

Prototype 3 - Figures A.13 through A.18
- Approximate peak force developed by source = 738.9 lbs. (3286.8 N)
- Swept mode of operation
- Source: Wilcoxon Model F8 piezoelectric shaker
- Receiver: Wilcoxon Model 728T accelerometer

Prototype 4 - Figures A.19 through A.24
- Approximate peak force developed by source = 562.5 lbs. (2502.1 N)
- Swept mode of operation
- Source: Wilcoxon Model F8 piezoelectric shaker
- Receiver: Wilcoxon Model 728T accelerometer

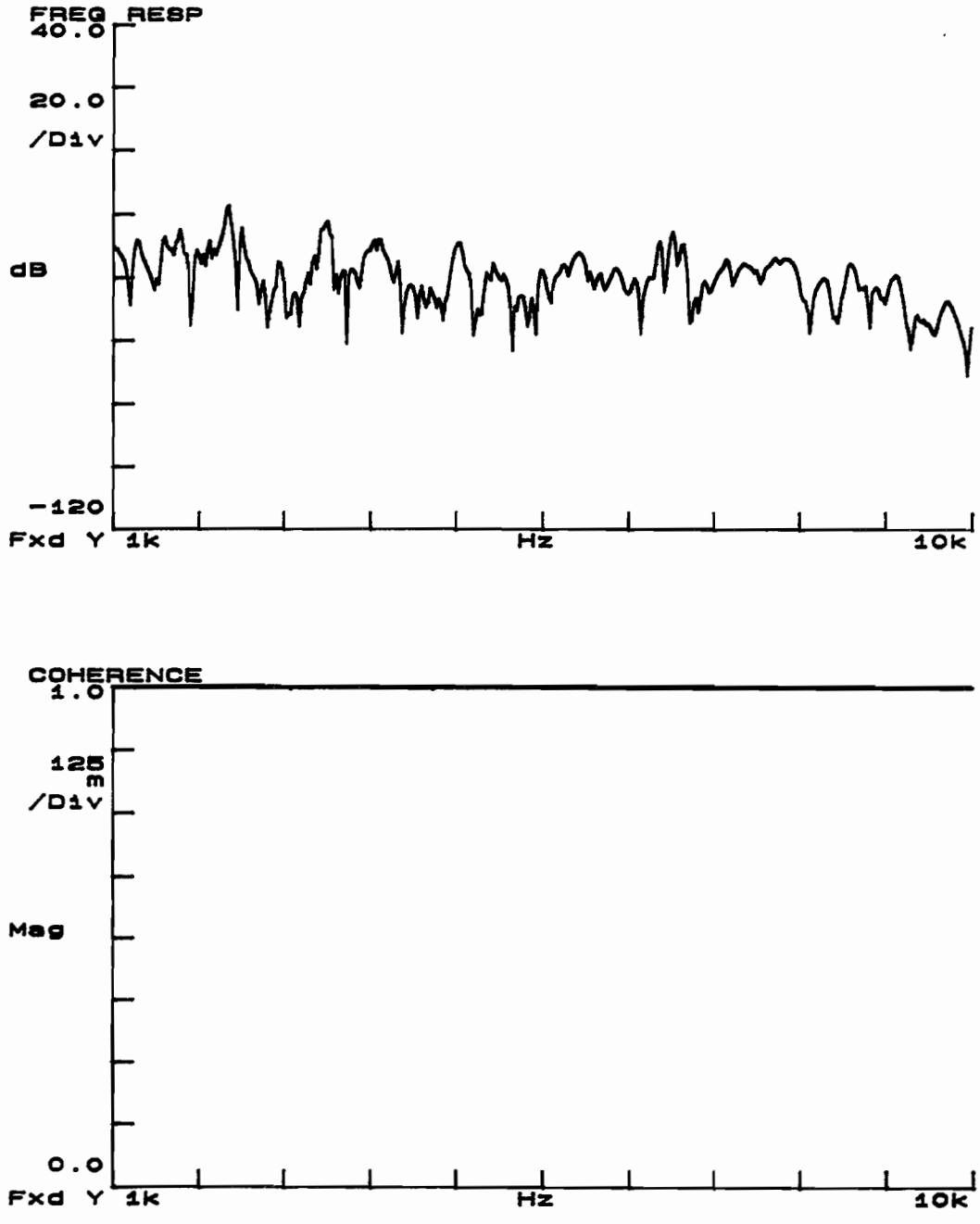

Figure A.1: Frequency Response and Coherence for Testing Signal Transmission Capabilities on Prototype 1 at Location A from Figure 3.13

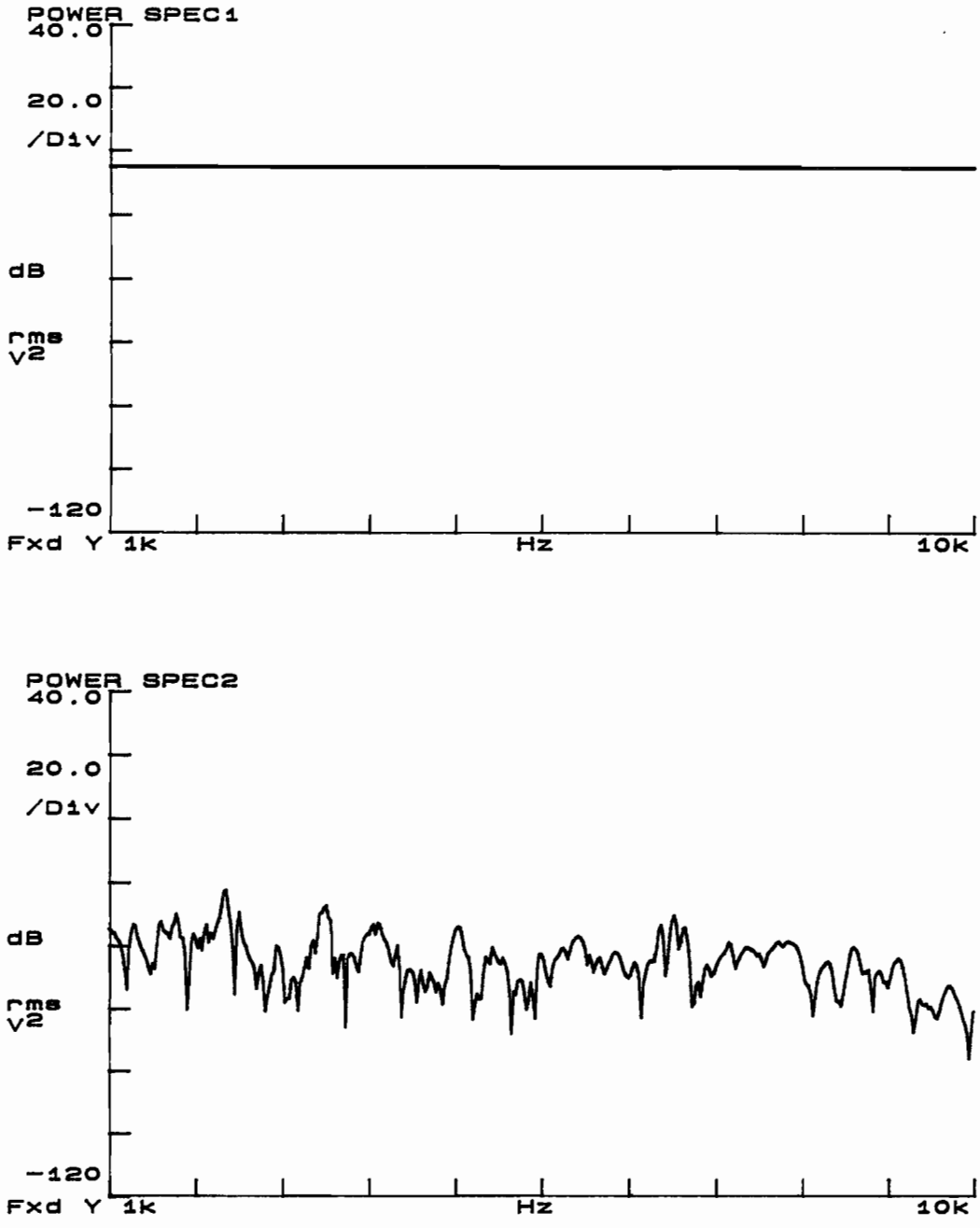

Figure A.2: Power Spectra for Testing Signal Transmission Capabilities on Prototype 1 at Location A from Figure 3.13

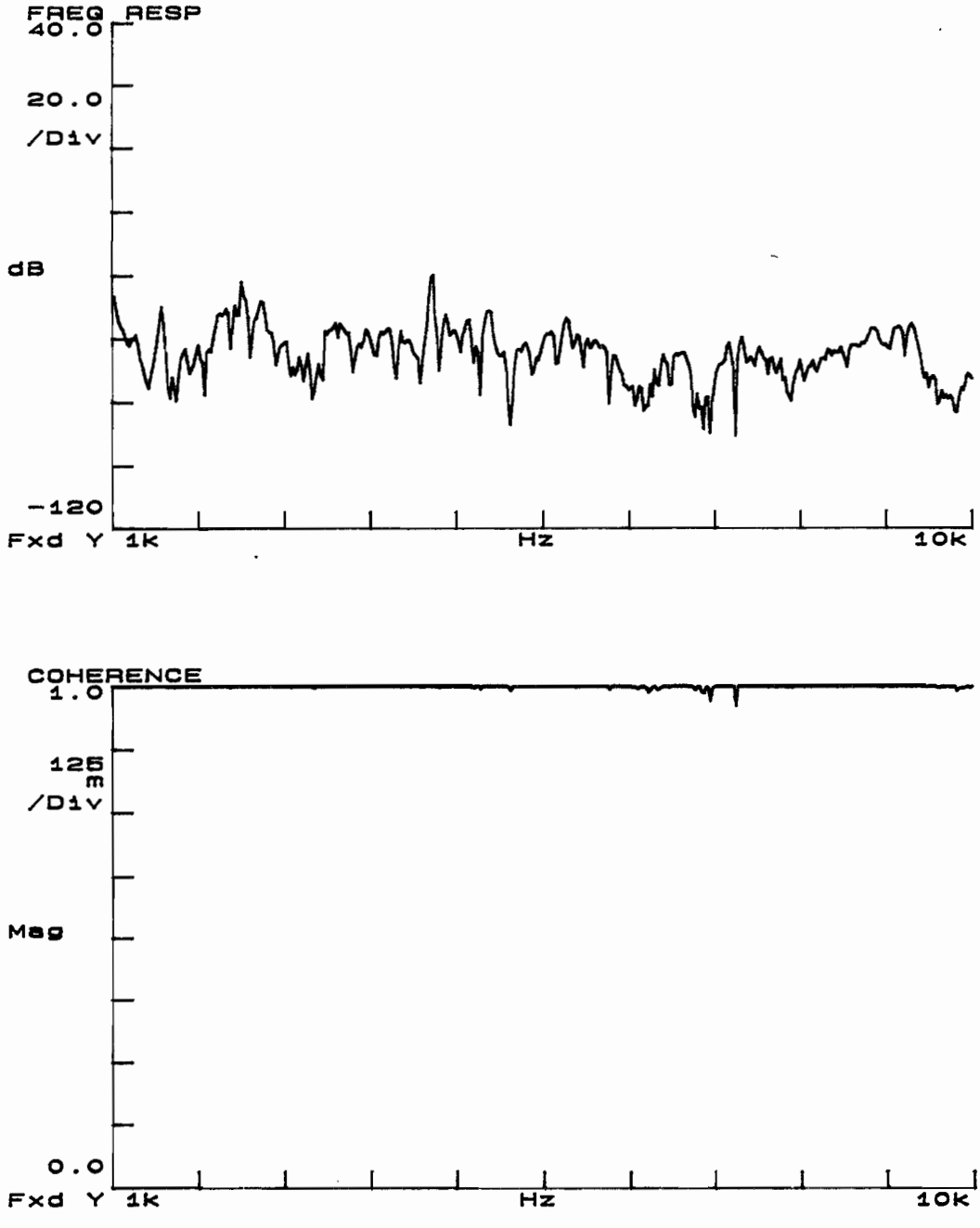

Figure A.3: Frequency Response and Coherence for Testing Signal Transmission Capabilities on Prototype 1 at Location B from Figure 3.13

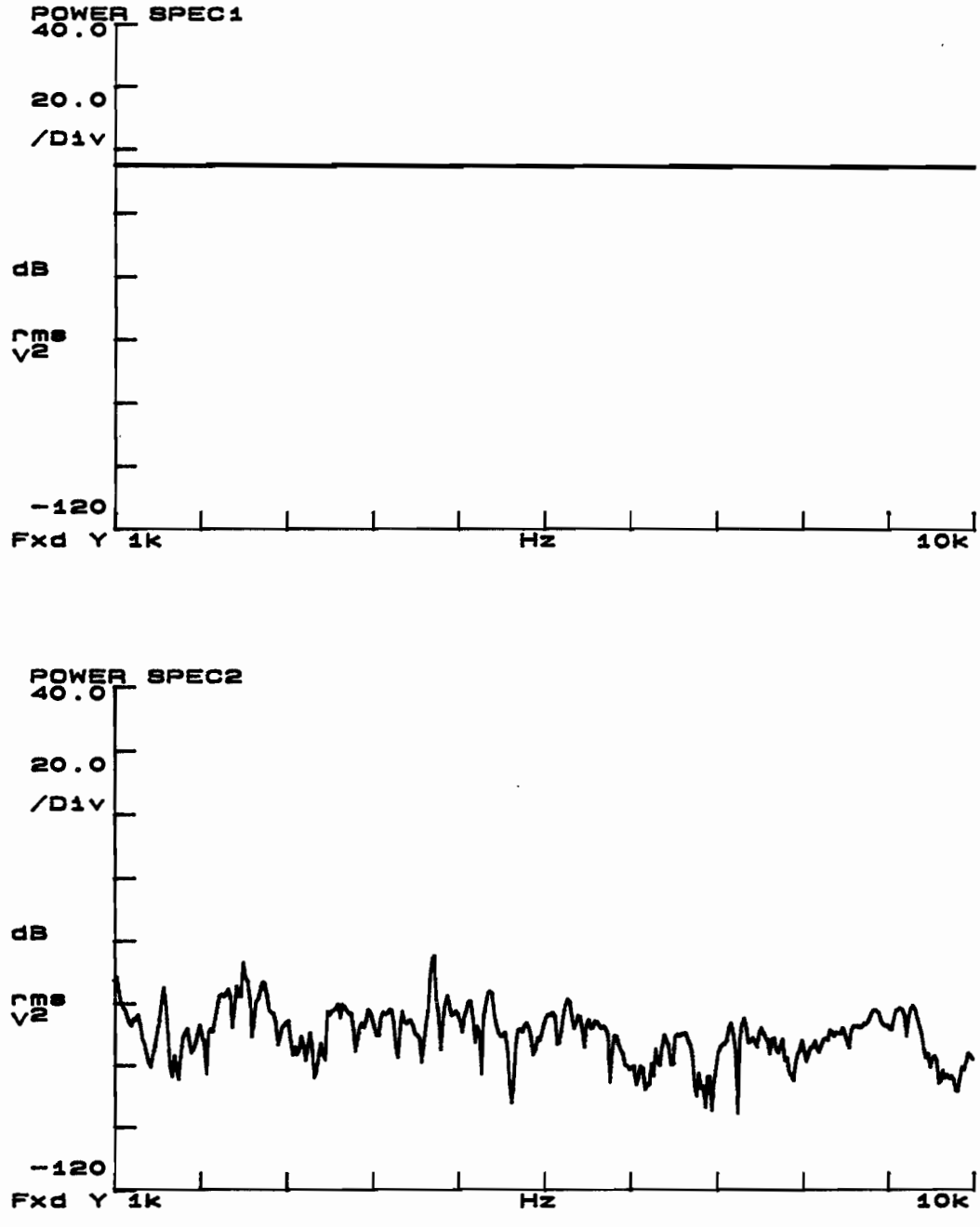

Figure A.4: Power Spectra for Testing Signal Transmission Capabilities on Prototype 1 at Location B from Figure 3.13

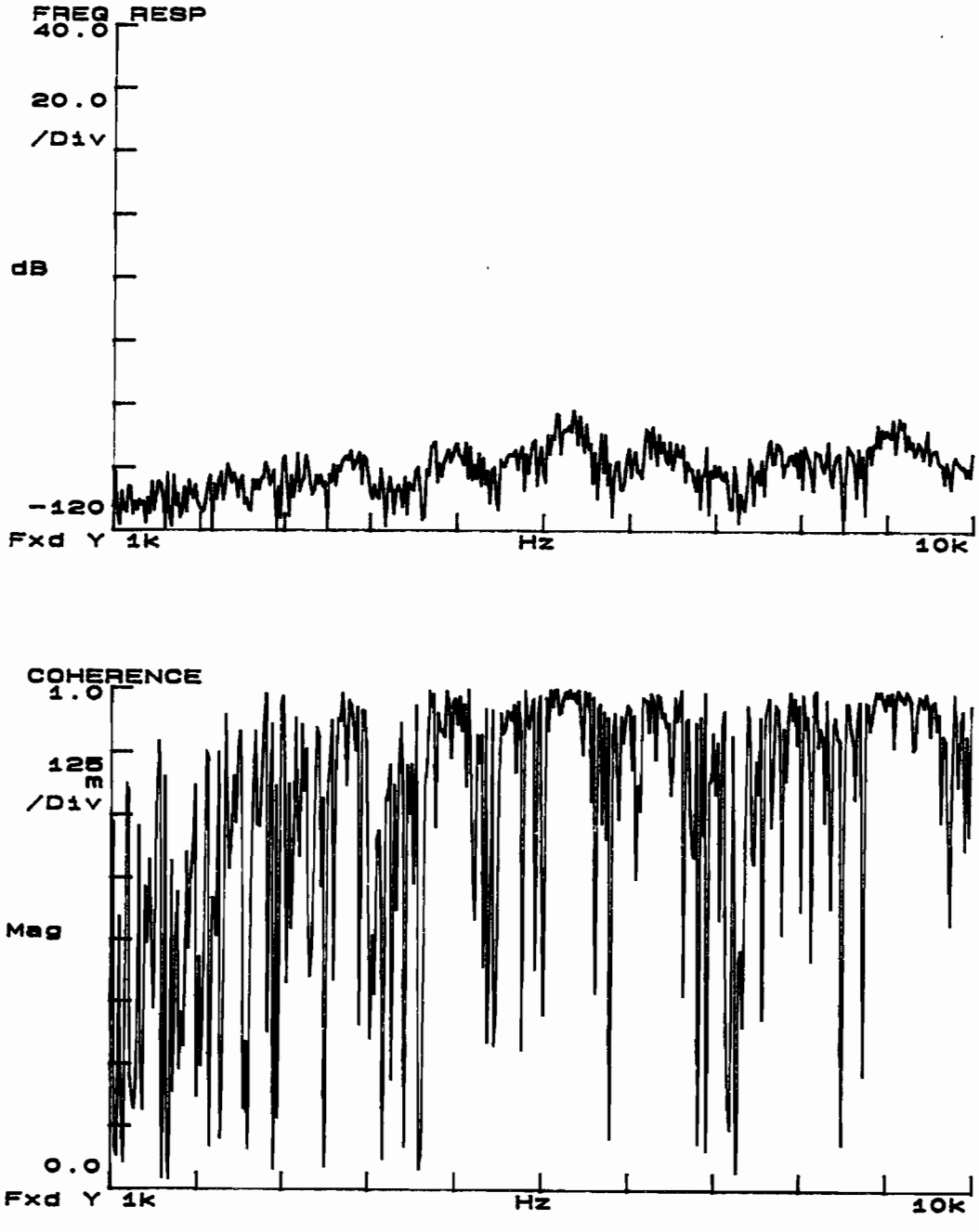

Figure A.5: Frequency Response and Coherence for Testing Signal Transmission Capabilities on Prototype 1 at Location C from Figure 3.13

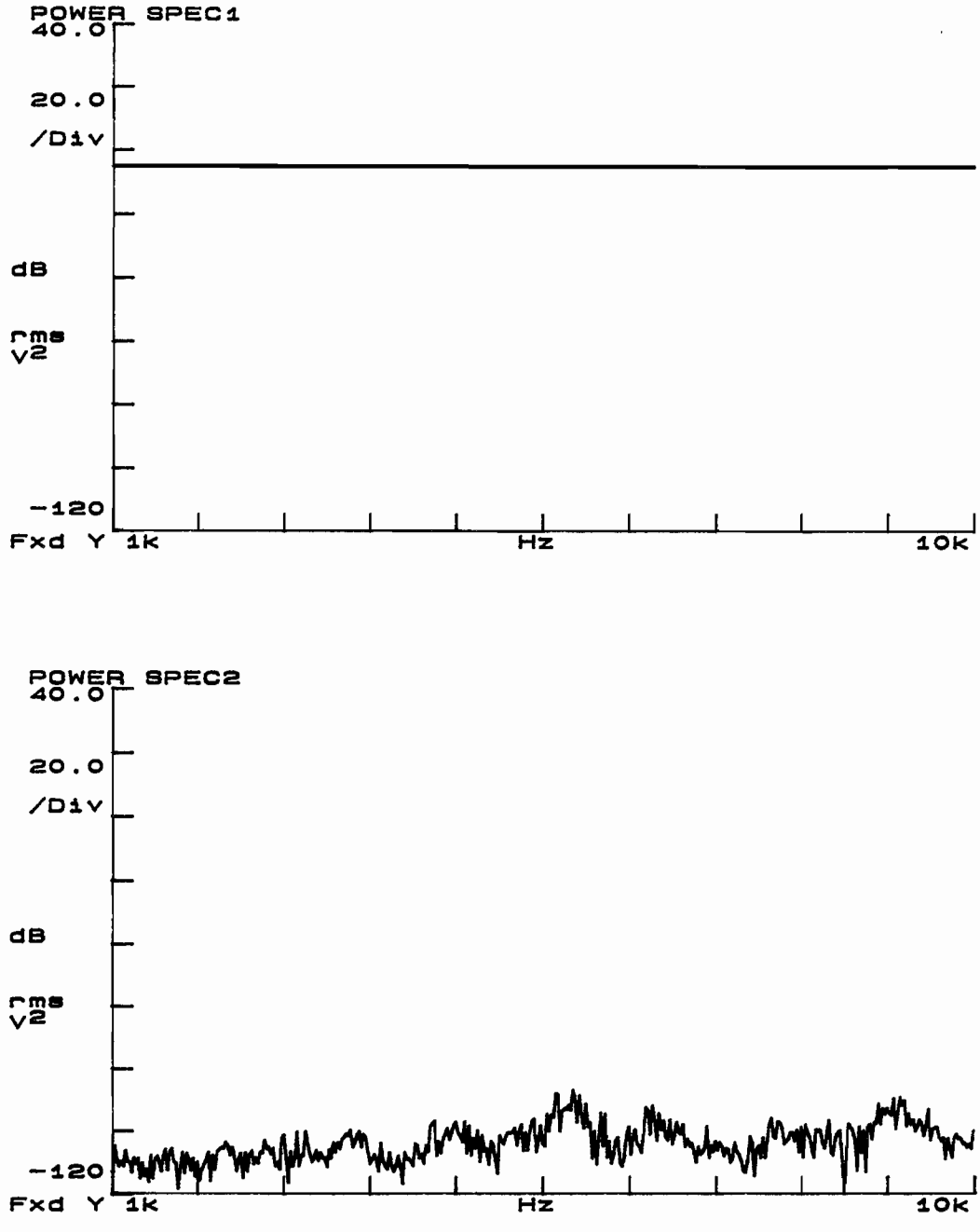

Figure A.6: Power Spectra for Testing Signal Transmission Capabilities on Prototype 1 at Location C from Figure 3.13

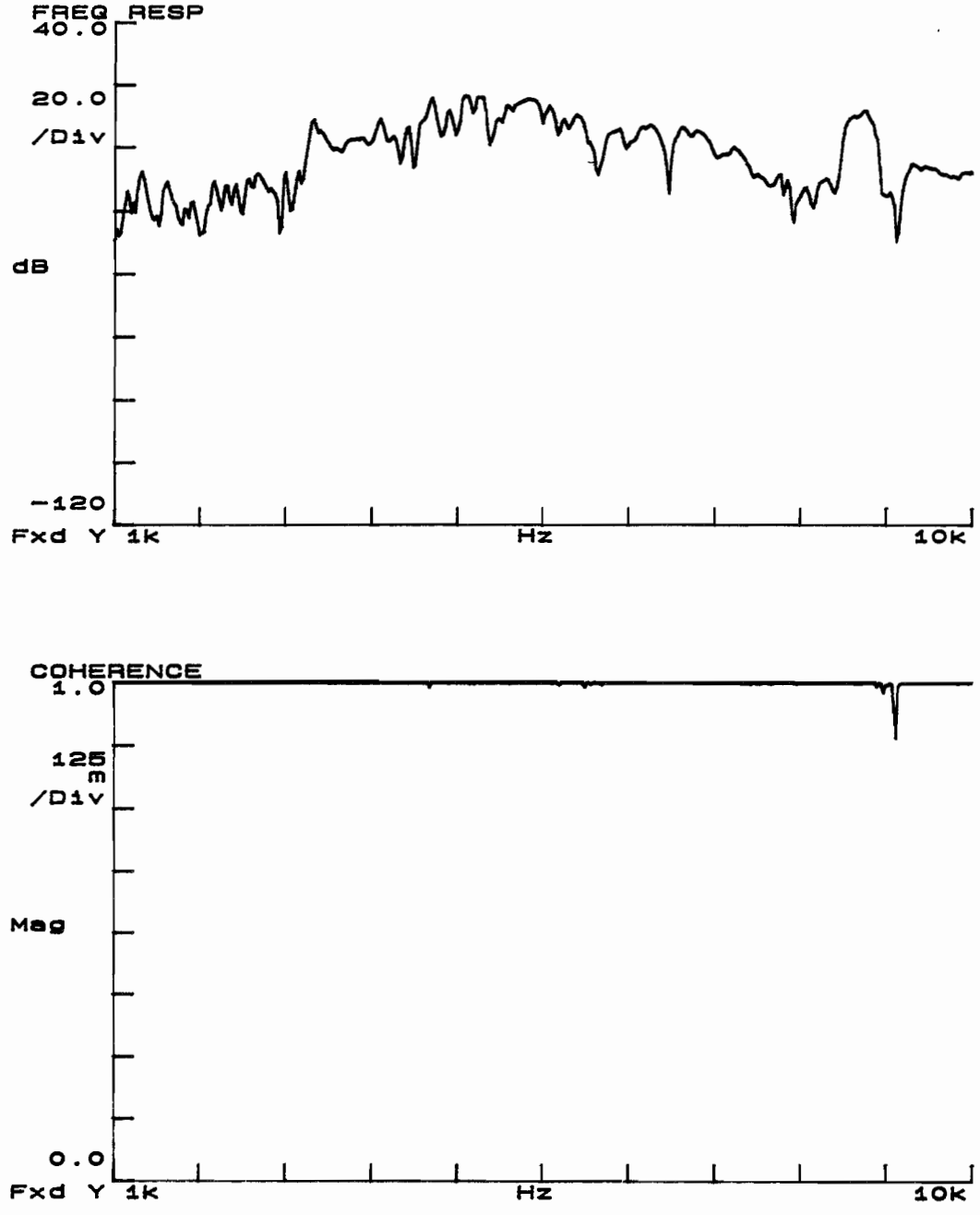

Figure A.7 Frequency Response and Coherence for Testing Signal Transmission Capabilities on Prototype 2 at Location A from Figure 3.13

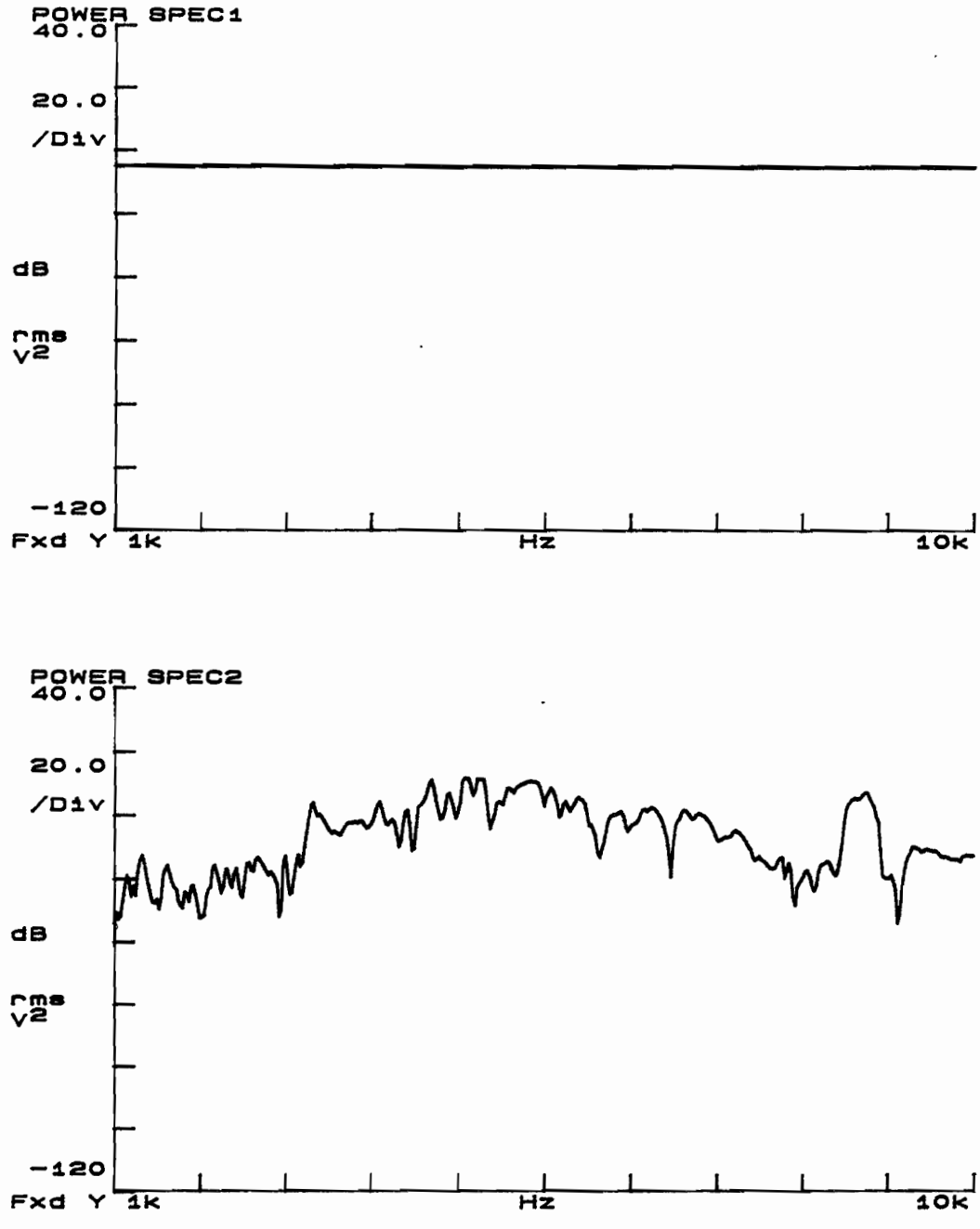

Figure A.8: Power Spectra for Testing Signal Transmission Capabilities on Prototype 2 at Location A from Figure 3.13

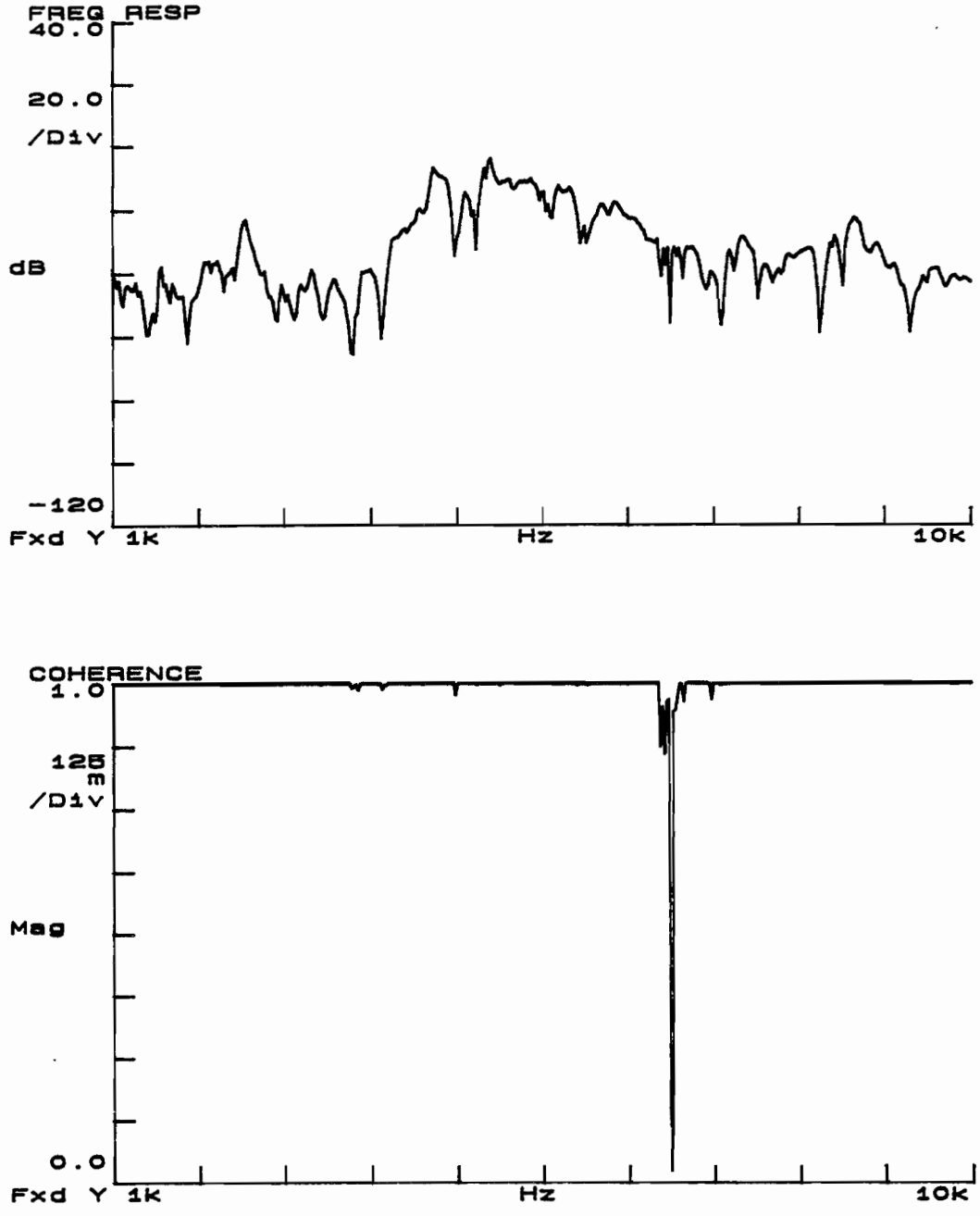

Figure A.9 Frequency Response and Coherence for Testing Signal Transmission Capabilities on Prototype 2 at Location B from Figure 3.13

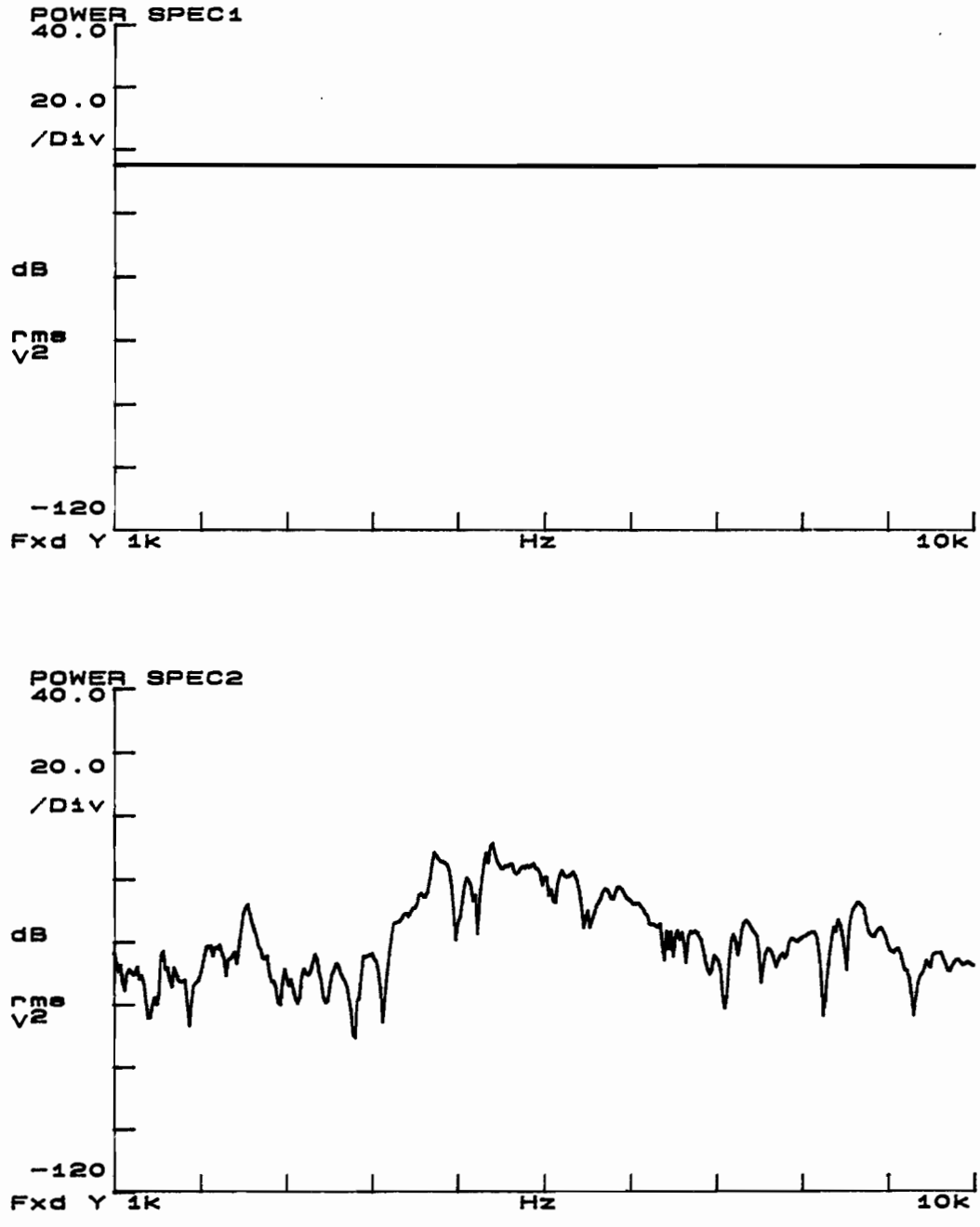

Figure A.10 Power Spectra for Testing Signal Transmission Capabilities on Prototype 2 at Location B from Figure 3.13

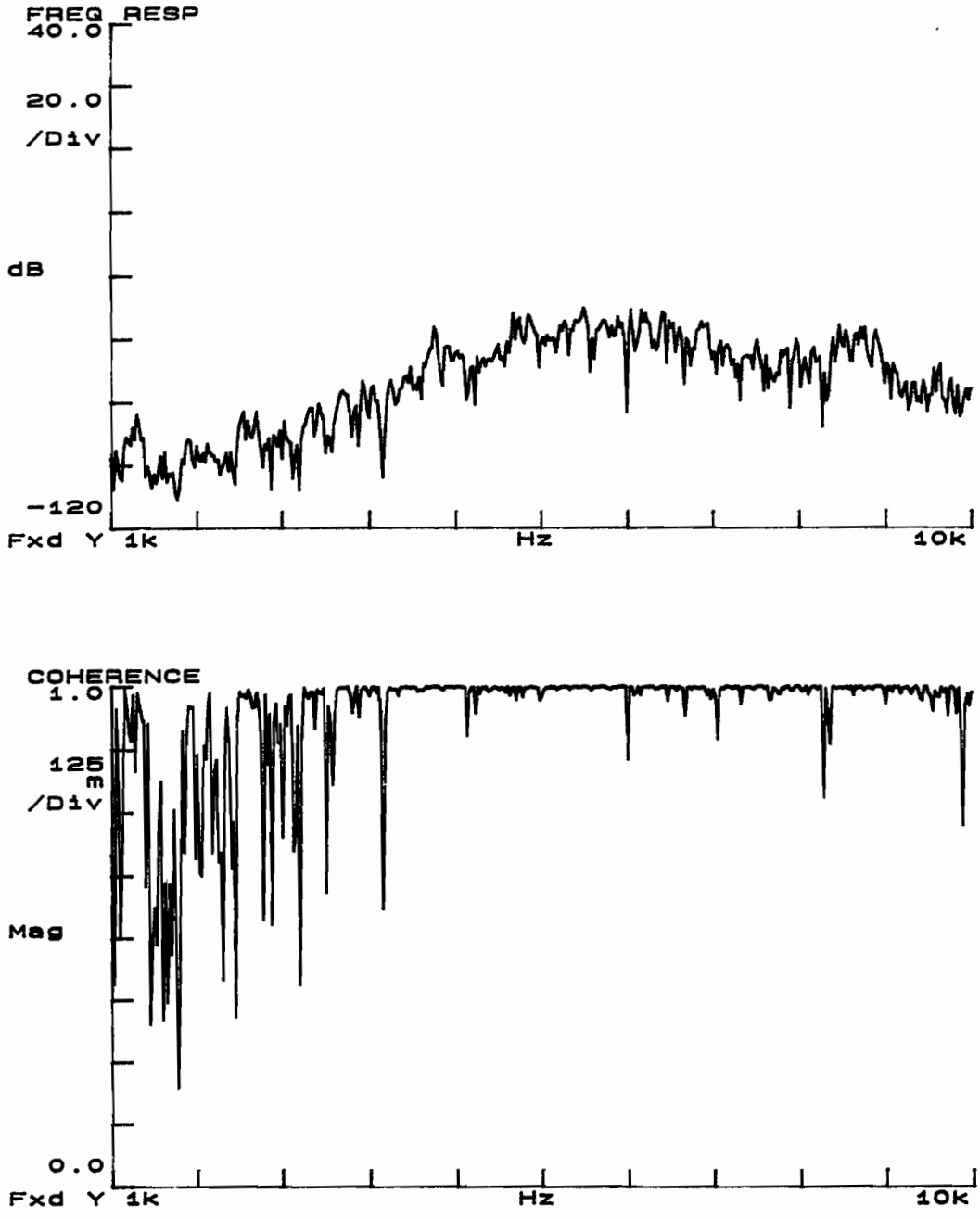

Figure A.11 Frequency Response and Coherence for Testing Signal Transmission Capabilities on Prototype 2 at Location C from Figure 3.13

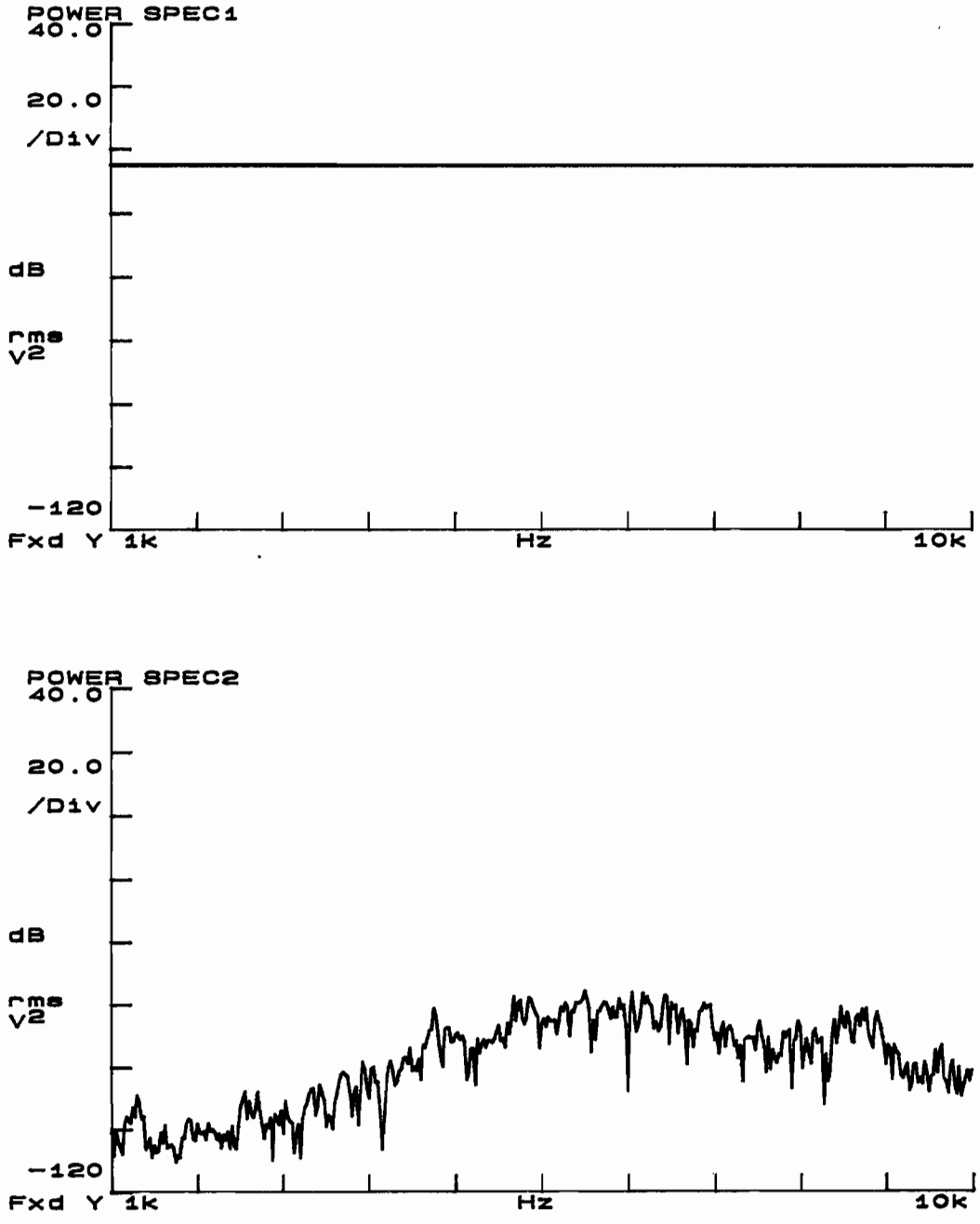

Figure A.12 Power Spectra for Testing Signal Transmission Capabilities on Prototype 2 at Location C from Figure 3.13

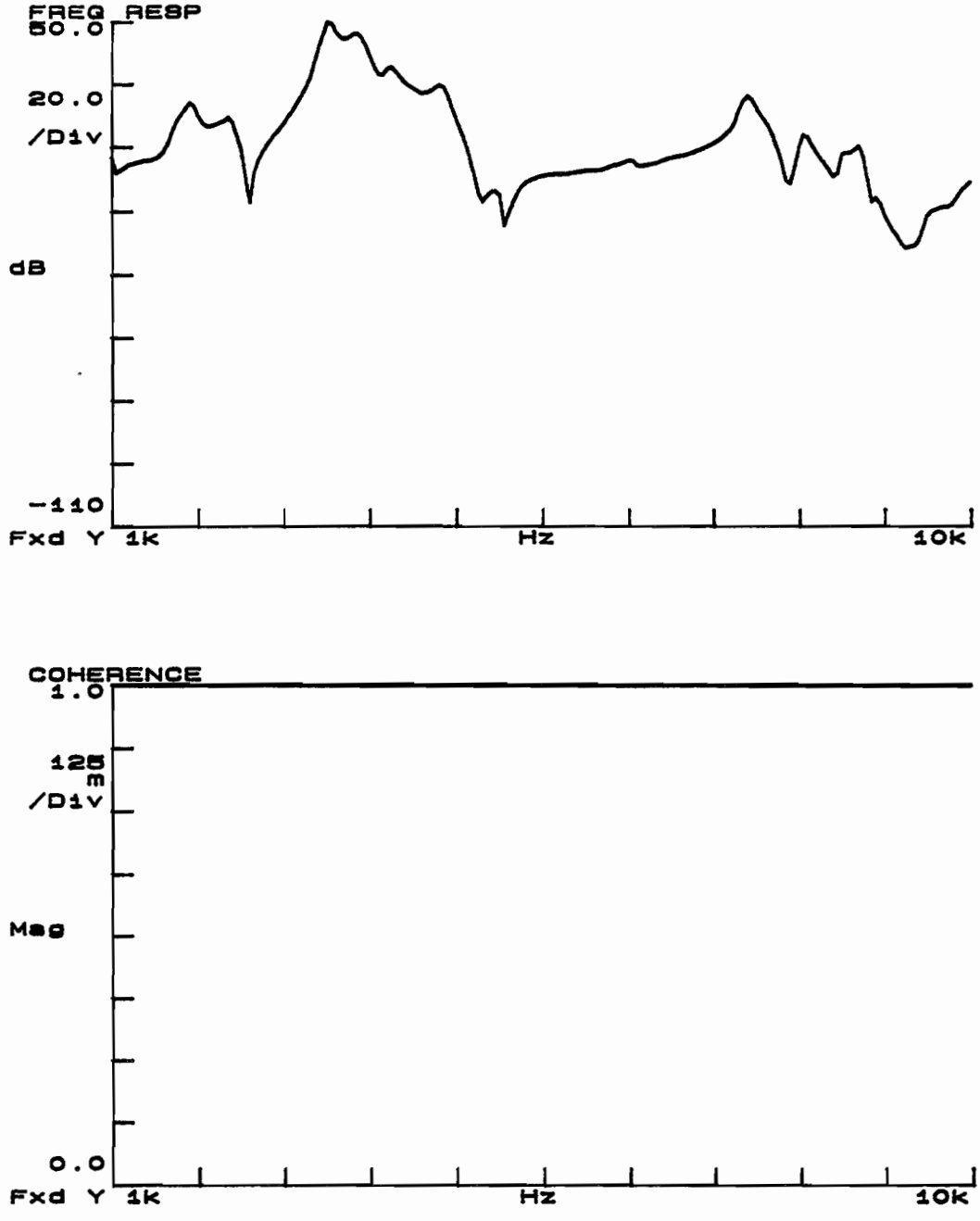

Figure A.13 Frequency Response and Coherence for Testing Signal Transmission Capabilities on Prototype 3 at Location A from Figure 4.4

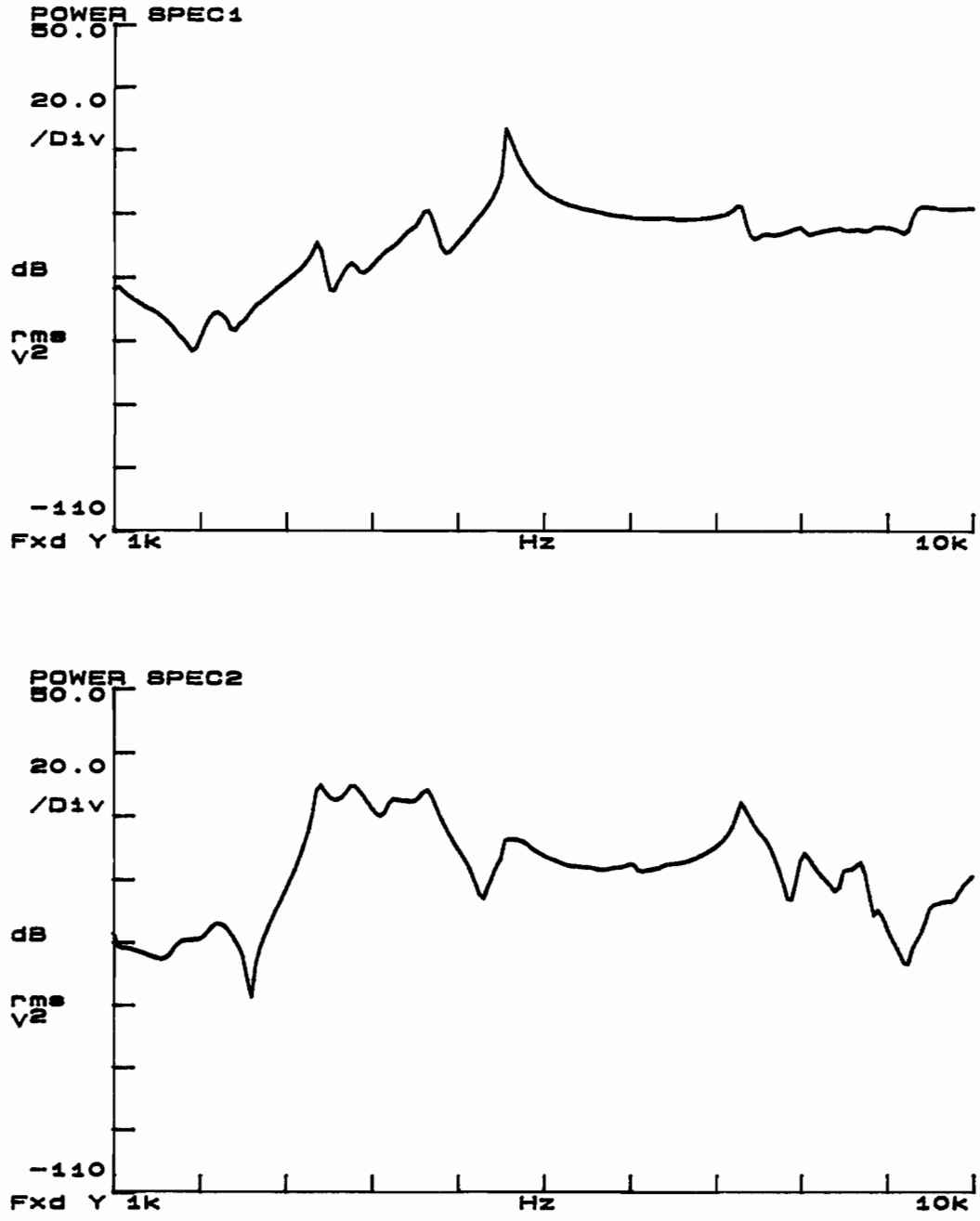

Figure A.14 Power Spectra for Testing Signal Transmission Capabilities on Prototype 3 at Location A from Figure 4.4

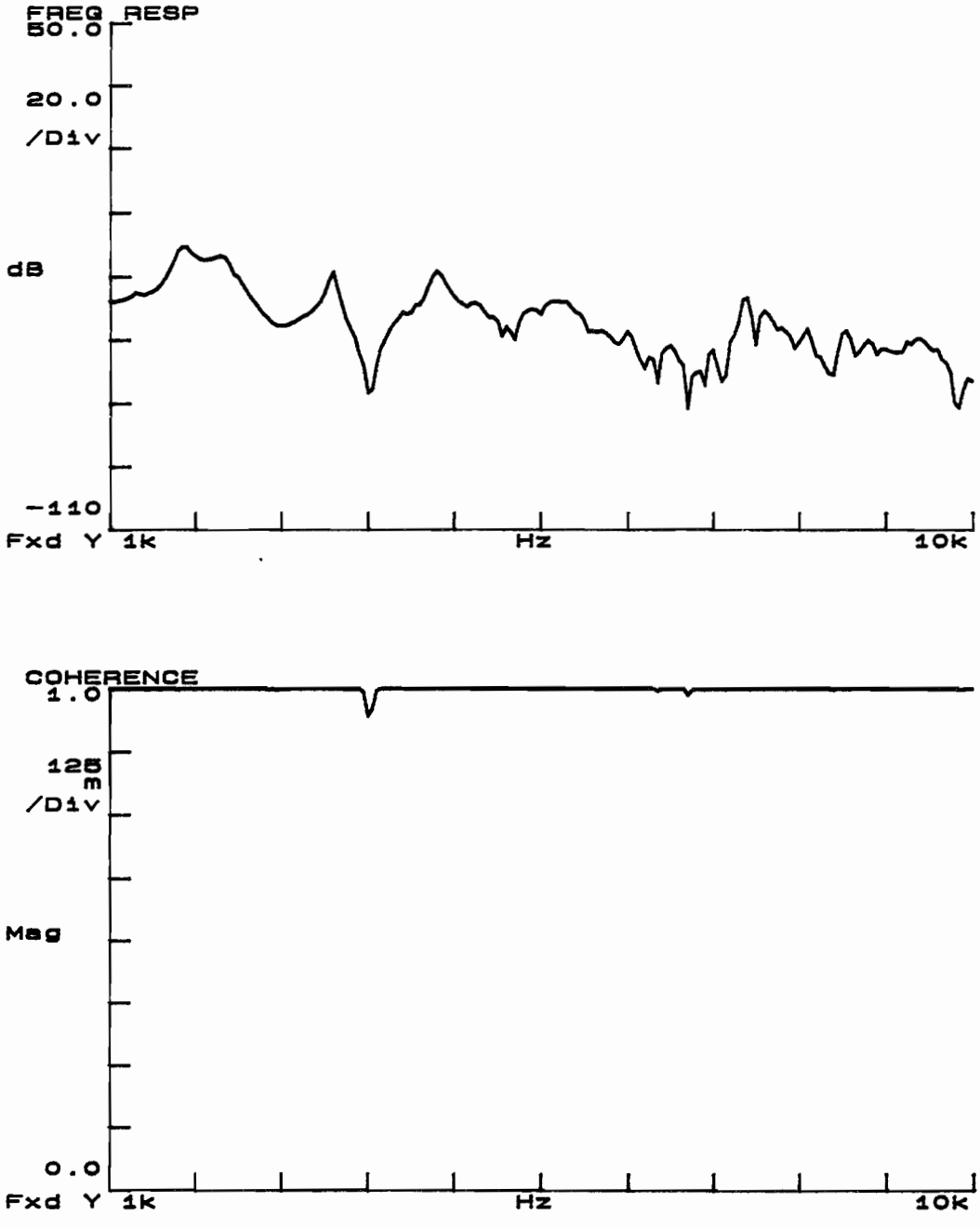

Figure A.15 Frequency Response and Coherence for Testing Signal Transmission Capabilities on Prototype 3 at Location B from Figure 4.4

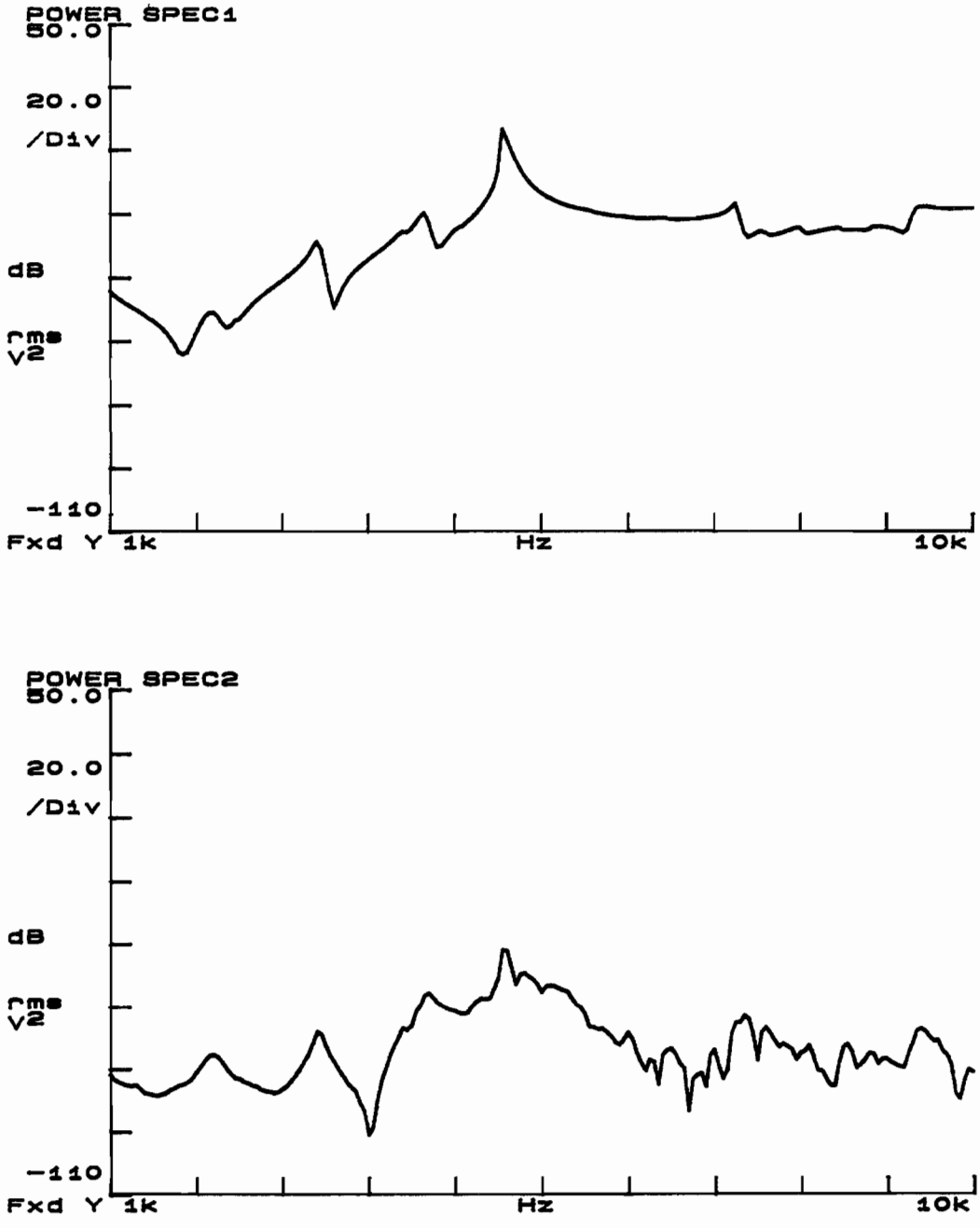

Figure A.16 Power Spectra for Testing Signal Transmission Capabilities on Prototype 3 at Location B from Figure 4.4

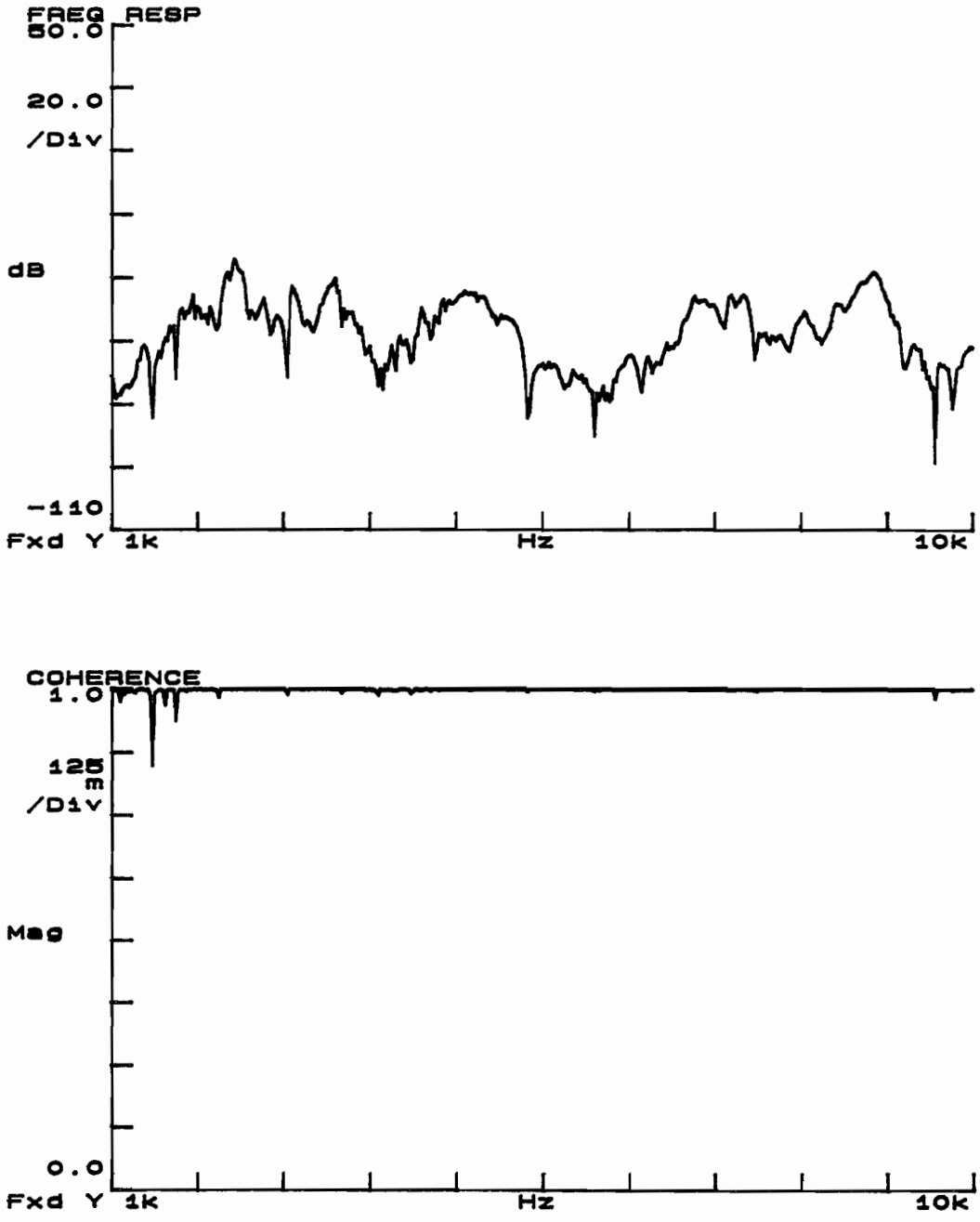

Figure A.17 Frequency Response and Coherence for Testing Signal Transmission Capabilities on Prototype 3 at Location C from Figure 4.4

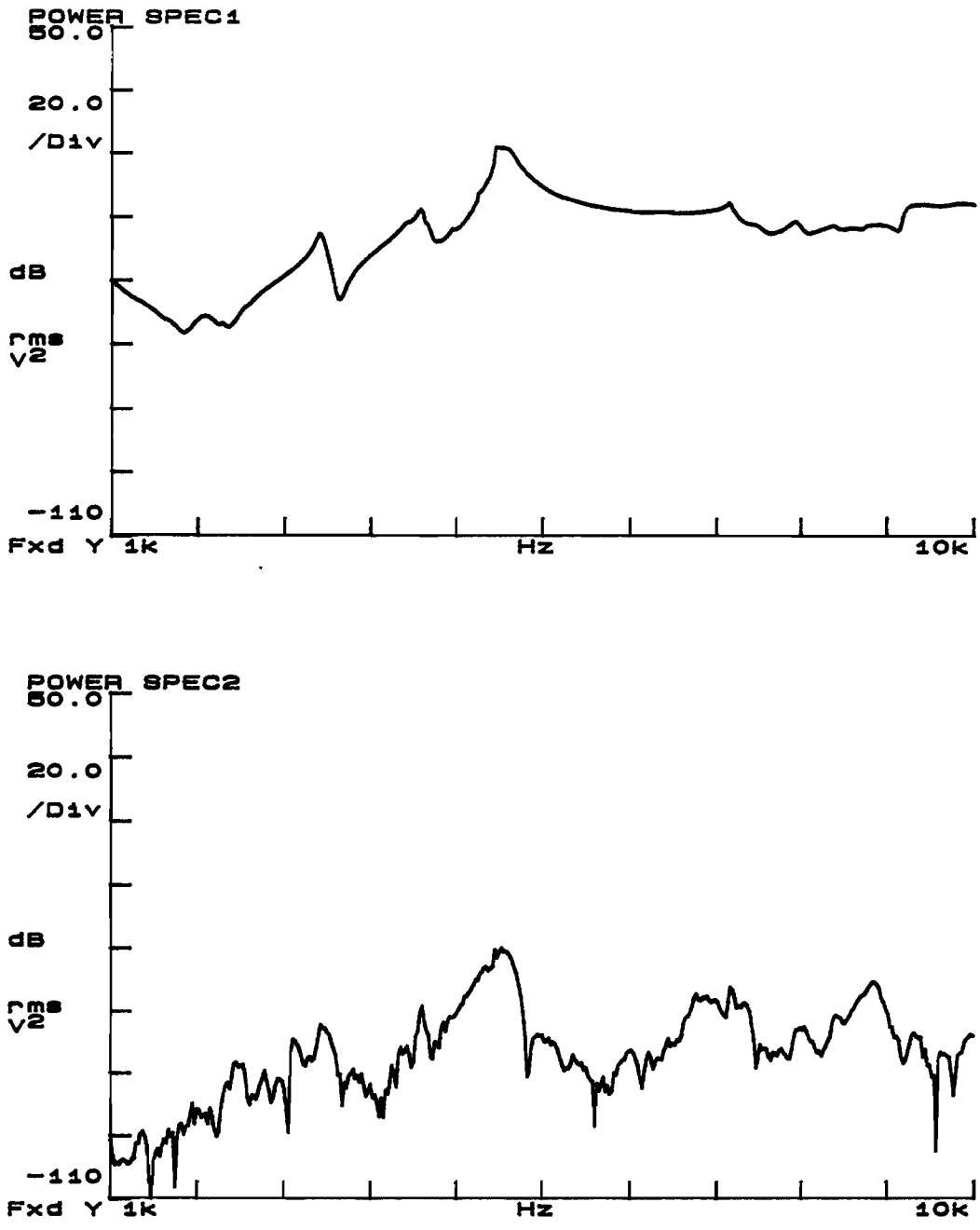

Figure A.18 Power Spectra for Testing Signal Transmission Capabilities on Prototype 3 at Location C from Figure 4.4

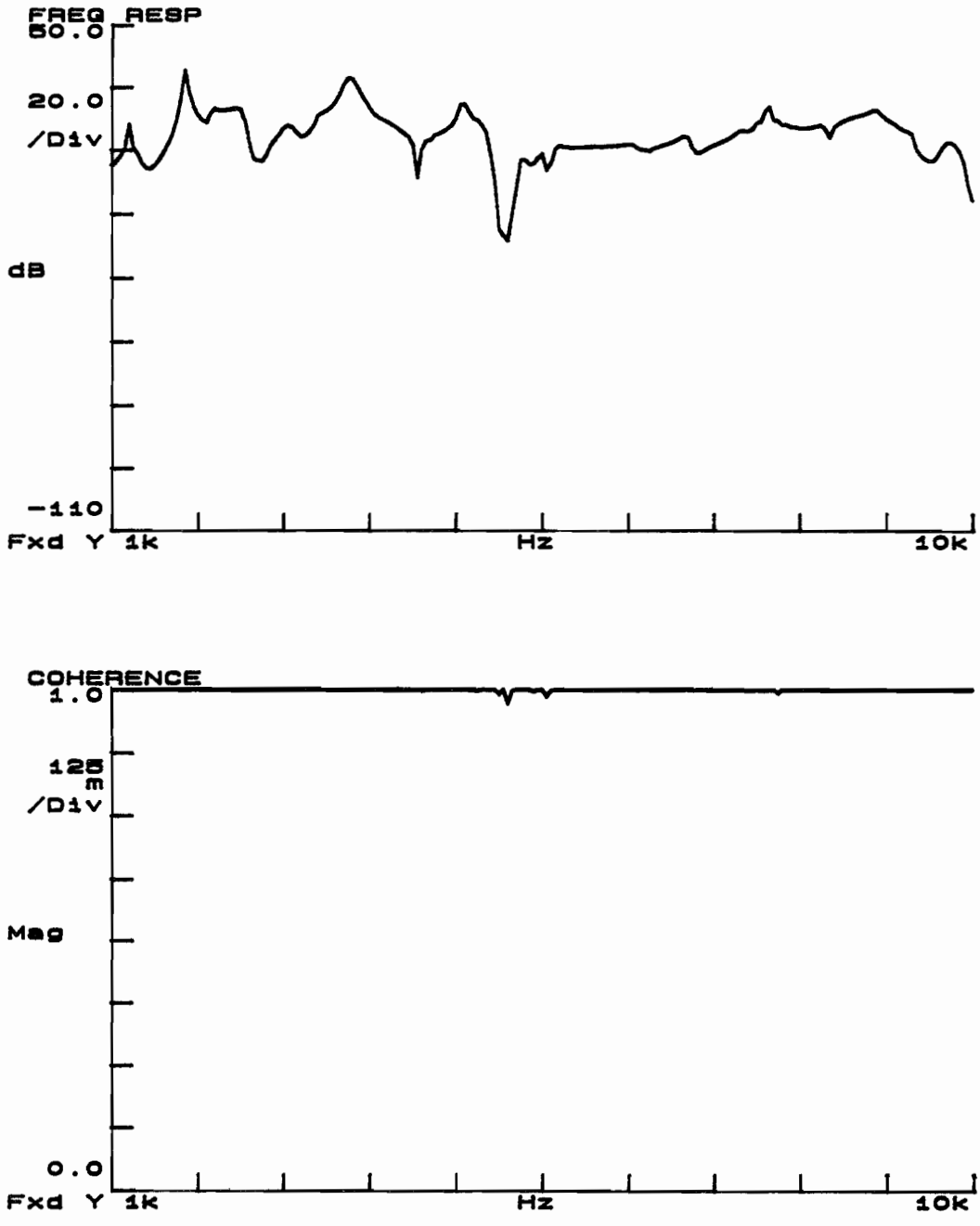

Figure A.19 Frequency Response and Coherence for Testing Signal Transmission Capabilities on Prototype 4 at Location A from Figure 4.4

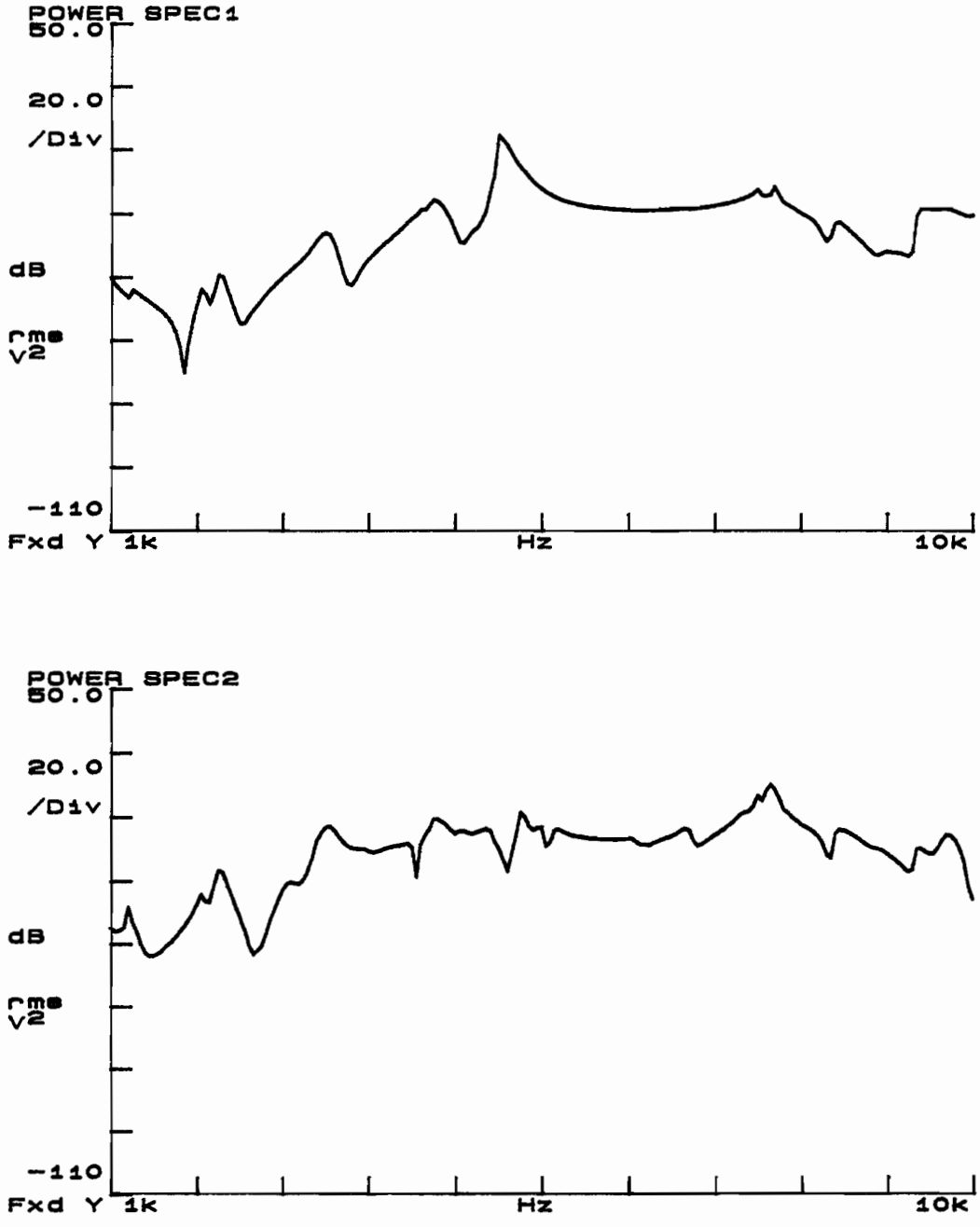

Figure A.20 Power Spectra for Testing Signal Transmission Capabilities on Prototype 4 at Location A from Figure 4.4

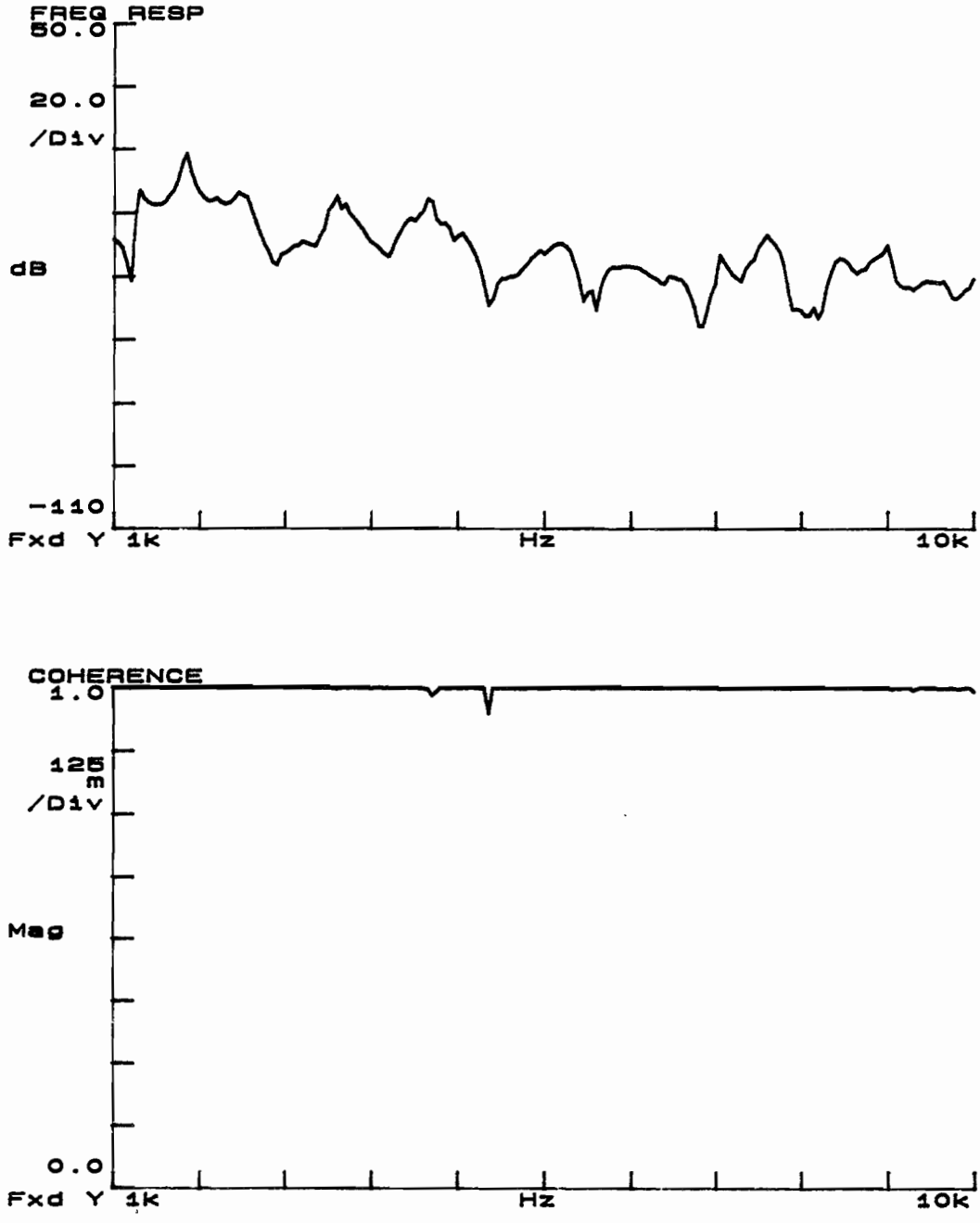

Figure A.21 Frequency Response and Coherence for Testing Signal Transmission Capabilities on Prototype 4 at Location B from Figure 4.4

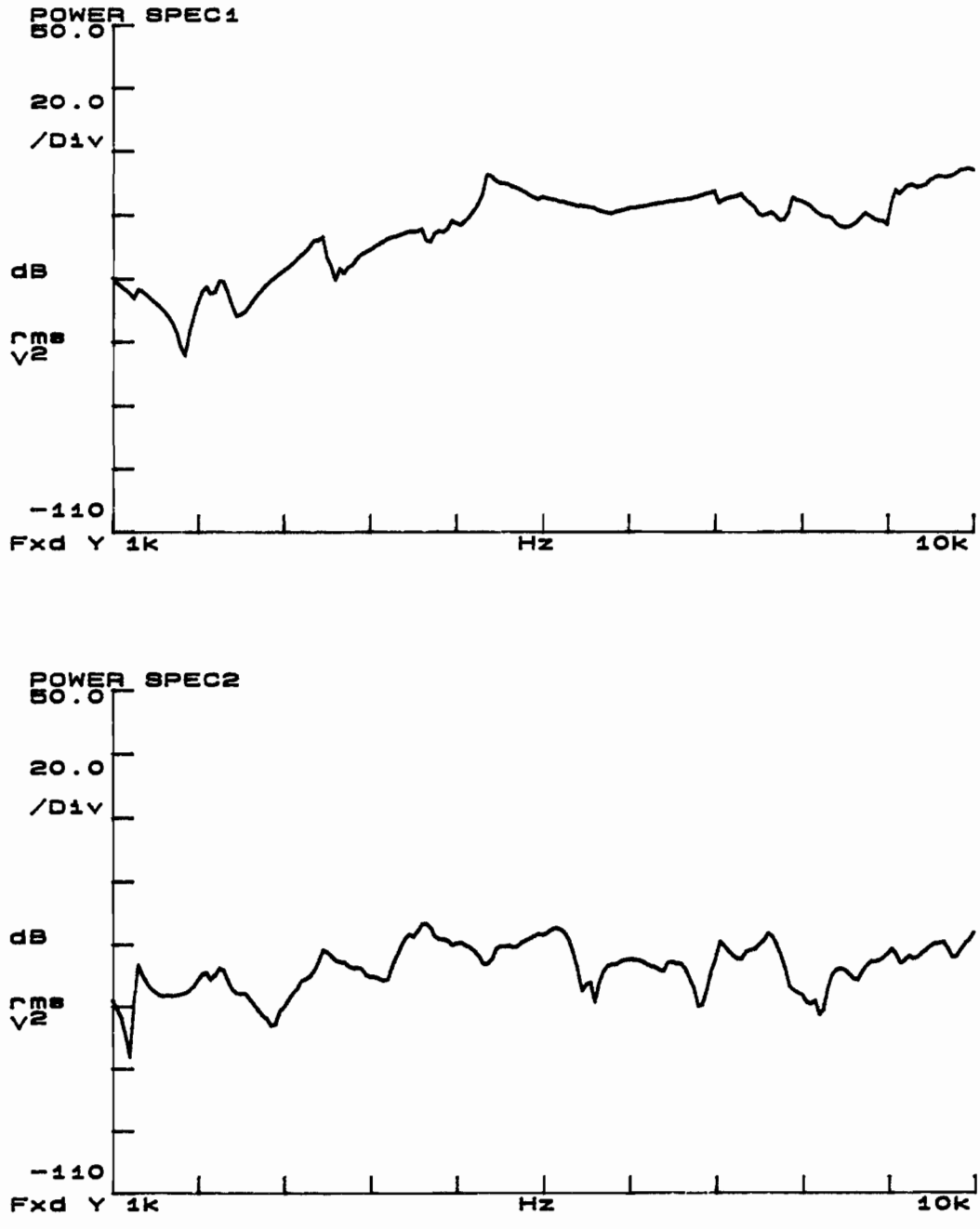

Figure A.22 Power Spectra for Testing Signal Transmission Capabilities on Prototype 4 at Location B from Figure 4.4

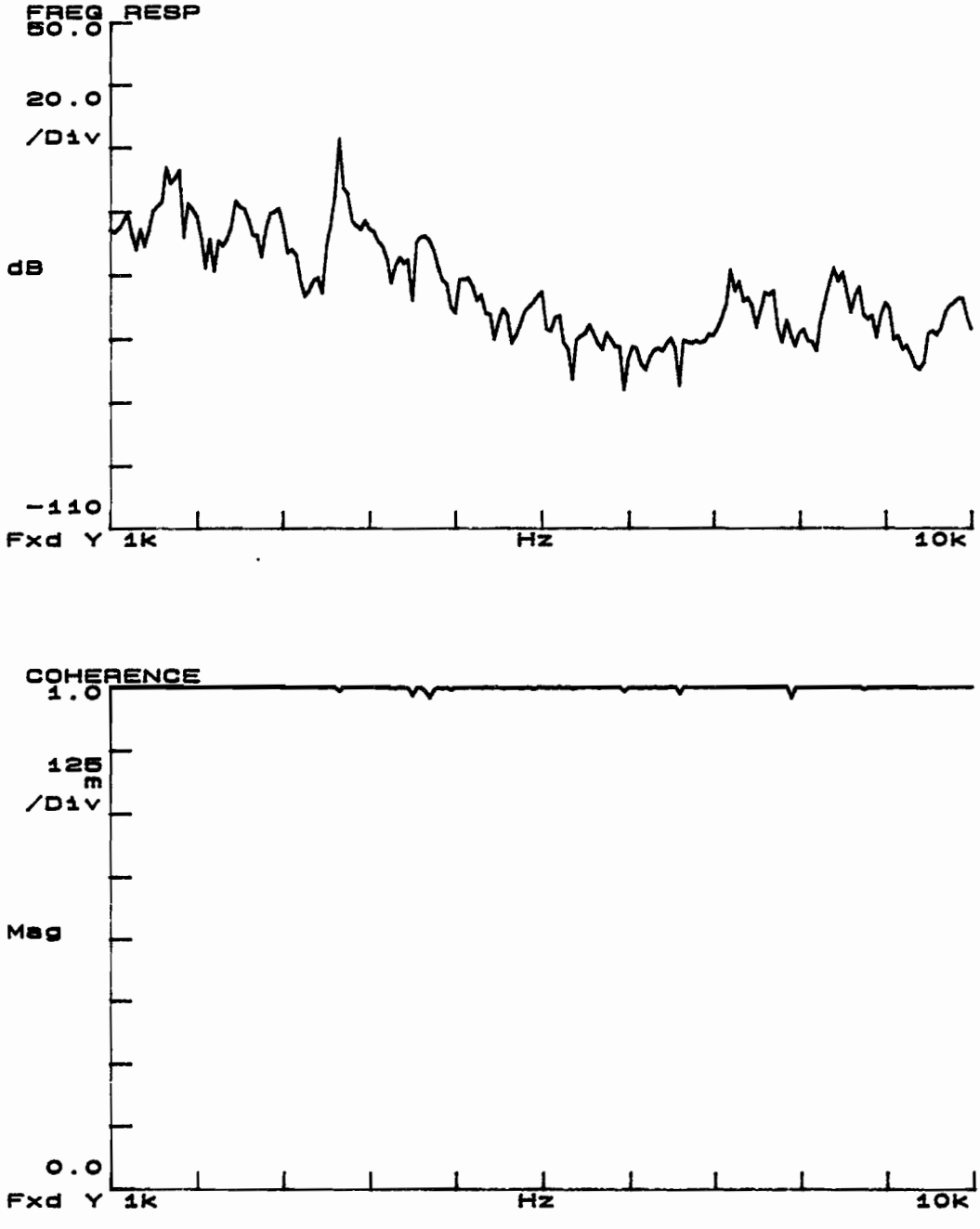

Figure A.23 Frequency Response and Coherence for Testing Signal Transmission Capabilities on Prototype 4 at Location C from Figure 4.4

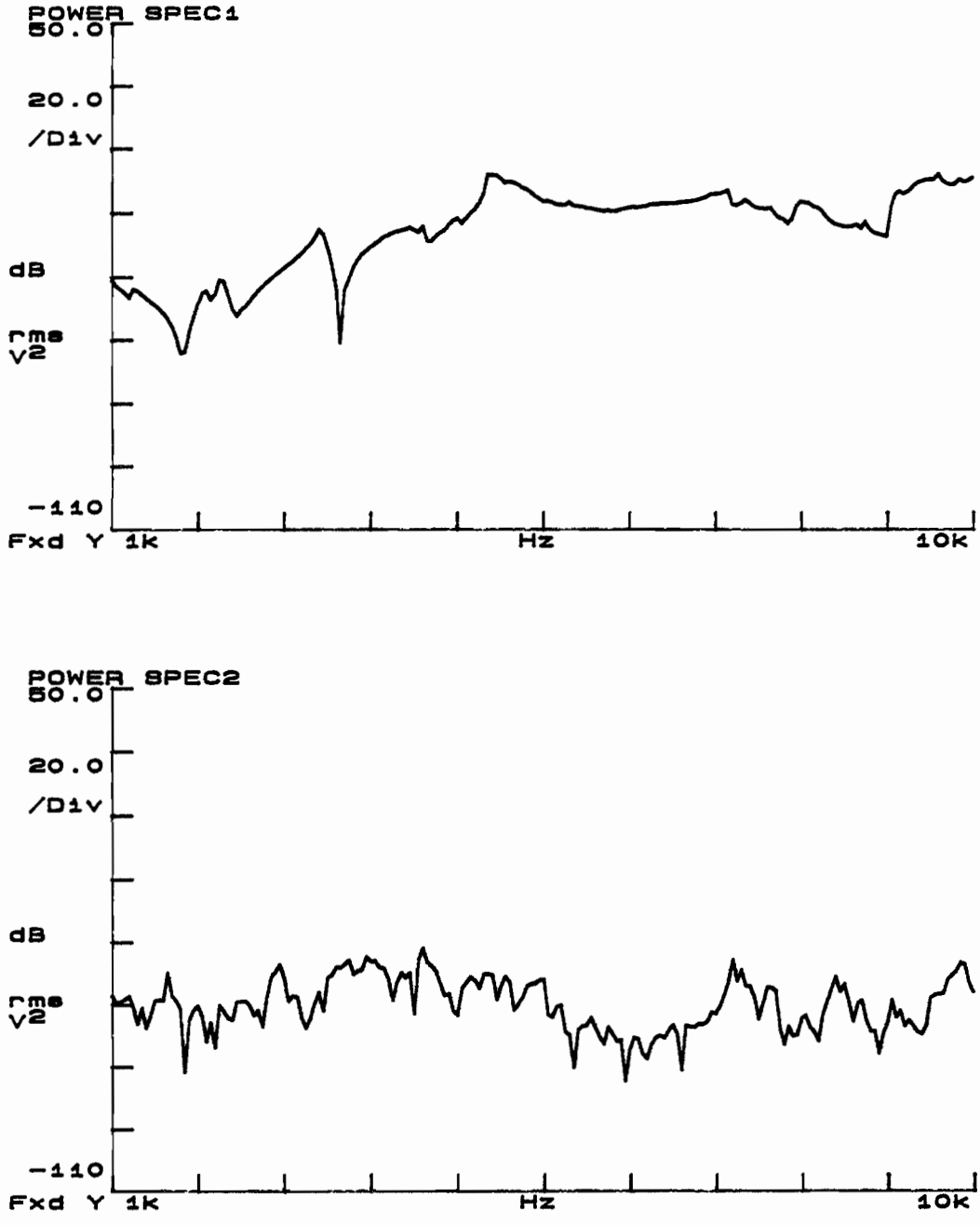

Figure A.24 Power Spectra for Testing Signal Transmission Capabilities on Prototype 4 at Location C from Figure 4.4

Appendix B

Spectral Functions Measured During Component Testing of Prototype 4 in the Laboratory

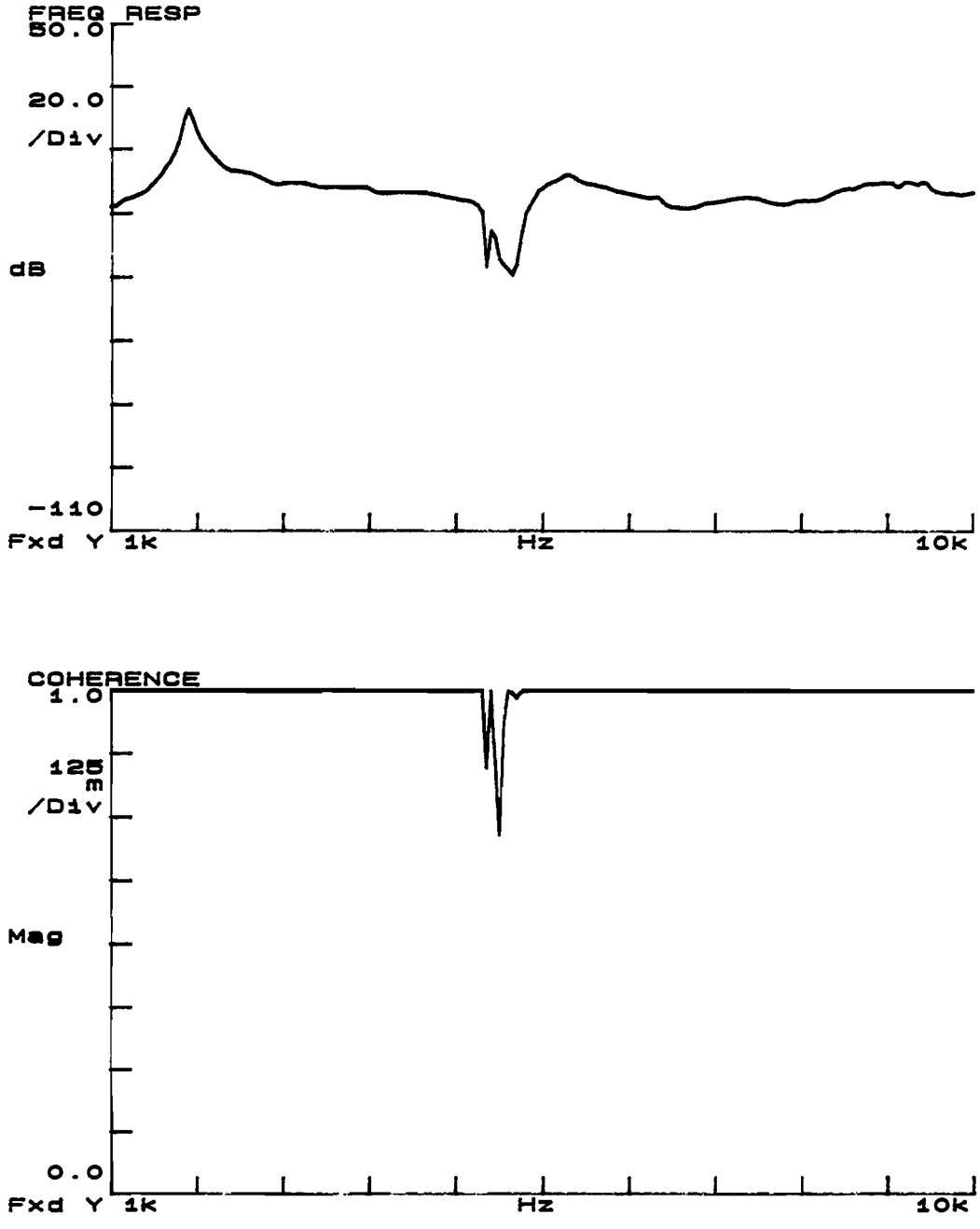

Figure B.1: Frequency Response and Coherence for Prototype 4 Component Testing with both the Source and Receiver Directly on the Ground

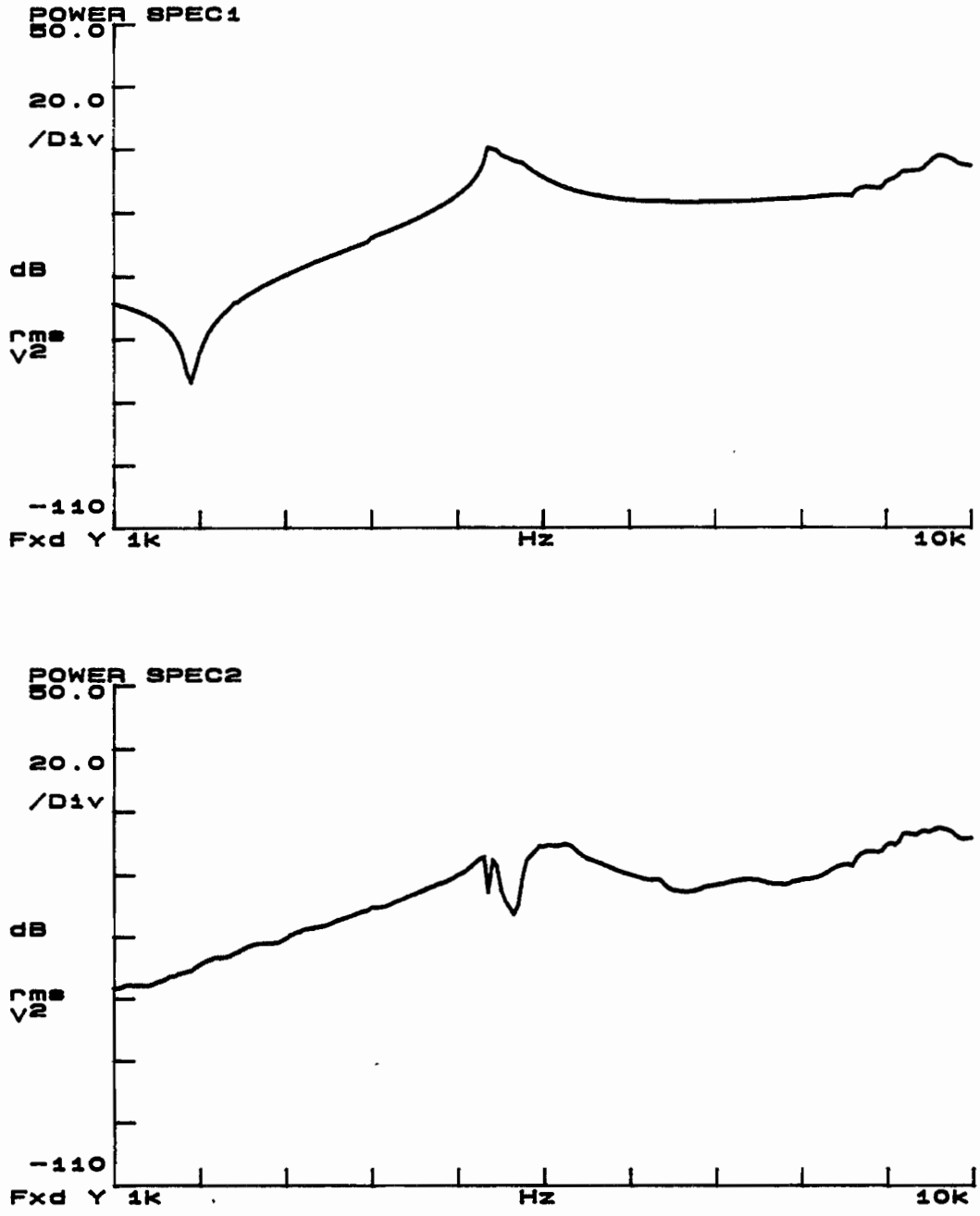

Figure B.2: Power Spectra for Prototype 4 Component Testing with both the Source and Receiver Directly on the Ground

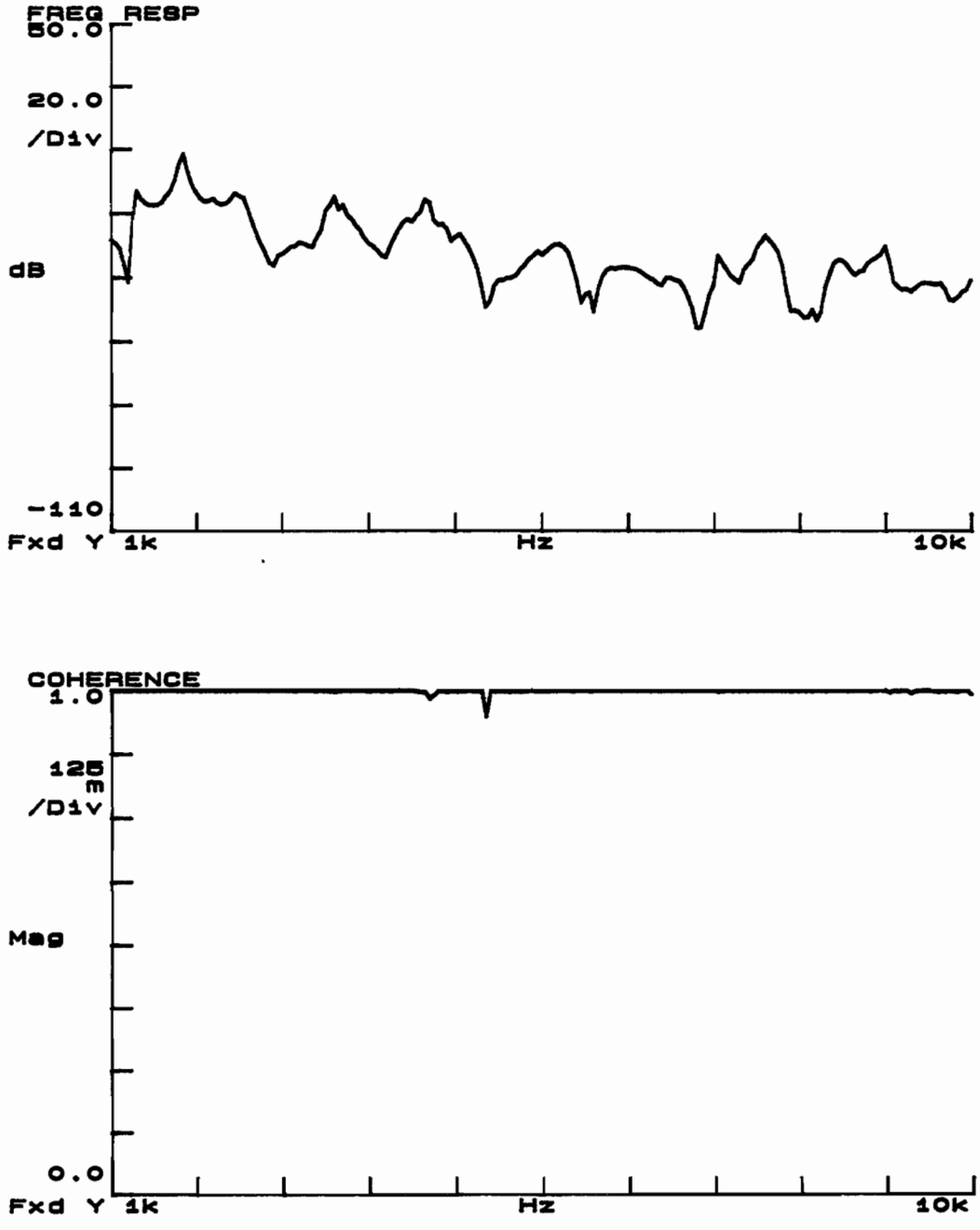

Figure B.3: Frequency Response and Coherence for Prototype 4 Component Testing with the Source on the "Source Wheel" and the Receiver Directly on the Ground

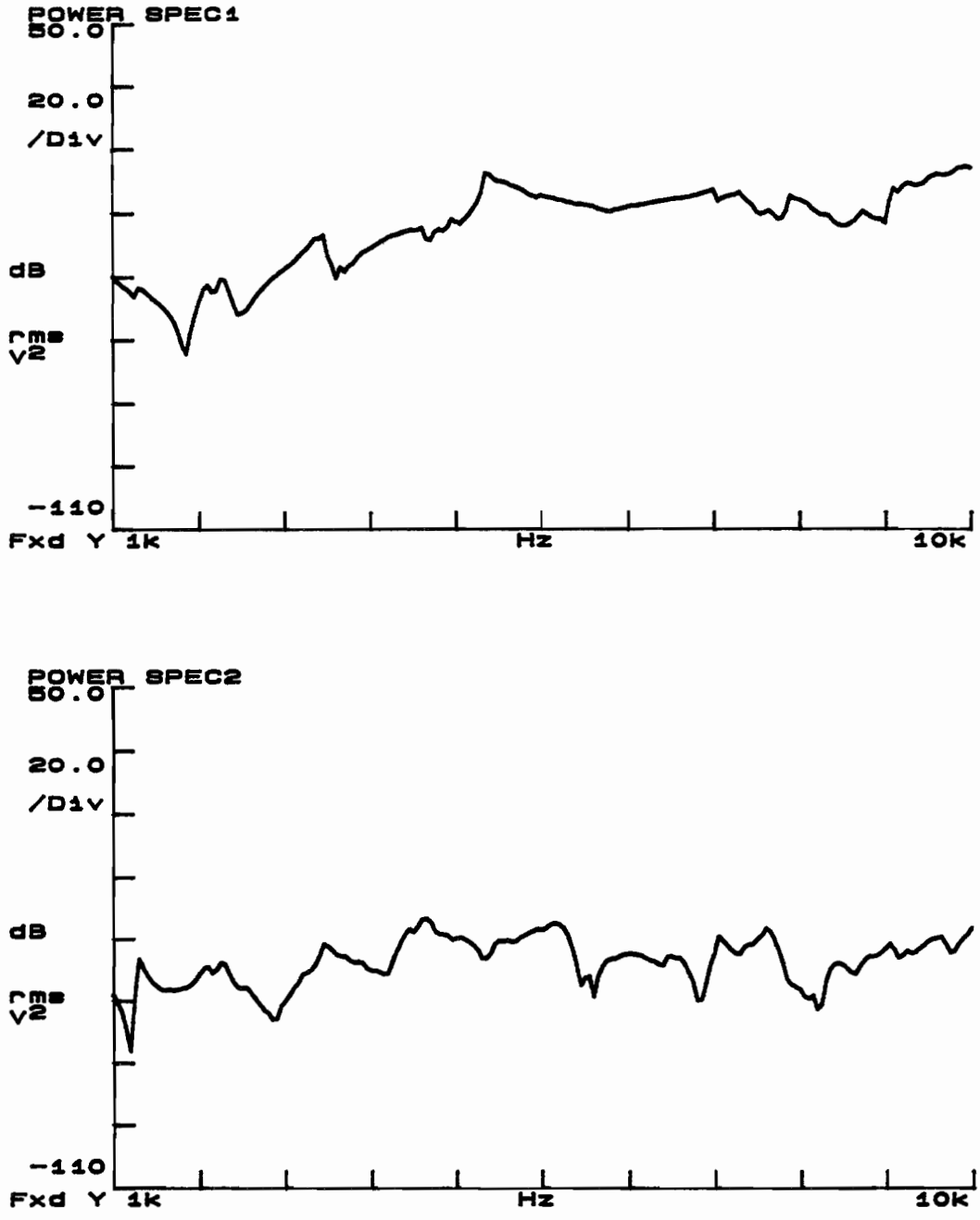

Figure B.4: Power Spectra for Prototype 4 Component Testing with the Source on the "Source Wheel" and the Receiver Directly on the Ground

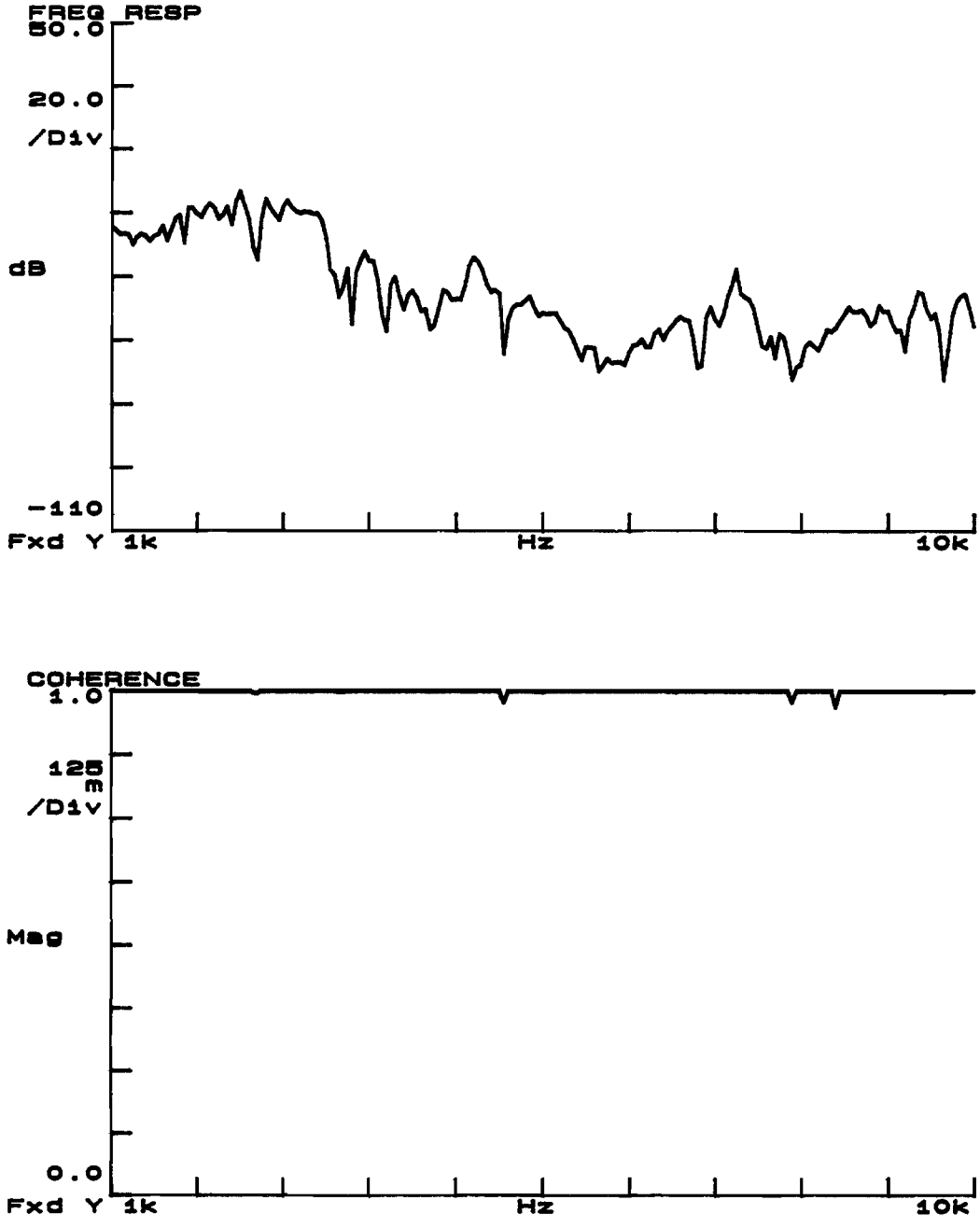

Figure B.5: Frequency Response and Coherence for Prototype 4 Component Testing with the Source Directly on the Ground and the Receiver on the "Receiver Wheel"

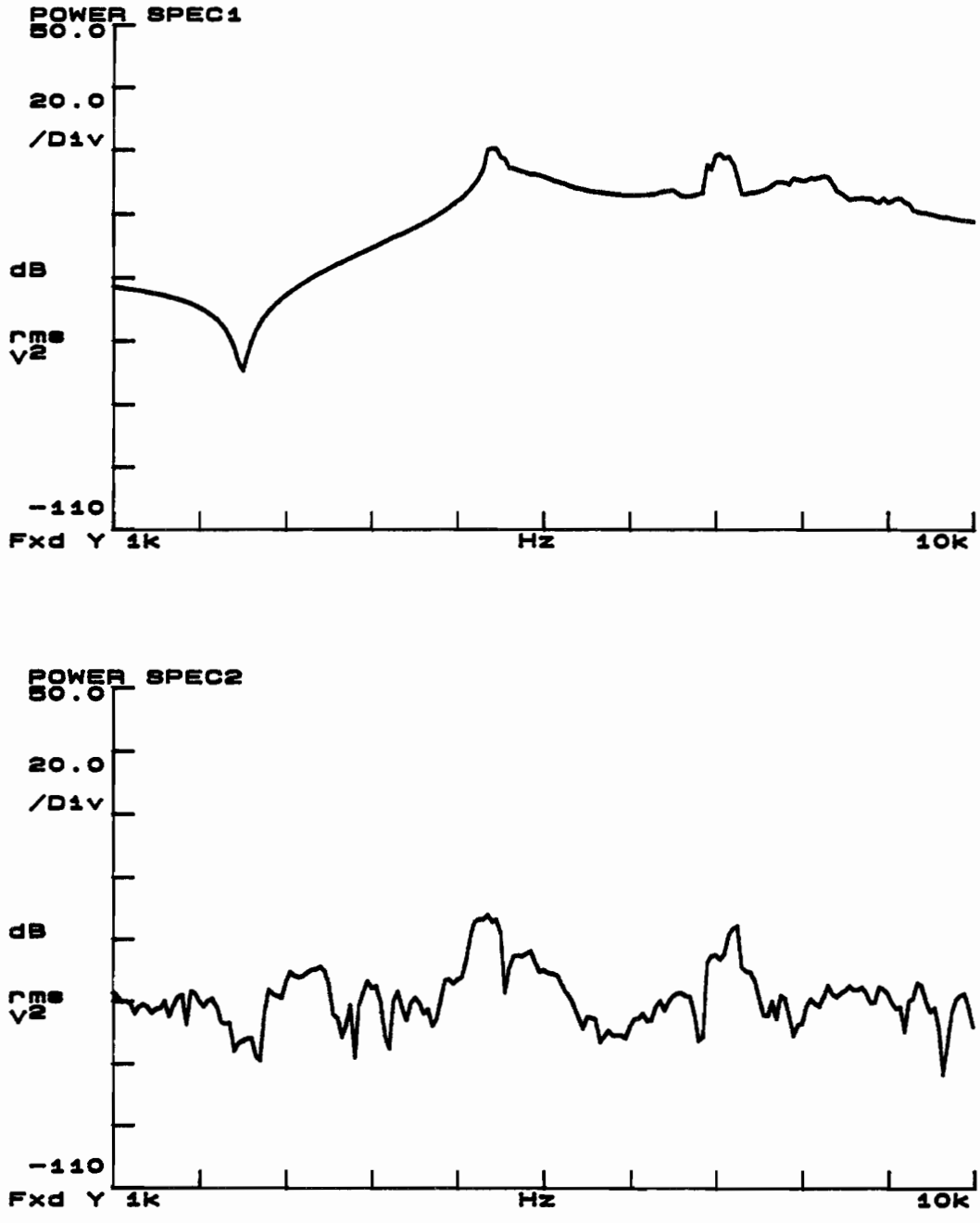

Figure B.6: Power Spectra for Prototype 4 Component Testing with the Source Directly on the Ground and the Receiver on the "Receiver Wheel"

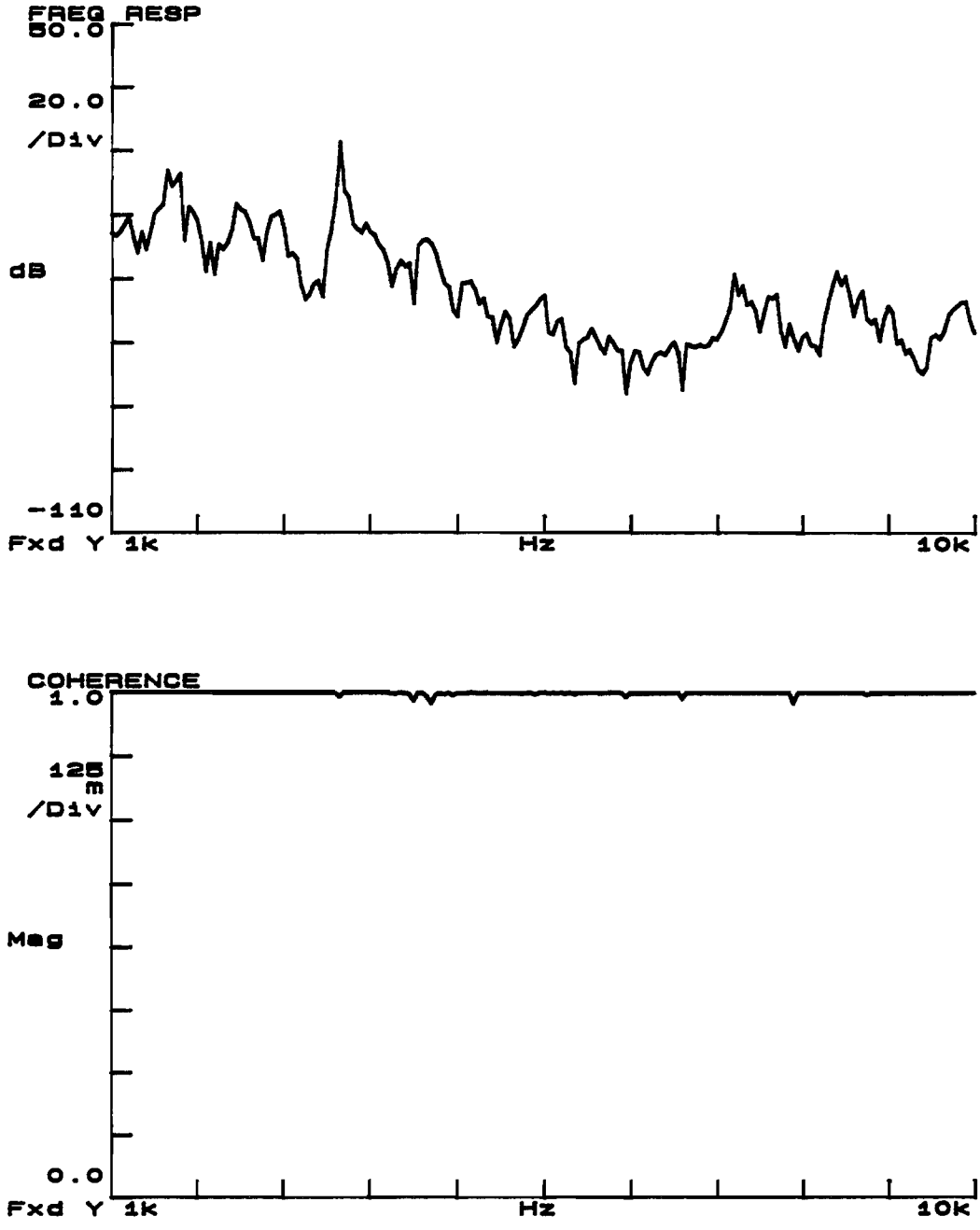

Figure B.7 Frequency Response and Coherence for Prototype 4 Component Testing with the Source on the "Source Wheel" and the Receiver on the "Receiver Wheel"

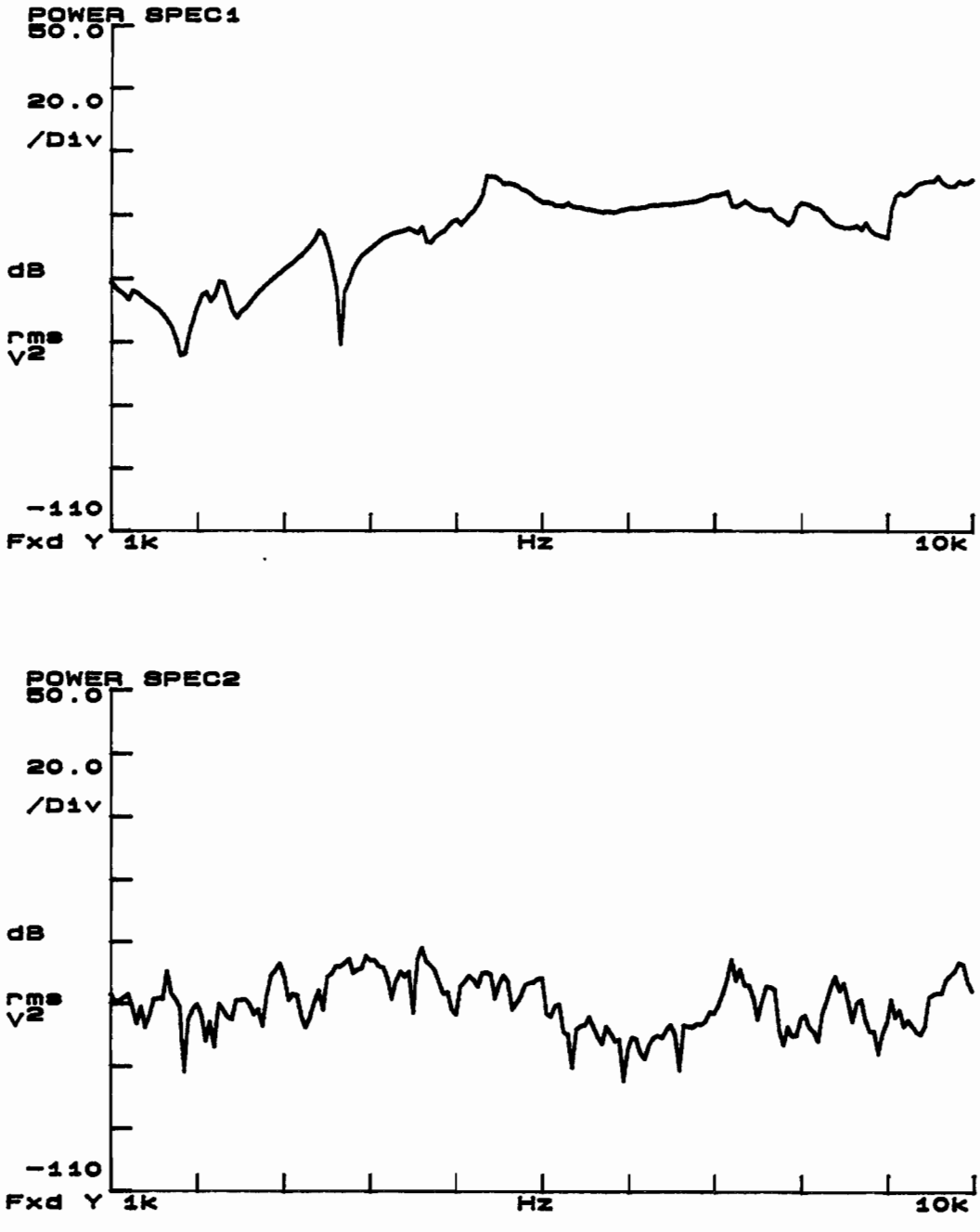

Figure B.8: Power Spectra for Prototype 4 Component Testing with the Source on the "Source Wheel" and the Receiver on the "Receiver Wheel"

Appendix C

Spectral Functions Measured During Signal Transmission Testing of Prototype 4 in the Laboratory

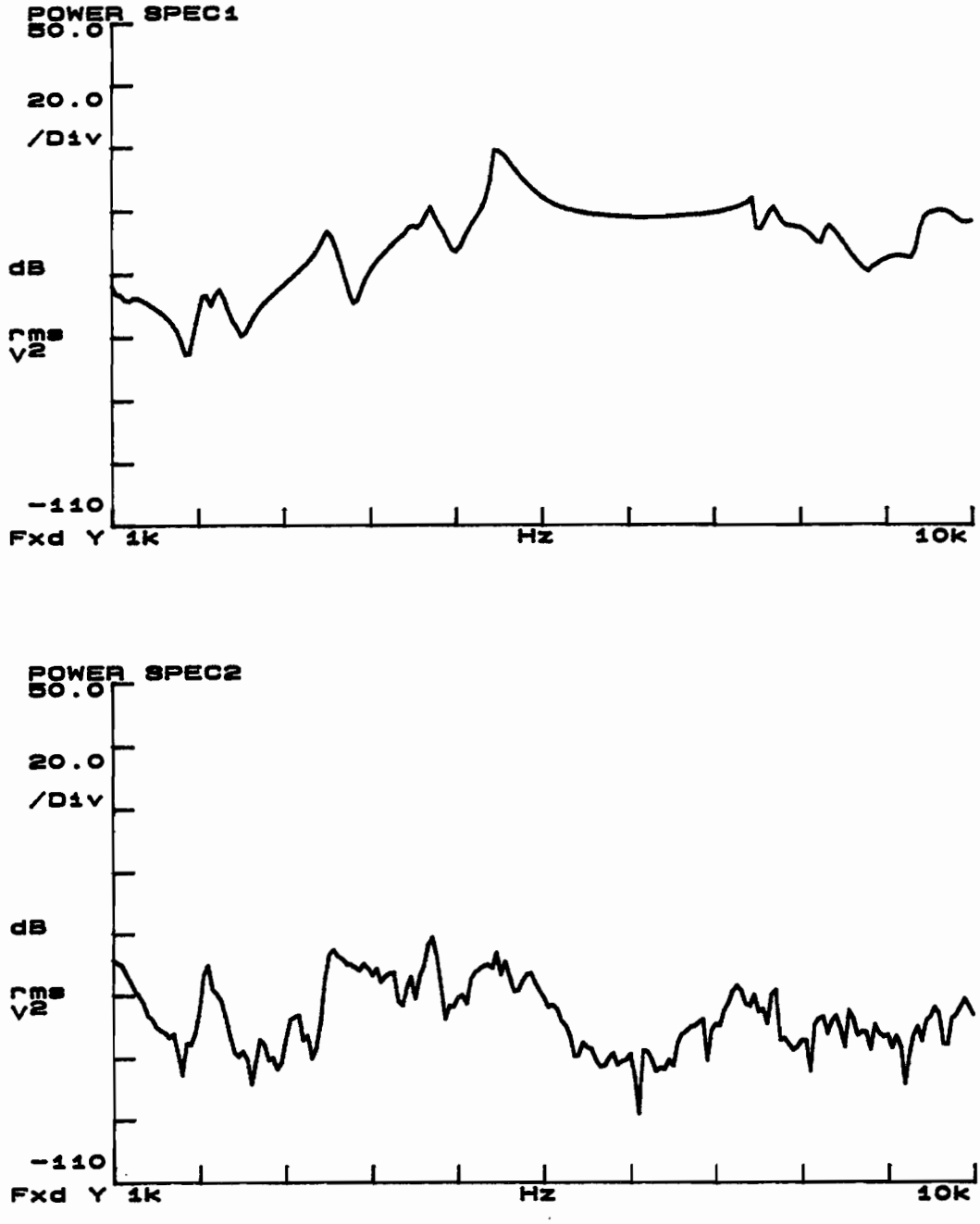

Figure C.1: Power Spectra for Signal Transmission Testing on Prototype 4 with Channel 1 Connected to the F8 Shaker Output and Channel 2 Connected to the Accelerometer on the "Receiver Wheel"

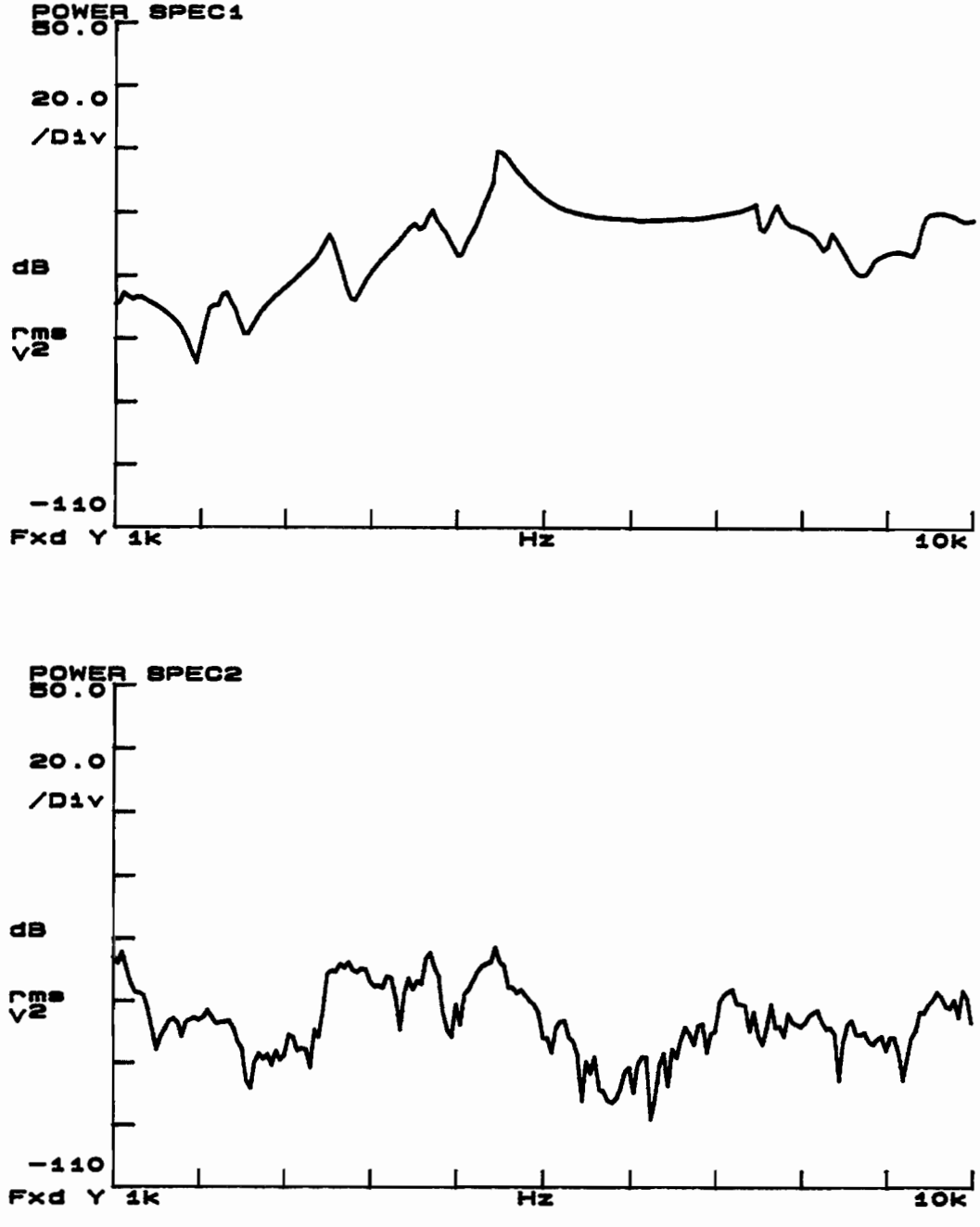

Figure C.2: Power Spectra for Signal Transmission Testing on Prototype 4 with the Hinge Disconnected, Channel 1 Connected to the F8 Shaker Output, and Channel 2 Connected to the Accelerometer on the "Receiver Wheel"

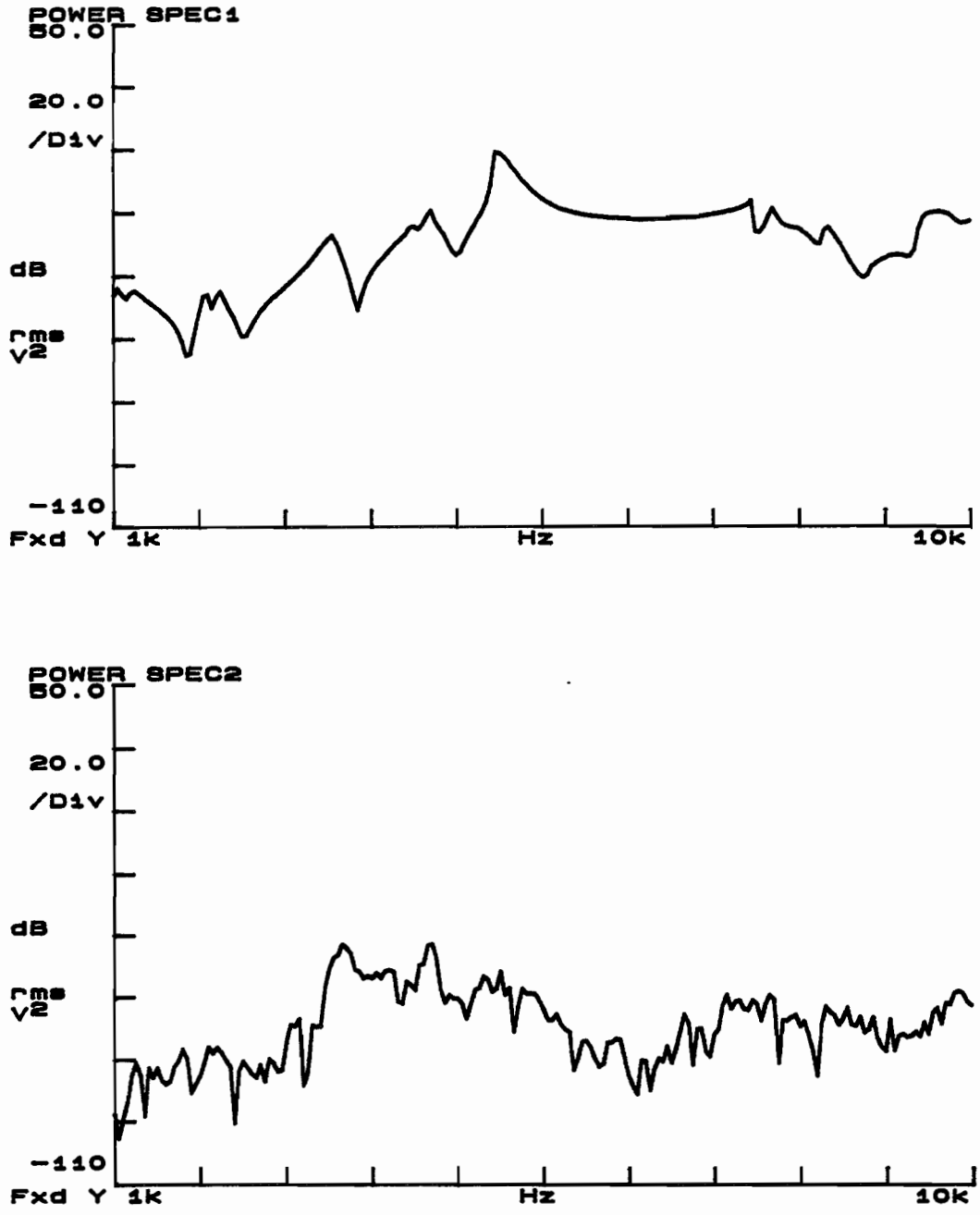

Figure C.3: Power Spectra for Signal Transmission Testing on Prototype 4 with the "Receiver Wheel" Suspended, Channel 1 Connected to the F8 Shaker Output, and Channel 2 Connected to the Accelerometer on the "Receiver Wheel"

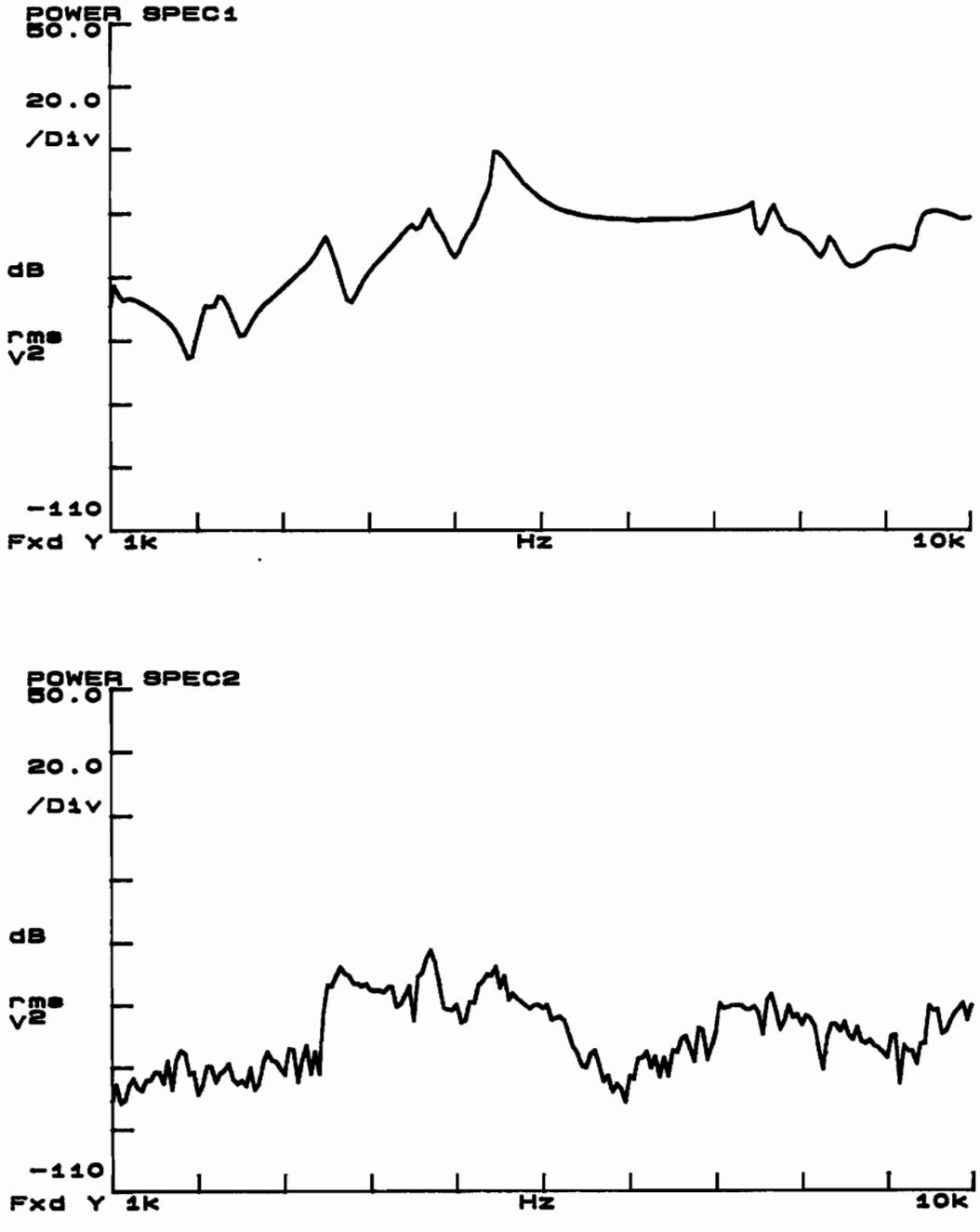

Figure C.4: Power Spectra for Signal Transmission Testing on Prototype 4 with the "Receiver Wheel" Suspended, the Hinged Connection Disconnected, Channel 1 Connected to the F8 Shaker Output, and Channel 2 Connected to the Accelerometer on the "Receiver Wheel"

Appendix D

Spectral Functions Measured During Testing of the Sensitivity of the Receiver Accelerometer

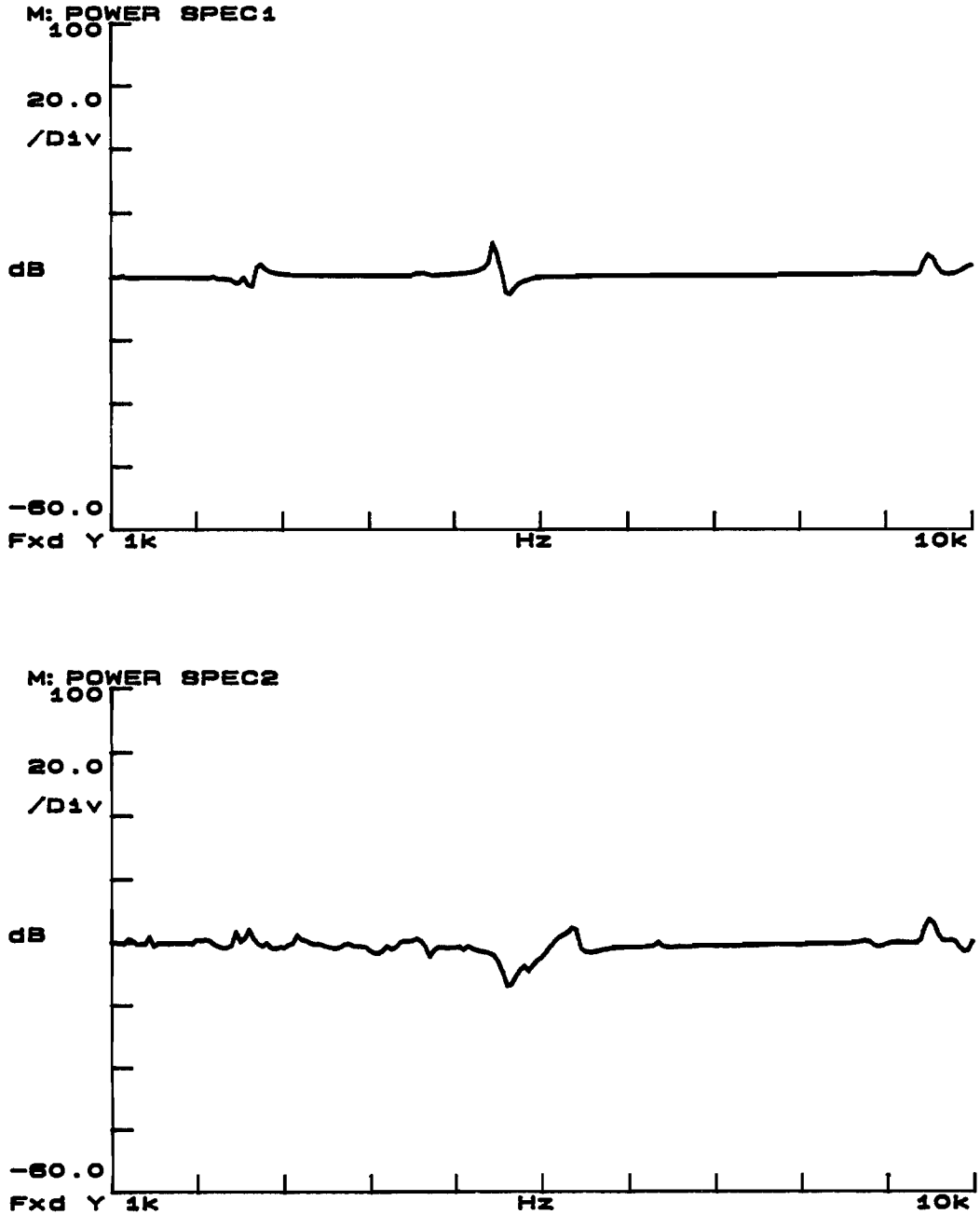

Figure D.1: Power Spectra for Evaluating the Sensitivity of the Receiver Accelerometer with both Source and Receiver Directly on the Ground Obtained by Dividing the 750mV Signal Results by the 75mV Signal Results

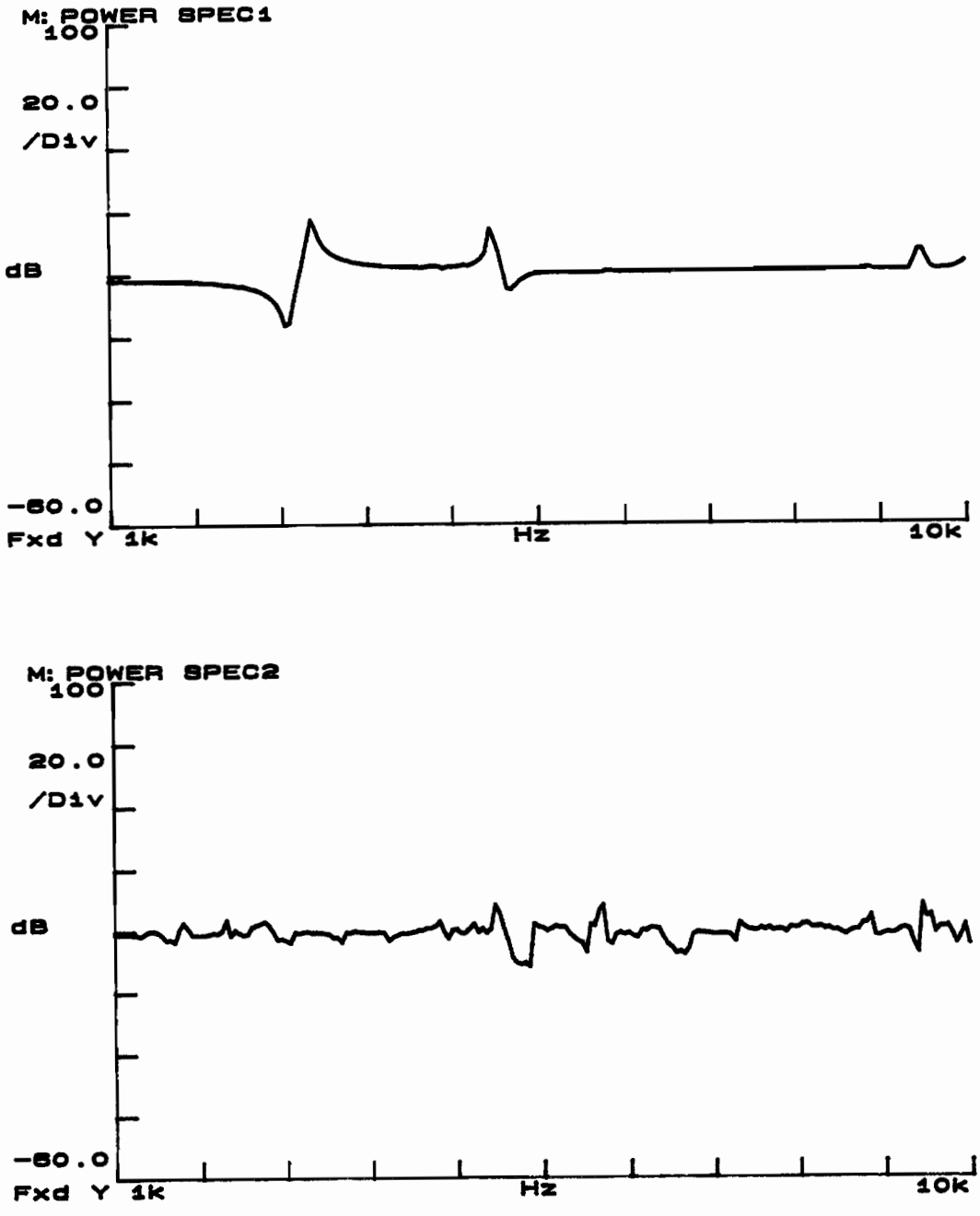

Figure D.2: Power Spectra for Evaluating the Sensitivity of the Receiver Accelerometer with the Source on the Ground and the Receiver on the "Receiver Wheel" Obtained by Dividing the 750mV Signal Results by the 75mV Signal Results

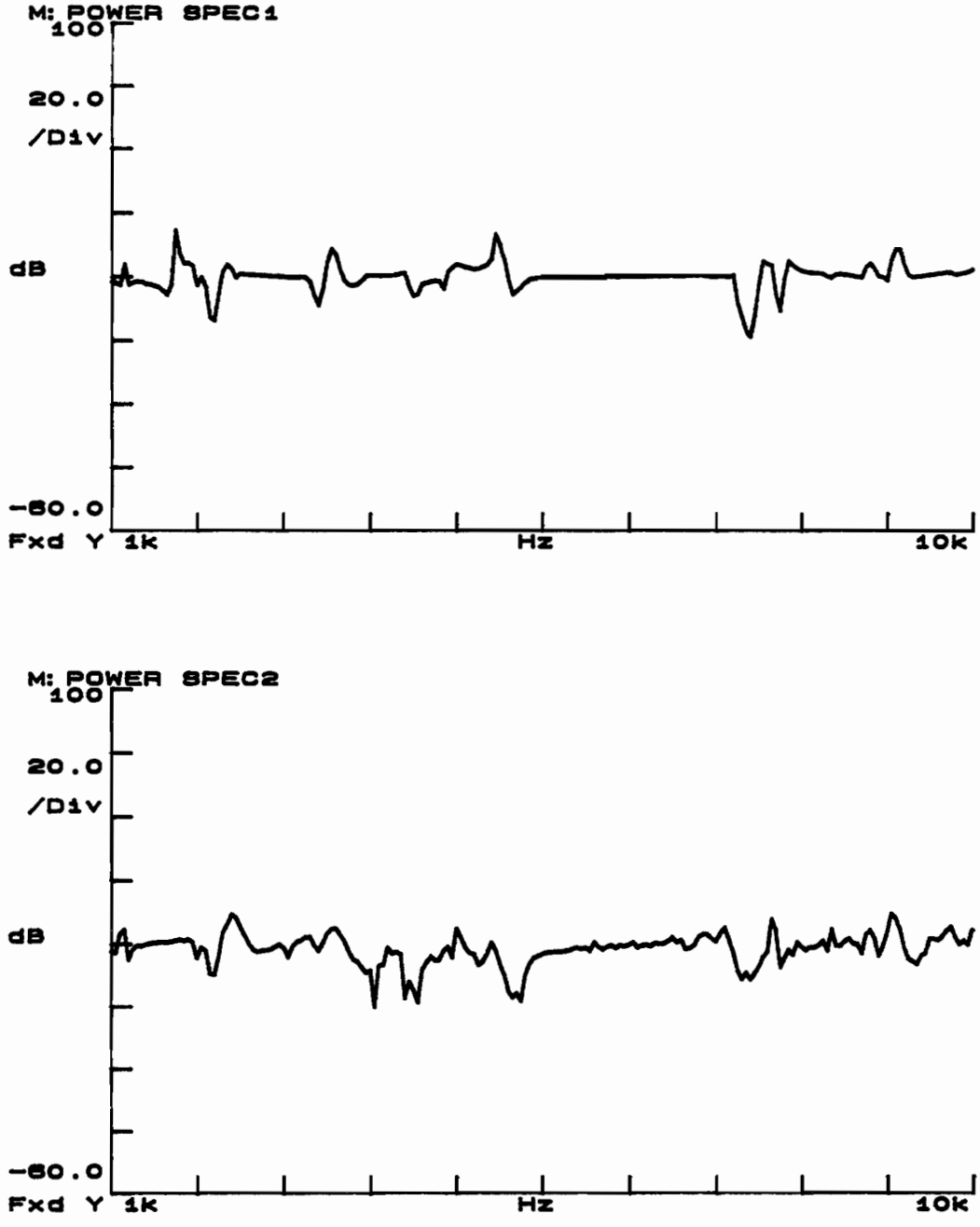

Figure D.3: Power Spectra for Evaluating the Sensitivity of the Receiver Accelerometer with the Source on the "Source Wheel" and the Receiver on the Ground Obtained by Dividing the 750mV Signal Results by the 75mV Signal Results

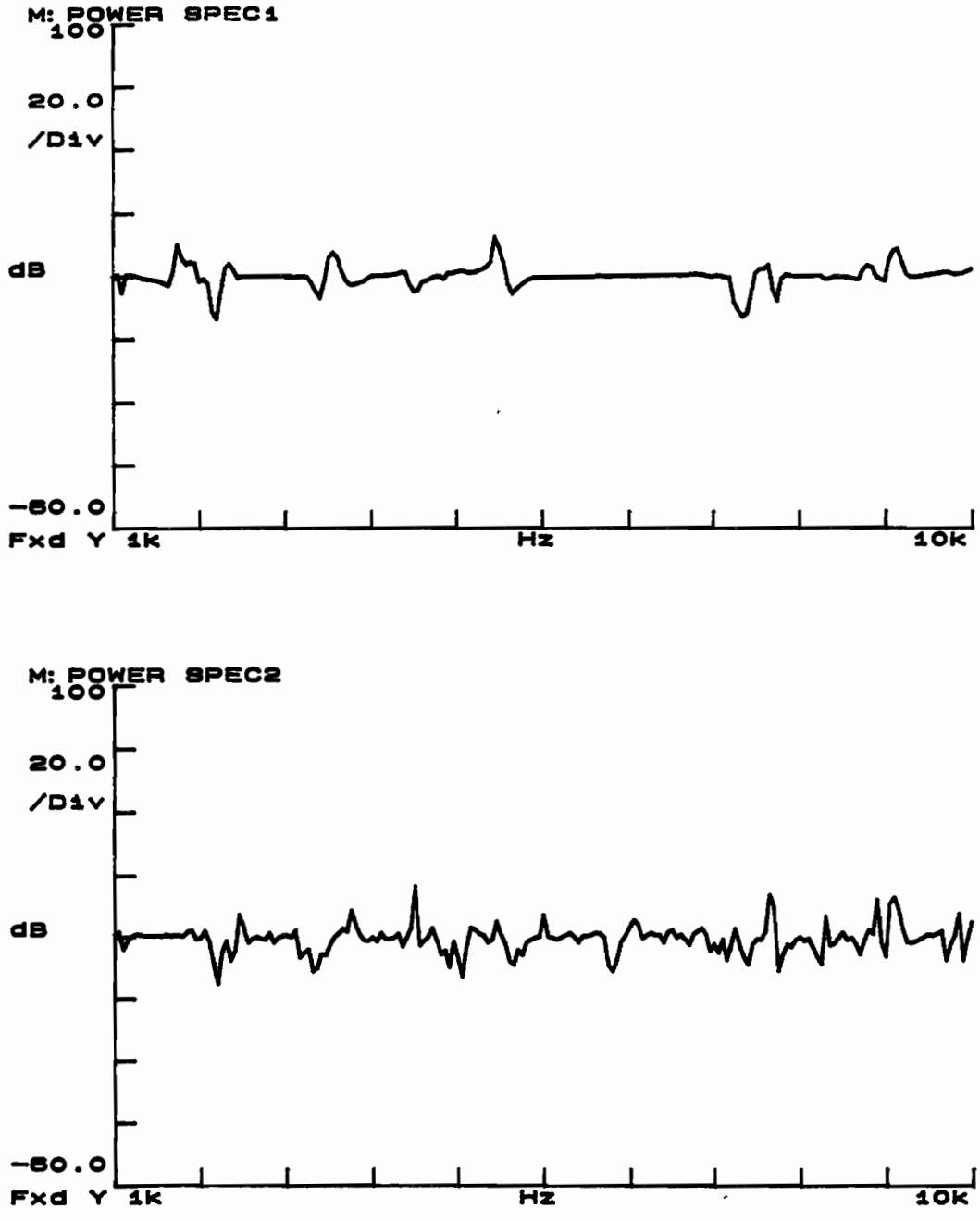

Figure D.4: Power Spectra for Evaluating the Sensitivity of the Receiver Accelerometer with the Source on the "Source Wheel" and the Receiver on the "Receiver Wheel" Obtained by Dividing the 750mV Signal Results by the 75mV Signal Results

Appendix E

Spectral Functions Measured During Transmission Testing for Airborne Signals on the Prototype Trailer-Mounted System

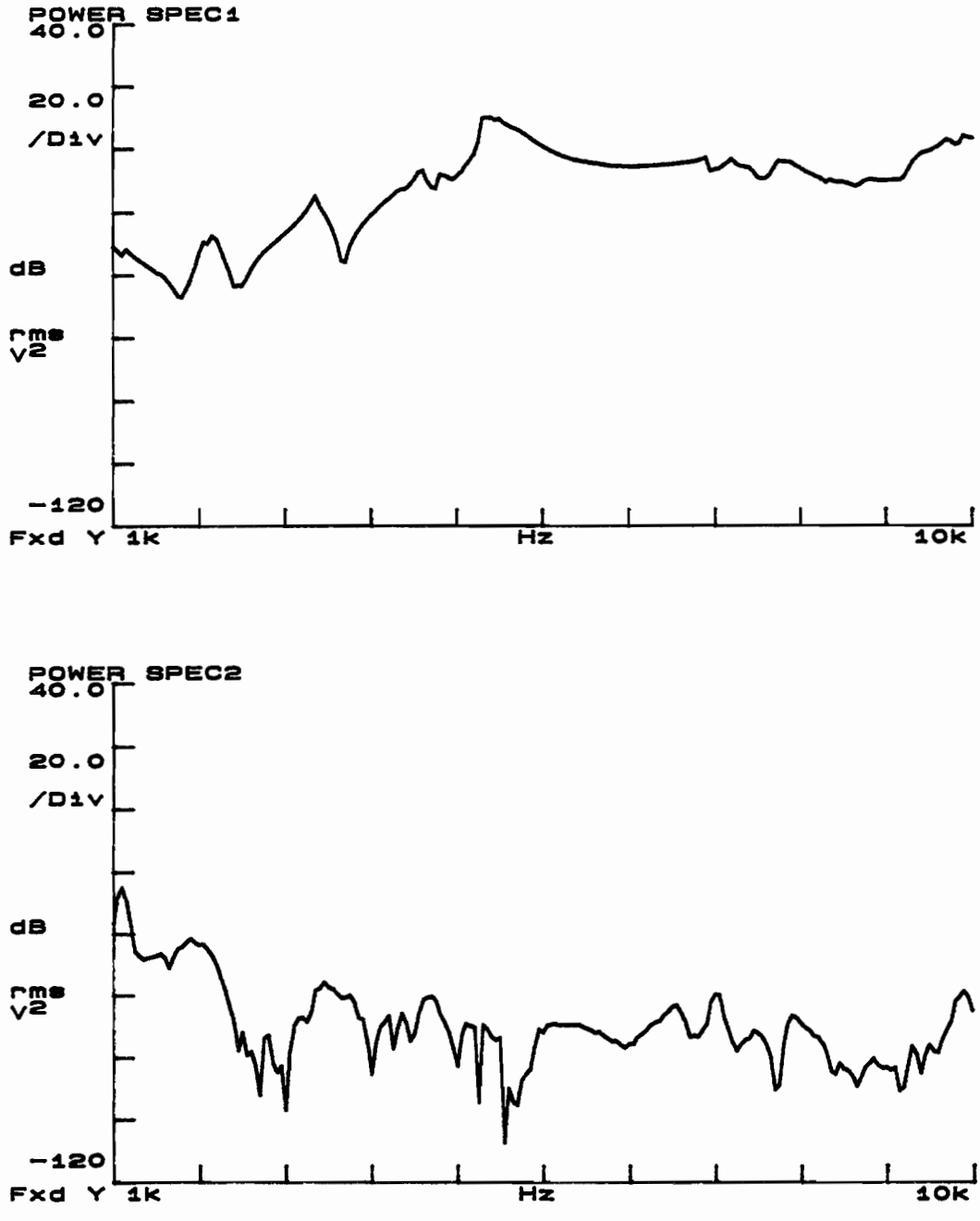

Figure E.1: Power Spectra for Signal Transmission Testing on Prototype Trailer-Mounted System with Channel 1 Connected to the F8 Shaker Output and Channel 2 Connected to the Accelerometer on the "Receiver Wheel"

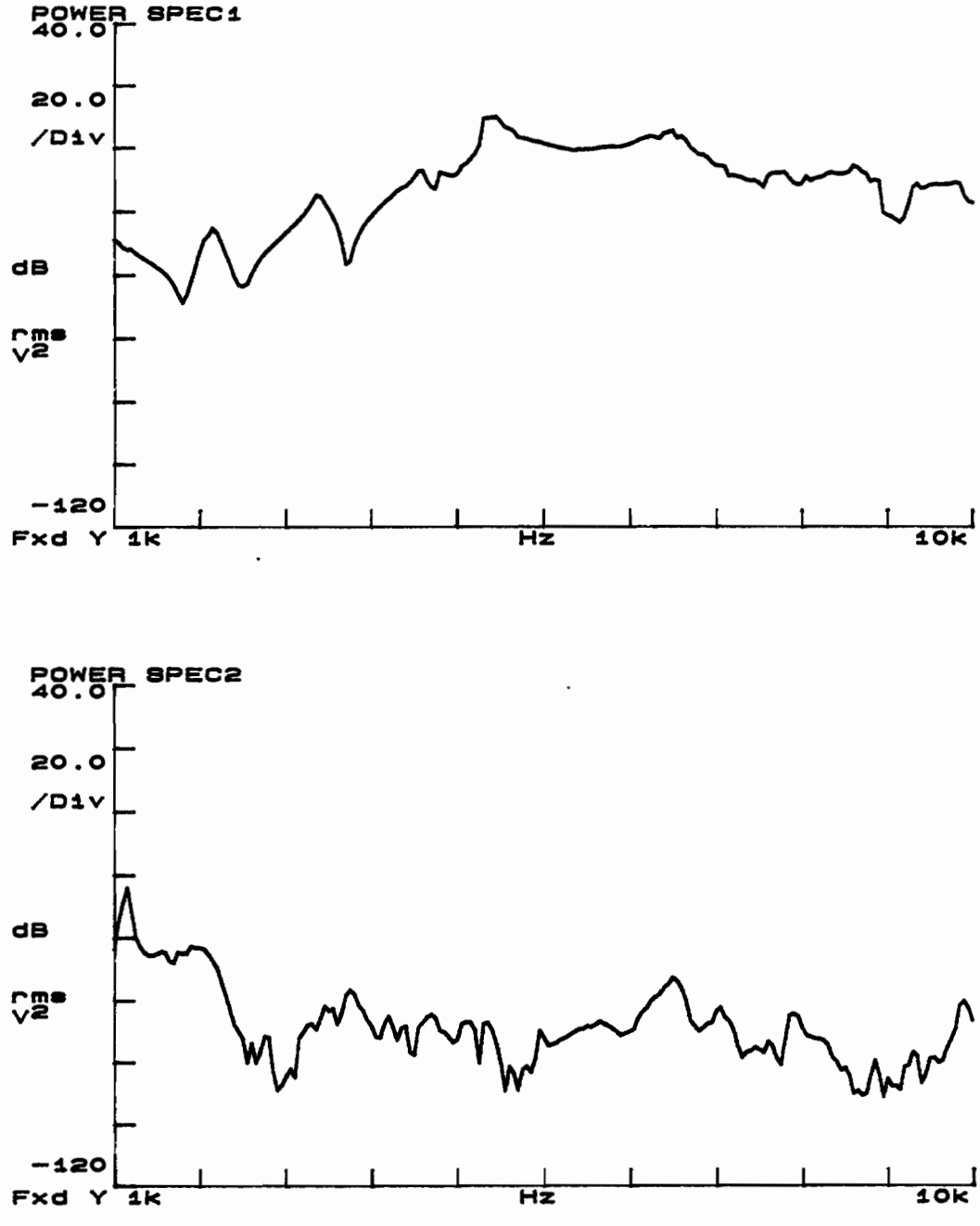

Figure E.2: Power Spectra for Signal Transmission Testing on Prototype Trailer-Mounted System with the Hinge Disconnected, Channel 1 Connected to the F8 Shaker Output, and Channel 2 Connected to the Accelerometer on the "Receiver Wheel"

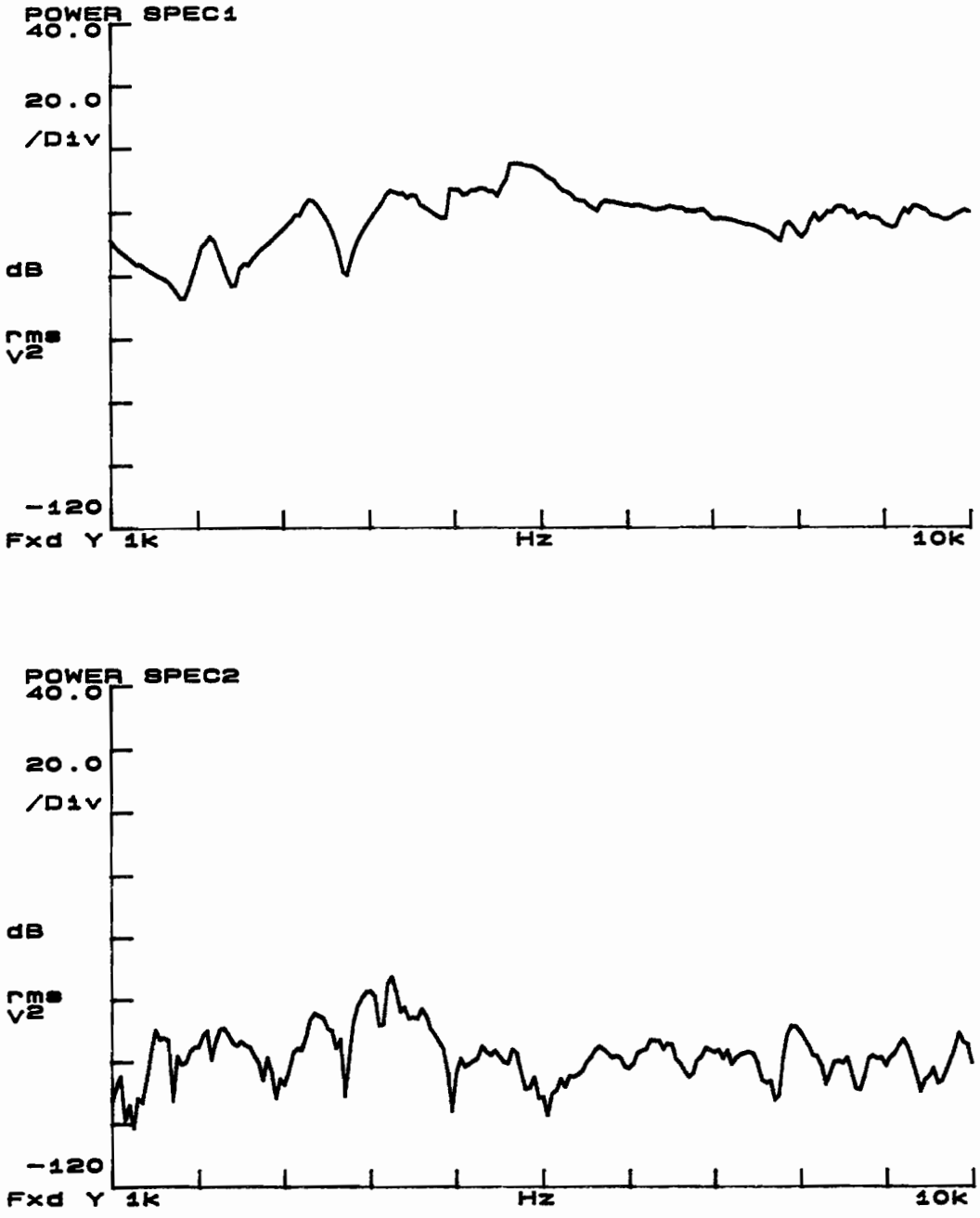

Figure E.3: Power Spectra for Signal Transmission Testing on Prototype Trailer-Mounted System with the "Receiver Wheel" Suspended, Channel 1 Connected to the F8 Shaker Output, and Channel 2 Connected to the Accelerometer on the "Receiver Wheel"

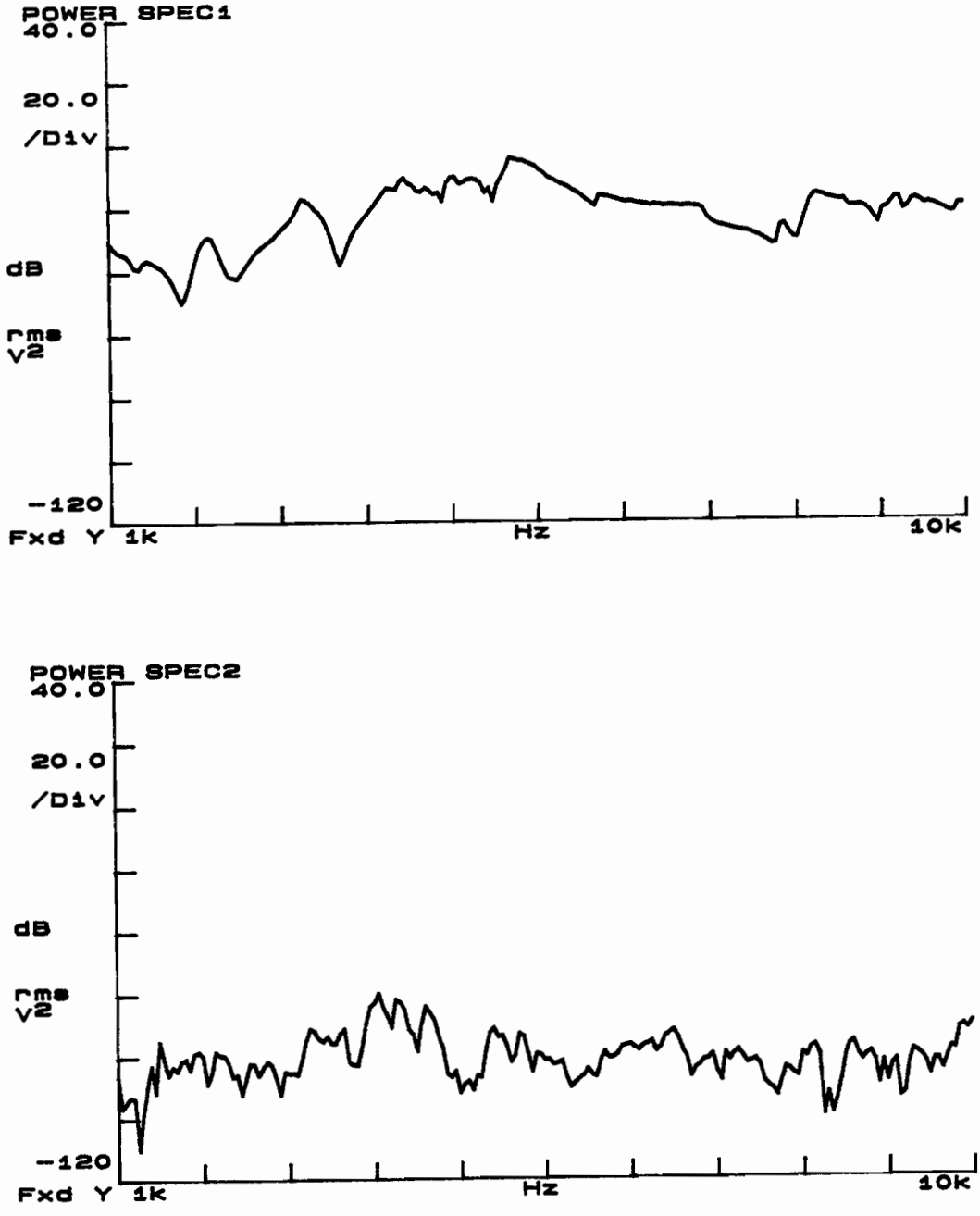

Figure E.4: Power Spectra for Signal Transmission Testing on Prototype Trailer-Mounted System with the "Receiver Wheel" Suspended, the Hinged Connection Disconnected, Channel 1 Connected to the F8 Shaker Output, and Channel 2 Connected to the Accelerometer on the "Receiver Wheel"

Appendix F

Spectral Functions Measured During Component Testing for Airborne Transmission on Prototype the Trailer-Mounted System

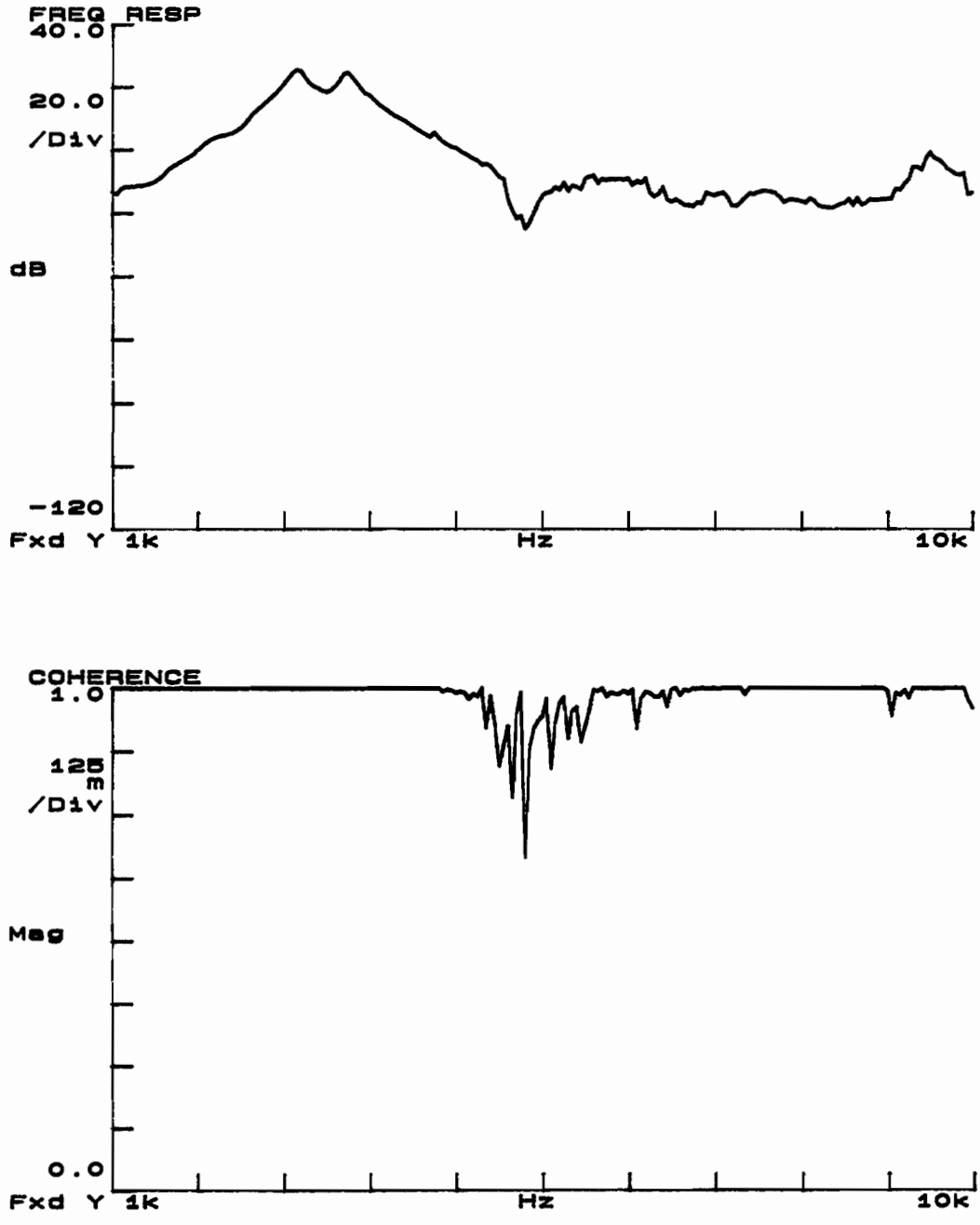

Figure F.1: Frequency Response and Coherence for Prototype Trailer-Mounted System Component Testing with both the Source and Receiver Directly on the Ground

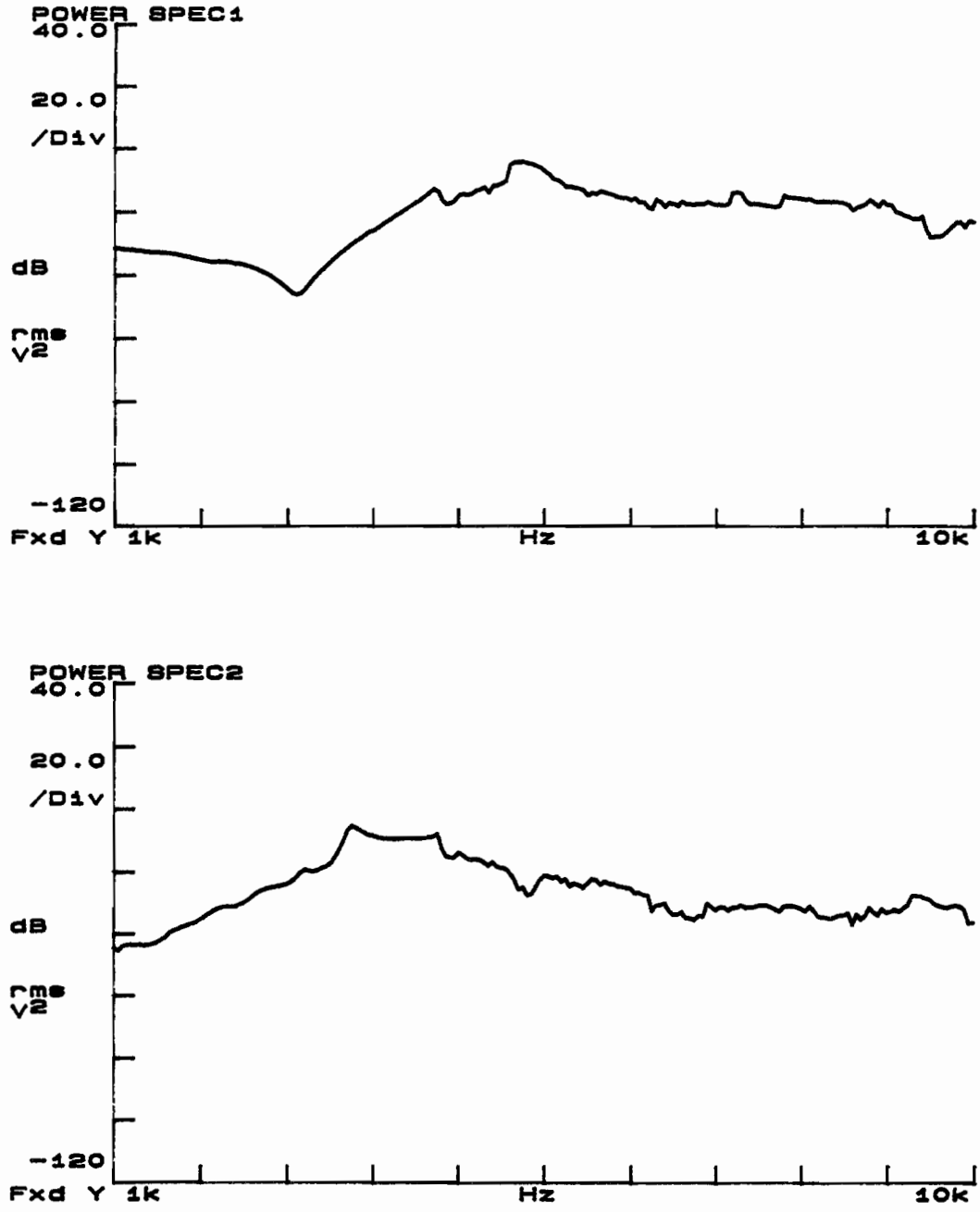

Figure F.2: Power Spectra for Prototype Trailer-Mounted System Component Testing with both the Source and Receiver Directly on the Ground

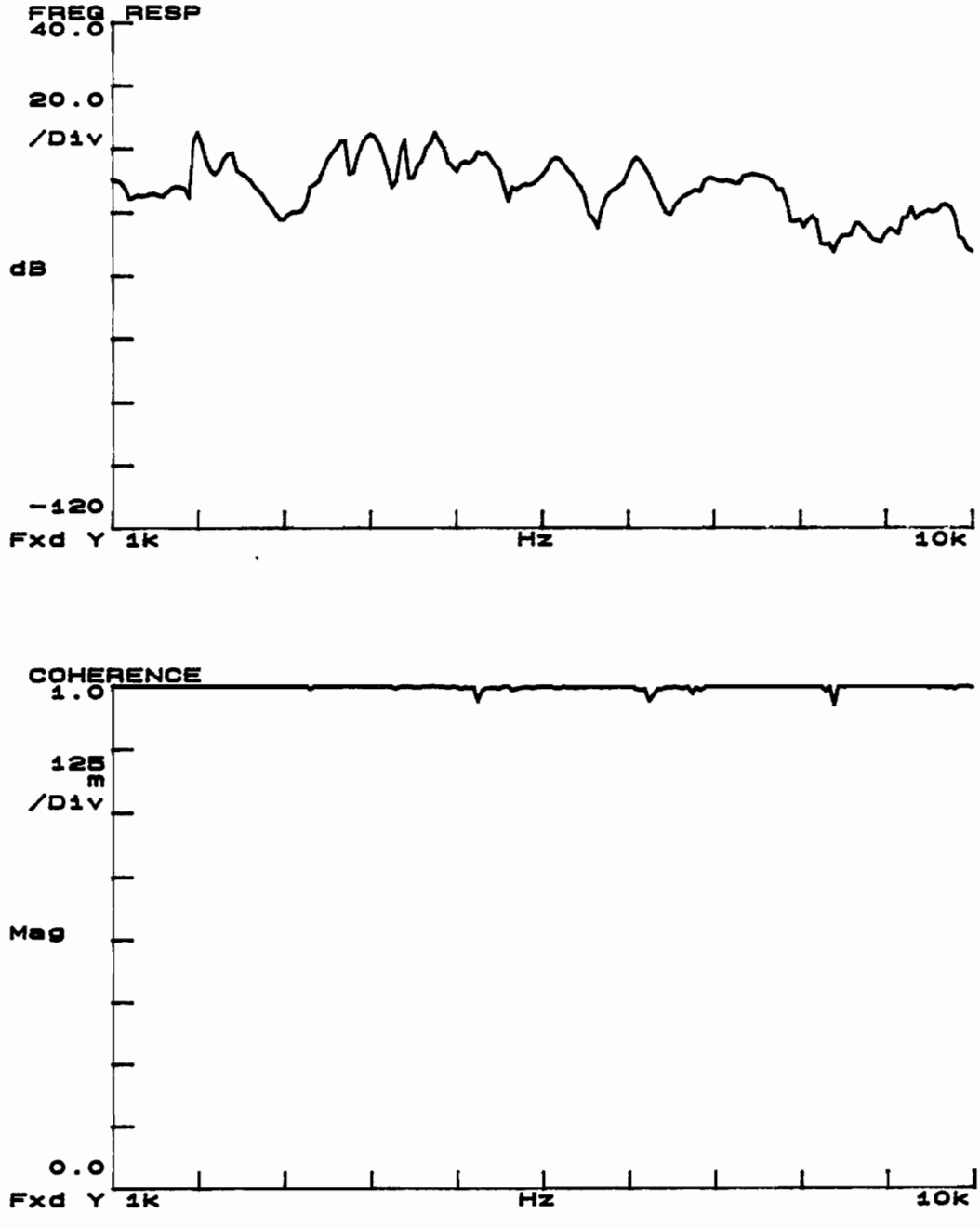

Figure F.3: Frequency Response and Coherence for Prototype Trailer-Mounted System Component Testing with the Source on the "Source Wheel" and the Receiver Directly on the Ground

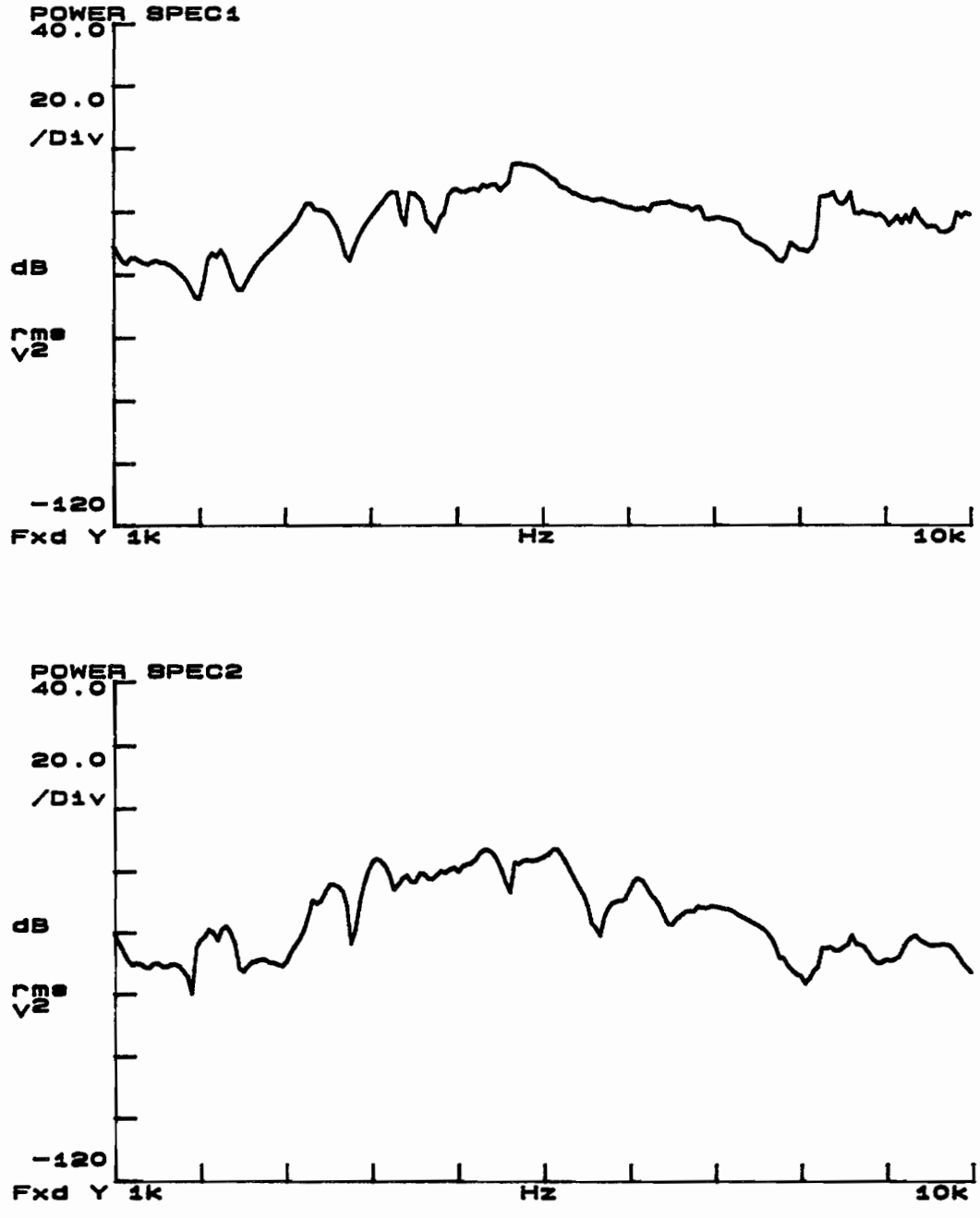

Figure F.4: Power Spectra for Prototype Trailer-Mounted System Component Testing with the Source on the "Source Wheel" and the Receiver Directly on the Ground

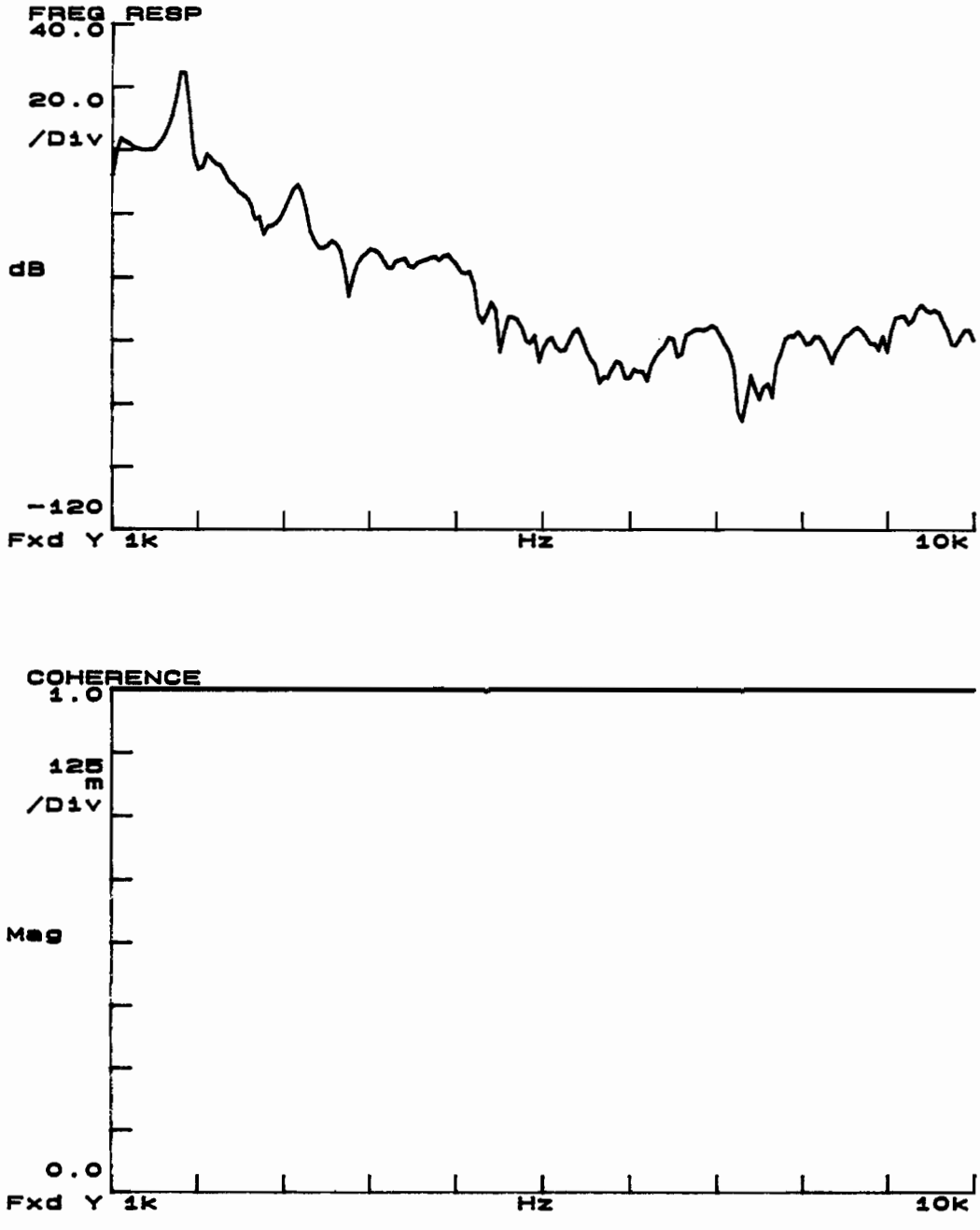

Figure F.5: Frequency Response and Coherence for Prototype Trailer-Mounted System Component Testing with the Source Directly on the Ground and the Receiver on the "Receiver Wheel"

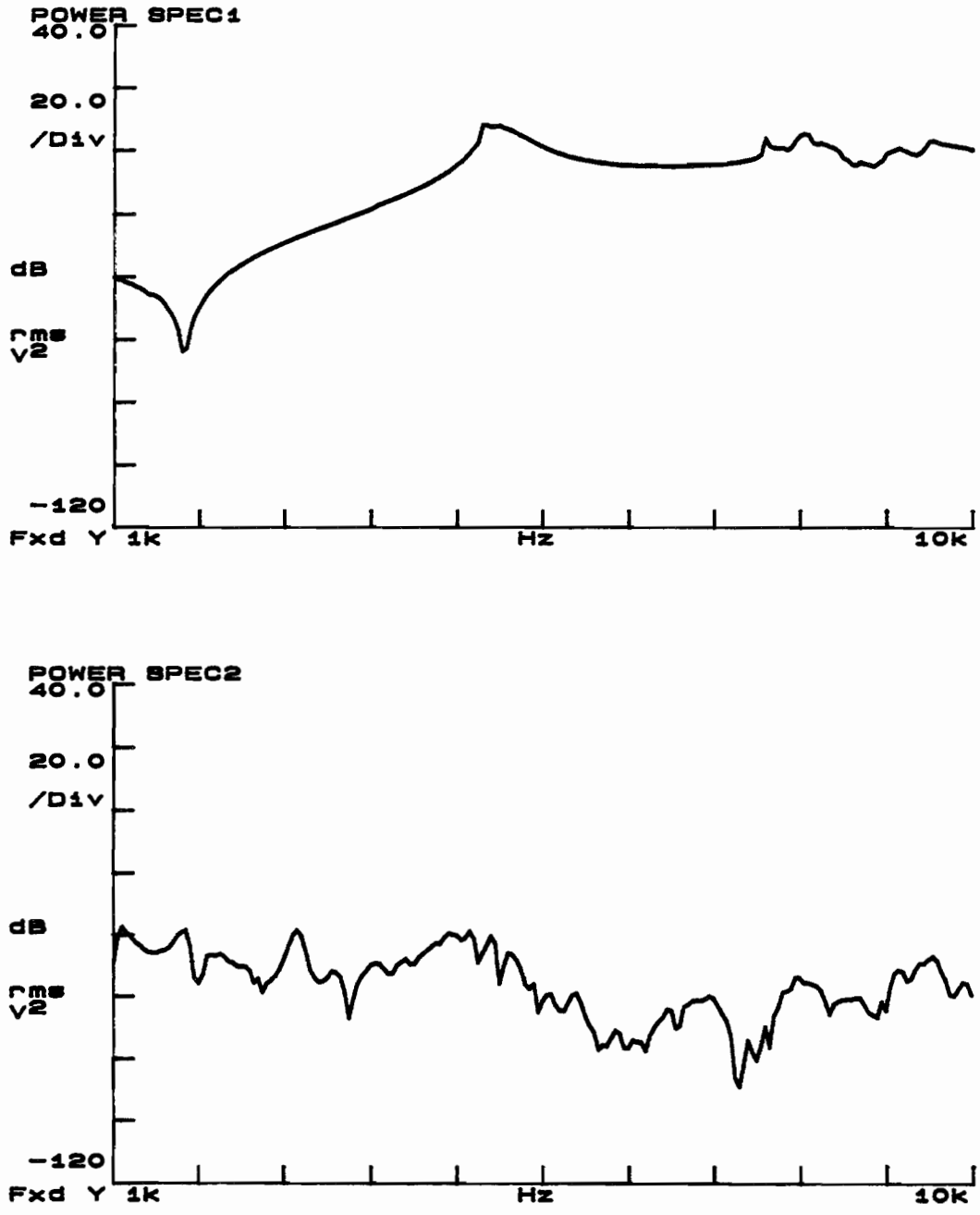

Figure F.6: Power Spectra for Prototype Trailer-Mounted System Component Testing with the Source Directly on the Ground and the Receiver on the "Receiver Wheel"

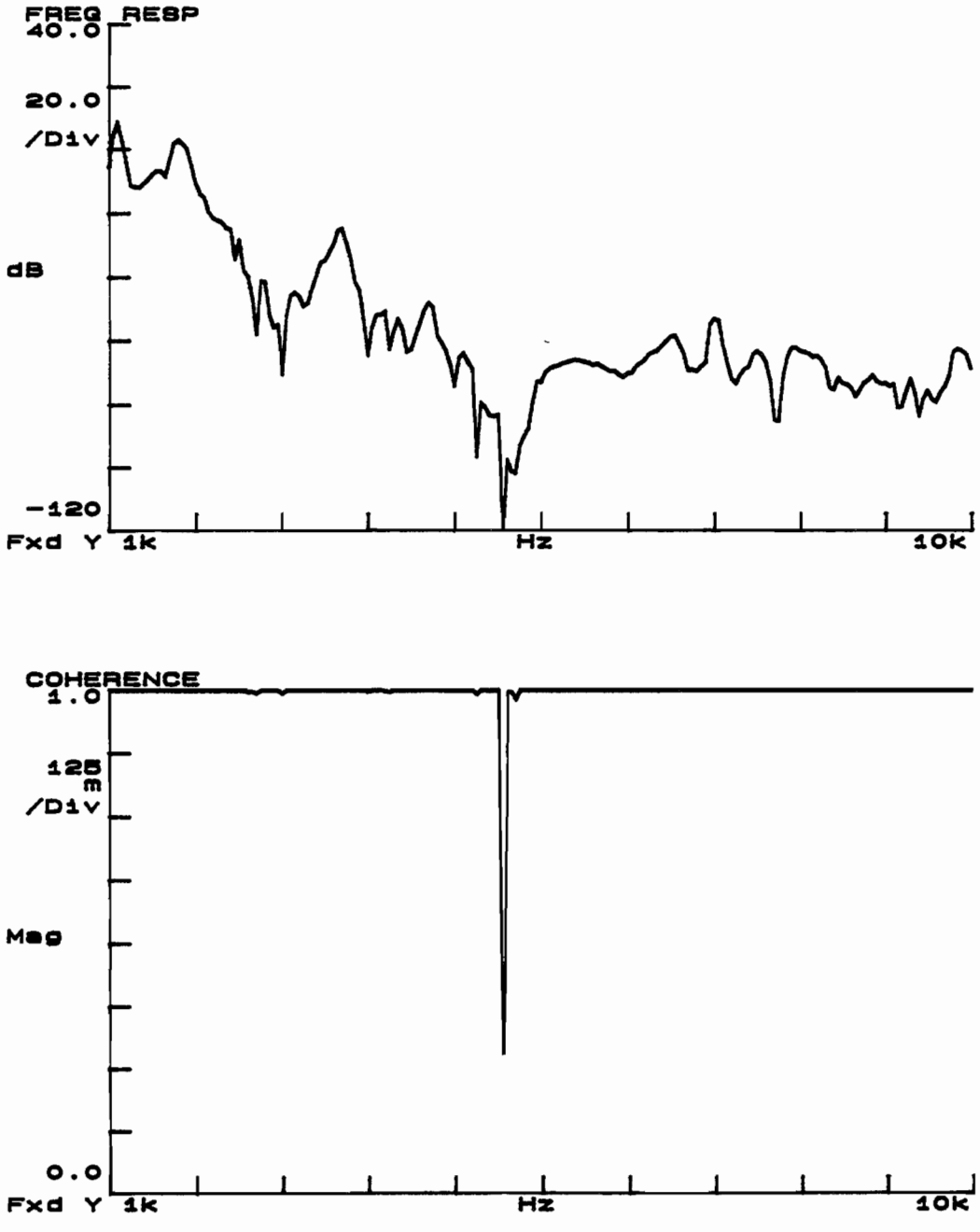

Figure F.7 Frequency Response and Coherence for Prototype Trailer-Mounted System Component Testing with the Source on the "Source Wheel" and the Receiver on the "Receiver Wheel"

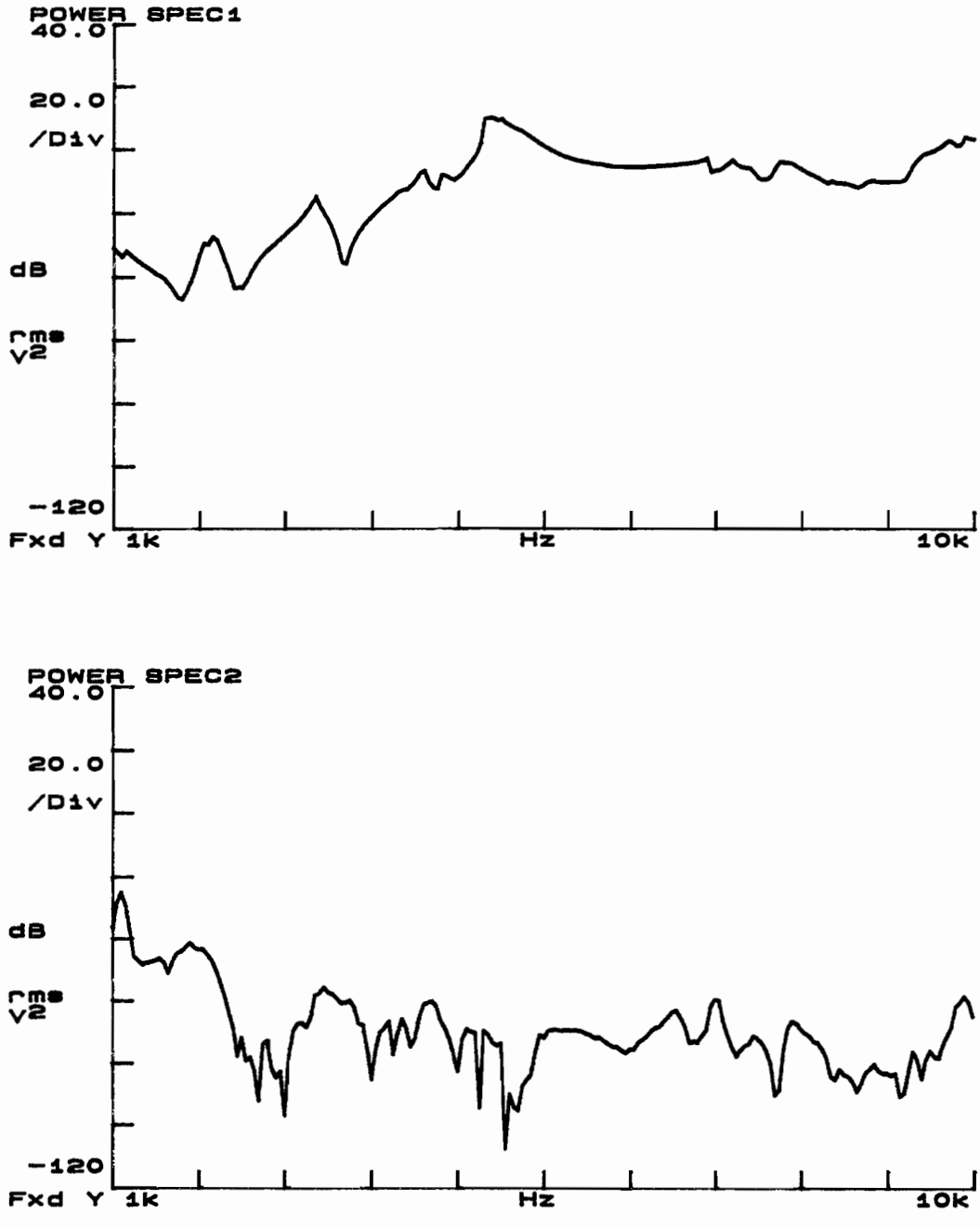

Figure F.8: Power Spectra for Prototype Trailer-Mounted System Component Testing with the Source on the "Source Wheel" and the Receiver on the "Receiver Wheel"

Appendix G

AC Voltmeter Voltage Data for Variable Frequency Testing Over the Void at the BRC Test Facility

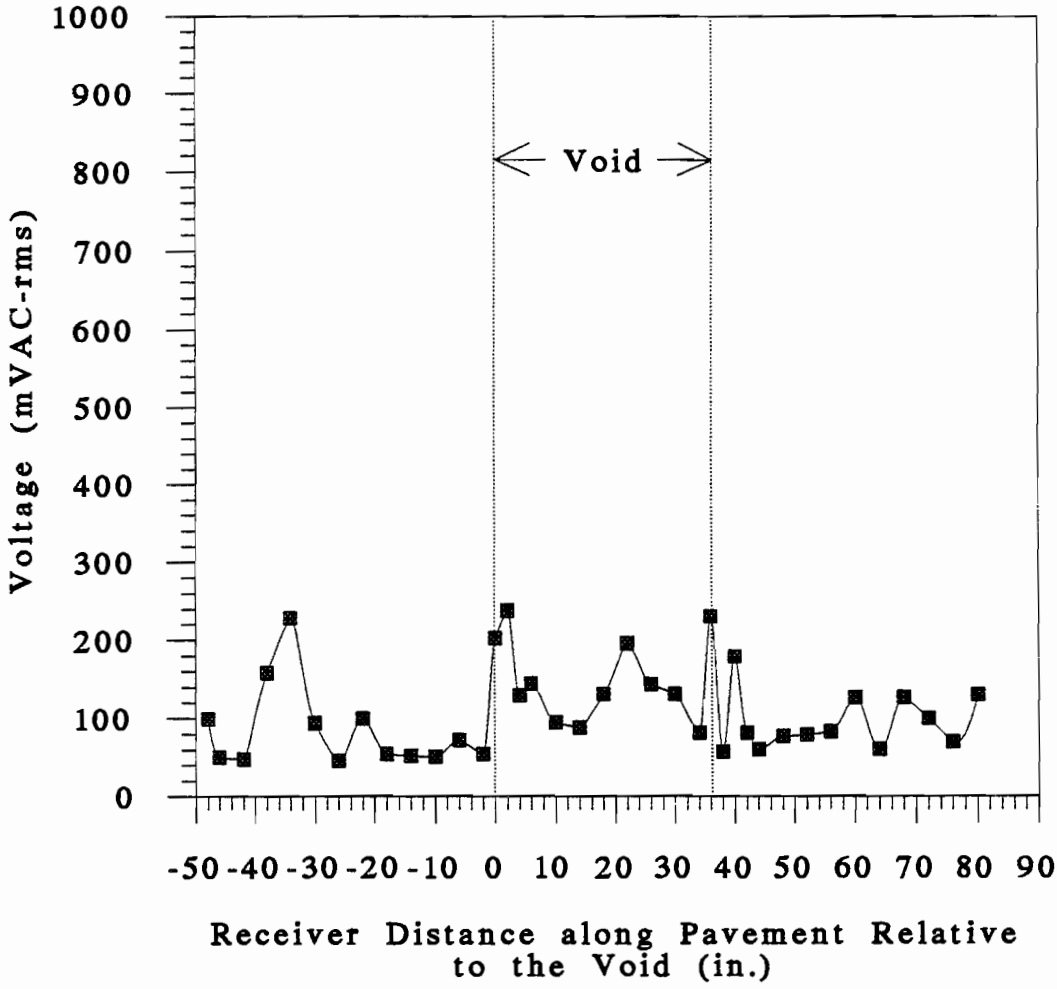

Figure G1: AC Voltmeter Voltage Output Versus Distance for Testing Across Pavement Void at the BRC Test Facility (Source Operating at 1.5KHz)

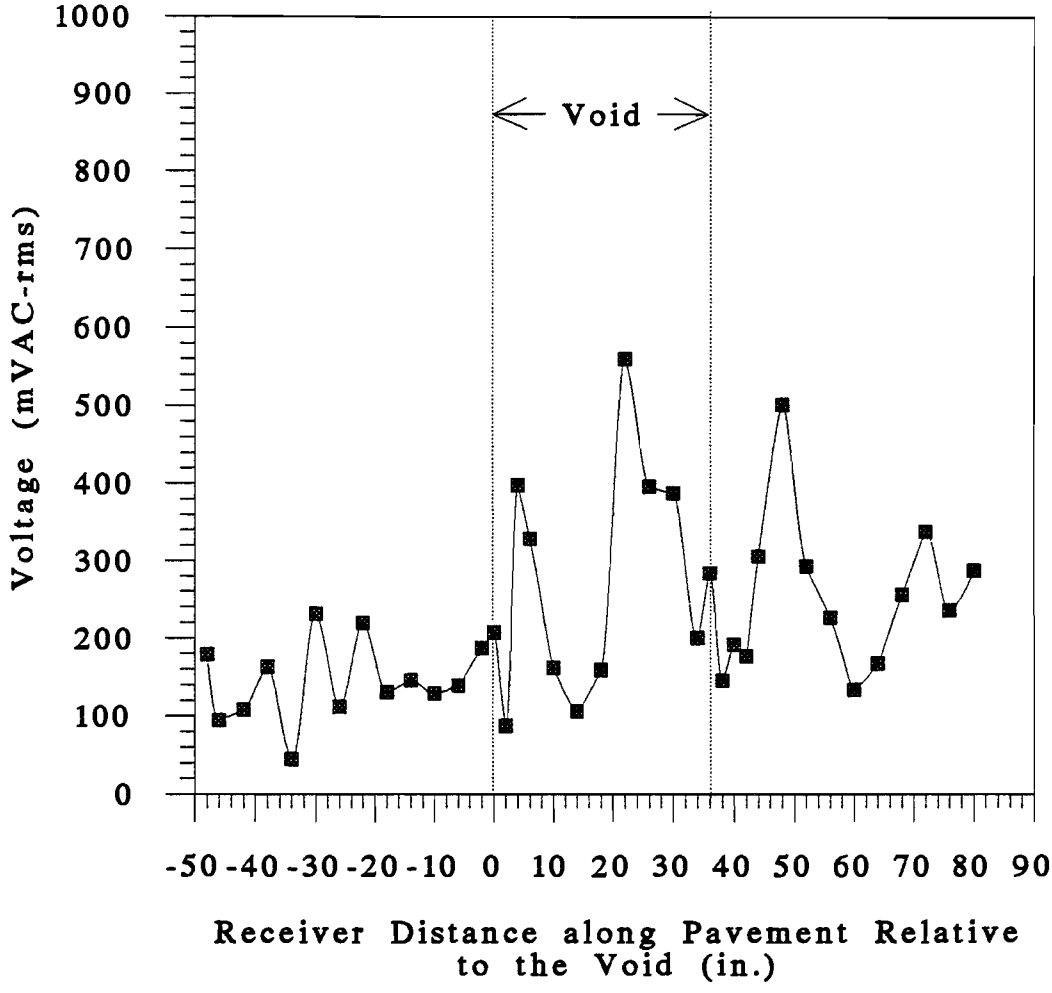

Figure G2: AC Voltmeter Voltage Output Versus Distanace for Testing Across Pavement Void at the BRC Test Facility (Source Operating at 2.175KHz)

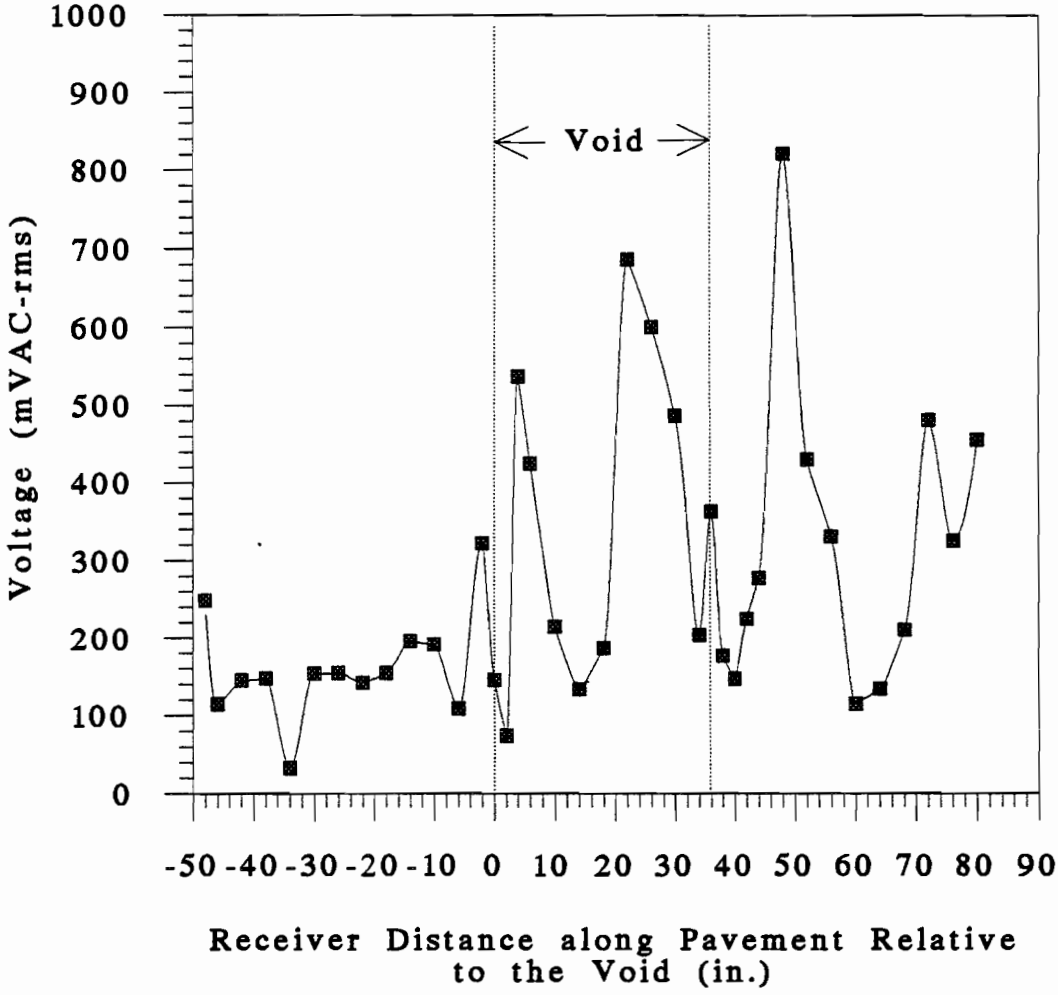

Figure G3: AC Voltmeter Voltage Output Versus Distance for Testing Across Pavement Void at the BRC Test Facility (Source Operating at 2.35KHz)

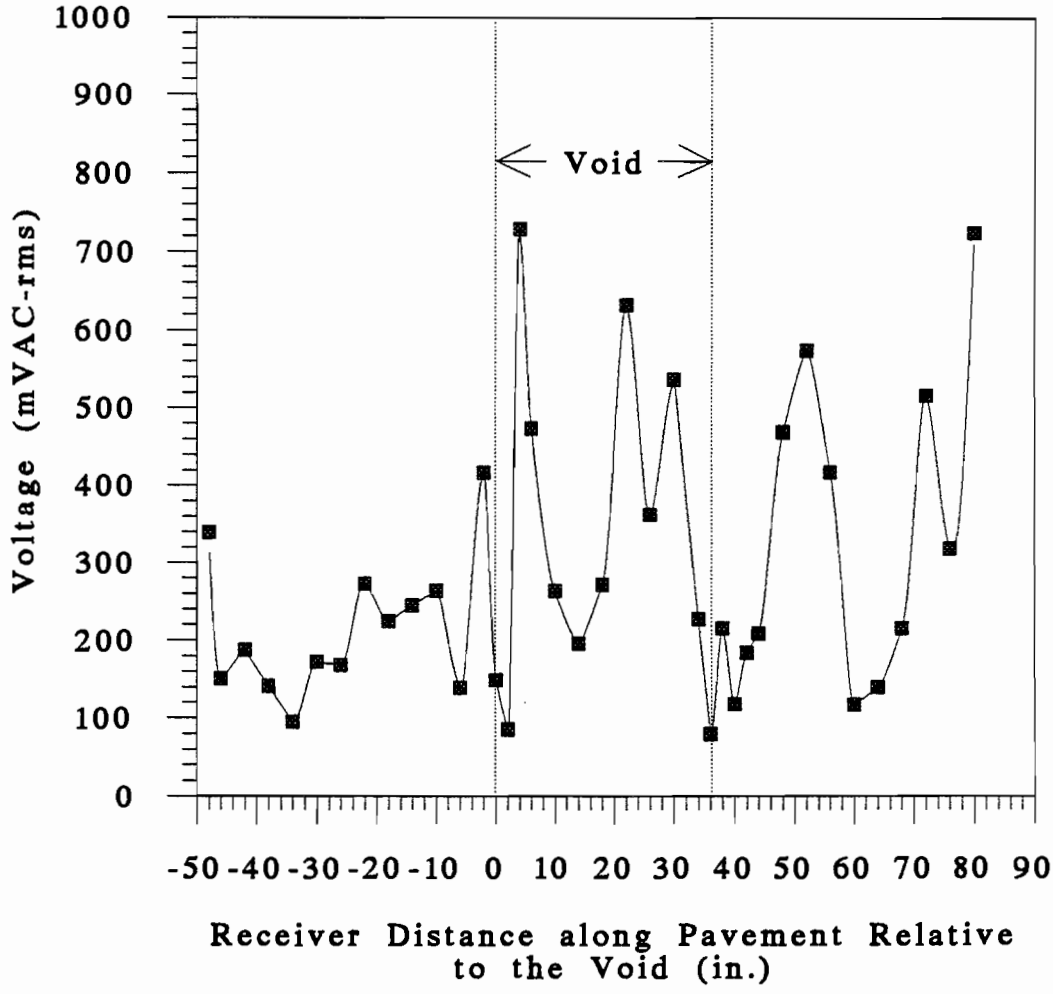

Figure G4: AC Voltmeter Voltage Output Versus Distance for Testing across Pavement Void at the BRC Test Facility (Source Operating at 2.5KHz)

References

Ayyub, B.M., and R. White, (1987), "Detection of Delamination and Cavities in Concrete", AW087-313-046 Task G, Maryland Department of Transportation, Maryland, 93pp.

Barenberg, E.J., D.A. Dietz, and M.L. Woods, (1988), "Evaluation of Concrete Pavements using Nondestructive Testing Techniques", Project 1HR-512, Transportation Research Laboratory, Department of Civil Engineering, Engineering Experiment Station, University of Illinois at Urbana-Champaign, pp. 3-40.

Birkoff, J.W., and B.F. McCullough, (1979), "Detection of Voids Underneath Continuously Reinforced Concrete Pavements", Research Report Number 177-18, Development and Implementation of the Design, Construction, and Rehabilitation of Rigid Pavements, Research Project 3-8-75-177, Center for Highway Research, The University of Texas, Austin, Texas, 52pp.

Cable, J.K., and R. Dankbar, (1990), "Evaluation of the PAVDEX Road Survey System in Iowa", Report Number FHWA-TS-90-038, Iowa Department of Transportation, Iowa, 118pp.

Cantor, T.R., (1984), "Review of Penetrating Radar as Applied to Nondestructive Evaluation of Concrete", American Concrete Institute Publication, SP-82, In Situ Nondestructive Testing of Concrete, V.M. Malhorta, ed., pp. 581-601.

Christory, J. P., (1981), "Continuous Nondestructive Evaluation of Concrete Pavements - Some Aspects of the Method used in France for Government Operated Roads", Proceedings of the 2nd International Conference on Concrete Pavement Design, Purdue University, West Lafayette, Indiana, pp. 221-230.

Clemena, G.G., (1982), "Evaluation of Overlaid Bridge Decks with Ground Penetrating Radar", VHTRC 82-R42, Virginia Highway & Transportation Research Council, Virginia, 55pp.

Clemena, G.G., and W.T. McKeel, (1977), "The Applicability of Infrared Thermography in the Detection of Delamination in Bridge Decks", Virginia Highway & Transportation Research Council, Virginia, 39pp.

Clemena, G.G., M.M. Sprinkel, and R.R. Long, (1986), "Use of Ground Penetrating Radar for Detecting Voids Underneath a Jointed Concrete Pavement", VHTRC 86-R36, Virginia Highway & Transportation Research Council, Virginia, 39pp.

Geophysical Survey Systems, Inc., (1989), "Subsurface Detection Problems", GSSI Document 8529, North Salem, New Hampshire, 2pp.

Hafermann, G.R., (1983), "Detection of Delamination in CRCP using Infrared Thermography", Executive Summary, Wisconsin Department of Transportation and Donohue & Associates, Wisconsin, 7pp.

Hagen, M.G., (1984), "Infrared Thermography and the Delamtect: A Comparison of Methods for Locating and Measuring Delaminations", Minnesota Department of Transportation, Minnesota, 18pp.

Hewlett Packard, (1985), "The Fundamentals of Signal Analysis", Application Note 243, Hewlett Packard, California.

Hintz, R.J., J.D. Degner, B.E. Ruth, and C. Karakadas, (1988), "Construction and Statistical Evaluation of a Computerized Photologging System for Identification and Measurement of Pavement Cracking", FL/DOT/BMR/88-315, University of Florida, Civil Engineering, Florida, 183pp.

Holt, F.B., and J.W. Eales, (1987), "Nondestructive Evaluation of Pavements", Concrete International: Design and Construction, Volume 9, Number 6, June, pp. 41-45.

Joyce, R.P., (1985), "Rapid Nondestructive Delamination Detection", FHWA/RD-85?051, IIT Research Institute, Chicago Illinois, 186pp.

Le Laboratoire Central des Ponts et Chaussees, (1983), "Le Collographe", Bull. Liasison Labo. P. et Ch., Number 126, pp. 77-90.

Luxmoore, A., (1973), "Holographic Detection of Cracks in Concrete", Nondestructive Testing, Volume 6, Number 5, October, pp. 258-263.

Masliwec, T., (1990), "Optimizing Infrared Detection for Bridge Deck Deterioration", ME-88-10, Ontario Ministry of Transportation, Research and Development Branch, Downsview, Ontario, 58pp.

Mendelsohn, D.H., (1988), "Pavement Crack Recording (PCR) by Slit Integration, Volume I: Final Report", FHWA-RD-88-168, Ektron Applied Imaging, Inc., Massachusetts, 76pp.

Moore, W.M., G. Swift, and L.J. Milberger, (1970), "An Instrument for Detecting Delamination in Concrete Bridge Decks", Research Report Number 130-4, A Study of Reinforced Concrete Bridge Deck Deterioration: Diagnosis, Treatment, and Repair, Research Study Number 2-18-68-130, Texas Transportation Institute, Texas A&M University, College Station, Texas, 35pp.

Nazarian, S., (1992) Telephone interview, 17 Aug.

Nazarian, S., and M. Baker, (1992), "A New Nondestructive Testing Device for Comprehensive Pavement Evaluation", Proceedings Nondestructive Evaluation of Civil Structures and Materials, May, pp.437-452.

Olson-Church, Inc., (1986), "Preliminary Research Results: Slab Impulse-Response Testing to Detect Void, Balcones Research

Center Research Slab, The University of Texas at Austin, Austin, Texas", Job No. R-1, June 20.

Olson, L.D., (1990), "NDE of Structural Concrete with Stress Waves", Proceedings Nondestructive Evaluation of Civil Structures and Materials, October, pp.61-70.

Olson, L.D., C. Wright, and K.H. Stokoe II, (1990), "Strides in Nondestructive Testing", Civil Engineering, Volume 60, Number 5, May, pp. 52-55.

Payne, L.D., and R.S. Walker, (1988), "The Use of Lasers for Pavement Crack Detection", Research Report Number 1141-1, Crack Identification Using Lasers, Research Project 8-18-88-1141, University of Texas, Arlington, Texas, 74pp.

Ransom, R.C., and J.T. Kunz, (1986), "Nondestructive Detection of Voids Beneath Pavement", Public Works, Volume 117, Number 1, January, pp. 52-54.

Richart, F.E., J.R. Hall, Jr., and R.D. Woods, (1970), Vibrations of Soils and Foundations, Prentice-Hall, Inc., Englewood Cliffs, New Jersey.

Sansalone, M., and N.J. Carino, (1988), "Impact-Echo Method", Concrete International: Design & Construction, Volume 10, Number 4, April, pp. 38-46.

Sansalone, M., and N.J. Carino, (1989), "Detecting Delaminations in Concrete Slabs With and Without Overlays Using the Impact Echo Method", ACI Materials Journal, Volume 86, Number 2, March-April, pp. 175-184.

Scrivner, F., and C.H. Michalak, (1974), "Linear Elastic Layered Theory as a Model of Displacements Measured Within and Beneath Flexible Pavement Structures Loaded by the Dynaflect", Research Report 123-25, Texas Transportation Institute, Texas A&M University, College Station, Texas.

Sheu, Jiun-Chyuan, (1987), "Applications and Limitations of the Spectral-Analysis-of-Surface-Waves Method", Doctoral Dissertation, The University of Texas at Austin, Department of Civil Engineering, Austin, Texas.

Torres, F., and B.F. McCullough, (1983), "Void Detection and Grouting Process", Research Report Number 249-3, Implementation of Rigid Pavement Overlay and Design System, Research Project 3-8-79-249, Center for Transportation Research, The University of Texas at Austin, pp. 33-36.

Uddin, W., W.R. Hudson, G.E. Elkins, and K.T. Reilley, (1987), "Pavement Condition Monitoring Methods and Equipment: Evaluation of Equipment for Measuring Voids Under Pavements", Report Number FH6713, Prepared by ARE Inc. for the Federal Highway Administration, Austin, Texas, 173pp.

Uddin, W., V. Torres-Verdin, R.W. Hudson, A.H. Meyer, and F.B. McCullough, (1983), "Dynaflect Testing for Rigid Pavement Evaluation", Research Report Number 256-6F, The Study of New Technologies for Pavement Evaluation, Research Project 3-8-80-256, Center for Transportation Research, Bureau of Engineering Research, The University of Texas at Austin, 102pp.

White, R., R.W. Hudson, A.H. Meyer, K.H. and Stokoe, II, (1984), "Design and Construction of a Rigid Pavement Research Facility", Research Report 355-1, Construction of a Multipurpose Rigid Pavement Research Facility, Research Project 3-8-83-355, Center for Transportation Research, Bureau of Engineering Research, University of Texas, Austin, Texas, 108pp.

Wilcoxon Research, (1990), "Vibration Instrumentation", Catalog W-11, Rockville, Maryland, 91pp.

Wittmann, F.H., ed., (1983), "Fracture Mechanics of Concrete", Developments in Civil Engineering, Volume 7, Elsevier Science Publishers, Amsterdam, The Netherlands, pp. 85-93.

Yoder, E.J. and M.W. Witczak, (1975), Principles of Pavement Design, John Wiley & Sons, Inc., New York, New York.